TRANSITION METAL ACETYLIDE COMPLEXES FOR NONLINEAR OPTICS

Andrew Michael McDonagh

B. Sc. (Hons)

A thesis submitted for the degree of Doctor Of Philosophy of The Australian National University

November 1999

Contents

Statement

I certify that the content of this Thesis has never been submitted for any degree and is not currently being submitted for any other degree or qualification, that all the work and results described are original unless due reference is made, and that any help received has been acknowledged.

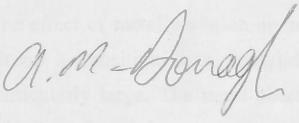

Andrew M. McDonagh

Summary

Nonlinear optical (NLO) effects are observed when there is an interaction of intense laser light with matter. Materials may be designed to harness these NLO phenomena for technological purposes, but a sound knowledge of the relationship between molecular structure and the NLO response is desirable in order to enhance the efficiency of such materials. Previous research in the area has begun to establish structure/NLO property relationships for a range of molecular systems, although there are many aspects yet to be explored. In the current work, the results of studies investigating the effect of variation in metal, charge-transfer ligands, and geometry on NLO properties are presented.

The effect of metal variation upon the second-order optical nonlinearity of several series of Group 8 transition-metal acetylide complexes was found to be significant, although not particularly large. The trend observed in molecular second-order optical nonlinearities for this type of complex was iron < ruthenium < osmium. This is in contrast to trends reported for transition-metal nitrile complexes, suggesting that factors other than the specific metal present in the complex may play a more dominant role in determining the second-order optical nonlinearity. A bulk-phase second-order response was detected for two complexes containing an optically active diphosphine ligand. This work represents the first time homologous iron, ruthenium and osmium acetylide complexes bearing the optically active 1,2-bis(methylphenylphosphino)benzene ligand were prepared. It led to the development of a synthetic route into *cis* and *trans* isomers of $[OsCl_2(\text{chiral-at-phosphorus diphosphine})_2]$ complexes, and the elucidation of a previously unreported all-S-bound Me_2SO geometry for $[OsCl_2(Me_2SO)_4]$.

The effect on the second-order optical nonlinearity of replacing the bridging atoms X = CH in complexes bearing the alkynyl ligand (*E*)-4,4´-$HC{\equiv}CC_6H_4X{=}XC_6H_4NO_2$ with the atoms X = N was examined. In order for these measurements to be made, synthetic routes into new terminal alkyne compounds and metal acetylide complexes were developed. NLO measurements revealed that ruthenium complexes bearing an alkynyl ligand that incorporates an N=N linkage have large molecular second-order optical nonlinearities, comparable in magnitude to previously reported complexes bearing the analogous CH=CH linked ligand. The optical nonlinearities of ruthenium complexes bearing an indoaniline alkynyl ligand were significantly lower. The measurements performed with the ruthenium-acetylide complexes were resonance enhanced. However, a gold complex incorporating the ligand containing the N=N linkage had little absorption at either the fundamental or second-harmonic wavelength, permitting a better comparison of the effect of ligand variation on second-order NLO merit. Second-order NLO measurements showed that the

gold complex bearing the N=N linked ligand has a larger second-order optical nonlinearity than the analogous complex bearing the CH=CH linked alkynyl ligand.

The effect of molecular geometry and size was examined. Branched and dendritic ruthenium-acetylide complexes containing extensive π-delocalized systems were examined, and an efficient synthesis of first generation dendrimers was developed. The alkynylruthenium dendrimers are soluble in a range of solvents and are oxidatively stable. Both second- and third-order NLO experiments were performed, revealing that varying the molecular size and geometry impacts significantly on the optical nonlinearity. Very large second-order nonlinearities were recorded for several of the branched complexes, comparable to some of the largest reported in the literature. Modification of the electronic properties of the molecule by the introduction of strong acceptor groups induced large increases in second-order optical nonlinearities. Third-order NLO measurements revealed significant two-photon absorption behaviour, again comparable to some of the largest reported in the literature. Both linear and nonlinear absorption coefficients increase in a nonlinear fashion with respect to the number of metal centres, arylalkynyl groups or molecular weight upon proceeding from the smaller complexes to the dendrimers.

Acknowledgements

I sincerely thank my supervisor, Dr Mark Humphrey, for his support and encouragement, and for a generous allocation of his time.

Dr Marek Samoc is thanked for assistance with Z-scan measurements and many helpful discussions.

Mr Stephan Houbrechts, Ms Inge Asselberghs, and Professors Koen Clays and André Persoons are thanked for hyper-Rayleigh scattering measurements.

Drs Ian Whittall, David Hockless and Tony Willis, and Mr Nigel Lucas are thanked for the crystal structure determinations.

Dr Bruce Wild is acknowledged for the gift of di-μ-chlorobis[(*R*)-dimethyl(α-methylbenzyl)aminato-2-*C*,*N*]dipalladium(II).

My personal thanks go to my friends and colleagues at the Australian National University.

Lastly, I wish to thank Aileen and Aidan for their understanding and patience.

Abbreviations

a.c.	alternating current
ADP	ammonium dihydrogen phosphate
bipy	2,2'-bipyridyl
Bu^n	normal butyl
Bu^t	tertiary butyl
c.c.	complex conjugate
CNDO	complete neglect of differential overlap
d.c.	direct current
DDQ	2,3-dichloro-5,6-dicyano-1,4-benzoquinone
DFM	density functional methods
DFWM	degenerate four-wave mixing
diph	1,2-bis(methylphenylphosphino)benzene
dmpz	3,5-dimethylpyrazolyl
dmso	dimethylsulfoxide
dppe	bis(diphenylphosphino)ethane
dppm	bis(diphenylphosphino)methane
diop	(1,2-dimethyl-1,3-dioxolane-4,5-diyl)bis(methylene) bis(diphenylphosphine)
EFISH	electric field-induced second harmonic generation
EI	electron impact
ESA	excited state absorption
Et	ethyl
FAB	fast atom bombardment
Fc	ferrocenyl
FWM	four-wave mixing
HOMO	highest occupied molecular orbital
HRS	hyper-Rayleigh scattering

IDS	intensity dependent absorption
INDO	intermediate neglect of differential overlap
KDP	potassium dihydrogen phosphate
KTP	potassium titanyl phosphate
LMCT	ligand to metal charge transfer
LUMO	lowest unoccupied molecular orbital
Me	methyl
mes	mesityl
MLCT	metal to ligand charge transfer
mppz	3-*p*-methoxyphenylpyrazol-1-yl
NLO	nonlinear optical
nmdpp	neomenthyldiphenylphosphine
Oc	octyl
OKG	optical Kerr gate
OPL	optical power limiting
Ph	phenyl
phen	1,10-phenanthroline
PPP	Parr-Pariser-Pople
PT	perturbation theory
RSA	reverse saturable absorption
SA	saturable absorption
SHG	second harmonic generation
TCNQ	7,7´,8,8´-tetracyanoquinodimethane
thf	tetrahydrofuran
THG	third harmonic generation
TPA	two-photon absorption
tpph	tetraphenylporphyrinyl
U	urea
ZINDO	Zerner's intermediate neglect of differential overlap

Published Results

1. A. M. McDonagh, M. G. Humphrey and D. C. R. Hockless.
Tetrahedron: Asymmetry, **1997**, *8*, 3579.
"Selective Preparation of *cis*- or *trans*-dichlorobis{(*R,R*)-1,2-phenylenebis(methylphenylphosphine-*P*)}osmium(II) from dimethylsulfoxide complex precursors"

2. I.R. Whittall, A.M. McDonagh, M.G. Humphrey and M. Samoc.
Adv. Organomet. Chem., **1998**, *42*, 291.
"Organometallic Complexes in Nonlinear Optics I: Second-Order Nonlinearities".

3. A. M. McDonagh, M. G. Humphrey and D. C. R. Hockless.
Aust. J. Chem., **1998**, *51*, 807.
"Preparation of *cis*- and *trans*-[$OsCl_2(Me_2SO)_4$], and X-ray Crystal Structures of the All-S-bound Isomers".

4. I.R. Whittall, A.M. McDonagh, M.G. Humphrey and M. Samoc.
Adv. Organomet. Chem., **1999**, *43*, 349.
"Organometallic Complexes in Nonlinear Optics II: Third-Order Nonlinearities and Optical Limiting Studies".

5. A. M. McDonagh, M. G. Humphrey, M. Samoc, B. Luther-Davies, S. Houbrechts, T. Wada, H. Sasabe and A. Persoons.
J. Am. Chem. Soc., **1999**, *121*, 1405.
"Organometallic Complexes for Nonlinear Optics 16. Second and Third Order Optical Nonlinearities of Octopolar Alkynylruthenium Complexes". (communication)

6. A. M. McDonagh, M. G. Humphrey, M. Samoc, B. Luther-Davies.
Organometallics, in press.
"Organometallic Complexes for Nonlinear Optics 17. Synthesis, Third-order Optical Nonlinearities and Two-Photon Absorption Cross Section of an Alkynylruthenium Dendrimer". (communication)

Chapter 1

Organo-transition Metal Complexes for Nonlinear Optics

Contents

Chapter 1

Organometallics for Nonlinear Optics

1.1. Introduction

Nonlinear optics arises from interactions of electromagnetic fields (light) with matter. Interactions in materials possessing nonlinear optical (NLO) properties change the nature of the incident light such that new field components with differing phase, frequency, amplitude, polarization, path or other propagation characteristics are produced. These materials are of technological importance in areas that utilize optical devices, with potential applications as optical signal processors, switches and frequency generators (exploiting such processes as harmonic generation, frequency mixing, optical parametric oscillation and Raman shifting). Such materials may also contribute to areas like optical data storage, optical communication, optical switching, image processing and, ultimately, optical computing.

Materials currently employed for their NLO properties are mostly inorganics: salts such as $LiNbO_3$ and KH_2PO_4 (KDP) are used for frequency mixing and electrooptic modulation while glasses such as silica are the materials of choice in applications where third-order nonlinear processes such as self-phase modulation are needed. In these materials the NLO effects of a purely electronic nature are often accompanied by lattice distortions. For example, loosely bound positive ions of lithium or potassium within crystals of the salts provide an asymmetric field giving rise to NLO effects with response times in the order of nanoseconds. This is of importance for relatively slow NLO processes such as the electrooptic effect, but is not ideal for frequency conversions which require a purely electronic NLO response. Advantages of inorganic salts include a large transparency range (UV to IR), high optical damage thresholds, high perfection of single crystals and very low optical losses. In many applications, such as doubling the frequency of lasers or optical parametric amplification, there is a need for synchronization of the phases of the interacting optical

fields (phase matching). This requirement is not always easy to satisfy, and severely limits the applicability of the nonlinearity of some materials. Quasi-phase matched second-harmonic generation in crystals such as $LiNbO_3$, $LiTaO_3$, and $KTiOPO_4$ (KTP) has, however, been achieved, with efficiencies up to 10 %.[1]

Semiconductors such as gallium arsenide or indium arsenide, particularly as reduced dimensionality species (quantum wells, quantum wires or quantum dots), possess nonlinear optical effects which originate from saturable absorption,[1] with third-order NLO responses that are amongst the largest known.[2] A disadvantage of NLO processes based on resonant interactions (such as one-photon or two-photon absorption) is, however, that the speed of the NLO response may be relatively slow. Although nonresonant nonlinearities of some semiconductors such as $Al_xGa_{1-x}As$ are reasonably high, many organics [for example π-conjugated polymers such as polyacetylene, polydiacetylenes and poly(*p*-phenylenevinylenes)] offer nonlinearities which are of similar or higher magnitudes, with the inherent flexibility of their design being an additional attractive feature.

Many organic molecules (in solution or as crystals, in polymers, or in guest-host systems) have been probed for their NLO responses (see, for examples, references 3-15). In these compounds, the main source of the NLO response is usually the electronic nonlinearities. Organic materials possess a number of advantages for NLO applications. Some have a higher optical damage threshold than inorganic crystals, and they are generally cheaper and easier to synthesize and fabricate than inorganic materials. They possess other advantages stemming from their structural diversity and architectural flexibility, which allow for molecular design and engineering. It is possible to grow single crystals of some organics, but many of them can also be used in other forms: for example, thin films of polymers can be electric field poled to introduce the asymmetry needed for the appearance of second-order NLO effects. Low lying electronic transitions in the UV-visible region improve the NLO efficiency in organic molecules, but a disadvantage of such molecules is a trade-off between nonlinear efficiency and optical transparency. Other disadvantages of organics may include lower thermal stability and facile relaxation of the chromophores to random orientation in poled guest-host systems.

During the evolution of the study of organic molecules for nonlinear optics, experimental observation has enabled certain structure/NLO property relationships to be developed, from which useful insights may be gained. Computational investigations utilizing quantum theory have also afforded general qualitative rules. High polarizability of any order is associated with the existence of low energy molecular excited states which, because they are close in energy to the ground state, mix easily when the molecule is perturbed.

Organic molecules containing conjugated π systems with charge asymmetry have been shown to exhibit extremely large second-order NLO properties. Donor-acceptor substituted azo dyes, Schiff bases and stilbenes are examples of molecules with an extensive cloud of π–electrons that are easily polarized, and which show large second-order nonlinearities. The nonlinearity of such molecules can be enhanced by either increasing the conjugation length, thereby increasing electron delocalization, or increasing the strength of donor or acceptor groups to improve electron asymmetry within a molecule.[2] NLO properties of polyene-like molecules can be increased further by controlling bond-length alternation (the difference in length between C—C single and double bonds in a π-conjugated system). Changing the alternation may alter the charge distribution in the electronic ground state. For optimized alternation, enhancements of up to a factor of five may be observed.[16,17]

Sizeable π-delocalization length (e.g. progressing from small molecules to π-conjugated polymers), the presence of donor and acceptor functional groups, chain orientation and packing density, conformation and dimensionality (e.g. progressing from one-dimensional oligomers to two-dimensional porphyrins and phthalocyanines)[18] all impact favourably on third-order nonlinearity.

Octopolar compounds have been studied as potential NLO materials. [19] Non-dipolar molecules may be effective in overcoming problems such as the NLO efficiency/transparency trade-off, and the proclivity of dipolar molecules to adopt centrosymmetric packing in the solid state. The presence of a three-fold symmetry axis in octopolar 1,3,5-substituted aromatic ring systems may lead to better transparency characteristics, and the lack of a molecular dipole enhances the prospects of noncentrosymmetric crystal packing.

Like organic molecules, organometallic complexes can possess large NLO responses, fast response times, ease of fabrication and integration into composites, as well as having the advantage over organic systems of much greater flexibility at the design stage. Variation in metal, oxidation state, ligand environment and geometry can in principle permit NLO responses to be tuned in ways not possible for purely organic molecules. Studying the nonlinear properties of a variety of metals, oxidation states and ligands in systematic series of "families" of organometallic compounds can lead to an understanding of structure/property relationships.

Novel bonding patterns and coordination geometries allow for spatial arrangements of atoms that may not be easily accessible in other systems. Organometallic compounds are often strong oxidizing or reducing agents, since metal centres may be electron rich or poor depending on their oxidation state and ligand environment. Thus, the metal centre may be an extremely strong donor or acceptor which is a requirement for electron asymmetry and

hence second-order nonlinearity within a molecule. Unusual and/or unstable organic fragments (e.g. carbenes) may be stabilized on metals, allowing the NLO properties of these species to be assessed. Organometallics can also form polymers or be included in polymers, either as side chains or in the polymer backbone, which affords the possibility of introducing more polarizable atoms in a polymer chain than may be accessible in purely organic systems.

The NLO properties of organometallic compounds have been reviewed previously together with those of some related coordination complexes.[18,20-24] The present work reviews the organo-transition metal-containing component of the field through mid-1999.[†]

[†] This Chapter draws partly on material from publications 2 and 4 (listed on page ix).

1.2. Background

1.2.1. Theory of nonlinear optics

Optical nonlinearities can be explained by considering the interaction of strong electric fields with matter. If the fields have optical frequencies, the phenomena resulting from the nonlinear interactions are called nonlinear optical (NLO) phenomena. Most texts on nonlinear optics (e.g. references 25-28) begin the discussion of this area from considerations of macroscopic relations between the vector quantities **P** (the polarization vector), **D** (the displacement vector) and **E** (the electric field vector). Chemists, however, consider the molecular origin of physical phenomena, so the description of NLO phenomena which follows starts from consideration of the behaviour of a single molecule in a strong electric field.

An electric field $\mathbf{E}_{loc}$ acting on a molecule is termed a *local* field since it may differ substantially from the macroscopic field outside the medium (because of the influence of neighbouring molecules). The field will, in general, distort the electron density distribution $\rho(\mathbf{r})$ in a molecule. Such a distortion may be described in terms of changes in the electron distribution moments. The first moment of the electron distribution, the dipole moment μ, is the most important quantity from the aspect of optical properties (hence, one often talks about a so-called dipolar approximation). The changes in the dipole moment induced by a relatively weak field can be expected to be linear with the magnitude of the field. However, this will not be the case for the field $\mathbf{E}_{loc}$ comparable in strength to the internal electric fields within the molecule. In these circumstances, the distortion and the induced dipole moment have to be treated as nonlinear functions of the field strength, usually being presented in terms of a power series:

$$\mu = \mu_0 + \alpha\mathbf{E}_{loc} + \beta\mathbf{E}_{loc}\mathbf{E}_{loc} + \gamma\mathbf{E}_{loc}\mathbf{E}_{loc}\mathbf{E}_{loc} + \ \ldots \qquad (1.1)$$

In many texts (e.g. some of those relating to quantum chemical calculations), equation (1.1) is treated as a Taylor series and therefore has 1/n! multipliers in front of the consecutive $(\mathbf{E}_{loc})^n$ terms.

The tensorial α, β and γ quantities defined by the above equation are called the linear polarizability, the second-order or quadratic hyperpolarizability (or, sometimes, the first hyperpolarizability) and the third-order or cubic hyperpolarizability (the second hyperpolarizability), respectively. As both μ and $\mathbf{E}_{loc}$ are vectors, the relation between the three cartesian components of μ and the three cartesian components of $\mathbf{E}_{loc}$ needs nine proportionality factors, and so α is a second-rank tensor (or a 3×3 matrix). A full description of the second-order and third-order interactions involves assessing the effect on the dipole moment

of *combinations* of cartesian components of the field, so β is a third-rank tensor (or a $3 \times 3 \times 3$ matrix) and γ is a fourth-rank tensor (or a $3 \times 3 \times 3 \times 3$ matrix). Fortunately, many of the tensor components of α, β, and γ are equivalent by various symmetry rules or equal to zero. The most straightforward simplification comes from permutation symmetry (the products of the cartesian components of the field can be freely permuted), which results in some indices in the tensor elements of the polarizabilities being permuted, too.[27] Additional simplification comes from polarizabilities being invariant with respect to all point group symmetry operations. The latter rule is especially important when considering the second-order hyperpolarizability β: in the same way that a vectorial property must be absent in an object which has a centre of symmetry (the only vector which stays invariant after inverting it through a centre of symmetry is a vector of zero length), all the components of β (and any third-rank tensor) must vanish in centrosymmetric point groups.

The electric field of a light wave can be expressed as:

$$\mathbf{E}(t) = \mathbf{E}_0 \cos(\omega t) = \frac{\mathbf{E}_0}{2}[\exp(i\omega t) + \exp(-i\omega t)]$$

Therefore, for an arbitrary point in space, Equation 1.1. can be written as:

$$\begin{aligned} \mu(t) &= \mu_0 + \alpha \mathbf{E}_0 \cos(\omega t) + \beta \mathbf{E}_0^2 \cos^2(\omega t) + \gamma \mathbf{E}_0^3 \cos^3(\omega t) + \ \ldots \\ &= \mu_0 + \tfrac{1}{2}\alpha \mathbf{E}_0 \exp(i\omega t) + \tfrac{1}{2}\beta \mathbf{E}_0^2 \\ &\quad + \tfrac{1}{4}\beta \mathbf{E}_0^2 \exp(2i\omega t) + \tfrac{3}{8}\gamma \mathbf{E}_0^3 \exp(i\omega t) + \tfrac{1}{8}\gamma \mathbf{E}_0^3 \exp(3i\omega t) + \text{c.c.} + \ \ldots \end{aligned} \tag{1.2}$$

where c.c. stands for complex conjugate terms. It is easily seen from the above expansions in terms of exponential factors or, equivalently, trigonometric relations such as $\cos^2(\omega t) = 1/2 + 1/2\cos(2\omega t)$ that the effect of the nonlinear terms in the dipole moment expansion has been to introduce contributions at different frequencies: the second order (β) term has introduced a time-independent (d.c.) contribution (optical rectification) as well as a term oscillating at the frequency of 2ω (the second harmonic generation component). It can readily be verified that the quadratic term also provides a frequency mixing phenomenon if the input field is a sum of two components with different frequencies, and that a constant (dc) field may influence an oscillating field if the two are combined in a medium containing second-order nonlinear molecules [the linear electrooptic (Pockels) effect]. In a similar way, the cubic term in Equation (1.1) leads to various nonlinear optical effects, one being oscillation of the induced dipoles at 3ω (third harmonic generation).

Equation (1.1) is, strictly speaking, not suitable for optical fields, which are rapidly varying in time. Even for linear polarization, the oscillation of the induced dipole moment may be damped (by material resonances) and thereby phase shifted with respect to the oscillation of the external electric field. The usual way of expressing this phase shift is by considering the

relationship between the Fourier components of the induced effect (oscillation of the induced dipole) and the stimulus (the electric field), with the damping and phase shift conveniently expressed by treating the terms involved as complex. Thus, the linear polarizability can be written as:

$$\Delta\mu^{(1)}(\omega) = \alpha(\omega)E(\omega)$$

where $\alpha(\omega)$ is complex, $E(\omega)$ is the Fourier amplitude of the field at frequency ω and $\Delta\mu^{(1)}(\omega)$ is the linear component of the oscillation of the dipole at the same frequency. Dispersion of α (the frequency dependence of the linear polarizability) will show characteristic rapid changes of the real part of α and enhanced values of the imaginary part of α near to the resonance frequencies of the molecule.

In the same way, frequency dependent hyperpolarizabilities can be defined as complex quantities by considering the relations between the nonlinear (quadratic and cubic) components of the induced dipole moment oscillations at particular frequencies. A complication is that, in general, more than a single field frequency is involved. The usual notation is:

$$\Delta\mu^{(2)}(\omega_3) = \beta(-\omega_3;\omega_1,\omega_2)E(\omega_1)E(\omega_2)$$

and:

$$\Delta\mu^{(3)}(\omega_4) = \gamma(-\omega_4;\omega_1,\omega_2,\omega_3)E(\omega_1)E(\omega_2)E(\omega_3)$$

for the quadratic and cubic nonlinear optical effects, respectively. The first frequency in the brackets describing the frequency dependence of the hyperpolarizability refers to the output frequency and the remaining frequencies are those of the input fields. Positive and negative signs of the frequencies can occur, depending on the type of interaction; for example, the β responsible for second harmonic generation is represented as $\beta(-2\omega;\omega,\omega)$ whereas β for optical rectification is written as $\beta(0;-\omega,\omega)$. Dispersion of β and γ is therefore quite complicated, the dispersion of β being a function in two-variable space (the frequency ω_3 is always $\omega_3 = \omega_1 + \omega_2$) and the dispersion of γ needing three-variable space for a full description. It should be noted that resonant behaviour of the hyperpolarizabilities (a rapidly changing real part and enhanced imaginary part) is expected not only when any of the frequencies in $\beta(-\omega_3;\omega_1,\omega_2)$ or $\gamma(-\omega_4;\omega_1,\omega_2,\omega_3)$ approaches a resonance but also for some combination of the input frequencies being close to a resonance. One of the best known examples of such behaviour is that the so-called degenerate third-order hyperpolarizability $\gamma(-\omega;\omega,-\omega,\omega)$ can be expected to exhibit resonant behaviour when 2ω approaches resonance.

Macroscopic description of the NLO phenomena is very similar to the microscopic approach presented above. The macroscopic quantities of interest are the susceptibilities of various orders defined by:

$$\mathbf{P} = \varepsilon_0(\chi^{(1)}\mathbf{E} + \chi^{(2)}\mathbf{E}^2 + \chi^{(3)}\mathbf{E}^3 + ...) \text{ in the SI system}$$

or:

$$\mathbf{P} = \chi^{(1)}\mathbf{E} + \chi^{(2)}\mathbf{E}^2 + \chi^{(3)}\mathbf{E}^3 + ... \text{ in the cgs system}$$

$\chi^{(i)}$ are tensors of the same ranks as their corresponding molecular analogues and, again, the equation relating the polarization to the macroscopic optical field is rewritten in terms of the Fourier components of the polarization and of the input fields. The important problem is, therefore, expressing the macroscopic NLO properties in terms of the molecular ones.

The usual way of treating the optical properties of systems containing organic molecules is in terms of the oriented gas model, i.e. the macroscopic property is treated as the sum of molecular contributions, allowing for orientation of the molecules and for differences between the local field and the macroscopic electrical field. By following the usual approach of transforming tensor properties from one coordinate system to another using matrices of orientational cosines, expressions for macroscopic nonlinear susceptibilities can be derived. For example, the second-order susceptibility $\chi^{(2)}$ of a crystal composed of organic molecules with second-order hyperpolarizability β will be equal to:[29]

$$\chi^{(2)}_{IJK}(-\omega_3;\omega_1,\omega_2) = L_I(\omega_3)L_J(\omega_1)L_K(\omega_2)\sum_{t=1}^{p} N_t b^t_{IJK}(-\omega_3;\omega_1,\omega_2)$$

where the L factors are the local field factors (often approximated by the Lorenz-Lorentz expression $L = (n^2+2)/3$ where n = refractive index) and:

$$b^t_{IJK}(-\omega_3;\omega_1,\omega_2) = \frac{1}{N_g}\sum_{ijk}\sum_{s=1}^{N_g}\cos\theta^{(s)}_{Ii_t}\cos\theta^{(s)}_{Jj_t}\cos\theta^{(s)}_{Kk_t}\beta_{ijk}(-\omega_3;\omega_1,\omega_2)$$

In the above, ijk denote the cartesian coordinates of a molecule, IJK those of a crystal (a unit cell), N_t is the number of molecules in a unit volume occupying each particular inequivalent site in the unit cell, p is the number of inequivalent positions of a molecule in a unit cell and N_g is the number of equivalent positions in a unit cell. The directional cosines are used to transform each of the molecular β components to those of the new coordinate system (b_{IJK}) and the contributions are summed.

Due to statistical orientation of molecules, orientation averaging can be performed which for fourth-rank tensors leads to substantial simplification; from symmetry considerations, the $\chi^{(3)}$ tensor for an isotropic medium can only have two independent components, namely $\chi^{(3)}{}_{1111}$ and $\chi^{(3)}{}_{1122}$. The component $\chi^{(3)}{}_{1111}$ can be related to components of the molecu-

lar hyperpolarizability tensor (those contributing to the so-called scalar part of the fourth-rank tensor) in the following way:

$$\chi^{(3)}{}_{1111}(-\omega_4;\omega_1,\omega_2,\omega_3) = L_{\omega 1}L_{\omega 2}L_{\omega 3}L_{\omega 4}N\langle\gamma(-\omega_4;\omega_1,\omega_2,\omega_3)\rangle$$

where $L_{\omega i}$ is the local field factor at frequency ω_i (often approximated by the Lorenz-Lorentz factor $L_\omega = (n_\omega{}^2 + 2)/3$) and:

$$\langle\gamma\rangle = \tfrac{1}{5}\left(\gamma_{1111} + \gamma_{2222} + \gamma_{3333} + 2\gamma_{1122} + 2\gamma_{1133} + 2\gamma_{2233}\right)$$

The simplest case is that of an isotropic medium containing molecules with a single dominant component of γ, say γ_{1111} (a reasonable approximation for rigid-rod π-conjugated molecules in which the hyperpolarizability component along the molecular axis is likely to be dominant); $\langle\gamma\rangle = \frac{1}{5}\gamma_{1111}$ is then a reasonable approximation.

1.2.2. Nonlinear optical processes

Second-order nonlinearities are mostly used for various frequency mixing schemes. Among the possible processes, there are several which have specific technological applications and are therefore of significant interest: (i) second harmonic generation, i.e. the $\omega + \omega \rightarrow 2\omega$ mixing process which doubles the energy of photons (e.g. to convert infrared into visible), (ii) the linear electrooptic (Pockels) effect, i.e. the $\omega + 0 \rightarrow \omega$ process which is often used to modulate the phase or amplitude of a light wave (to make it carry information), and (iii) parametric generation, i.e. the $\omega \rightarrow \omega_1 + \omega_2$ process which involves splitting an energetic photon into a sum of two less energetic ones (a popular way of generating laser beams at tunable wavelengths).

There are many possible third-order nonlinear processes, some of which are important as valuable tools for nonlinear spectroscopy, while others have technological significance. The presence of $\chi^{(3)}$ in any substance (even air) means that all materials exhibit third-harmonic generation of laser frequencies. The direct process of third-harmonic generation is, however, not usually exploited for generation of short wavelength laser beams, a cascade of two second-order mixing processes ($\omega + \omega = 2\omega$ and $2\omega + \omega = 3\omega$) being preferred for generation of 3ω from ω (one reason for this is that phase matching is virtually impossible to obtain for third-harmonic generation). From the technological point of view, the most interesting applications of $\chi^{(3)}$ are those which correspond to all-optical interactions of light beams. For interacting fields of the same frequency (the degenerate case), the frequency mixing scheme is $\omega - \omega + \omega \rightarrow \omega$, which means that the interaction of three fields of the same frequency generates a fourth field of the same frequency.

Optical power limiting has attracted considerable interest with applications such as the protection of sensors from damage resulting from exposure to high energy laser pulses. In

principle, the direct two-photon absorption process is suitable for optical limiting, but practical estimates show that power limiting properties of existing materials (even those with the largest two-photon absorption coefficients) are insufficient for the most important applications, namely, the protection of sensors from laser pulses of duration of the order of nanoseconds. Another important process which affords optical limiting behaviour is reverse saturable absorption (RSA). If a substantial proportion of the population of molecules is excited from the ground state to the excited state, then the absorption of the material is no longer the same as that of the population of ground state molecules. A common phenomenon is saturable absorption (absorption bleaching), i.e. increase of sample transmission as the ground state molecules are depleted. In order for reverse saturable absorption to take place, it is necessary that the excited state molecules exhibit a higher absorptivity at a given wavelength than the ground state molecules. The RSA phenomenon is thus a "photodarkening" effect. The difference between the RSA process and two-photon absorption is that the two-photon absorption is virtually instantaneous whereas processes involving intermediate absorbing states exhibit certain kinetic behaviour, which is dependent upon the lifetimes of the states which are involved. As with refractive third-order nonlinearity, time-resolved investigations of the changes of absorptive properties are necessary to evaluate the mechanism of power limiting in a given system.

1.2.3. Systems of units

The two common unit systems employed for the description of nonlinear optical properties are the SI (or MKS) and Gaussian (or cgs) systems (Boyd[27] mentions an alternative system of SI units which will not be discussed further in this review, as it has not been used with organometallic complexes). In the Gaussian system, properties are described in units of esu. The main source of confusion arises from the fact that not only do the units vary between each system, but the dimensions of the properties also vary: for example, the polarizability α has dimensions of length^3 in the Gaussian system (units: cm^3) but dimensions of charge length^2 potential^{-1} (units: C m^2 V^{-1}) in the SI system. Furthermore, vacuum permittivity ε_0 exists in the SI system (having units of F m^{-1}) but has no equivalent in the Gaussian system (i.e. $\varepsilon_0 = 1$). It is important to be able to convert between the two systems, but care must be taken to ensure that not only are the units converted correctly, but that the quantities of interest are treated according to their different definitions in different systems.

The dimensions of the first-, second- and third-order susceptibilities in both systems are simply derived from the polarizability power series equation.[27] In the Gaussian system, polarization $\mathbf{P}$ and electric field strength $\mathbf{E}$ have equivalent dimensions (units: statV cm^{-1} = statC cm^{-2} = (erg cm^{-3})$^{1/2}$), and are related by:

$$\mathbf{P} = \chi^{(1)}\mathbf{E} + \chi^{(2)}\mathbf{E}^2 + \chi^{(3)}\mathbf{E}^3 + \ldots$$

so that the electrostatic units of the susceptibilities are as follows:

$\chi^{(1)}$ dimensionless

units of $\chi^{(2)}$ = units of 1/E = cm statV^{-1} = (erg cm^{-3})$^{-1/2}$

units of $\chi^{(3)}$ = units of 1/E^2 = cm^2 statV^{-2} = (erg cm^{-3})$^{-1}$

The above units are traditionally written as esu for any of the above quantities.

In the SI system, **P** and **E** have different dimensions (units of **P**: C m^{-2}, and units of **E**: V m^{-1}), and **P** is related to **E** by:

$$\mathbf{P} = \varepsilon_0[\chi^{(1)}\mathbf{E} + \chi^{(2)}\mathbf{E}^2 + \chi^{(3)}\mathbf{E}^3 + ...]$$

where $\varepsilon_0 = 8.85 \times 10^{-12}$ F m^{-1}. The units of the susceptibilities in the SI system are:

$\chi^{(1)}$ dimensionless

units of $\chi^{(2)}$ = units of 1/E = m V^{-1}

units of $\chi^{(3)}$ = units of 1/E^2 = m^2 V^{-2}

Similarly, the units for α, β and γ in both SI and Gaussian systems can be derived from the equation describing polarization on the molecular scale (noting units μ_{SI}: C m, and units μ_{cgs}: statV cm^2) and are given in Table 1.1.

To convert $\chi^{(1)}$, $\chi^{(2)}$ and $\chi^{(3)}$ between the systems of units, it is also necessary to include a factor of 4π, as the displacement vector **D** is defined differently for the two systems. In the Gaussian system:

$$\mathbf{D}_{cgs} = \mathbf{E}_{cgs} + 4\pi\mathbf{P}_{cgs} = \mathbf{E}_{cgs}(1 + 4\pi\chi^{(1)}{}_{cgs})$$

and in the SI system:

$$\mathbf{D}_{SI} = \varepsilon_0\mathbf{E}_{SI} + \mathbf{P}_{SI} = \varepsilon_0\mathbf{E}_{SI}(1 + \chi^{(1)}{}_{SI})$$

so that:

$$4\pi\chi^{(1)}{}_{cgs} = \chi^{(1)}{}_{SI}$$

To convert α, β and γ between the systems of units, we utilize the fact that μ in SI (units: C m) and μ in cgs (units: StatC cm) are defined the same way and, since 1 C = 3×10^9 StatC, the conversion factor is $\mu_{SI} = 1/3 \times 10^{-11}\ \mu_{cgs}$. The unit system conversions for the polarizability and hyperpolarizabilities can be deduced by analogy to the derivation of the susceptibilities (i.e. rearranging the equations and equating $\alpha_{SI}E_{SI}/\mu_{0SI} = \alpha_{cgs}E_{cgs}/\mu_{0cgs}$, etc). A summary of units and conversion factors for important properties is shown in Table 1.1. Reference 26 provides a discussion of the pitfalls which arise when applying conversion procedures between nonlinear properties defined in different ways.

Table 1.1. Units and conversion factors for important properties.

Property		System of units		Conversion factor
		SI	cgs	
Dipole moment	μ	C m	statC cm = statV cm^2	$\mu_{SI} = 1/3 \times 10^{-11}\ \mu_{cgs}$
Electric field	E	V m^{-1}	statV cm^{-1} = (erg cm^{-2})$^{1/2}$	$E_{SI} = 3 \times 10^4\ E_{cgs}$
Linear polarizability	α	C m^2 V^{-1}	cm^3	$\alpha_{SI} = (1/3)^2 \times 10^{-15}\ \alpha_{cgs}$
Linear susceptibility	$\chi^{(1)}$	dimensionless	dimensionless	$\chi^{(1)}_{SI} = 4\pi\ \chi^{(1)}_{cgs}$
First hyperpolarizability	β	C m^3 V^{-2}	cm^2 $statV^{-1}$ = esu	$\beta_{SI} = (1/3)^3 \times 10^{-19}\ \beta_{cgs}$
Second-order susceptibility	$\chi^{(2)}$	m V^{-1}	cm $statV^{-1}$ = (cm^3 erg^{-1})$^{1/2}$ = esu	$\chi^{(2)}_{SI} = (4\pi/3) \times 10^{-4}\ \chi^{(2)}_{cgs}$
Second hyperpolarizability	γ	C m^4 V^{-3}	cm^5 $statV^{-2}$ = esu	$\gamma_{SI} = (1/3)^4 \times 10^{-23}\ \gamma_{cgs}$
Third-order susceptibility	$\chi^{(3)}$	m^2 V^{-2}	cm^2 $statV^{-2}$ = cm^3 erg^{-1} = esu	$\chi^{(3)}_{SI} = (4\pi/3^2) \times 10^{-8}\ \chi^{(2)}_{cgs}$
Nonlinear absorption coefficient	β_2	m W^{-1}	cm s erg^{-1} *a*	
Nonlinear refractive index intensity coefficient	n_2	m^2 W^{-1}	cm^2 s erg^{-1} *b*	$n_{2SI} = 10^3 \times n_{2cgs}$
Nonlinear refractive index coefficient	n_2'	m^2 V^{-2}	cm^2 $statV^{-2}$ = cm^3 erg^{-1} = esu	$n_2'_{SI} = (1/3)^2 \times 10^{-8}\ n_2'_{cgs}$

a Although these are the cgs units, the alternative non-cgs units cm W^{-1} or cm GW^{-1} are often used. *b* The alternative units cm^2 W^{-1} are often used.

1.3. Experimental techniques

A variety of experimental techniques have been used to obtain both qualitative and quantitative information about the optical nonlinearities of materials. This section includes descriptions of those techniques which have been used, or have potential use, for the measurements of nonlinear optical properties of organometallics. For an excellent source of information about other techniques the interested reader is directed to reference 28.

1.3.1. Kurtz powder technique[30]

In this technique a laser beam is directed onto a solid microcrystalline ("powder") sample that is sometimes immersed in an index matching liquid. The emitted second harmonic light is collected, filtered, detected and compared with a standard (usually a urea powder for the organometallic complexes measured to date). This technique is crude: the magnitude of the response depends on particle size, and care must be taken in preparation of samples (for example, sieving samples to ensure a narrow particle size range).

Materials can generally be classed as phase matchable or non-phase matchable (Figure 1.1). For a non-phase matchable material, the second harmonic is only generated effectively over distances smaller than the coherence length (the coherence length L_c for a second harmonic process is related to the fundamental wavelength λ_ω and the refractive indices of the material at the fundamental n_ω and second harmonic $n_{2\omega}$ by $L_c = [\lambda_\omega/4(n_{2\omega}-n_\omega)]$). For light paths smaller than the coherence length the intensity of the second harmonic increases with the square of the interaction distance, so for small crystal sizes there is an increase of the second harmonic intensity with the crystal size. However, when the crystal sizes are of the order of the coherence length (averaged over crystal orientations: the coherence length also depends on the direction of propagation of light in the crystal and on the polarization of the interacting fields), there is no further increase of the light intensity with the propagation distance and the powder SHG signal actually decreases, which can be understood as due to the fact that the number of crystals decreases as their sizes grow. For materials that are phase matchable, there is a direction of propagation for which the second harmonic intensity grows quadratically with the propagation path without a limit (the coherence length is formally infinite in such a direction). It follows that the SHG intensity should not show a falling-off behaviour in such a case because the decrease in the number of crystallites as they become bigger will now be compensated by the contribution from phase-matched interactions. Figure 1.1 shows the difference between the non-phase matched and phase-matched cases as predicted by Kurtz.[30]

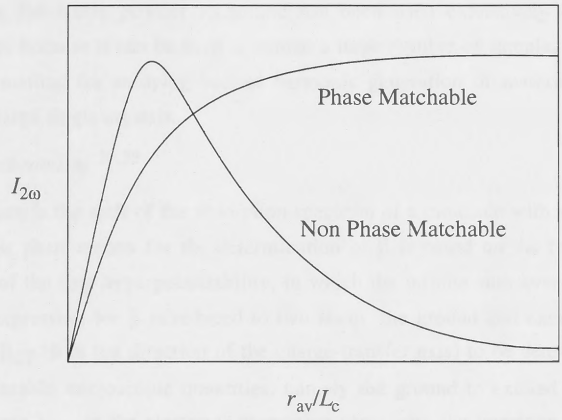

Figure 1.1. Dependence of the second-harmonic intensity on particle size.

Results from Kurtz powder SHG studies do not have quantitative significance as the light intensities measured in the powder SHG technique depend on several factors. The magnitude of the tensor components of the molecular hyperpolarizability β is only one of these factors. A very important issue is how the molecules are oriented in the unit cell of the crystal: in a centrosymmetric arrangement, the unit cell hyperpolarizability tensor components are all identically equal to zero, but even in noncentrosymmetric groups there may be very substantial differences in the nonlinear coefficients arising from packing the nonlinear molecules in different ways. Unit cell hyperpolarizability is transformed into macroscopic second-order susceptibility with the contribution of local field factors; this can modify the properties also. The efficiency for second harmonic generation depends critically on the coherence lengths, which depend in turn on crystal optics. The measured second harmonic intensities also depend on factors such as reflection coefficients at the crystal/air interfaces (introduction of an index matching fluid is therefore important) and absorption and scattering of fundamental and second harmonic light. Given these complicating factors, the powder technique cannot be considered to give quantitative information about the molecular properties of molecules in the crystals being investigated. Observation of high power SHG is a good indication of large β for a compound while the absence of strong powder SHG does not necessarily preclude high molecular nonlinearities.

Materials which crystallize in centrosymmetric space groups theoretically cannot exhibit second harmonic generation, so the applicability of this technique is limited as about three quarters of organometallic complexes crystallize centrosymmetrically. Despite the need for

noncentrosymmetric crystal packing and the reservations concerning the quantitative nature of the results, the Kurtz powder technique has been used extensively to characterize organometallics because it can be used to screen a large number of samples quickly, and is a convenient method for studying second harmonic generation of materials without the need to grow large single crystals.

1.3.2. Solvatochromism [31,32]

Solvatochromism is the shift of the absorption spectrum of a molecule with varying solvent. The use of this phenomenon for the determination of β is based on the two-level microscopic model of the first hyperpolarizability, in which the infinite sum-over-states quantum perturbation expression for β is reduced to two states, the ground and excited states. This model allows β_{CT} (β in the direction of the charge-transfer axis) to be determined in terms of other measurable microscopic quantities, namely the ground to excited state transition energy ω_{eg} (from λ_{max} in the electronic absorption spectrum), the transition dipole moment μ_{eg} (from integration of the absorption band in the UV-vis spectrum), the ground state dipole moment μ_g (measured separately) and the excited state dipole moment μ_e. The last quantity is found by measuring the solvatochromic shift of λ_{max} of the solute, in solvents of varying polarity for which the dielectric constant and refractive index are known (or can be measured). The value for β_{CT} is then obtained from:

$$\beta_{CT} = \frac{3}{2}\hbar^2\left[\frac{\mu_{eg}^2(\mu_e - \mu_g)}{(\omega_{eg}^2 - \omega^2)(\omega_{eg}^2 - 4\omega^2)}\right]$$

This technique has been applied to organic compounds where charge-transfer is dominated by one transition; this is not often the case for organometallics. The applicability of this technique to organometallics thus far has not been tested; there are no reports where solvatochromism has been used to examine the second order nonlinearities of transition metal organometallics, and only one report of its application to two organoboron compounds.[33]

1.3.3. SHG measurements of single crystals and films[34]

Detailed information about the components of the second-order susceptibility $\chi^{(2)}(-2\omega;\omega,\omega)$ can be obtained from second harmonic measurements on well defined samples such as single crystals or oriented thin films, the latter obtained by procedures such as the asymmetric Langmuir-Blodgett deposition technique or electric-field poling of NLO chromophore-doped polymers. In the case of single crystal samples the second harmonic is generated by a crystal with plane parallel surfaces and the distance of interaction of the fundamental and second harmonic radiation is varied by rotation of the sample about an axis perpendicular to the laser beam axis. This produces minima and maxima of the second harmonic which are called Maker fringes. Alternatively, a wedge made out of a crystal may

be used to vary the interaction length. The amplitude of the second harmonic is proportional to $(\chi^{(2)})^2[L_c\sin(L/L_c)]^2$, L being the variable interaction distance and L_c the coherence length. Comparison of measurements with a well characterized material, such as quartz, allows $\chi^{(2)}$ to be determined. The coherence length is obtained from the periodicity of the signal and can be compared to that obtained from measurements of crystal refractive indices. The major disadvantage of the technique is the requirement for large (of the order of mm^3) single crystals. Large crystals are difficult to obtain for organometallic complexes, and this is probably the main reason this technique has never been applied to purely organometallic materials.

A second harmonic signal can also be obtained from thin films of some compounds if the films are made noncentrosymmetric. A technique similar to that of Maker fringe measurements can then be used to determine the second-order nonlinearity. Rotating a second-order optically nonlinear thin film deposited on a second-order inactive substrate (e.g. glass) will result in an angularly dependent second harmonic with no fringes, whereas a glass plate covered on both sides with an NLO film shows an angular dependence of the second harmonic with fringes similar to those obtainable from a crystal. Both for films and crystals, additional information about individual tensor components of $\chi^{(2)}$ can be obtained by varying the polarization of the fundamental radiation. An important issue is that these measurements determine the macroscopic nonlinearity and obtaining information about the molecular hyperpolarizabilities usually requires certain assumptions, e.g. about the nature of local field corrections.

1.3.4. Electric-field induced second harmonic generation (EFISH)

In the EFISH technique, a liquid or solution sample is subjected to a high voltage d.c. pulse to align molecules, the pulse being synchronized with the laser beam pulse. $\chi^{(2)}$ can then be observed in what was previously an isotropic medium. All materials will produce an EFISH signal as it is formally a third-order nonlinear process described by the susceptibility $\chi^{(3)}(-2\omega;\omega,\omega,0)$. There are two contributions to this susceptibility, one of them arising from the sum of the orientationally-averaged third-order hyperpolarizabilities $\gamma(-2\omega;\omega,\omega,0)$ of the medium, and another due to the vectorial sum of the components of the second-order hyperpolarizabilities. Molecules that possess a permanent dipole μ partially align with the d.c. field, the degree of the alignment usually described in terms of the Langevin function. The net second-order effect can be shown to depend on the $\mu\cdot\beta_{vec}$ product where μ is the dipole moment of the molecule and β_{vec} is the vectorial component of the second-order hyperpolarizability (the hyperpolarizability β is a symmetric third-rank tensor which can be treated as being composed of a vector part and a septor part).[35] In general, the directions of β_{vec} and of μ do not coincide. The effective hyperpolarizability measured by the EFISH

technique can be defined as β_{EFISH}, and is given by $\mu \cdot \beta_{vec} = \mu\beta_{EFISH}$. For molecules with strong electron donor and acceptor groups (at opposing ends of the molecule), β_{CT} (the hyperpolarizability along the charge-transfer axis) usually accounts for most of β_{EFISH}.

A wedge shaped cell is used to hold a solution of the sample. This is translated in a direction perpendicular to the incident laser beam, creating Maker fringes whose periodicity is related to the wedge design and to the coherence length, which can therefore be determined. An analogous measurement can also be made on a reference wedge such as quartz, but most often a measurement on a pure solvent of well-known properties, e.g. chloroform, is used to calibrate the system.

The EFISH third-order macroscopic susceptibility defined as $\Gamma = 3\chi^{(3)}(-2\omega;\omega,\omega,0)$ is related to the microscopic second hyperpolarizability γ' by local field factors and the molecule number density. In turn, β can be obtained from $\gamma' = \gamma + \mu\beta_{EFISH}/(5k_bT)$, where γ' is the effective second hyperpolarizability (third-order hyperpolarizability), γ is the intrinsic second hyperpolarizability consisting of electronic and vibrational parts, k_b is Boltzmann's constant and T is the temperature in K. In the experiment, comparison against a reference enables Γ values to be determined. In order to determine the $\mu\beta_{EFISH}$ product of an unknown substance, one usually performs EFISH measurements as a function of concentration in a well-characterized solvent; this concentration dependence study is necessary in order to resolve ambiguities occurring because the $\mu\beta_{EFISH}$ products for the solvent and the solute may be of the same or of opposite signs, and the SHG signal is proportional to the square of the EFISH susceptibility. Other quantities that may be required for the interpretation of the results are the dielectric constant, the permanent dipole moment, and the intrinsic second hyperpolarizability of the solute (found from a separate experiment or ignored).

The application of EFISH to organometallics is limited to neutral complexes. The presence of ionic species makes it impossible to apply high electric fields to a solution. It is also not possible to utilize EFISH when the complex has no net dipole moment.

1.3.5. Hyper-Rayleigh scattering (HRS) [36,37]

The HRS technique involves detecting the incoherently scattered second harmonic light generated from an isotropic solution in order to determine the first hyperpolarizability. HRS is due to orientational fluctuations of asymmetric molecules in solution which give rise to local asymmetry, on a microscopic scale, in an isotropic liquid.[37] The light scattered from such a system can have a component at the second harmonic that depends only on the first hyperpolarizability of the solute molecules, and varies quadratically with the incident intensity; an example of the data obtained from an HRS experiment is displayed in Figure 1.2.

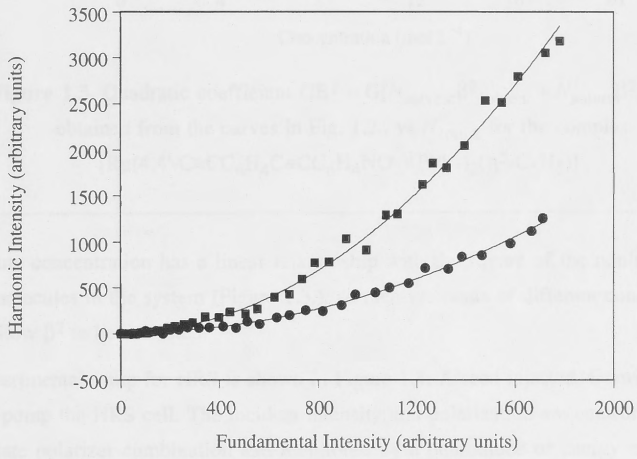

Figure 1.2. Quadratic dependence of $I_{2\omega}$ vs I_{ω} for $[Ru(4,4'\text{-}C{\equiv}CC_6H_4C{\equiv}CC_6H_4NO_2)(PPh_3)_2(\eta^5\text{-}C_5H_5)]$.

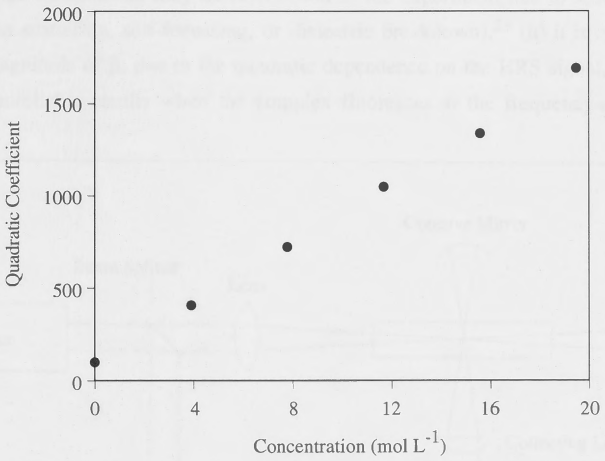

Figure 1.3. Quadratic coefficient $GB^2 = G[N_{solvent}\beta^2_{solvent} + N_{solute}\beta^2_{solute}]$, obtained from the curves in Fig. 1.2., vs N_{solute} for the complex $[Ru(4,4'\text{-}C{\equiv}CC_6H_4C{\equiv}CC_6H_4NO_2)(PPh_3)_2(\eta^5\text{-}C_5H_5)]$.

The solute concentration has a linear relationship with the square of the nonlinearity of all of the molecules in the system (Figure 1.3.), so measurements of different concentrations of solute allow β^2 to be extracted.

The experimental setup for HRS is shown in Figure 1.4. A seed injected, Q-switched laser is used to pump the HRS cell. The incident intensity and polarization are controlled by a half-wave plate polarizer combination and monitored by a photodiode or energy meter. The incident beam is focussed into the sample solution. A concave mirror, with its focus at the interaction focal volume, and a lens are used to collect the scattered light which is filtered to isolate the second harmonic light, detected by a photomultiplier tube and averaged by a gated integrator.

Advantages of HRS are: (i) its simplicity when compared to EFISH (there is no need for a d.c. field to be applied, and it does not need complementary measurements of μ or γ), (ii) its sensitivity to non-vector components of the β tensor and (iii) unlike EFISH, it can be used to measure octopolar molecules and ionic molecules, the latter having important implications for organometallics where a particular system may have a range of accessible

oxidation states. Disadvantages of HRS include: (i) the need for sensitive detection and high intensity of the fundamental, due to the low intensity of the second harmonic light (high intensity of the fundamental may be detrimental to the experiment due to stimulated Raman or Brillouin scattering, self-focussing, or dielectric breakdown),[28] (ii) it is only possible to find the magnitude of β, due to the quadratic dependence on the HRS signal, and (iii) HRS can give unreliable results when the complex fluoresces at the frequency-doubled wavelength.[38]

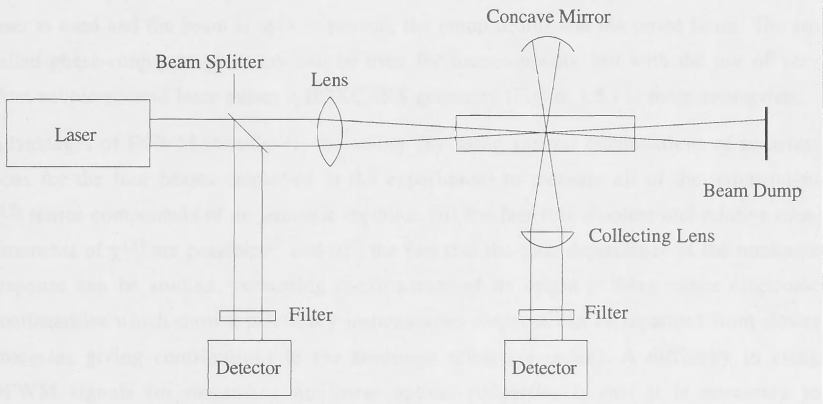

Figure 1.4. Schematic diagram of the HRS experiment.

1.3.6. Third harmonic generation (THG)

Third harmonic generation is used to study the purely electronic molecular second hyperpolarizability of centrosymmetric materials; no other mechanism but the nonresonant electron cloud distortion can respond rapidly enough to produce a nonlinear polarization oscillating at the third harmonic.[28] It is technically difficult because all materials exhibit THG, including any glass used for a sample cell and even air. One technique that avoids some of these problems involves placing the sample in a vacuum sealed cell inside a vacuum chamber. A simpler method involves using thick glass windows which allow the contribution from air to be ignored; the third-order susceptibility of the glass and solvent must be known. THG has been used to study $\chi^{(3)}$ in many organic and organometallic molecules, particularly those measured by EFISH for which an estimation of γ is required to extract an accurate value of β.

1.3.7. Degenerate four-wave mixing (DFWM)

In this technique, two coherent "pump" beams interact within a material creating an interference pattern of light intensity. As the change in refractive index of a third-order material depends on the intensity of the applied field, a refractive index grating results which in the simplest case can be described by the dependence $\Delta n(r) = n_2 I(r)$. When a third beam is incident on this grating, a fourth beam is generated, with the intensity of this beam proportional to the product of all the input intensities and to the square of the absolute value of the complex third-order susceptibility, i.e. $I_4 \sim |\chi^{(3)}|^2 I_1 I_2 I_3$. Experimentally, one laser is used and the beam is split to provide the pump beams and the probe beam. The so-called phase-conjugate geometry can be used for measurements, but with the use of very short subpicosecond laser pulses a BOXCARS geometry (Figure 1.5.) is more appropriate.

Advantages of DFWM include: (i) the ability (by using various combinations of polarizations for the four beams employed in the experiment) to measure all of the independent $\chi^{(3)}$ tensor components of an isotropic medium, (ii) the fact that absolute and relative measurements of $\chi^{(3)}$ are possible,[28] and (iii) the fact that the time dependence of the nonlinear response can be studied, permitting confirmation of its origin (off-resonance electronic nonlinearities which show a practically instantaneous response can be separated from slower processes giving contributions to the nonlinear refractive index). A difficulty in using DFWM signals for measuring nonlinear optical properties is that it is necessary to distinguish between contributions from the real and imaginary part of the third-order susceptibility. One way of doing this is to perform a series of measurements on solutions of a compound with varying concentrations in a non-absorbing solvent, and then interpret the concentration dependence of the DFWM signal as:

$$I_{DFWM} \propto \left|\chi^{(3)}\right|^2 \propto [N_{solvent}\gamma_{solvent} + N_{solute}\,\mathrm{Re}(\gamma_{solute})]^2 + [N_{solute}\,\mathrm{Im}(\gamma_{solute})]^2$$

where it is assumed that the solvent contributes only to the real part of the solution susceptibility, whereas the solute can contribute to both the real (refractive) and imaginary (absorptive) components.

Degenerate four-wave mixing has been widely used for the study of organometallics. At present, it forms a complementary technique to the technically less difficult Z-scan, in that it can be used to verify that the origin of the observed nonlinearity is electronic in nature.

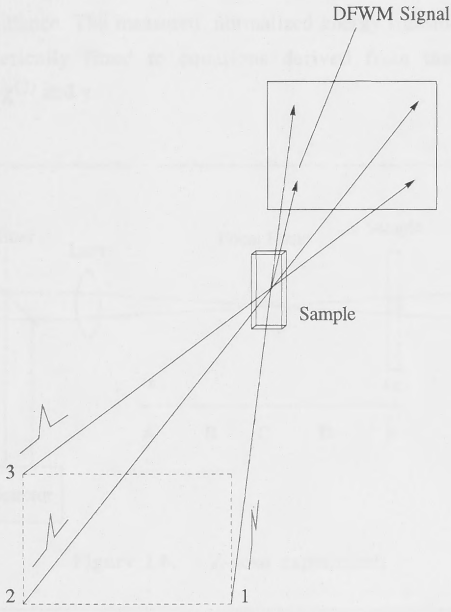

Figure 1.5. Geometry of degenerate four-wave mixing (BOXCARS geometry) for short-pulse, time-resolved measurements of the nonlinear response. Beams 1, 2 and 3 are derived from a single laser beam by the use of a beam splitter and the beam paths are adjusted for the pulses to arrive simultaneously at the sample. By delaying one of the beams with respect to the others, time-resolved measurements can be performed.

1.3.8. Z-scan [39]

Z-scan is a technique used to derive the nonlinear refractive index intensity coefficient n_2 (from which $\chi^{(3)}$ and γ can be determined) by examining self-focussing or self-defocussing phenomena in a nonlinear material. Using a single Gaussian laser beam in a tight focus geometry (Figure 1.6.), the transmittance of a nonlinear medium through a fixed aperture in the far field is measured as the position of the material is varied through the z direction. An example of a Z-scan trace is shown in Figure 1.7. for a nonlinear material with a positive nonlinear refractive index. At the start (A) (and end (E)) of the scan the sample is far from the focal plane, the intensity of the beam is low and so lensing is not observed. As the material approaches the focal-plane (B), lensing causes the beam to focus earlier and hence

reduces the measured transmittance. At the focal plane, z = 0 (C), there will be no change in transmittance as a thin lens at the focus will cause no change in the far-field. After the focal plane (D), slight focussing of the beam by the lensing of the material causes an increase in the measured transmittance. The measured, normalized energy transmittance from a Z-scan experiment is numerically fitted to equations derived from theory and allows the determination of n_2, $\chi^{(3)}$ and γ.

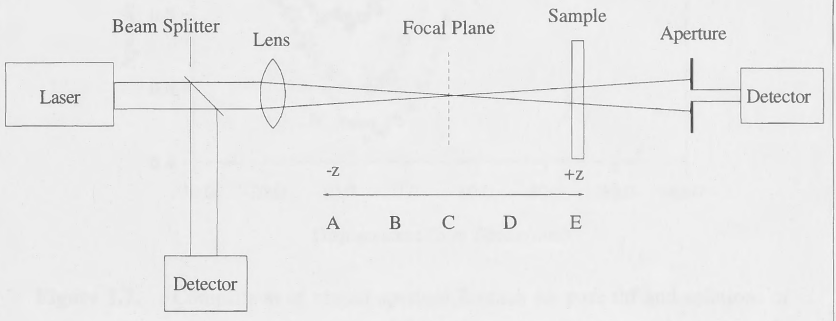

Figure 1.6. Z-scan experiment.

The shape of the Z-scan curve can be modified if a nonlinear absorption or nonlinear transmission (absorption bleaching) takes place in the sample, e.g. due to the presence of an imaginary part of $\chi^{(3)}$ of the material. The curves then become asymmetrical due to increased absorption or transmission when the sample is close to the focal plane. By analyzing the shape of such a modified Z-scan curve one can determine the nonlinear absorption coefficient β_2 or the related imaginary part of $\chi^{(3)}$. Alternatively, to determine the nonlinear absorption properties of a sample, the total transmission through the sample can be monitored, i.e. the total intensity of the transmitted beam can be measured without an aperture, as a function of the sample position with respect to the focal plane. Such an experiment is usually referred to as an "open aperture Z-scan". It is often used for the investigations of materials with potential optical limiting properties. For solutions, the changes of the nonlinearity with concentration of the solution can be determined and measurements performed in an absolute manner, or results can be referenced to a known standard (e.g. the nonlinear refractive index of silica equal to $n_2 = 3 \times 10^{-16}$ cm^2 W^{-1} can be used).

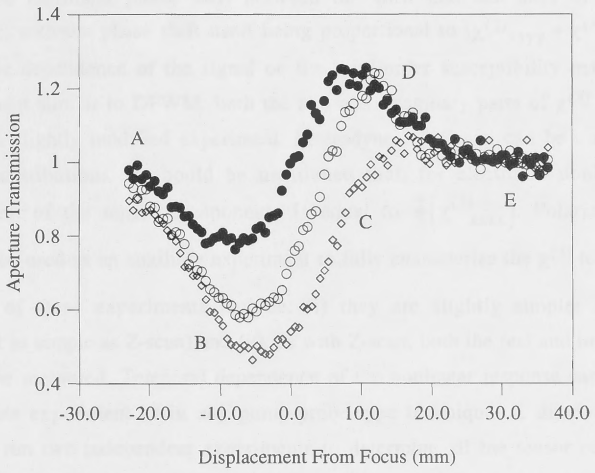

Figure 1.7. Comparison of closed aperture Z-scans for pure thf and solutions of $[Au(4,4'\text{-}C{\equiv}CC_6H_4C{\equiv}CC_6H_4NO_2)(PPh_3)]$; • thf, ○ 1.56 weight %, ◊ 3.08 weight %.

Advantages of the Z-scan technique include: (i) the ability to determine the sign and magnitude of the nonlinear refractive index, (ii) the ability to determine both the real and imaginary parts of $\chi^{(3)}$, and (iii) simplicity (compared to DFWM) due to the single beam configuration. Disadvantages of Z-scan include: (i) the necessity for a high quality Gaussian beam and good optical quality of samples, and (ii) the absence of information on the temporal behaviour of the nonlinear response. The Z-scan technique has been used to determine the third-order nonlinear optical properties of organometallics as solutions and as thin films.

1.3.9. Optical Kerr gate[28]

In the optical Kerr gate experiment (Figure 1.8.), the sample is subjected to a linearly polarized pump beam which induces optical birefringence (and also, in some cases, optical dichroism, i.e. different absorption for different polarization sense). An almost collinear probe beam of known linear polarization (usually at 45° to that of the pump beam) is then

allowed to pass through the material, and the resultant intensity of the light that passes through a crossed polarizer is measured. The Kerr gate transmittance is proportional to the square of the nonlinear phase shift between the slow and fast axes of the induced birefringence, with the phase shift itself being proportional to $(\chi^{(3)}_{xxyy} + \chi^{(3)}_{xyyx}) I_{pump}$. The quadratic dependence of the signal on the third-order susceptibility makes the Kerr gate experiment similar to DFWM: both the real and imaginary parts of $\chi^{(3)}$ contribute to the signal. A slightly modified experiment, heterodyne Kerr gate, can be used to resolve these two contributions. It should be mentioned that, for electronic nonlinearity, the measured sum of the tensor components is equal to $\frac{2}{3}\left(\chi^{(3)}_{xxxx}\right)$. Polarization ellipse rotation can be used as an auxiliary experiment to fully characterize the $\chi^{(3)}$ tensor.

Advantages of these experiments include: (i) they are slightly simpler than DFWM (although not as simple as Z-scan) and (ii), as with Z-scan, both the real and imaginary parts of $\chi^{(3)}$ can be measured. Temporal dependence of the nonlinear response can be followed in a Kerr gate experiment as in any pump-probe type technique. A disadvantage is the necessity to run two independent experiments to determine all the tensor components of $\chi^{(3)}$. These techniques were developed before DFWM and Z-scan, and have largely been superseded as Z-scan and DFWM reveal more information from one experiment.

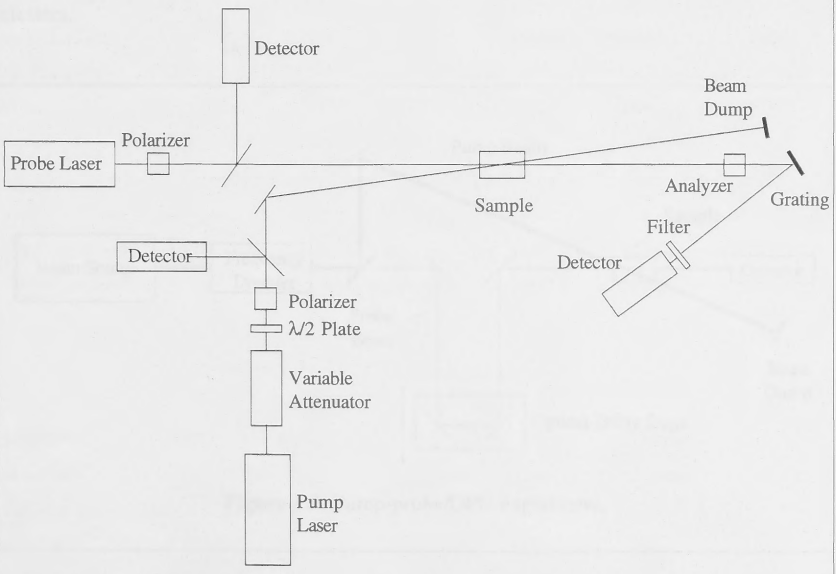

Figure 1.8. Setup of an optical Kerr gate experiment.

1.3.10. Power dependent transmission

Information about nonlinear absorptive properties of a sample can be derived simply by measuring the sample transmission as a function of the incident light intensity. A linear dependence of the inverse transmission on the incident intensity can be used to determine the value of the nonlinear absorption coefficient (β_2). Because of the ease of determining the value of β_2 with open-aperture Z-scan, Z-scan is often the preferred method for quickly determining the nonlinear absorption coefficient.

1.3.11. Pump-probe experiments for excited state absorption (ESA) measurements

Figure 1.9. shows an experimental setup to measure nonlinear transmittance by the pump-probe method. The pump is used to excite the sample and the transmission of the probe is measured. The probe beam may be delayed relative to the pump beam in order to perform time delay experiments. A continuum of frequencies may be used as the probe, thereby allowing a complete nonlinear absorption spectrum to be generated rather than investigate the change of absorption at a single frequency.[28] The pump-probe technique has advantages such as the capability of generating information on a single laser shot, as well as the possibility of observing absorption changes at varying intervals after excitation. Pump-probe measurements of optical limiting have been carried out on very few organometallic complexes; results from these studies thus far are restricted to a range of tetrahedral metal clusters.

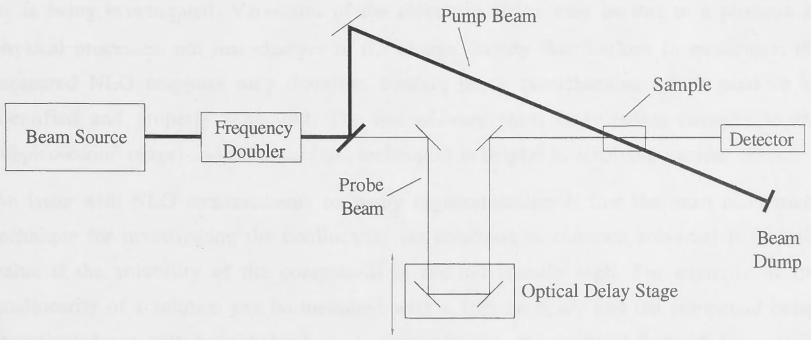

Figure 1.9. Pump-probe/OPL experiment.

1.3.12. Comparisons between experimental results

There are several problems in comparing results obtained by different groups using the many experimental techniques which are available to investigate the NLO properties of molecules; the most important of these include dispersion effects, the measurement of different tensorial components, different physical processes contributing to nonlinearity, and solubility problems.

The dispersion of NLO properties is a major source of problems. Measurements are frequently available at one wavelength only and the degree to which the results are influenced by material resonances close to the measurement wavelength is often difficult to quantify. It is possible to compensate for some of the dispersion effects in certain cases. For example, off-resonant dispersion of the second-order hyperpolarizability for linear intramolecular charge-transfer type molecules is reasonably well described by a two-state model in which parameters of the dominant excited state are assumed. A two-state model is probably not sufficient for more complicated second-order molecules, e.g. those with significant contribution to the nonlinearity from octopolar origins. Also, the simple two-state model is generally considered insufficient for describing the dispersion of the third-order nonlinearity; at least two excited states have to be considered.

The tensorial character of the nonlinear polarizabilities is another experimental complication. Experimental techniques only provide access to specific tensorial components or combinations thereof, e.g. the vector part of β or orientationally averaged γ. An especially challenging issue is the correct measurement and interpretation of the third-order nonlinear effects when the degenerate susceptibility $\chi^{(3)}(-\omega;\omega,-\omega,\omega)$ or the nonlinear refractive index n_2 is being investigated. Variations of the refractive index may be due to a plethora of physical processes, not just changes in the charge density distributions in molecules; the measured NLO response may therefore contain many contributions which need to be identified and properly separated. The use of very short laser pulses (usually in the subpicosecond range) and time-resolved techniques is helpful in resolving unclear cases.

An issue with NLO measurements on many organometallics is that the most convenient technique for investigating the nonlinearity (as solutions in common solvents) is of little value if the solubility of the compounds is not sufficiently high. For example, if the nonlinearity of a solution can be measured with a 10% accuracy and the compound being investigated can only be dissolved at 1% concentration, the practical limit of detection is that the nonlinearity of the organometallic has to be at least 10 times higher than that of the solvent.

Finally, a source of major frustration for anybody trying to compare NLO results obtained by different techniques and from different research groups is the use of varying definitions

of the measured quantities and of varying measurement standards. This problem has been discussed in several monographs.[26-28] Several different definitions of $\chi^{(3)}$ are possible depending, for example, on the use or absence of the factor of 1/2 before the Fourier components of the a.c. electric field, and on the inclusion or exclusion in $\chi^{(3)}$ of so-called degeneracy factors which are dependent on the type of nonlinear process considered [as seen, for example, in Equation (1.2), different multipliers are present in front of the nonlinear terms responsible for different processes]. Thus, it is very helpful if the optical nonlinearities of well-known standards used or determined in a given series of experiments are provided by the authors of original papers in which data on new compounds are published. In many cases, because of the factors mentioned above, direct comparison of numbers quoted in different papers is unfortunately not possible: trends observed for a series of compounds in a single set of experimental results are relatively reliable, though.

1.4. Organo-transition Metal Complexes for Second-order Nonlinear Optics

1.4.1. Bulk second-order measurements

The SHG efficiencies of over three hundred organo-transition metal complexes measured utilizing the Kurtz powder method have been reported, but most responses are either very low or zero. Table 1.2. contains data for samples with reported Kurtz powder efficiencies greater than or equal to twice that of urea, with Figure 1.10. containing the structural formulae of complexes with very large (> 60 × urea) responses.

Ferrocenyl-type complexes are prominent in Table 1.2., with many having SHG efficiencies comparable to efficient organic compounds (although these data are significantly smaller than the largest reported powder measurement for an organic: 1000 × urea for [*N*-MeC_5H_4N-4-(*E*)-$CH{=}CHC_6H_4$-4'-NMe_2][$MeC_6H_4SO_3$]).[40] Complexes with ferrocenyl groups as donors and either organic or metal-organic acceptors are responsible for all of the very large powder responses for organometallics reported thus far. Large bulk nonlinearities are a function of both significant molecular nonlinearities and favourable crystal packing. As many types of organometallic complexes have been the subject of powder measurements, and have comparable molecular nonlinearities to ferrocenyl complexes, the implication is that ferrocenyl-based complexes have a greater proclivity for optimal lattice alignment. Two ruthenocenyl and osmocenyl complexes having identical cyclopentadienyl substituents feature in Table 1.2.; these complexes show little difference in their SHG efficiencies, but comment on the significance of intramolecular structural changes (metal variation in this case) upon bulk NLO merit is not warranted (this shortcoming of the powder technique was discussed in Section 1.3.1.). The iron analogue of these compounds has also been prepared and measured[41] but has an SHG efficiency of only 0.8 × urea, in contrast to molecular measurements of the effect of metal variation where ferrocenyl complexes have been shown to be significantly more efficient than ruthenocenyl analogues (see Section 1.6.). Phosphine-containing complexes exhibit low to moderate SHG efficiencies, although they mostly have the donor-π conjugated bridge-acceptor structure which should favour enhanced molecular nonlinearity. Comparison of the significant number of data for the group 10 $MX(C_6H_4$-4-A$)(PEt_3)_2$ complexes reveals little difference in observed efficiency for systematic structural modifications. The usefulness of the Kurtz technique is to rapidly identify SHG activity; structure-NLO property correlations are not justified.

Table 1.2. Complexes with Kurtz powder efficiencies ≥ 2 × urea.

Complex	SHG (Urea = 1)	Fund. (μm)	Ref.
[Fc-(*E*)-CH=CH-4-C_5H_4N-1-Me][I]	125 - 240	1.91	42-45
[Fc-(*E*)-CH=CH-4-C_5H_4N-1-Me][Br]	165-170	1.91	42-45
[Fc-(*E*)-CH=CH-4-C_5H_4N-1-Me][NO_3]	75-120	1.91	42-45
[Fc-(*E*)-CH=CH-4-C_5H_4N-1-Me][BF_4]	50	1.91	42-45
[Fc-(*E*)-CH=CH-4-C_5H_4N-1-Me][BPh_4]	13	1.91	42-45
[Fc-(*E*)-CH=CH-4-C_5H_4N-1-Me][MeC_6H_4-4-SO_3]	13	1.91	42-45
[Fc-(*Z*)-CH=CHC_6H_4-4-NO_2]	62	1.91	46-49
[Fc-(*E*)-CH=CHC_6H_3-2,4-$(NO_2)_2$]	21	1.91	50
[(*S*)-Fe(η^5-C_5H_5)(η^5-C_5H_3-2-Me-(*E*)-CH=CHC=CHCH=(NO_2)O]	17-17.5	1.91	47-49
[(*S*)-Fe(η^5-C_5H_5)(η^5-C_5H_3-2-Me-(*E*)-CH=CHC_6H_4-4-NO_2)]	8.0-8.4	1.91	47-49
[(*R*)-Fe(η^5-C_5H_5)(η^5-C_5H_3-2-Me-(*E*)-CH=CHC_6H_4-4-NO_2)]	6	1.91	51
[(*S*)-Fe(η^5-C_5H_5)(η^5-C_5H_3-2-Me-(*E*)-CH=CH-(*E*)-CH=CHC_6H_4-4-NO_2)]	6.4	1.91	47-49
[(*S*)-Fe(η^5-C_5H_5)(η^5-C_5H_3-2-Me-(*E*)-CH=CHC_6H_4-4-CHO)]	1.8-2.5	1.91	47-49
[(*R*)-Fe(η^5-C_5H_5)(η^5-C_5H_3-2-CH_2OH-(*E*)-CH=CHC_6H_4-4-NO_2)]	20	1.91	51
[(*S*)-Fe(η^5-C_5H_5)(η^5-C_5H_3-2-$SiMe_3$-(*E*)-CH=CHC_6H_4-4-NO_2)]	80-100	1.91	51
[(η^5-C_5H_5)$_2$$Fe_2$$(CO)_2$(μ-CO)(μ-C-(*E*)-CH=$CHC_6H_4$-4-$NMe_2$)][$CF_3SO_3$]	3.6	1.91	52
[(*S*)-Ru(η^5-C_5H_5)(η^5-C_5H_4CHMeSC_6H_4-4-NO_2)]	27	1.06	41
[(*S*)-Os(η^5-C_5H_5)(η^5-C_5H_4CHMeSC_6H_4-4-NO_2)]	21	1.06	41
[MoCl(NO)(NHC_6H_3-3-Me-4-N=NC_6H_4-4-Fc){HB(dmpz)$_3$}]	50-123	1.91	53-55
[MoI(NO)(NHC_6H_4-4-(*E*)-CH=CHC_6H_4-4-Fc){HB(dmpz)$_3$}]	85	1.91	56
[MoCl(NO)(NHC_6H_4-4-N=NC_6H_4-4-Fc){HB(dmpz)$_3$}]	30-59	1.91	54,55
[WCl(NO)(NHC_6H_3-3-Me-4-N=NC_6H_4-4-Fc){HB(dmpz)$_3$}]	8-53	1.91	54,56
[MoCl(NO)(NHC_6H_4-4-(*E*)-CH=CHC_6H_4-4-Fc){HB(dmpz)$_3$}]	35	1.91	56
[MoBr(NO)(NHC_6H_3-3-Me-4-N=NC_6H_4-4-Fc){HB(dmpz)$_3$}]	25	1.91	55
[WCl(NO)(NHC_6H_4-4-N=NC_6H_4-4-Fc){HB(dmpz)$_3$}]	12	1.91	55
[WCl(NO)(NHC_6H_4-4-(*E*)-CH=CHC_6H_4-4-Fc){HB(dmpz)$_3$}]	8	1.91	56
[Cr$(CO)_3$(η^6-C_6H_6)]:thiourea, 1:3	2.3	1.06	57-60
[Cr$(CO)_3$(η^6-C_6H_5F)]:thiourea, 1:3	2.0	1.06	58-60

Table 1.2. (continued) Complexes with Kurtz powder efficiencies ≥ 2 × urea.

Complex	SHG (Urea = 1)	Fund. (μm)	Ref.
$[PtBr(C_6H_3\text{-}2\text{-}Me\text{-}4\text{-}NO_2)(PEt_3)_2]$	2.0-14.0	1.06	61
$[PdBr(C_6H_3\text{-}2\text{-}Me\text{-}4\text{-}NO_2)(PEt_3)_2]$	5.0-10.0	1.06	61
$[PtI(C_6H_4\text{-}4\text{-}NO_2)(PEt_3)_2]$	5.0-8.0	1.06	61,62
$[Pt(NCO)(C_6H_4\text{-}4\text{-}NO_2)(PEt_3)_2]$	6.7-9.2	1.06	62
$[PdBr(C_6H_4\text{-}4\text{-}NO_2)(PEt_3)_2]$	2.1-7.2	1.06	61
$[PtBr(C_6H_4\text{-}4\text{-}NO_2)(PEt_3)_2]$	4.2	1.06	61,62
$[PtBr(C_6H_4\text{-}4\text{-}CHO)(PEt_3)_2]$	1.5-3.4	1.06	61
$[PtCl(C_6H_4\text{-}4\text{-}NO_2)(PEt_3)_2]$	3.0	1.06	62
$[PdI(C_6H_4\text{-}4\text{-}NO_2)(PEt_3)_2]$	2.3	1.06	61
$[PdBr(C_6H_4\text{-}4\text{-}CHO)(PEt_3)_2]$	2.3	1.06	61,62
$[Pt(CN)(C_6H_4\text{-}4\text{-}NO_2)(PEt_3)_2]$	2.0	1.06	62
$[Fe(N{\equiv}CC_6H_4\text{-}4\text{-}Ph)((+)\text{-diop})(\eta^5\text{-}C_5H_5)][PF_6]$	4.2	1.91	63
$[Fe(N{\equiv}C\text{-}(E)\text{-}CH{=}CHC_6H_4\text{-}4\text{-}NMe_2)((+)\text{-diop})(\eta^5\text{-}C_5H_5)][PF_6]$	3.3	1.91	63
$[Fe(N{\equiv}CC_6H_4\text{-}4\text{-}C_6H_4\text{-}4\text{-}NO_2)((+)\text{-diop})(\eta^5\text{-}C_5H_5)][PF_6]$	38.0	1.91	63
$[Ru(N{\equiv}CC_6H_4\text{-}4\text{-}NO_2)((+)\text{-diop})(\eta^5\text{-}C_5H_5)][CF_3SO_3]$	10	1.06	64
$[Ru(N{\equiv}CC_6H_4\text{-}4\text{-}NO_2)((+)\text{-diop})(\eta^5\text{-}C_5H_5)][ClO_4]$	2.9	1.06	64
$[Ru(N{\equiv}CC_6H_4\text{-}4\text{-}NO_2)((+)\text{-diop})(\eta^5\text{-}C_5H_5)][PF_6]$	2.7	1.06	64
$[Au(C{\equiv}CC_6H_4\text{-}4\text{-}NO_2)((+)\text{-nmdpp})]$	2	1.06	65

The powder technique can establish that a basic structural type is SHG active; once NLO activity of this type is confirmed, molecular modification has most impact when it affects packing in the solid state. Variation of counter ions can have a significant effect on the SHG efficiencies (see, for example, the first six entries in Table 1.2.). Marder and co-workers have shown that variation of counter-ions is a highly successful and very straightforward method to rapidly sample different lattice arrangements and thus engineer materials with large nonlinearities.[44] Meredith has explained these results by proposing that Coulombic interactions in salts may negate deleterious dipolar interactions, enhancing the possibility of favourable noncentrosymmetric packing.[66]

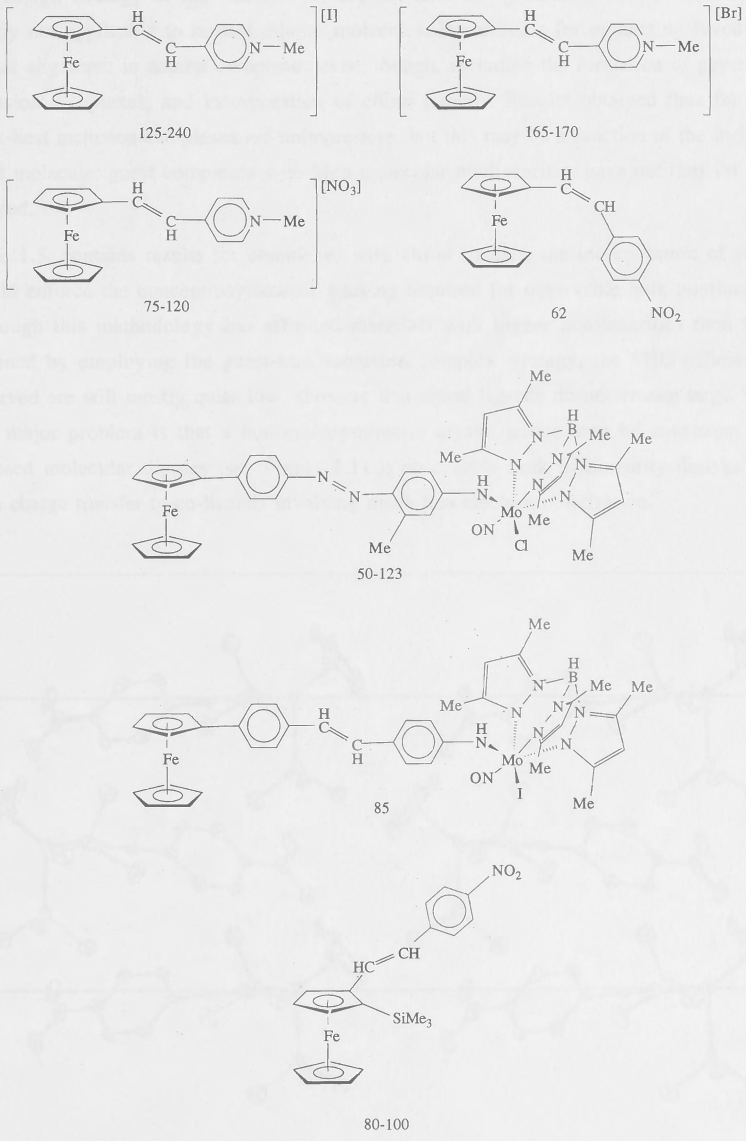

Figure 1.10. Organometallic complexes with large $\chi^{(2)}$ measured by the Kurtz powder technique (units: multiples of urea response).

The design strategy of the variation of counter ions for optimizing bulk nonlinearity is clearly not applicable to neutral dipolar molecules. Possibilities for organizing favourable crystal alignment in neutral complexes exist, though, including the formation of guest-host inclusion complexes, and incorporation of chiral ligands. Results obtained thus far with guest-host inclusion complexes are unimpressive, but this may be a function of the included guest molecule; guest complexes with high molecular nonlinearities have not thus far been assayed.

Table 1.3. contains results for complexes with chiral ligands, the incorporation of which should enforce the noncentrosymmetric packing required for observable bulk nonlinearity. Although this methodology has afforded materials with higher nonlinearities than those obtained by employing the guest-host inclusion complex strategy, the SHG efficiencies observed are still mostly quite low, showing that chiral ligands do not ensure large SHG. One major problem is that a noncentrosymmetric crystal lattice may be consistent with opposed molecular dipoles (see Figure 1.11.); observable bulk nonlinearity derives then from charge transfer to co-ligands involving much less electron polarization.

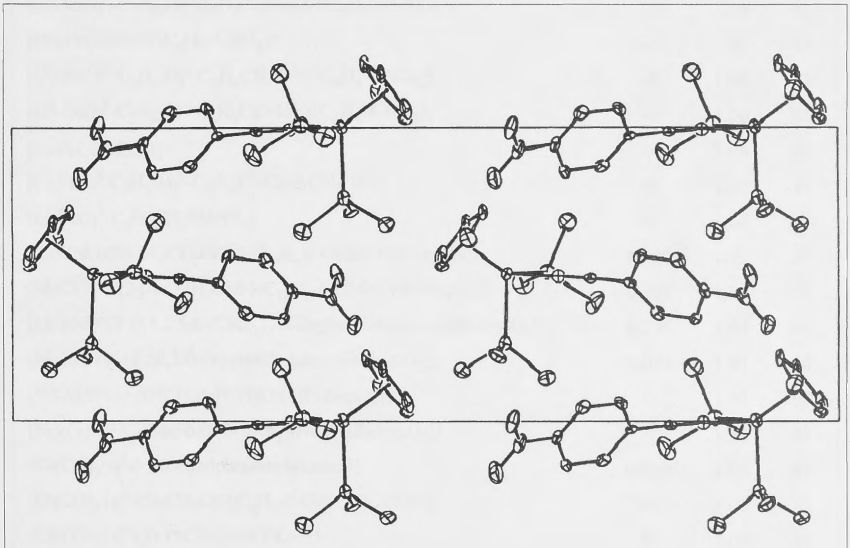

Figure 1.11. Cell packing diagram for $[Ru(C{\equiv}CC_6H_4\text{-}4\text{-}NO_2)(PMe_3)_2(\eta^5\text{-}C_5H_5)]$.

Table 1.3. Kurtz powder measurements of complexes containing chiral ligands.

Complex	SHG (urea = 1)	Fund. (μm)	Ref.
[(*S*)-Fe(η^5-C_5H_5)(η^5-C_5H_3-2-$SiMe_3$-(*E*)-CH=CHC_6H_4-4-NO_2)]	80-100	1.91	51
[(*R*)-Fe(η^5-C_5H_5)(η^5-C_5H_3-2-CH_2OH-(*E*)-CH=CHC_6H_4-4-NO_2)]	20	1.91	51
[(*R*)-Fe(η^5-C_5H_5)(η^5-C_5H_3-2-Me-(*E*)-CH=CHC_6H_4-4-NO_2)]	6	1.91	51
[(*S*)-Fe(η^5-C_5H_5)(η^5-C_5H_3-2-Me-(*E*)-CH=CHC_6H_4-4-NO_2)]	8.0-8.4	1.91	47-49
[(*S*)-Fe(η^5-C_5H_5)(η^5-C_5H_3-2-Me-(*E*)-CH=CHC_6H_4-4-CN)]	1.2-1.6	1.91	47-49
[(*S*)-Fe(η^5-C_5H_5)(η^5-C_5H_3-2-Me-(*E*)-CH=CHC_6H_4-4-CHO)]	1.8-2.5	1.91	47-49
[(*S*)-Fe(η^5-C_5H_5)(η^5-C_5H_3-2-Me-(*E*)-CH=CH-(*E*)-CH=CHC_6H_4-4-NO_2)]	6.4	1.91	47-49
[(*S*)-Fe(η^5-C_5H_5){η^5-C_5H_3-2-Me-(*E*)-CH=CHC=CHCH=C(NO_2)O}]	17.0-17.5	1.91	47-49
[(*R*)-FcCHMeSC_5H_4-4-NO_2)]	0.8	1.06	41
[(*S*)-Ru(η^5-C_5H_5)(η^5-C_5H_4CHMeSC_6H_4-4-NO_2)]	27	1.06	41
[(*S*)-Os(η^5-C_5H_5)(η^5-C_5H_4CHMeSC_6H_4-4-NO_2)]	21	1.06	41
[(*R*)-FcCHMe-2-SC_5H_3N-5-NO_2)]	~0	1.06	41
[(*S*)-Ru(η^5-C_5H_5)(η^5-C_5H_4CHMe-2-SC_5H_3N-5-NO_2)]	1.9	1.06	41
[(*R*)-FcCHMeNHC_6H_4-4-NO_2)]	~0	1.06	41
[(*S*)-Ru(η^5-C_5H_5)(η^5-C_5H_4CHMeNHC_6H_4-4-NO_2)]	~0	1.06	41
[(*S*)-Os(η^5-C_5H_5)(η^5-C_5H_4CHMeNHC_6H_4-4-NO_2)]	~0	1.06	41
[(-)-FcCHMeOH]	0	1.06	41
[(-)-Fe(η^5-C_5H_5){η^5-C_5H_3(CHO)-2-CH_2OH}]	0	1.06	41
[(-)-Fe(η^5-$C_5H_4CH_2$SMeO)$_2$]	0	1.06	41
[MoI(NO)(2-(-)-OCH_2CHMe$C_{10}H_6$-6-OMe){HB(dmpz)$_3$}]	0.007	1.91	54
[MoCl(NO)(2-(-)-OCH_2CHMe$C_{10}H_6$-6-OMe){HB(dmpz)$_3$}]	0.004	1.91	54
[MoI(NO)(3-*O*-1,2:5,6-(CMe_2)$_2$-α-D-glucofuranose){HB(dmpz)$_3$}]	0.245	1.91	54
[MoI(NO)((1*S*,2*R*,5*S*)-(+)-mentholate){HB(dmpz)$_3$}]	0.074	1.91	54
[WCl((*R*)-(+)-NHCHMePh)(NO){HB(dmpz)$_3$}]	0	1.91	54
[Mo((+)-NHCHMePh)(*p*-*O*-tpph$_2$)(NO){HB(dmpz)$_3$}]	0	1.91	54
[Cr($CO)_3$(η^6-(-)-α-ethylphenethylalcohol)]	0.003[a]	1.06	67
[Cr($CO)_3${η^6-(*S*)-CH_3C(O)C_6H_4-2-CH(OH)COOH}]	0[a]	1.06	67
[Cr($CO)_3${η^6-(*S*)-PhCH(OH)COOH}]	0[a]	1.06	67
[Cr($CO)_3${η^6-(*R*)-PhCH(OH)COOH}]	0[a]	1.06	67
[Cr($CO)_3$(η^6-(*S*)-PhCH$_2$CHMeEt]	0.5[a]	1.06	67
[Cr($CO)_3$(η^6-L-phenylaniline ethyl ester hydrochloride)]	0.2[a]	1.06	67

Table 1.3. (continued) Kurtz powder measurements of complexes containing chiral ligands.

Complex	SHG (urea = 1)	Fund. (μm)	Ref.
$[Cr(CO)_3(\eta^6\text{-}PhCHMeCH_2OH)]$	0[a]	1.06	67
$[(+)\text{-}Cr(CO)_3(\eta^6\text{-}C_6H_4Me\text{-}2\text{-}CHO)]$	0	1.06	41
$[(+)\text{-}Cr(CO)_3\{\eta^6\text{-}C_6H_4\text{-}2\text{-}CH_2OHCH_2OC(O)C_{15}H_{31}\}]$	0	1.06	41
$[(+)\text{-}Cr(CO)_3(\eta^6\text{-}C_6H_4\text{-}2\text{-}Me\text{-}COOH)]$	0	1.06	41
$[Cr(CO)_2(nmdpp)(\eta^6\text{-}C_6H_4\text{-}1,4\text{-}Me_2)]$	0.003[a]	1.06	67
$[Fe(CO)_4(nmdpp)]$	0.003[a]	1.06	67
$[Mo(CO)_5(nmdpp)]$	< 0.003[a]	1.06	67
$[W(CO)_5(nmdpp)]$	0.02[a]	1.06	67
$[Fe(N{\equiv}CC_6H_4\text{-}4\text{-}NH_2)((+)\text{-}diop)(\eta^5\text{-}C_5H_5)][PF_6]$	0.0	1.06	63
$[Fe(N{\equiv}CC_6H_4\text{-}4\text{-}NMe_2)((+)\text{-}diop)(\eta^5\text{-}C_5H_5)][PF_6]$	0.2	1.91	63
$[Fe(N{\equiv}CC_6H_4\text{-}4\text{-}Ph)((+)\text{-}diop)(\eta^5\text{-}C_5H_5)][PF_6]$	4.2	1.91	63
$[Fe(N{\equiv}C\text{-}(E)\text{-}CH{=}CHC_6H_4\text{-}4\text{-}NMe_2)((+)\text{-}diop)(\eta^5\text{-}C_5H_5)][PF_6]$	3.3	1.91	63
$[Fe(N{\equiv}CC_6H_4\text{-}4\text{-}NO_2)((+)\text{-}diop)(\eta^5\text{-}C_5H_5)][PF_6]$	38.0	1.91	63
$[Fe(N{\equiv}C\text{-}(E)\text{-}CH{=}CHC_6H_4\text{-}4\text{-}NO_2)((+)\text{-}diop)(\eta^5\text{-}C_5H_5)][PF_6]$	0.0	1.06	63
$[Fe(N{\equiv}CC_6H_4\text{-}4\text{-}C_6H_4\text{-}4\text{-}NO_2)((+)\text{-}diop)(\eta^5\text{-}C_5H_5)][PF_6]$	0.0	1.91	63
$[Ru(N{\equiv}CC_6H_4\text{-}4\text{-}NO_2)((+)\text{-}diop)(\eta^5\text{-}C_5H_5)][MeC_6H_4\text{-}4\text{-}SO_3]$	0.4	1.06	64
$[Ru(N{\equiv}CC_6H_4\text{-}4\text{-}NO_2)((+)\text{-}diop)(\eta^5\text{-}C_5H_5)][Cl]$	0.5	1.06	64
$[Ru(N{\equiv}CC_6H_4\text{-}4\text{-}NO_2)((+)\text{-}diop)(\eta^5\text{-}C_5H_5)][NO_3]$	1.2	1.06	64
$[Ru(N{\equiv}CC_6H_4\text{-}4\text{-}NO_2)((+)\text{-}diop)(\eta^5\text{-}C_5H_5)][BF_4]$	1.9	1.06	64
$[Ru(N{\equiv}CC_6H_4\text{-}4\text{-}NO_2)((+)\text{-}diop)(\eta^5\text{-}C_5H_5)][PF_6]$	2.7	1.06	64
$[Ru(N{\equiv}CC_6H_4\text{-}4\text{-}NO_2)((+)\text{-}diop)(\eta^5\text{-}C_5H_5)][ClO_4]$	2.9	1.06	64
$[Ru(N{\equiv}CC_6H_4\text{-}4\text{-}NO_2)((+)\text{-}diop)(\eta^5\text{-}C_5H_5)][CF_3SO_3]$	10	1.06	64
$[Au(C{\equiv}CC_6H_4\text{-}4\text{-}NO_2)((+)\text{-}nmdpp)]$	2	1.06	65

[a] Measured relative to ADP: conversion of ADP = 0.3 × U was used.[68]

Optimizing molecular alignment is important for enhancing SHG efficiencies in noncentrosymmetric space groups. As was discussed above, the introduction of chiral ligands theoretically ensures noncentrosymmetry (although it does not preclude pseudocentrosymmetric arrangements), but it does not ensure the most favourable molecular arrangement in the lattice. Table 1.4. contains results for complexes with non-zero SHG for which the crystal structures have been reported, emphasizing the range of SHG intensities observed for complexes that crystallize in noncentrosymmetric space groups (and, incidentally, the range of values obtained *for a single complex* and the consequent lack of quantitative significance of Kurtz powder results). The complexes $[(\eta^5\text{-}C_5H_5)_2Fe_2(CO)_2(\mu\text{-}CO)(\mu\text{-}C\text{-}(E)\text{-}CH{=}CHC_6H_4\text{-}4\text{-}NMe_2)][BF_4]$, $[MoCl(p\text{-}O\text{-}tpph_2)(NO)\{HB(dmpz)_3\}]$ and $[Ru(C{=}CPhN{=}NC_6H_4\text{-}4\text{-}OMe)(PPh_3)_2(\eta^5\text{-}C_5H_5)][BF_4]$ crystallize in centric space groups but surprisingly give non-zero responses.[52,53,69,70] A variety of reasons have been proposed to explain these results including SHG by the particle surfaces (which must of necessity be noncentrosymmetric), crystal defects (i.e. the existence of a noncentrosymmetric phase), decomposition in the laser beam due to the high power of the laser, or fluorescence.

Second-order susceptibilities of a further 300 complexes have been reported,[41-44,47-49,52-55,57-62,64,67,69-82] all of which are less than 2 × urea, with about 200 examples giving a zero response. About 100 complexes have been reported relative to ADP[67,82] and 7 relative to quartz[43,77] but, assuming conversion factors ADP = 0.3 × urea and quartz = 0.1 × urea,[68] all of their nonlinearities are low. The complexes listed in Table 1.2. are not representative of all complex types that have been assayed; all examples investigated of $[M(CO)_3(\eta^6\text{-arene})]$ (M = Cr, Mo, W), $[M(CO)_4(L)(\eta^1\text{-}N\text{-pyridine})]$ (M = Cr, Mo, W; L = CO, PR_3),[67] $[M(CO)_4(bipy)]$ (M = Cr, Mo, W),[73] $[Ru(\eta^5\text{-}C_5H_5)(\eta^6\text{-arene})]^+$ salts,[74] $[Ru(C{=}CPhN{=}NR)(PPh_3)_2(\eta^5\text{-}C_5H_5)]^+$ salts,[70] $[Pt(C{\equiv}CR)(C{\equiv}CR')(PR''_3)_2]$,[77,78,83] $[WI(\eta^2\text{-}RC{\equiv}CR')(CO)\{HB(dmpz)_3\}]$,[80] [(pentane-2,4-dionato)ML_2] (M = Pd, Rh, Ir; L = CO, PPh_3),[81] and $[HgX\{C_6H_3(2\text{-}R)\text{-}4\text{-}Y\}]$ complexes gave low (less than 2 × urea) responses.

While most bulk material second-order measurements have been made on powders, other material forms have also been examined. Table 1.5. contains data of bulk second-order measurements performed on Langmuir-Blodgett monolayers containing organometallics. The molecular alignment achieved in Langmuir-Blodgett monolayers leads, perhaps not surprisingly, to little anion dependence compared with that observed in Kurtz powder measurements; the anions do not affect film-forming properties to the same degree as they affect crystal packing.

Table 1.4. Complexes with non-zero SHG for which the crystal structures are known.

Complex	SHG urea = 1	Fund. (μm)	Space Group	Ref.
[(*S*)-Fe(η^5-C_5H_5)(η^5-C_5H_3-2-$SiMe_3$-(*E*)-CH=CHC_6H_4-4-NO_2)]	80-100	1.91	$P2_1$	51
[(*R*)-Fe(η^5-C_5H_5)(η^5-C_5H_3-2-CH_2OH-(*E*)-CH=CHC_6H_4-4-NO_2)]	20	1.91	$P2_1$	51
[(*R*)-Fe(η^5-C_5H_5)(η^5-C_5H_3-2-Me-(*E*)-CH=CHC_6H_4-4-NO_2)]	6	1.91	$P2_12_12_1$	51
[Fc-(*E*)-CH=CH-4-C_5H_4NMe)][NO_3]	75-120	1.91	*Cc*	42-44
[Fc-(*Z*)-CH=CHC_6H_4-4-NO_2)]	62	1.91	*Cc*	46,48,49
[FcCH=NC_6H_4-4-NO_2)]	0.33	1.91	$P2_12_12_1$	71
[MoCl(NO){NHC_6H_3-3-Me-4-N=NC_6H_4-4-(η^5-C_5H_4)Fe(η^5-C_5H_5)}{HB(dmpz)$_3$}]	50-123	1.91	$P2_1$	53,54
[WCl(NO){NHC_6H_3-3-Me-4-N=NC_6H_4-4-(η^5-C_5H_4)Fe(η^5-C_5H_5)}{HB(dmpz)$_3$}]	8-53	1.91	$P2_1$	53,54
[Re(OSO_2CF_3)(CO)$_3$(bipy)]	1.7-2	1.06	$P2_1$	73
[Cr(CO)$_3$(η^6-C_6H_6)]:thiourea, 1:3	2.3	1.06	*R*3*c*	57-60
[Fe(CO)$_3$(η^4-1,3-cyclohexadienyl)]:thiourea, 1:3	0.4	1.06	$Pna2_1$	57-60
[Mn(CO)$_3$(η^4-1,3-cyclohexadienyl)]:thiourea, 1:3	0.4	1.06	*R*3*c*	57-60
[Fe(CO)$_3$(trimethylenemethane)]:thiourea, 1:3	0.3	1.06	*R*3*c*	57-60
[Cr(CO)$_3$(η^6-tetrahydronaphthalene):tris(*o*-thymotide), 1:1	0.1	1.06	$Pca2_1$	58,60,84

Table 1.4. (continued) Complexes with non-zero SHG for which the crystal structures are known.

Complex	SHG urea = 1	Fund. (μm)	Space Group	Ref.
$[PtI(C_6H_4\text{-}4\text{-}NO_2)(PEt_3)_2]$	5.0-8.0	1.06	$Cmc2_1$	61,62
$[Pt(SnCl_3)(C_6H_4\text{-}4\text{-}NO_2)(PEt_3)_2]$	0.8	1.06	$P2_1$	62
$[Pt(SPh)(C_6H_4\text{-}4\text{-}NO_2)(PEt_3)_2]$	0.6	1.06	$Pca2_1$	62
$[1,3\text{-}(FcCH_2)_2\text{-}2\text{-}(=CCN_2)\text{-diazolidine}]$	0.67	1.06	$P3_22_1$	76
$[Fe_2(\mu\text{-}C\text{-}(E)\text{-}CH{=}CHC_6H_4\text{-}4\text{-}NMe_2)(\mu\text{-}CO)(CO)_2(\eta^5\text{-}C_5H_5)_2][BF_4]$	0.77	1.91	$P2_1/n$	52,69
$[MoCl(p\text{-}O\text{-}tpph_2)(NO)\{HB(dmpz)_3\}]$	1.93	1.91	$P\bar{1}$	53,54
$[Ru(C{=}CPhN{=}NC_6H_4\text{-}4\text{-}OMe)(PPh_3)_2(\eta^5\text{-}C_5H_5)][BF_4]$	1.05	1.06	$P\bar{1}$	70

Table 1.6. contains data of bulk second-order measurements performed on poled polymers containing organometallics. The three non-zero components of the second-order susceptibility, $\chi_{ij}^{(2)}$, have been measured for bimetallic complexes having a donor ferrocenyl group linked to either a 16 electron molybdenum-containing moiety or a nitro group. The data show that the off-diagonal component $\chi_{31}^{(2)}$ is greater than the diagonal component, $\chi_{33}^{(2)}$, suggesting that the transition dipole moment associated with the low-energy CT transitions has a component perpendicular to the permanent dipole moment and thus to the effective molecular axis. The 'bent' *ortho* substituted ferrocenyl derivatives have reduced susceptibilities in comparison with their *para* substituted analogues.

Decay of SHG signals has been used to monitor the long-term stability of ferrocenyl chromophores copolymerized with methylmethacrylate[85,86] or 1,6-diisocyanatohexane,[86] and pentacarbonyltungsten attached to polyvinylpyridine or styrene-vinylpyridine copolymer.[87] The long term stability of the electro-optic response in polymers has also been probed; the electro-optic coefficient r_{33}[13] for *p*-dimethylaminonitrobenzene in a polycarbosilane was invariant after sixteen days.[88]

Table 1.5. Results of bulk second-order measurements on Langmuir-Blodgett monolayers.

Material	$\chi^{(2)}$ (10^{-7} esu)	β (10^{-30} esu)	λ_{max} (nm)	Technique	Fund. (μm)	Ref.
[Fc-(*E*)-CH=CH-4-C_5H_4N-1-$C_{16}H_{33}$)][Dy{4,4,4-F_3-1-(2-naphthyl)-1,3-butanedionato)}$_4$]	2.8	150	560,330,286,256	SHG	1.06	89
[Fc-(*E*)-CH=CHCH_2-4-C_5H_4N-1-$C_{16}H_{33}$)][La(dibenzoylmethanato)$_4$]	2.3	158	~349,~250	SHG	1.06	90
[Fc-(*E*)-CH=CHCH_2-4-C_5H_4N-1-$C_{16}H_{33}$)][Nd(dibenzoylmethanato)$_4$]	2.2	137	~349,~250	SHG	1.06	90
[Fc-(*E*)-CH=CHCH_2-4-C_5H_4N-1-$C_{16}H_{33}$)][Dy(dibenzoylmethanato)$_4$]	2.4	150	~349,~250	SHG	1.06	90
[Fc-(*E*)-CH=CHCH_2-4-C_5H_4N-1-$C_{16}H_{33}$)][Yb(dibenzoylmethanato)$_4$]	2.9	144	~349,~250	SHG	1.06	90
[Fc-(*E*)-CH=CHCH_2-4-C_5H_4N-1-$C_{16}H_{33}$)]Br	2.9	110	240, 360	SHG	1.06	91
[Fc-(*E*)-CH=CHCH_2-4-C_5H_4N-1-$C_{16}H_{33}$)]I	2.8	120	240, 360	SHG	1.06	91
[Fe{η^5-C_5H_4-(*E*)-CH=CH-4-C_6H_4-1-N($C_{18}H_{37}$)$_2$}{η^5-C_5H_4CH=C(CN)C(O)NH_2}]		60	~320	SHG	1.06	92
[Fe{η^5-C_5H_4-(*E*)-CH=CH-4-C_6H_4-1-N($C_{18}H_{37}$)$_2$}{η^5-C_5H_4CH=CC(O)NHC(O)NHC(O)}]		180		SHG	1.06	93
[Ru(N≡CC_6H_4-4-C_6H_4-4-C_6H_4-4-C_5H_{11})(PPh_3)$_2$(η^5-C_5H_5)][PF_6]		40×10^{-50} C^3 m^3 J^{-2}	332	SHG	1.06	94

Table 1.6. Results of bulk second-order measurements on poled polymers.

Material	$\chi_{31}^{(2)}$ (10^{-7} esu)	$\chi_{15}^{(2)}$ (10^{-7} esu)	$\chi_{33}^{(2)}$ (10^{-7} esu)	d (pm V^{-1})	Technique	Fund. (μm)	Ref.
[MoCl(NO)(NHC_6H_4-4-Fc){HB($mppz)_3$}]	1.3	-0.5	0.4		Maker Fringe	1.06	95
[MoCl(NO)(NHC_6H_4-4-N=NC_6H_4-4-Fc){HB($mppz)_3$}]	1.9	-0.7	0.6		Maker Fringe	1.06	95
[MoCl(NO)(NHC_6H_3-3-Me-4-N=NC_6H_4-4-Fc){HB($mppz)_3$}]	1.4	-0.4	0.4		Maker Fringe	1.06	95
[MoCl(NO)(NHC_6H_3-3-Me-4-N=NC_6H_4-3-Me-4-Fc){HB($mppz)_3$}]	1.5	-0.4	0.7		Maker Fringe	1.06	95
[MoCl(NO)(NHC_6H_4-4-CH=CHC_6H_4-4-Fc){HB($mppz)_3$}]	2.4	-1.0	0.7		Maker Fringe	1.06	95
[Fc-(*E*)-CH=CHC_6H_4-4-NO_2]	6.6	-4.2	-2.4		Maker Fringe	1.06	95
[FcC_6H_3-4-Me-2-N=NC_6H_3-2-Me-4-NO_2]	1.4	-0.9	-0.5		Maker Fringe	1.06	96
[MoCl(NO)(NHC_6H_3-3-Me-4-N=NC_6H_3-3-Me-2-Fc){HB($mppz)_3$}]	0.4	-0.4	0.3		Maker Fringe	1.06	96
[Fe{η^5-C_5H_4CH=C(CN)CO_2Et}{η^5-$C_5H_4CH_2OC(O)CMeCH_2$}]	α	α	α	1.72	SHG	1.06	97

α Not reported.

1.4.2. Molecular second-order measurements

As can be readily ascertained from the Tables in this Section, researchers have mostly employed the EFISH or HRS techniques to measure second-order nonlinearities of organometallics. Although the initial interest in this field was in metal carbonyl-based complexes, the majority of the measurements are now of ferrocenyl-based complexes or metal acetylides. One reason for this may be pragmatic; despite the vast panoply of possible complex types which exists, ferrocenyl or acetylide complexes can be synthesized in high yield by well-established methodologies, both revealed large molecular nonlinearities in initial studies, and both are (comparatively) oxidatively and thermally stable, the latter an important consideration for (putative) longer-term device applications.

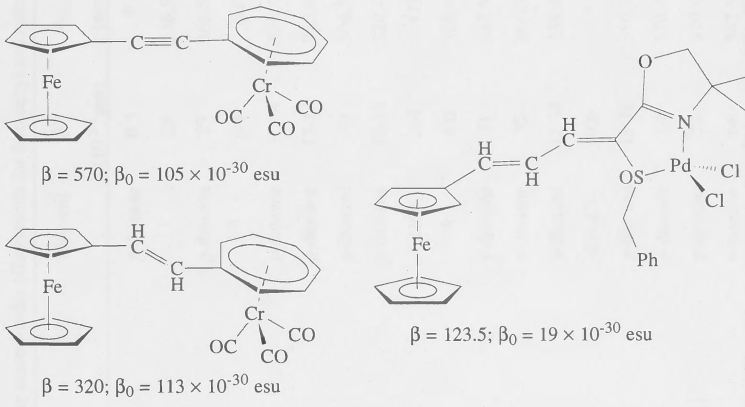

Figure 1.12. Ferrocenyl complexes with large β.

Table 1.7. contains molecular second-order data for ferrocenyl and ruthenocenyl complexes. Ferrocenyl-type compounds had been shown to exhibit large bulk material SHG efficiencies and, as a consequence, their molecular nonlinearities were investigated. Some of the observed nonlinearities are large, with the highest values corresponding to bimetallic species with metal-based acceptors as well as ferrocenyl donors (Figure 1.12.). The data are consistent with the ferrocenyl moiety acting as a reasonable donor in these donor-bridge-acceptor complexes, with observed nonlinearities comparable to those of analogous methoxyphenyl organics.[98]

Table 1.7. Molecular second-order NLO results for ferrocenyl and ruthenocenyl complexes.

Complex	Solvent	β [a] (10^{-30} esu)	λ_{max} (nm)	β_o (10^{-30} esu)	Technique	Fund. (μm)	Ref.
[$FcCOCH_3$]	*p*-dioxane	0.3	[b]	[b]	EFISH	1.91	43,98,99
[Fc-(*E*)-CH=CHC_6H_3-2,4-$(NO_2)_2$]	[b]	20	536,545	[b]	EFISH	1.91	50
	p-dioxane	23	366,536	[b]	EFISH	1.91	99
[Fc-(*E*)-CH=CHC_6H_4-4-NO_2]	[b]	34	500	[b]	EFISH	1.91	50
	p-dioxane	31-34	356,496	[b]	EFISH	1.91	43,98-101
[Fc-(*Z*)-CH=CHC_6H_4-4-NO_2]	*p*-dioxane	13-14	325,480	[b]	EFISH	1.91	43,98-100
[Fc^*-(*E*)-CH=CHC_6H_4-4-NO_2]	*p*-dioxane	40	366,533	[b]	EFISH	1.91	43,98-100
[Fc-(*E*)-CH=CHC_6H_4-4-CN]	*p*-dioxane	10-11	324,466	[b]	EFISH	1.91	98,100
	$CHCl_3$	203	473	34	HRS	1.06	102
[Fc-(*Z*)-CH=CHC_6H_4-4-CN]	[b]	4.0	308,460	[b]	EFISH	1.91	98
[Fc-(*E*)-CH=$C(CN)C_6H_4$-4-NO_2]	*p*-dioxane	21	348,526	[b]	EFISH	1.91	99
[Fc^*-(*E*)-CH=$C(CN)C_6H_4$-4-NO_2]	*p*-dioxane	35	366,560	[b]	EFISH	1.91	99
[Fc-(*E*)-CH=CHC_6H_4-4-CHO]	*p*-dioxane	12-34	338,474	[b]	EFISH	1.91	43,98,100
[Ru(η^5-C_5Me_5)(η^5-$C_5H_4NO_2$)]	CH_2Cl_2	0.6	[b]	[b]	EFISH	1.91	43,98,99
[Ru(η^5-C_5H_5)(η^5-C_5H_4-(*E*)-CH=CHC_6H_4-4-NO_2)]	*p*-dioxane	12-16	350,390	[b]	EFISH	1.91	43,98-100
[Ru(η^5-C_5Me_5)(η^5-C_5H_4-(*E*)-CH=CHC_6H_4-4-NO_2)]	*p*-dioxane	24	370,424	[b]	EFISH	1.91	43,98-100
[Ru(η^5-C_5Me_5){η^5-C_5H_4-(*E*)-CH=$C(CN)C_6H_4$-4-NO_2}]	*p*-dioxane	24	370,443	[b]	EFISH	1.91	99
[Fc-(*E*)-CH=CH-(*E*)-CH=CHC_6H_4-4-NO_2]	*p*-dioxane	66	382,500	[b]	EFISH	1.91	43,98-100

Table 1.7. (continued) Molecular second-order NLO results for ferrocenyl and ruthenocenyl complexes.

Complex	Solvent	β [a] (10^{-30} esu)	λ_{max} (nm)	β_o (10^{-30} esu)	Technique	Fund. (μm)	Ref.
[Fc-(*E*)-CH=CH-6-(4,8-dimethylazulene)]	$CHCl_3$	8.6	334,396	[b]	HRS	1.5	103
[(*S*)-Fe(η^5-C_5H_5)(η^5-C_5H_3-2-$SiMe_3$-(*E*)-CH=CHC_6H_4-4-NO_2)]	*p*-dioxane	36	357	[b]	EFISH	1.91	51
[(*R*)-Fe(η^5-C_5H_5)(η^5-C_5H_3-2-CH_2OH-(*E*)-CH=CHC_6H_4-4-NO_2)]	*p*-dioxane	43	362	[b]	EFISH	1.91	51
[(*R*)-Fe(η^5-C_5H_5)(η^5-C_5H_3-2-Me-(*E*)-CH=CHC_6H_4-4-NO_2)]	*p*-dioxane	24	359	[b]	EFISH	1.91	51
[FcH]	CH_3CN	[b]	380	0.8	HRS	1.06	104
[FcH]·I_3	CH_3CN	[b]	420	2.8	HRS	1.06	104
[FcH]·(DDQ)	CH_3CN	[b]	470	4.6	HRS	1.06	104
[FcH]·(TCNQ)	CH_3CN	[b]	580	5.9	HRS	1.06	104
[FcCH=NPh]	CH_3CN	[b]	460	14.2	HRS	1.06	104
[FcCH=NPh]·I_3	CH_3CN	[b]	550	111.2	HRS	1.06	104
[FcCH=NPh]·(DDQ)	CH_3CN	[b]	567	121.6	HRS	1.06	104
[FcCH=NPh]·(TCNQ)	CH_3CN	[b]	589	132.0	HRS	1.06	104
[FcCH=N-4-C_6H_4N=CHFc]	CH_3CN	[b]	465	20.8	HRS	1.06	104
[FcCH=N-4-C_6H_4N=CHFc]·I_3	CH_3CN	[b]	556	161.0	HRS	1.06	104
[FcCH=N-4-C_6H_4N=CHFc]·(DDQ)	CH_3CN	[b]	572	201.0	HRS	1.06	104
[FcCH=N-4-C_6H_4N=CHFc]·(TCNQ)	CH_3CN	[b]	588	246.0	HRS	1.06	104

Table 1.7. (continued) Molecular second-order NLO results for ferrocenyl and ruthenocenyl complexes.

Complex	Solvent	β [a] (10^{-30} esu)	λ_{max} (nm)	β_o (10^{-30} esu)	Technique	Fund. (μm)	Ref.
[Fc-(*E*)-CH=CHC≡CRu(PPh_3)$_2$(η^5-indenyl)]	CH_2Cl_2	273	345	141	HRS	1.06	105
[Fc-(*E*)-CH=CHCH=C=Ru(PPh_3)$_2$(η^5-indenyl)][BF_4]	CH_2Cl_2	117	301	73	HRS	1.06	105
[Fc-(*E*)-CH=CH(η^6-C_6H_5)Cr(CO)$_3$]	$CHCl_3$	193	304	119	HRS	1.06	102
[Fc-(*E*)-(CH=CH)$_2$(η^6-C_6H_5)Cr(CO)$_3$]	$CHCl_3$	300	334	164	HRS	1.06	102
[Fc-(*E*)-CH=CH-4-C_5H_4N]	$CHCl_3$	21	468	4	HRS	1.06	102
[Fc-(*E*)-CH=CH-4-C_5H_4NCr(CO)$_5$]	$CHCl_3$	63	401	23	HRS	1.06	102
[Fc-(*E*)-CH=CH-4-C_5H_4NMo(CO)$_5$]	$CHCl_3$	95	487	12	HRS	1.06	102
[Fc-(*E*)-CH=CH-4-C_5H_4NW(CO)$_5$]	$CHCl_3$	101	491	12	HRS	1.06	102
[Fc-(*E*)-CH=CHC_6H_4-4-CNCr(CO)$_5$]	$CHCl_3$	271	481	39	HRS	1.06	102
[Fc-(*E*)-CH=CHC_6H_4-4-CNW(CO)$_5$]	$CHCl_3$	375	487	48	HRS	1.06	102
[FcC≡C(η^7-C_7H_6)Cr(CO)$_3$]	CH_2Cl_2	570	600	105	HRS	1.06	106
[Fc-(*E*)-CH=CH(η^7-C_7H_6)Cr(CO)$_3$]	CH_2Cl_2	320	670	113	HRS	1.06	106
[(Fc-(*E*)-CH=CH-4-C_5H_4N)$_2$ReBr(CO)$_3$]	$CHCl_3$	24	501	[b]	HRS	1.3	107
[Fc(η^6-BC_5H_5)Co(η^5-C_5H_5)][PF_6]	CH_2Cl_2	[b]	370,410(sh),650	90±30	HRS	1.06	108
[Fc-(*E*)-CH=CHB(mes)$_2$]	$CHCl_3$	-24	336	[b]	EFISH	1.91	109
[FcC≡CB(mes)$_2$]	$CHCl_3$	4.4	336	[b]	EFISH	1.91	109
[(Fc-2-η^5-C_4H_3S)Mn(CO)$_3$][BF_4]	CH_3NO_2	260	514	13	HRS	1.06	110
[(Fc-(*E*)-CH=CH-2-η^5-C_4H_3S)Mn(CO)$_3$][BF_4]	CH_3NO_2	670	536	-8	HRS	1.06	110
[{Fc-((*E*)-CH=CH)$_2$-2-η^5-C_4H_3S}Mn(CO)$_3$][BF_4]	CH_3NO_2	771	548	-34	HRS	1.06	110

Table 1.7. (continued) Molecular second-order NLO results for ferrocenyl and ruthenocenyl complexes.

Complex	Solvent	β [a] (10^{-30} esu)	λ_{max} (nm)	β_o (10^{-30} esu)	Technique	Fund. (μm)	Ref.
[(Fc-(*E*)-CH=CH-3-η^5-C_4H_3S)Mn(CO)$_3$][BF_4]	CH_3NO_2	305	480	45	HRS	1.06	110
[($FcCH_2$-2-η^5-C_4H_3S)Mn(CO)$_3$][BF_4]	CH_3NO_2	220	[b]	[b]	HRS	1.06	110
[FcCH=C(SCH_2Ph)C=NCMe_2CH_2O]	$CHCl_3$	4.5	472	2.0	EFISH	1.34	111-113
	$CHCl_3$	2.9	472	2.1	EFISH	1.91	112,113
[Fc-CH=CC(O)N(Et)C(S)N(Et)C(O)]	$CHCl_3$	26	377	[b]	EFISH	1.91	114
[Fc-(*E*)-CH=CHCH=CC(O)N(Et)C(S)N(Et)C(O)]	$CHCl_3$	177	430	[b]	EFISH	1.91	114
[Fc-((*E*)-CH=CH)$_2$CH=CC(O)N(Et)C(S)N(Et)C(O)]	$CHCl_3$	380	457	[b]	EFISH	1.91	114
[FcCH=CC{=C(CN)$_2$}-2-$C_6H_4S(O)_2$]	$CHCl_3$	29	419	[b]	EFISH	1.91	114
[Fc-(*E*)-CH=CHCH=CC{=C(CN)$_2$}-2-$C_6H_4S(O)_2$]	$CHCl_3$	192	475	[b]	EFISH	1.91	114
[Fc-((*E*)-CH=CH)$_2$CH=CC{=C(CN)$_2$}-2-$C_6H_4S(O)_2$]	$CHCl_3$	405	517	[b]	EFISH	1.91	114
[FcCH=C{S(O)CH_2Ph} C=NCMe_2CH_2O]	$CHCl_3$	8.4	470	3.7	EFISH	1.34	111-113
[FcCH=C{$S(O)_2CH_2Ph$} C=NCMe_2CH_2O]	$CHCl_3$	6.3	477	1.6	EFISH	1.34	112,113
[Fc-(*E*)-CH=CHCH=C(SCH_2Ph) C=NCMe_2CH_2O]	$CHCl_3$	13.3	482	5.6	EFISH	1.34	112,113
	$CHCl_3$	8.8	482	6.1	EFISH	1.91	112,113
[Fc-(*E*)-CH=CHCH=C{S(O)CH_2Ph} C=NCMe_2CH_2O]	$CHCl_3$	11.0	494	4.6	EFISH	1.34	112,113
[FcC≡CCH=C(SCH_2Ph) C=NCMe_2CH_2O]	$CHCl_3$	2.6	460	1.2	EFISH	1.34	112,113
[FcCH=C(SCH_2Ph)C=NCMe_2CH_2O -*N*,*S*-$NiCl_2$]	$CHCl_3$	10.3	500	3.9	EFISH	1.34	112,113

Table 1.7. (continued) Molecular second-order NLO results for ferrocenyl and ruthenocenyl complexes.

Complex	Solvent	β [a] (10^{-30} esu)	λ_{max} (nm)	β_o (10^{-30} esu)	Technique	Fund. (μm)	Ref.
[FcCH=C(SCH$_2$Ph)C=NCMe$_2$CH$_2$O -*N*,*S*-NiBr$_2$]	$CHCl_3$	7.14	511	2.55	EFISH	1.34	112,113
[FcCH=C(SCH$_2$Ph)C=NCMe$_2$CH$_2$O -*N*,*S*-PdCl$_2$]	$CHCl_3$	12.2	530	4.13	EFISH	1.34	111-113
	$CHCl_3$	9	530	5.8	EFISH	1.91	112,113
[FcCH=C(SCH$_2$Ph)C=NCMe$_2$CH$_2$O -*N*,*S*-PtCl$_2$]	$CHCl_3$	16	523	5.2	EFISH	1.34	112,113
[FcCH=C{S(O)CH$_2$Ph}C=NCMe$_2$CH$_2$O -*N*,*S*-NiCl$_2$]	$CHCl_3$	15.8	498	6.0	EFISH	1.34	112,113
[FcCH=C{S(O)CH$_2$Ph}C=NCMe$_2$CH$_2$O -*N*,*S*-NiBr$_2$]	$CHCl_3$	5.85	494	2.3	EFISH	1.34	112,113
[FcCH=C{S(O)CH$_2$Ph}C=NCMe$_2$CH$_2$O -*N*,*S*-PdCl$_2$]	$CHCl_3$	30.2	540	7.6	EFISH	1.34	111-113
[FcCH=C{S(O)CH$_2$Ph}C=NCMe$_2$CH$_2$O -*N*,*S*-PtCl$_2$]	$CHCl_3$	28.0	548	7.7	EFISH	1.34	112,113
[Fc-(*E*)-CH=CHCH=C(SCH$_2$Ph)C=NCMe$_2$CH$_2$O -*N*,*S*-PdCl$_2$]	$CHCl_3$	58	567	14	EFISH	1.34	112,113
	$CHCl_3$	18.2	567	10.8	EFISH	1.91	112,113
[Fc-(*E*)-CH=CHCH=C{S(O)CH$_2$Ph}C=NCMe$_2$CH$_2$O -*N*,*S*-PdCl$_2$]	$CHCl_3$	123.5	602	19	EFISH	1.34	112,113
[FcC≡CCH=C(SCH$_2$Ph)C=NCMe$_2$CH$_2$O -*N*,*S*-PdCl$_2$]	$CHCl_3$	33.6	558	8.5	EFISH	1.34	112,113

[a] The uncertainties are quoted as ±10%. For lower responses (~1×10^{-30} esu) the uncertainty may be higher. [b] Not reported.

The donor characteristic of the ferrocenyl group has been attributed to the low binding energy of the metal electrons,[99] oxidation from the ferrocene to the analogous ferrocenium being a facile process. The overall effectiveness of the metal as a donor has been questioned, though, with the poor coupling between the metal centre and the substituent cited as a shortcoming of this class of complex;[100] it is believed that the orthogonal relationship of the MLCT axis and organic chromophore is unfavourable.

The UV-visible spectra of many of these complexes exhibit absorptions near the second harmonic region for the irradiating frequencies being employed; many of the reported β values are therefore resonance enhanced. It is possible to apply the two-level correction to compute frequency-independent nonlinearities. However, both the π-π* and MLCT transitions are reported by Marder *et al* to be significant,[100] and the validity of a two-level approximation has therefore been questioned. In contrast to Marder's comments, it has been suggested by Loucif-Saïbi *et al* that the MLCT is dominant for monometallic ferrocenyl derivatives.[112] The latter group has used a two-level correction to calculate the static hyperpolarizability β_0 for some bimetallic ferrocenyl derivatives;[112] based on the good correlation of β_0 values obtained at two different frequencies, they argue that the MLCT is dominant and that the π-π* transition is not an important contributor. The two-level correction has also been applied to some bimetallic sesquifulvalene complexes,[106] where the ferrocenyl group is the donor and a (cycloheptatrienyl)tricarbonylchromium moiety is the acceptor. The evidence thus far is consistent with the two-level correction having some utility with organometallics when applied to a closely-related and systematically varied class of complexes, but that it must be applied with caution; examples exist of structural variations affecting both the MLCT and π-π* transitions significantly,[98] and in these instances the two-level model is not justified.

The effect of metal replacement on β has been investigated using analogous ferrocenyl and ruthenocenyl complexes. Replacement of iron by ruthenium in $[M(\eta^5\text{-}C_5H_5)(\eta^5\text{-}C_5H_4\text{-}(E)\text{-}CH{=}CHC_6H_4\text{-}4\text{-}NO_2]$ leads to a reduction in β, perhaps not surprisingly as ruthenium has a higher ionization potential than iron. Bimetallic complexes coupling $[FcCH{=}C(SCH_2Ph)\overline{C{=}NCMe_2CH_2O}]$ to ligated group 10 metals have been investigated,[112] with the second metal in almost all cases enhancing β compared to the monometallic ferrocenyl precursor; for the acceptor ligated metals, the efficiency series $PtCl_2 \approx PdCl_2 > NiCl_2 > NiBr_2$ was observed. Significantly, coordination of the functionalized ferrocenyl group to a ligated metal results in a larger two-level corrected β_0 than coordination of the dimethylanilino group to the same metal, emphasizing once again that the ferrocenyl group is comparable in strength to the best organic donors. A correlation between Δμ (the difference in dipole moment between ground and excited

states) and β_0 has been found with the monometallic ferrocenyl derivatives, but not with the bimetallic derivatives.[113] Examination of nonamethylferrocenyl analogues has permitted comment on the effect of making the iron more electron rich; the iron is the donor in these donor-bridge-acceptor complexes, and permethylating both rings results in an increase in nonlinearity over that of the related ferrocenyl complexes, as expected. An interesting comparison which was performed for $[Ru(\eta^5\text{-}C_5R_5)(\eta^5\text{-}C_5H_4\text{-}(E)\text{-}CH{=}CHC_6H_4\text{-}4\text{-}NO_2)]$ (R = H, Me) is the effect of permethylating only one of the rings; modifying the ring remote from the chromophore resulted in a 50 to 100 % increase in nonlinearity. The borabenzene derivative $[Fc(\eta^6\text{-}BC_5H_5)Co(\eta^5\text{-}C_5H_5)][PF_6]$ has a surprisingly large β_0 value despite the absence of linking units between the ferrocenyl and (borabenzene)cobalt moieties; related sesquifulvalene complexes lacking bridging units do not show measurable β.

A study[104] of ferrocenyl derivatives of the type [FcR] (where R = H, CH=NPh, CH=N-4-C_6H_4N=CH-Fc) partially oxidized with a variety of reagents (I_2, DDQ, TCNQ) found that β increased as the strength of the oxidant decreased. Each of the partially oxidized complexes has β values an order of magnitude greater than the neutral complexes. The authors suggest that electron transfer from the ferrocene unit to the oxidant, resulting in a significant change in the dipole moment between the ground and excited states, is the reason for the increased optical nonlinearity.

Related nitro $[Fc\text{-}(E)\text{-}CH{=}CHC_6H_4\text{-}4\text{-}NO_2]$ and dinitro $[Fc\text{-}(E)\text{-}CH{=}CHC_6H_3\text{-}2,4\text{-}(NO_2)_2]$ ferrocene derivatives have been assessed,[50] with the 4-nitro complex having a larger β than the 2,4-dinitro complex. Two reasons have been suggested to rationalize this surprising observation. Firstly, EFISH measures the β component in the dipolar direction and the two complexes have different dipole moments, with the dipole of the dinitro complex less aligned with β_{CT} than is the dipole of the 4-nitro complex. Secondly, introduction of the second nitro group may saturate the polarizability, with the second nitro group competing for oscillator strength in the excited state.[50] Table 1.7. also permits comment on relative efficiencies of the bridging groups. For example, the *trans*-complex $[Fc\text{-}(E)\text{-}CH{=}CHC_6H_4\text{-}4\text{-}NO_2]$ has a higher nonlinearity than its *cis*-isomer, and $[Fc\text{-}(E)\text{-}CH{=}CHB(mes)_2]$ has a greater β value than $[FcC{\equiv}CB(mes)_2)]$; the greater efficiencies of *E* versus *Z* stereochemistry and double bond versus triple bond in linking units have been established previously with organic compounds.

Table 1.8. contains data for a series of ferrocenyl complexes for which only $\mu{\cdot}\beta$ values are extant; in the absence of reported dipole moments, only an internal comparison is possible. The results are resonance enhanced and, as the applicability of the two-level correction is

Table 1.8. Molecular second-order NLO results for ferrocenyl, ruthenocenyl and di-iron complexes for which μ·β values have been reported.[a]

Complex	Solvent	μ·β (10^{-48} esu)	λ_{max} (nm)	$\mu\cdot\beta_o$[c] (10^{-48} esu)	Ref.
[Fc-(*E*)-CH=CHCHO]	Acetone/$CHCl_3$	60	367,480	42-49 [45]	114,115
[Fc-((*E*)-CH=CH)$_2$CHO]	Acetone/$CHCl_3$	215	330,494	147-184 [165]	114,115
[Fc-(*E*)-CH=CH-(*E*)-CMe=CH-(*E*)-CH=CH-(*E*)-CH=CMeCHO]	Acetone	560	398[b]	440	115
[Fc-((*E*)-CH=CH)$_2$-(*E*)-CMe=CH-(*E*)-CH=CH-(*E*)-CH=CMe-(*E*)-CH=CHCHO]	Acetone	1150	430[b]	870	115
[FcCH=C(CN)$_2$]	Acetone/$CHCl_3$	92	320,526	60-80 [70]	114,115
[Fc-(*E*)-CH=CHCH=C(CN)$_2$]	Acetone/$CHCl_3$	420	370,556	250-340 [300]	114,115
[Fc-((*E*)-CH=CH)$_2$CH=C(CN)$_2$]	Acetone/$CHCl_3$	1120	406,568	660-875 [770]	114,115
[Fc-(*E*)-CH=CH-(*E*)-CMe=CH-(*E*)-CH=CH-(*E*)-CH=CMeCH=C(CN)$_2$]	Acetone	4600	458[b]	3300	115
[Ru(η^5-C_5H_5){η^5-C_5H_4-((*E*)-CH=CH)$_2$CHO}]	$CHCl_3$	140	369, 381		114
[Ru(η^5-C_5H_5){η^5-C_5H_4CH=C(CN)$_2$}]	$CHCl_3$	65	321,411		114
[Ru(η^5-C_5H_5){η^5-C_5H_4-(*E*)-CH=CHCH=C(CN)$_2$}]	$CHCl_3$	410	362,449		114
[Ru(η^5-C_5H_5){η^5-C_5H_4-((*E*)-CH=CH)$_2$CH=C(CN)$_2$}]	$CHCl_3$	750	397,472		114
[Ru(η^5-C_5H_5){η^5-C_5H_4-CH=CC(O)N(Et)C(S)N(Et)C(O)}]	$CHCl_3$	90	368,458		114
[Ru(η^5-C_5H_5){η^5-C_5H_4-(*E*)-CH=CHCH=CC(O)N(Et)C(S)N(Et)C(O)}]	$CHCl_3$	390	409,508		114
[Ru(η^5-C_5H_5){η^5-C_5H_4-((*E*)-CH=CH)$_2$CH=CC(O)N(Et)C(S)N(Et)C(O)}]	$CHCl_3$	1000	530		114
[Ru(η^5-C_5H_5)(η^5-C_5H_4-CH=CC{=C(CN$_2$)}-2-C_6H_4-S(O)$_2$)]	$CHCl_3$	105	414,541		114
[Ru(η^5-C_5H_5)(η^5-C_5H_4-(*E*)-CH=CHCH=CC{=C(CN$_2$)}-2-C_6H_4-S(O)$_2$)]	$CHCl_3$	630	464,595		114
[Ru(η^5-C_5H_5)(η^5-C_5H_4-((*E*)-CH=CH)$_2$CH=CC{=C(CN$_2$)}-2-C_6H_4-S(O)$_2$)]	$CHCl_3$	1900	623		114

Table 1.8. (continued) Molecular second-order NLO results for ferrocenyl, ruthenocenyl and diiron complexes for which μ·β values have been reported.[a]

Complex	Solvent	μ·β (10^{-48} esu)	λ_{max} (nm)	μ·β_o[c] (10^{-48} esu)	Ref.
[Fc-(*E*)-CH=CHC_6H_4-4-NO_2]	$CHCl_3$	140	362,508		116
[Fc-((*E*)-CH=CH)$_2C_6H_4$-4-NO_2]	$CHCl_3$	300	390,510		116
[FcCH= CC(O)N(Et)C(S)N(Et)C(O)]	$CHCl_3$	100	379,579		116
[Fc-(*E*)-CH=CHCH= CC(O)N(Et)C(S)N(Et)C(O)]	$CHCl_3$	850	427,618		116
[Fc-((*E*)-CH=CH)$_2$CH= CC(O)N(Et)C(S)N(Et)C(O)]	$CHCl_3$	1900	457,632		116
[FcCH= CC{=C(CN_2)}-2-C_6H_4-S($O)_2$)]	$CHCl_3$	160	422,670		116
[Fc-(*E*)-CH=CHCH= CC{=C(CN_2)}-2-C_6H_4-S($O)_2$)]	$CHCl_3$	1400	476,724		116
[Fc-((*E*)-CH=CH)$_2$CH= CC{=C(CN_2)}-2-C_6H_4-S($O)_2$)]	$CHCl_3$	3000	516,745		116
[Fe_2(μ–C=CHCH= CC(O)N(Et)C(S)N(Et)C(O) }(μ-CO)$(CO)_2(\eta^5$-$C_5H_5)_2$]	[d]	179	474	120	117
[Fe_2(μ–C=CH-(*E*)-CH=CHCH= CC(O)N(Et)C(S)N(Et)C(O) }(μ-CO)$(CO)_2(\eta^5$-$C_5H_5)_2$]	[d]	1100	564	660	117
[Fe_2(μ–C=CH-((*E*)-CH=CH)$_2$CH= CC(O)N(Et)C(S)N(Et)C(O) }(μ-CO)$(CO)_2(\eta^5$-$C_5H_5)_2$]	[d]	3100	646	1500	117

[a] Measured by EFISH at 1.91 μm. Uncertainty of 5-20 %. [b] Lower energy band obscured by band to higher energy. [c] Since the UV-vis show two distinct bands, the two-level model was deemed unsuitable and not applied. The range of values (and average in square brackets) derived from the two-level model is shown. [d] Not reported.

questionable (see above), a range of values was calculated for some examples; approximate static values were obtained by taking the average of this range. Two other assumptions were made in order to draw conclusions about β in the absence of experimental μ: (i) that the major β component is nearly parallel to the dipolar direction and (ii) that μ values exhibit a weak length dependence, both of which appear reasonable. The results from these studies suggest a $\mu \cdot \beta_0 = kn^a$ relationship for n ene-linkages, with a values of 1.6 and 2.4 for the formyl and dicyanovinyl acceptor groups, respectively; larger $\mu \cdot \beta_0$ values and larger increases upon chain lengthening were obtained with the stronger acceptor. A metal comparison may be made between homologous iron and ruthenium complexes.[114] The ruthenocene derivatives yield smaller $\mu \cdot \beta$ values than their ferrocene analogues but consideration should be given to the proximity of the absorption bands to the second harmonic, the effect of resonance enhancement being somewhat greater for the ferrocene complexes. Coupling of the metal centre to the polyene chain was also examined.[115] The two absorption bands assigned to MLCT and π-π^* transitions approach one another with increasing chain length; for sufficiently long chain length, the bands overlap, suggesting mixing of these two bands resulting in increased coupling between the metal centre and the acceptor.

Table 1.9. contains results from metal carbonyl complexes. In many cases, the dominant contribution to the nonlinearity is presumed to derive from the other ligands present, namely pyridines, arenes, carbenes and acetylides. The pyridine and arene complexes have negative β values, indicative of a decrease or even change in direction of dipole moment between ground and excited state. The data show that introduction of an electron accepting group onto the *N*-ligand leads to larger β;[118,119] the acceptor substituent facilitates back-transfer of charge upon MLCT excitation, as well as providing lower energy π^* orbitals. The expected increase in β values with increased conjugation length is also seen.

Varying the metal has minimal impact on nonlinearity in *N*-ligand complexes, in contrast to its effects upon β values in *C*-ligand compounds. Metal substitution across the series $[M(CO)_4(1,10\text{-phen})]$ (M = Cr, Mo, W)[118] has little effect on β values, but metal replacement for the carbene complexes $[M(CO)_5\{C(OMe)\text{-}(E)\text{-}CH{=}CHNMe_2\}]$ (M = Cr, W) results in a significant difference in β. Both metal and halogen replacement in $[MX(CO)_2(NC_5H_4\text{-}4\text{-}(E)\text{-}CH{=}CHC_6H_4\text{-}4\text{-}OCH_2CHMeEt)]$ had minimal impact upon β.

The chromium arene complexes have much lower second-order responses than the chromium carbene complexes; unlike the arene complexes, the carbene complexes satisfy a suggested organometallic NLO chromophore design strategy (the metal positioned along the chromophore axis, and the presence of some M-C multiple bonding).[98]

Table 1.9. Molecular second-order NLO measurements for metal carbonyl complexes.

Complex	Solvent	β [a] (10^{-30} esu)	λ_{max} (nm)	β_o (10^{-30} esu)	Technique	Fund. (μm)	Ref.
$[W(CO)_5(NC_5H_4\text{-}4\text{-}NH_2)]$	dmso	-2.1 ± 0.3	290		EFISH	1.91	99,118,119
$[W(CO)_5(NC_5H_4\text{-}4\text{-}Bu^n)]$	*p*-dioxane	-3.4	328		EFISH	1.91	99,118,119
$[W(CO)_5(NC_5H_5)]$	toluene	-4.4	332		EFISH	1.91	99,118,119
$[W(CO)_5(NC_5H_4\text{-}4\text{-}Ph)]$	$CHCl_3$	-4.5	330-340		EFISH	1.91	99,118,119
$[W(CO)_5(NC_5H_4\text{-}4\text{-}COMe)]$	$CHCl_3$	-9.3	420-440		EFISH	1.91	99,118,119
$[W(CO)_5(NC_5H_4\text{-}4\text{-}CHO)]$	$CHCl_3$	-12	420-440		EFISH	1.91	99,118,119
$[W(CO)_5(NC_5H_4\text{-}4\text{-}(E)\text{-}CH{=}CHPh)]$	$CHCl_3$	-5.7	302,440		EFISH	1.91	118
$[W(CO)_5(NC_5H_4\text{-}4\text{-}(E)\text{-}CH{=}CHC_6H_4\text{-}4'\text{-}CHO)]$	$CHCl_3$	-17	320,420		EFISH	1.91	118
$[W(CO)_5(NC_5H_4\text{-}4\text{-}(E)\text{-}CH{=}CHC_6H_4\text{-}4'\text{-}NO_2)]$	$CHCl_3$	-20	322,425		EFISH	1.91	101,118
$[W(CO)_5(\text{pyrazine})]$	$CHCl_3$	6.0 [b]	c		EFISH	1.91	118
$[Cr(CO)_4(1,10\text{-phen})]$	CH_2Cl_2	-13	500		EFISH	1.91	118
$[Mo(CO)_4(1,10\text{-phen})]$	CH_2Cl_2	-13	496		EFISH	1.91	118
$[W(CO)_4(1,10\text{-phen})]$	CH_2Cl_2	-13	492		EFISH	1.91	118
$[W(CO)_4(5\text{-}NO_2\text{-}1,10\text{-phen})]$	CH_2Cl_2	-18	c		EFISH	1.91	118
$[Cr(CO)_3(\eta^6\text{-}C_6H_6)]$	toluene	-0.8 ± 0.08	310		EFISH	1.91	99
$[Cr(CO)_3(\eta^6\text{-}C_6H_5OMe)]$	toluene	-0.9 ± 0.09	310		EFISH	1.91	99,118,119
$[Cr(CO)_3(\eta^6\text{-}C_6H_5NH_2)]$	*p*-dioxane	-0.6 ± 0.06	313		EFISH	1.91	99,118,119
$[Cr(CO)_3(\eta^6\text{-}C_6H_5NMe_2)]$	toluene	-0.4 ± 0.04	318		EFISH	1.91	99,118,119
$[Cr(CO)_3(\eta^6\text{-}C_6H_5CO_2Me)]$	toluene	-0.7 ± 0.07	318		EFISH	1.91	99,118,119

Table 1.9. (continued) Molecular second-order NLO measurements for metal carbonyl complexes.

Complex	Solvent	β^a (10^{-30} esu)	λ_{max} (nm)	β_o (10^{-30} esu)	Technique	Fund. (μm)	Ref.
$[Cr(CO)_3(\eta^6\text{-}C_6H_5\text{-}(E)\text{-}CH{=}CHPh)]$	*p*-dioxane	-2.2 ± 0.22	410		EFISH	1.91	99,118,119
$[Cr(CO)_5\{C(N\text{-pyrrole})\text{-}5\text{-}(2,2'\text{-bithiophene})\}]$	$CHCl_3$	18	335	10	HRS	1.06	120
$[Cr(CO)_5\{C(OMe)\text{-}(E)\text{-}CH{=}CHNMe_2\}]$	$CHCl_3$	16	420	5	HRS	1.06	120
$[W(CO)_5\{C(OMe)\text{-}(E)\text{-}CH{=}CHNMe_2\}]$	$CHCl_3$	34	411	12	HRS	1.06	120
$[Cr\{C{=}C{=}C(NMe_2)_2\}(CO)_5]$	DMF	21	372	9.5	HRS	1.06	121
$[W\{C{=}C{=}C(NMe_2)_2\}(CO)_5]$	DMF	25	368	11	HRS	1.06	121
$[Cr\{C{=}C{=}C(NMe_2)CH{=}C(NMe_2)_2\}(CO)_5]$	DMF	22	388	9	HRS	1.06	121
$[Cr\{C{=}C{=}C{=}C{=}C(NMe_2)_2\}(CO)_5]$	DMF	100	424	31	HRS	1.06	121
$[W\{C{=}C{=}C{=}C{=}C(NMe_2)_2\}(CO)_5]$	DMF	102	424	31	HRS	1.06	121
$[Cr\{C{=}C{=}C{=}C{=}C(NEt_2)C(Me){=}C(NMe_2)_2\}(CO)_5]$	DMF	125	418	40	HRS	1.06	121
$[IrCl(CO)_2(NC_5H_4\text{-}4\text{-}(E)\text{-}CH{=}CHC_6H_4\text{-}4\text{-}OCH_2CHMeEt)]$	$CHCl_3$	24.4	364		EFISH	1.91	122
$[RhCl(CO)_2(NC_5H_4\text{-}4\text{-}(E)\text{-}CH{=}CHC_6H_4\text{-}4\text{-}OCH_2CHMeEt)]$	$CHCl_3$	20.1	355		EFISH	1.91	122
$[RhBr(CO)_2(NC_5H_4\text{-}4\text{-}(E)\text{-}CH{=}CHC_6H_4\text{-}4\text{-}OCH_2CHMeEt)]$	$CHCl_3$	23.9	357		EFISH	1.91	122
$[Ru\{C{\equiv}C\text{-}(E)\text{-}CH{=}CH\text{-}4\text{-}C_5H_4N\text{-}1\text{-}Cr(CO)_5\}(PPh_3)_2(\eta^5\text{-indenyl})]$	CH_2Cl_2	260 ± 26	451	60	HRS	1.06	105,123,124
$[Ru\{C{\equiv}C\text{-}(E)\text{-}CH{=}CH\text{-}4\text{-}C_5H_4N\text{-}1\text{-}W(CO)_5\}(PPh_3)_2(\eta^5\text{-indenyl})]$	CH_2Cl_2	535 ± 54	462	71	HRS	1.06	105,123,124
$[Ru\{C{\equiv}C\text{-}(E)\text{-}CH{=}CHC_6H_4\text{-}4\text{-}C{\equiv}NCr(CO)_5\}(PPh_3)_2(\eta^5\text{-indenyl})]$	CH_2Cl_2	465 ± 47	442	119	HRS	1.06	105,123,124
$[Ru\{C{\equiv}C\text{-}(E)\text{-}CH{=}CHC_6H_4\text{-}4\text{-}C{\equiv}NW(CO)_5\}(PPh_3)_2(\eta^5\text{-indenyl})]$	CH_2Cl_2	700 ± 70	456	150	HRS	1.06	105,123,124
$[Ru\{C{\equiv}NCr(CO)_5\}(PPh_3)_2(\eta^5\text{-indenyl})]$	CH_2Cl_2	25 ± 2.5	392	10	HRS	1.06	105,123,124
$[Ru\{C{\equiv}NW(CO)_5\}(PPh_3)_2(\eta^5\text{-indenyl})]$	CH_2Cl_2	40 ± 4	392	15	HRS	1.06	105,123,124

Table 1.9. (continued) Molecular second-order NLO measurements for metal carbonyl complexes.

Complex	Solvent	β [a] (10^{-30} esu)	λ_{max} (nm)	β_o (10^{-30} esu)	Technique	Fund. (μm)	Ref.
[Fc-2-C_4H_3S{$Mn(CO)_3$}][BF_4]	CH_3NO_2	260	514	13	HRS	1.06	110
[Fc-(*E*)-CH=CH-2-{η^5-$C_4H_3SMn(CO)_3$}][BF_4]	CH_3NO_2	670	536	-8	HRS	1.06	110
[Fc-((*E*)-CH=CH)$_2$-2-{η^5-$C_4H_3SMn(CO)_3$}][BF_4]	CH_3NO_2	771	548	-34	HRS	1.06	110
[Fc-(*E*)-CH=CH-3-{η^5-$C_4H_3SMn(CO)_3$}][BF_4]	CH_3NO_2	305	480	45	HRS	1.06	110
[$FcCH_2$-2-{η^5-$C_4H_3SMn(CO)_3$}][BF_4]	CH_3NO_2	220	[c]		HRS	1.06	110
[$Mn(CO)_3$(η^5-C_4H_3S-2-(*E*)-CH=CHC_6H_4-4-OMe)][BF_4]	CH_3NO_2	252	415	84	HRS	1.06	110
[$Mn(CO)_3$(η^5-C_4H_3S-2-(*E*)-CH=CHC_6H_4-4-Me)][BF_4]	CH_3NO_2	355	405	127	HRS	1.06	110
[$Mn(CO)_3$(η^5-C_4H_3S-2-(*E*)-CH=CHPh)][BF_4]	CH_3NO_2	413	390	165	HRS	1.06	110
[$Mn(CO)_3$(η^5-C_4H_3S-2-(*E*)-CH=CHC_6H_4-4-Br)][BF_4]	CH_3NO_2	534	393	209	HRS	1.06	110
[$Mn(CO)_3$(η^5-C_4H_3S-2-(*E*)-CH=CHC_6H_4-4-NO_2)][BF_4]	CH_3NO_2	613	400	229	HRS	1.06	110
[$Mn(CO)_2(PPh_3)$(η^5-C_4H_3S-2-(*E*)-CH=CHC_6H_4-4-NO_2)][BF_4]	CH_3NO_2	700	384	292	HRS	1.06	110
[$Mn(CO)_3$(η^6-$C_6H_4NMe_2$-4-(*E*)-CH=CHC_4H_3S)][BF_4]	CH_3NO_2	377	470	67	HRS	1.06	110
[$Mn(CO)_3$(η^5-$C_5H_4C_7H_6$)][BF_4]	CH_2Cl_2	45	536		HRS	1.06	125
	MeCN	38	506		HRS	1.06	125
[$Mn(CO)_2${$P(OMe)_3$}(η^5-$C_5H_4C_7H_6$)][BF_4]	CH_2Cl_2	54	612		HRS	1.06	125
	MeCN	53	581		HRS	1.06	125
[$Mn(CO)_2(PPh_3)$(η^5-$C_5H_4C_7H_6$)][BF_4]	CH_2Cl_2	29	643		HRS	1.06	125
	MeCN	39	630		HRS	1.06	125

Table 1.9. (continued) Molecular second-order NLO measurements for metal carbonyl complexes.

Complex	Solvent	β [a] (10^{-30} esu)	λ_{max} (nm)	β_o (10^{-30} esu)	Technique	Fund. (μm)	Ref.
$[Mn(CO)_3(\eta^5\text{-}C_5H_4C{\equiv}CC_7H_6)][BF_4]$	CH_2Cl_2	40	537		HRS	1.06	125
	MeCN	94	491		HRS	1.06	125
$[Mn(CO)_2\{P(OMe)_3\}(\eta^5\text{-}C_5H_4C{\equiv}CC_7H_6)][BF_4]$	CH_2Cl_2	50	649		HRS	1.06	125
	MeCN	151	583		HRS	1.06	125
$[Mn(CO)_2(PPh_3)(\eta^5\text{-}C_5H_4C{\equiv}CC_7H_6)][BF_4]$	CH_2Cl_2	44	740		HRS	1.06	125
	MeCN	73	650		HRS	1.06	125
$[FcC{\equiv}C(\eta^7\text{-}C_7H_6)Cr(CO)_3]$	CH_2Cl_2	570	600	105	HRS	1.06	106
[Fc-(*E*)-CH=CH(η^7-C_7H_6)Cr(CO)$_3$]	CH_2Cl_2	320	670	113	HRS	1.06	106
$[Fc(\eta^6\text{-}BC_5H_5)Co(\eta^5\text{-}C_5H_5)]$	CH_2Cl_2	[c]	370,410(sh),650	90 ± 30	HRS	1.06	108

[a] Uncertainties not shown have not been quoted. [b] Absolute value of β. [c] Not reported.

The sesquifulvalene complexes have significantly larger nonlinearities, illustrating one important advantage of organometallics, namely stabilization of reactive organic species. Sesquifulvalenes were predicted computationally to have large nonlinearities, but their high reactivity has prevented experimental confirmation. Stabilization by coordination to transition metal(s) permits assessment experimentally.

The metallacumulene complexes also show minimal impact of metal variation upon nonlinearity. The measured β values show a chain length dependence but, interestingly, the insertion of a conjugated C_2 unit only slightly enhances β while the insertion of a cumulated unit leads to a quadrupling.

Each of the (thiophene)manganese complexes shows substantial β values,[110] although a large resonance enhancement contribution is present. The (thiophene)$Mn(CO)_3^+$ centre is reported to act as an effective excited state acceptor.

The ruthenium indenyl complexes have second-order data that are strongly resonance enhanced; there is little difference between the two-level corrected β_0 values of the related chromium- and tungsten-containing complexes, the lack of significance of metal replacement being consistent with the observations in the [$M(CO)_4$(1,10-phen)] series above. The β_0 values are much larger than those of the other carbonyl-containing complexes, and amongst the largest values reported thus far for organometallic complexes.

Table 1.10. contains data from acetylide complexes, with Figure 1.13. showing representative examples with large nonlinearities. Humphrey, Gimeno, Persoons and their co-workers have prepared and measured systematically-varied series of ruthenium, nickel and gold acetylides. Dispersion-enhanced experimentally-obtained and two-level-corrected quadratic nonlinearities for the ruthenium examples increase on chain-lengthening from one-ring to biphenyl and yne-linked two-ring acetylide ligand, with the ene-linked two-ring acetylide the most efficient. Although the data for ruthenium acetylide complexes are substantially resonance enhanced, their absolute values (both experimentally-observed and two-level-corrected) are much larger than those for the gold complexes, consistent with the 18 valence electron, more easily oxidizable, ruthenium(II) being a better donor than the 14 valence electron, less readily oxidizable, gold(I). The $Ph_3PAu(C{\equiv}C)$ unit has comparable efficiency to the strongest organic donors, suggesting that the more efficient oxidizable 18 valence electron organometallic complexes can provide access to stronger donors than are possible in organic systems. Data from the (cyclopentadienyl)(triphenylphosphine)nickel acetylides with an 18 electron, but less easily oxidizable metal are also substantially resonance enhanced, although the relative orderings were maintained with two-level-corrected values.

Table 1.10. Molecular second-order NLO measurements for metal acetylide complexes.

Complex	Solvent	β^a (10^{-30} esu)	λ_{max} (nm)	β_o (10^{-30} esu)	Ref.
$[Ru(C{\equiv}CPh)(PPh_3)_2(\eta^5\text{-}C_5H_5)]$	thf	89	310	45	123,126
$[Ru(C{\equiv}CC_6H_4\text{-}4\text{-}NO_2)(PPh_3)_2(\eta^5\text{-}C_5H_5)]$	thf	468	382,460	96	123,127
$[Ru(C{\equiv}CC_6H_4\text{-}4\text{-}NO_2)(PMe_3)_2(\eta^5\text{-}C_5H_5)]$	thf	248	279,477	39	123,127
$[Ru(C{\equiv}CC_6H_4\text{-}4\text{-}C_6H_4\text{-}4\text{-}NO_2)(PPh_3)_2(\eta^5\text{-}C_5H_5)]$	thf	560	310,448	134	123,126
$[Ru(C{\equiv}CC_6H_4\text{-}4\text{-}(E)\text{-}CH{=}CHC_6H_4\text{-}4\text{-}NO_2)(PPh_3)_2(\eta^5\text{-}C_5H_5)]$	thf	1455	341,476	232	123,127
	thf	1464[c]	341,476	234	123,127
	CH_2Cl_2	186[d]	478	105	128
$[Ru(C{\equiv}C\text{-}2\text{-}C_5H_4N)(PPh_3)_2(\eta^5\text{-}C_5H_5)]$	thf	18	331	10	129
$[Ru(C{\equiv}C\text{-}2\text{-}C_5H_3N\text{-}5\text{-}NO_2)(PPh_3)_2(\eta^5\text{-}C_5H_5)]$	thf	622	468	113	129
$[Ru(C{\equiv}CC_6H_4\text{-}4\text{-}C{\equiv}CC_6H_4\text{-}4\text{-}NO_2)(PPh_3)_2(\eta^5\text{-}C_5H_5)]$	thf	865	340,446	212	123,126
$[Ru(C{\equiv}CC_6H_4\text{-}4\text{-}N{=}CHC_6H_4\text{-}4\text{-}NO_2)(PPh_3)_2(\eta^5\text{-}C_5H_5)]$	thf	840	298,496	86	123,127
	thf	760[c]	298,496	78	123,127
$[Ru(C{\equiv}CC_6H_4\text{-}4\text{-}(E)\text{-}CH{=}CH\text{-}2\text{-}C_4H_2S\text{-}5\text{-}NO_2)(PPh_3)_2(\eta^5\text{-}C_5H_5)]$	CH_2Cl_2	294	533	138	128
$[Ru(C{\equiv}C\text{-}2\text{-}C_4H_2S\text{-}5\text{-}(E)\text{-}CH{=}CHC_6H_4\text{-}4\text{-}NO_2)(PPh_3)_2(\eta^5\text{-}C_5H_5)]$	CH_2Cl_2	333	522	163	128
$[Ru(C{\equiv}CC_6H_4\text{-}4\text{-}C{\equiv}C\text{-}2\text{-}C_4H_2S\text{-}5\text{-}NO_2)(PPh_3)_2(\eta^5\text{-}C_5H_5)]$	CH_2Cl_2	210	505	109	128
$[Ru\{C{\equiv}C\text{-}(2\text{-}C_4H_2S\text{-}5\text{-}(E)CH{=}CH)_2C_6H_4\text{-}4\text{-}NO_2\}(PPh_3)_2(\eta^5\text{-}C_5H_5)]$	CH_2Cl_2	419	536	195	128
$[Ru(C{\equiv}CC_6H_4\text{-}4\text{-}N{=}CH\text{-}2\text{-}C_4H_2S\text{-}5\text{-}NO_2)(PPh_3)_2(\eta^5\text{-}C_5H_5)]$	CH_2Cl_2	308	562	129	128
$[Ru(C{\equiv}CC_5H_4NMe)(PPh_3)_2(\eta^5\text{-}C_5H_5)][PF_6]$	CH_2Cl_2	80	460	16	130
$[Ru(C{\equiv}CC_6H_4\text{-}4\text{-}(E)\text{-}CH{=}CH\text{-}4\text{-}C_5H_4NMe)(PPh_3)_2(\eta^5\text{-}C_5H_5)][PF_6]$	CH_2Cl_2	1600	582	154	130

Table 1.10. (continued) Molecular second-order NLO measurements for metal acetylide complexes.

Complex	Solvent	β^a (10^{-30} esu)	λ_{max} (nm)	β_o (10^{-30} esu)	Ref.
$[Ru(C{\equiv}CC_6H_4\text{-}4\text{-}C{\equiv}C\text{-}4\text{-}C_5H_4NMe)(PPh_3)_2(\eta^5\text{-}C_5H_5)][PF_6]$	CH_2Cl_2	1400	558	102	130
$[Ru(C{\equiv}CC_6H_4\text{-}4\text{-}NO_2)(PPh_3)_2(\eta^5\text{-indenyl})]$	CH_2Cl_2	746	476	119	105,123,124
$[Ru(C{\equiv}CC_6H_4\text{-}4\text{-}NO_2)(dppe)(\eta^5\text{-indenyl})]$	CH_2Cl_2	516	459	107	105
$[Ru(C{\equiv}CC_6H_4\text{-}4\text{-}NO_2)(dppm)(\eta^5\text{-indenyl})]$	CH_2Cl_2	540	456	117	105
$[Ru(C{\equiv}C\text{-}(E)\text{-}CH{=}CHC_6H_4\text{-}4\text{-}NO_2)(PPh_3)_2(\eta^5\text{-indenyl})]$	CH_2Cl_2	1257	507	89	105,123,124
$[Ru(C{\equiv}C\text{-}(E)\text{-}CH{=}CHC_6H_4\text{-}4\text{-}CN)(PPh_3)_2(\eta^5\text{-indenyl})]$	CH_2Cl_2	238	427	71	105,123,124
$[Ru(C{\equiv}C\text{-}(E)\text{-}CH{=}CH\text{-}(E)\text{-}CH{=}CHC_6H_4\text{-}4\text{-}NO_2)(PPh_3)_2(\eta^5\text{-indenyl})]$	CH_2Cl_2	1320	523	34	105,123,124
$[Ru(C{\equiv}C\text{-}(E)\text{-}CH{=}CH\text{-}4\text{-}C_5H_4N)(PPh_3)_2(\eta^5\text{-indenyl})]$	CH_2Cl_2	100	399	37	123,124
$[Ru(C{\equiv}CC_6H_4\text{-}4\text{-}C{\equiv}CC_6H_4\text{-}4\text{-}NO_2)(PPh_3)_2(\eta^5\text{-indenyl})]$	CH_2Cl_2	1027	463	202	105
$[Ru(C{\equiv}CC_6H_4\text{-}4\text{-}N{=}CHC_6H_4\text{-}4\text{-}NO_2)(PPh_3)_2(\eta^5\text{-indenyl})]$	CH_2Cl_2	1295	509	85	105
$[Ru(C{\equiv}C\text{-}(E,Z)\text{-}CH{=}CH\text{-}2\text{-}C_4H_2O\text{-}5\text{-}NO_2)(PPh_3)_2(\eta^5\text{-indenyl})]$	CH_2Cl_2	908	550	43	105
$[Ru(C{\equiv}C\text{-}(E)\text{-}CH{=}CH\text{-}2\text{-}C_4H_2S\text{-}5\text{-}NO_2)(PPh_3)_2(\eta^5\text{-indenyl})]$	CH_2Cl_2	487	598	88	105
$[Ru\{C{\equiv}CCH{=}C(C_6H_4\text{-}3\text{-}NO_2)_2\}(PPh_3)_2(\eta^5\text{-indenyl})]$	CH_2Cl_2	48	345	25	105
$[Ru\{C{\equiv}C\text{-}(E)\text{-}CH{=}CH\text{-}4\text{-}C_5H_4N\text{-}1\text{-}Cr(CO)_5\}(PPh_3)_2(\eta^5\text{-indenyl})]$	CH_2Cl_2	260	451	60	105,123,124
$[Ru\{C{\equiv}C\text{-}(E)\text{-}CH{=}CH\text{-}4\text{-}C_5H_4N\text{-}1\text{-}W(CO)_5\}(PPh_3)_2(\eta^5\text{-indenyl})]$	CH_2Cl_2	535	462	71	105,123,124
$[Ru\{C{\equiv}C\text{-}(E)\text{-}CH{=}CHC_6H_4\text{-}4\text{-}C{\equiv}NCr(CO)_5\}(PPh_3)_2(\eta^5\text{-indenyl})]$	CH_2Cl_2	465	442	119	105,123,124
$[Ru\{C{\equiv}C\text{-}(E)\text{-}CH{=}CHC_6H_4\text{-}4\text{-}C{\equiv}NW(CO)_5\}(PPh_3)_2(\eta^5\text{-indenyl})]$	CH_2Cl_2	700	456	150	105,123,124
$[Ru\{C{\equiv}C\text{-}(E)\text{-}CH{=}CHC_6H_4\text{-}4\text{-}C{\equiv}NRu(NH_3)_5\}(PPh_3)_2(\eta^5\text{-indenyl})]^{3+}$	acetone	315	442	80	105,123,124
$[Fc\text{-}(E)\text{-}CH{=}CHC{\equiv}CRu(PPh_3)_2(\eta^5\text{-indenyl})]$	CH_2Cl_2	273	345	141	105

Table 1.10. (continued) Molecular second-order NLO measurements for metal acetylide complexes.

Complex	Solvent	β^a (10^{-30} esu)	λ_{max} (nm)	β_o (10^{-30} esu)	Ref.
trans-[Ru(C≡CPh)Cl(dppm)$_2$]	thf	20	308	12	132
trans-[Ru(C≡CC$_6$H$_4$-4-NO$_2$)Cl(dppm)$_2$]	thf	767	473	129	132
trans-[Ru(C≡CC$_6$H$_4$-4-C$_6$H$_4$-4-NO$_2$)Cl(dppm)$_2$]	thf	933	465	178	132
trans-[Ru(C≡CC$_6$H$_4$-4-(*E*)-CH=CHC$_6$H$_4$-4-NO$_2$)Cl(dppm)$_2$]	thf	1964	490	235	132
trans-[Ru(C≡C-2-C$_5$H$_4$N)Cl(dppm)$_2$]	thf	35	351	19	132
trans-[Ru(C≡C-2-C$_5$H$_3$N-5-NO$_2$)Cl(dppm)$_2$]	thf	468	490	56	132
[1-(HC≡C)-3,5-C$_6$H$_3${*trans*-C≡CRuCl(dppm)$_2$}$_2$]	thf	< 42	323	< 24	133
[Au(C≡CPh)(PPh$_3$)]	thf	6	268,282,296	4	123,134
[Au(C≡CC$_6$H$_4$-4-NO$_2$)(PPh$_3$)]	thf	22	338	12	123,134
[Au(C≡CC$_6$H$_4$-4-C$_6$H$_4$-4-NO$_2$)(PPh$_3$)]	thf	39	274,287,350	20	123,134
[Au(C≡CC$_6$H$_4$-4-(*E*)-CH=CHC$_6$H$_4$-4-NO$_2$)(PPh$_3$)]	thf	120	303,386	49	123,134
[Au(C≡CC$_6$H$_4$-4-(*Z*)-CH=CHC$_6$H$_4$-4-NO$_2$)(PPh$_3$)]	thf	58	298,362	28	123,134
[Au(C≡CC$_6$H$_4$-4-C≡CC$_6$H$_4$-4-NO$_2$)(PPh$_3$)]	thf	59	301,362	28	123,134
[Au(C≡CC$_6$H$_4$-4-N=CHC$_6$H$_4$-4-NO$_2$)(PPh$_3$)]	thf	85	297,392	34	123,134
[Au(C≡C-2-C$_5$H$_4$N)(PPh$_3$)]	thf	7	300	4	129
[Au(C≡C-2-C$_5$H$_3$N-5-NO$_2$)(PPh$_3$)]	thf	38	339	20	129
[Au(C≡C-2-C$_5$H$_3$N-5-NO$_2$)(PMe$_3$)]	thf	12	340	6	129
[1,3,5-C$_6$H$_3$(C≡CAuPPh$_3$)$_3$]	thf	6	298	4	133

Table 1.10. (continued) Molecular second-order NLO measurements for metal acetylide complexes.

Complex	Solvent	β^a (10^{-30} esu)	λ_{max} (nm)	β_o (10^{-30} esu)	Ref.
$[Ni(C{\equiv}CPh)(PPh_3)(\eta^5\text{-}C_5H_5)]$	thf	24[b]	307	15	135
$[Ni(C{\equiv}CC_6H_4\text{-}4\text{-}NO_2)(PPh_3)(\eta^5\text{-}C_5H_5)]$	thf	221	368,439	59	135
$[Ni(C{\equiv}CC_6H_4\text{-}4\text{-}C_6H_4\text{-}4\text{-}NO_2)(PPh_3)(\eta^5\text{-}C_5H_5)]$	thf	193	263,310,413	65	135
$[Ni(C{\equiv}CC_6H_4\text{-}4\text{-}(E)\text{-}CH{=}CHC_6H_4\text{-}4\text{-}NO_2)(PPh_3)(\eta^5\text{-}C_5H_5)]$	thf	445	313,437	120	135
$[Ni(C{\equiv}CC_6H_4\text{-}4\text{-}(Z)\text{-}CH{=}CHC_6H_4\text{-}4\text{-}NO_2)(PPh_3)(\eta^5\text{-}C_5H_5)]$	thf	145	307,417	47	135
$[Ni(C{\equiv}CC_6H_4\text{-}4\text{-}C{\equiv}CC_6H_4\text{-}4\text{-}NO_2)(PPh_3)(\eta^5\text{-}C_5H_5)]$	thf	326	313,417	106	135
$[Ni(C{\equiv}CC_6H_4\text{-}4\text{-}N{=}CHC_6H_4\text{-}4\text{-}NO_2)(PPh_3)(\eta^5\text{-}C_5H_5)]$	thf	387	282,448	93	135
$[Ni(C{\equiv}C\text{-}2\text{-}C_5H_4N)(PPh_3)(\eta^5\text{-}C_5H_5)]$	thf	25	415	8	129
$[Ni(C{\equiv}C\text{-}2\text{-}C_5H_3N\text{-}5\text{-}NO_2)(PPh_3)(\eta^5\text{-}C_5H_5)]$	thf	186	456	41	129
$[1\text{-}(C{\equiv}C)\text{-}3,5\text{-}C_6H_3\{C{\equiv}CNi(PPh_3)(\eta^5\text{-}C_5H_5)\}_2]$	thf	94	316	55	133

[a] Uncertainty of ±10%. Measured by HRS at 1.06 μm. [b] Uncertainty of ±20%. [c] Measured by EFISH at 1.06 μm.[d] Measured by HRS at 1.54 μm.

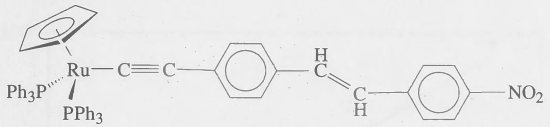

$\beta = 1464$; $\beta_0 = 234 \times 10^{-30}$ esu

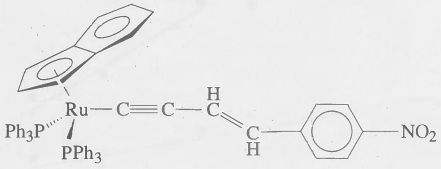

$\beta = 1257$; $\beta_0 = 89 \times 10^{-30}$ esu

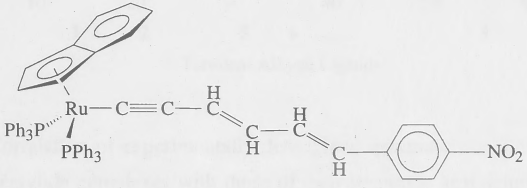

$\beta = 1320$; $\beta_0 = 34 \times 10^{-30}$ esu

Figure 1.13. Acetylide complexes with large β.

Trends observed in chromophore variation are consistent across the ruthenium, gold and nickel complexes. Figure 1.14. shows the relative merit of these varying ligated metal centres, with the $Ru(PPh_3)_2(\eta^5\text{-}C_5H_5)$ unit ten and three times as efficient as the $Au(PPh_3)$ and $Ni(PPh_3)(\eta^5\text{-}C_5H_5)$ moieties, respectively (experimental data).

These structural changes involve the donor group of a donor-bridge-acceptor system; it was therefore expected that a more electron donating (electron rich) ligand at the donor metal would increase the molecular hyperpolarizability. This was confirmed in the substitution of cyclopentadienyl by the more electron rich indenyl group for $[Ru(C{\equiv}CC_6H_4\text{-}4\text{-}NO_2)(PPh_3)_2(\eta^5\text{-}C_5H_4R)]$ (R = H, C_4H_7). Further modification in the ligand environment of the metal centre to include four phosphorus centres (as in $[Ru(C{\equiv}CC_6H_4\text{-}4\text{-}NO_2)Cl(dppm)_2]$) leads to an increase in the molecular hyperpolarizability. However, the replacement of triphenylphosphine by the stronger base trimethylphosphine for the

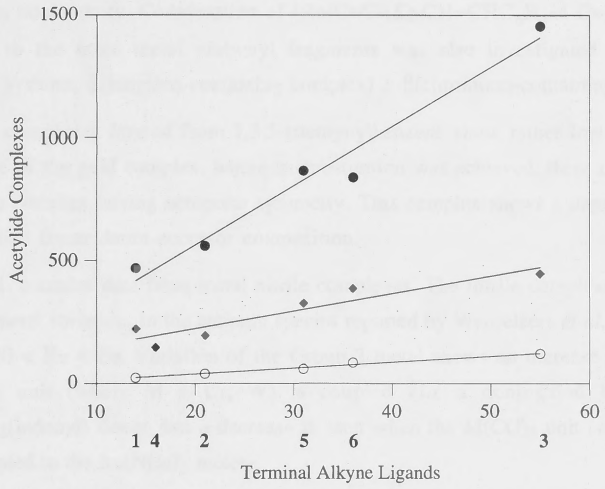

Figure 1.14. Correlation of experimentally determined quadratic nonlinearities of metal acetylide complexes with those of their precursor acetylenes; ◦ [Au(C≡CR)(PPh_3)], ♦ [Ni(C≡CR)(PPh_3)(η^5-C_5H_5)], • [Ru(C≡CR)(PPh_3)$_2$(η^5-C_5H_5)]; (R = 4-$C_6H_4NO_2$, **1**; 4,4'-$C_6H_4C_6H_4NO_2$, **2**; (*E*)-4,4'-$C_6H_4CH{=}CHC_6H_4NO_2$, **3**; (*Z*)-4,4'-$C_6H_4CH{=}CHC_6H_4NO_2$, **4**; 4,4'-$C_6H_4C{\equiv}CC_6H_4NO_2$, **5**; 4,4'-$C_6H_4N{=}CHC_6H_4NO_2$ **6**).

complexes [Ru(C≡CC_6H_4-4-NO_2)L_2(η^5-C_5H_5)] (L = PPh_3, PMe_3) resulted in a decrease of the observed hyperpolarizability; this result is consistent with the recent report that *N*-phenyl substitution of 4-nitroaniline produces a greater increase in β than *N*-methyl substitution,[136] but further data assessing ligand replacement are required to confirm this observation.

Chain lengthening in proceeding from [Ru(C≡CC_6H_4-4-NO_2)(PPh_3)$_2$(η^5-indenyl)] to [Ru(C≡C-(*E*)-CH=CHC_6H_4-4-NO_2)(PPh_3)$_2$(η^5-indenyl)] and then [Ru(C≡C-(*E*)-CH=CH-(*E*)-CH=CHC_6H_4-4-NO_2)(PPh_3)$_2$(η^5-indenyl)] leads to a dramatic increase in observed nonlinearity upon introduction of the first ene-linkage, but results in no significant difference upon introduction of the second alkene group. Surprisingly, examination of the two-level corrected data reveals a dramatic *decrease* in nonlinearity upon stepwise

introduction of the ene-linkers. Coordination of the free pyridine in [Ru(C≡C-(*E*)-CH=CH-4-C_5H_4N)$(PPh_3)_2(\eta^5$-indenyl)] to $M(CO)_5$ (M = Cr, W) centres leads to a substantial increase in nonlinearity. Coordination of [Ru(C≡C-(*E*)-CH=CHC_6H_4-4-C≡N)$(PPh_3)_2(\eta^5$-indenyl)] to the same metal carbonyl fragments was also investigated and, for both bimetallic systems, β(tungsten-containing complex) > β(chromium-containing complex).

Acetylide complexes formed from 1,3,5-triethynylbenzene show rather low nonlinearities. In the case of the gold complex, where tri-substitution was achieved, there is no molecular dipole, the complex having octopolar symmetry. This complex shows a departure from the much-studied linear donor-acceptor composition.

Table 1.11. contains data from metal nitrile complexes. The nitrile complexes reveal some trends in metal variation. In the cationic species reported by Wenseleers *et al*,[137] β increases as Co < Ni < Ru < Fe. Variation of the Group 3 metal shows an increase in β when the $M(CO)_5$ unit (where M = Cr, W) is coupled *via* a conjugated bridge to the $Ru(PPh_3)_2$(indenyl) donor, but a decrease is seen when the $M(CO)_5$ unit (where M = Mo, W) is coupled to the $Ru(NH_3)_5$ moiety.

Given the increased nonlinearities obtained by incorporating one metal into organic chromophores, it is not surprising that introduction of two metals has been assayed. Examples have been met in earlier Tables organized by various metal-ligand groupings, but Table 1.12. contains collected data for all bimetallic complexes for which β values have been reported. Figure 1.15. displays representative examples with large nonlinearities.

The complex [Ru{C≡NRu$(NH_3)_5$}$(PPh_3)_2(\eta^5$-$C_5H_5)$][$CF_3SO_3]_3$ is a mixed valence Ru^{II}/Ru^{III} compound. The very large β value reported in 1993[138] has been revised down quite substantially.[139] The discrepancy was attributed to fluorescence, alerting many to the problems associated with this phenomenon. Results with the sesquifulvalene complexes in Figure 1.15. have been mentioned above and are strongly resonance enhanced. The difference in measured β values for the two tabulated examples suggests that the triple bond linkage leads to a higher nonlinearity than the double bond linkage; however, the two-level corrected β_0 values do not support this conclusion. The two ferrocene derivatives containing the dimesitylboranyl acceptor group show that there is a marked effect on nonlinearity observed upon replacing a triple bond by a double bond, with a significantly smaller |β| for the triple bond-containing complex. As both complexes were measured far from resonance and have very similar λ_{max} values, an ene- vesus yne-linkage comparison seems valid in this instance. The series of ferrocenyl bimetallic complexes with group 10 metals has been discussed previously; while ligated nickel is a poor acceptor, replacing $PdCl_2$ by $PtCl_2$ has only a weak influence on the measured nonlinearity.

Table 1.11. Molecular second-order NLO measurements for metal nitrile complexes.

Complex	Solvent	β^a (10^{-30} esu)	λ_{max} (nm)	β_o (10^{-30} esu)	Ref.
$[Ni(N{\equiv}CC_6H_4\text{-}4\text{-}Ph)(PPh_3)(\eta^5\text{-}C_5H_5)]^+$	MeOH	17	267		137,140
	$CHCl_3$	18	282		137
$[Ni(N{\equiv}CC_6H_4\text{-}4\text{-}NMe_2)(PPh_3)(\eta^5\text{-}C_5H_5)]^+$	MeOH	18	291		137,140
	$CHCl_3$	14	298		137
$[Ni(N{\equiv}CC_6H_4\text{-}4\text{-}C_6H_4\text{-}4\text{-}NO_2)(PPh_3)(\eta^5\text{-}C_5H_5)]^+$	$CHCl_3$	45	299		137
$[Ni(N{\equiv}CC_6H_4\text{-}4\text{-}NO_2)(PPh_3)(\eta^5\text{-}C_5H_5)]^+$	$CHCl_3$	93	419		137
$[Co(N{\equiv}CC_6H_4\text{-}4\text{-}Ph)(dppe)(\eta^5\text{-}C_5H_5)]^{2+}$	MeOH	<25	298		137
$[Co\{N{\equiv}CC_6H_4\text{-}4\text{-}NMe_2)(dppe)(\eta^5\text{-}C_5H_5)]^{2+}$	MeOH	<40	332		137
$[Co(N{\equiv}CC_6H_4\text{-}4\text{-}C_6H_4\text{-}4\text{-}NO_2)(dppe)(\eta^5\text{-}C_5H_5)]^{2+}$	MeOH	~35	420		137
$[Co(N{\equiv}CC_6H_4\text{-}4\text{-}NO_2)(dppe)(\eta^5\text{-}C_5H_5)]^{2+}$	MeOH	~45	419		137
$[Ru(N{\equiv}CC_6H_4\text{-}4\text{-}C_6H_4\text{-}4\text{-}NO_2)(dppe)(\eta^5\text{-}C_5H_5)]^+$	MeOH	96	288		137
	$CHCl_3$	85	293		137
$[Ru(N{\equiv}CC_6H_4\text{-}4\text{-}NO_2)(dppe)(\eta^5\text{-}C_5H_5)]^+$	MeOH	138	358		137
	$CHCl_3$	126	358		137
$[Fe(N{\equiv}CC_6H_4\text{-}4\text{-}C_6H_4\text{-}4\text{-}NO_2)(dppe)(\eta^5\text{-}C_5H_5)]^+$	MeOH	276	375		137
	$CHCl_3$	240	372		137
$[Fe(N{\equiv}CC_6H_4\text{-}4\text{-}NO_2)(dppe)(\eta^5\text{-}C_5H_5)]^+$	MeOH	410	468		137
	$CHCl_3$	375	460		137

Table 1.11. (continued) Molecular second-order NLO measurements for metal nitrile complexes.

Complex	Solvent	β^a (10^{-30} esu)	λ_{max} (nm)	β_o (10^{-30} esu)	Ref.
$[Ru\{C{\equiv}NRu(NH_3)_5\}(PPh_3)_2(\eta^5\text{-}C_5H_5)][CF_3SO_3]_3$	H_2O	1080	~700		138
	$MeNO_2$	157	716	69	141
$[Ru\{C{\equiv}NOs(NH_3)_5\}(PPh_3)_2(\eta^5\text{-}C_5H_5)]^{3+}$	dmso	65	440	16	141
$[Mo\{C{\equiv}NRu(NH_3)_5\}(CO)_5]^{2+}$	acetone	225	693	90	141
$[W\{C{\equiv}NRu(NH_3)_5\}(CO)_5]^{2+}$	acetone	130	708	56	141
$[Ru(C{\equiv}N)(PPh_3)_2(\eta^5\text{-indenyl})]$	CH_2Cl_2	13	396	5	105
$[Ru\{C{\equiv}NCr(CO)_5\}(PPh_3)_2(\eta^5\text{-indenyl})]$	CH_2Cl_2	25	392	10	105,123,124
$[Ru\{C{\equiv}NW(CO)_5\}(PPh_3)_2(\eta^5\text{-indenyl})]$	CH_2Cl_2	40	392	15	105,123,124
$[Ru\{C{\equiv}NRu(NH_3)_5\}(PPh_3)_2(\eta^5\text{-indenyl})]^{3+}$	acetone	108	621	26	105,123,124
$[Ru\{C{\equiv}C\text{-}(E)\text{-}CH{=}CHC_6H_4\text{-}4\text{-}C{\equiv}NCr(CO)_5\}(PPh_3)_2(\eta^5\text{-indenyl})]$	CH_2Cl_2	465	442	119	105,123,124
$[Ru\{C{\equiv}C\text{-}(E)\text{-}CH{=}CHC_6H_4\text{-}4\text{-}C{\equiv}NW(CO)_5\}(PPh_3)_2(\eta^5\text{-indenyl})]$	CH_2Cl_2	700	456	150	105,123,124
$[Ru\{C{\equiv}C\text{-}(E)\text{-}CH{=}CHC_6H_4\text{-}4\text{-}C{\equiv}NRu(NH_3)_5\}(PPh_3)_2(\eta^5\text{-indenyl})]^{3+}$	acetone	315	442	80	105,123,124
$[Fc\text{-}(E)\text{-}CH{=}CHC_6H_4\text{-}4\text{-}C{\equiv}NCr(CO)_5]$	$CHCl_3$	271	481	39	102
$[Fc\text{-}(E)\text{-}CH{=}CHC_6H_4\text{-}4\text{-}C{\equiv}NW(CO)_5]$	$CHCl_3$	375	487	48	102

[a] Measured by HRS at 1.06 μm

Some of the ruthenium indenyl complexes have also been discussed above; their nonlinearities are amongst the largest observed for bimetallic complexes. The differences observed between the bimetallic compounds and their precursor monometallic complexes can be explained by the differences in the effectiveness of the metal σ-acceptor groups; the metal may usefully tune and in many instances enhance the NLO response. For the ruthenium indenyl complexes, the tungsten-containing complexes have larger hyperpolarizabilities than their chromium analogues, probably due to the electron density at tungsten being better reduced by back donation to carbonyl ligands than it is at chromium.

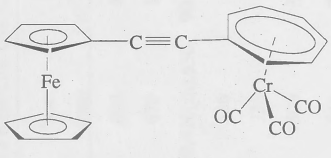

$\beta = 570$; $\beta_0 = 105 \times 10^{-30}$ esu

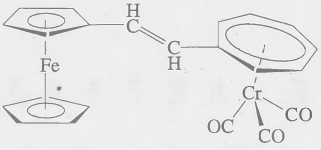

$\beta = 320$; $\beta_0 = 113 \times 10^{-30}$ esu

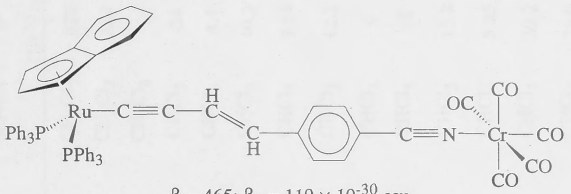

$\beta = 465$; $\beta_0 = 119 \times 10^{-30}$ esu

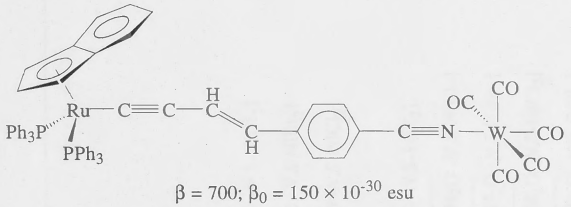

$\beta = 700$; $\beta_0 = 150 \times 10^{-30}$ esu

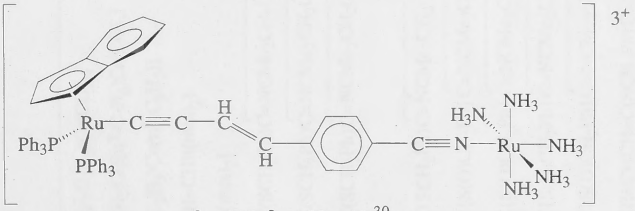

$\beta = 315$; $\beta_0 = 80 \times 10^{-30}$ esu

Figure 1.15. Bimetallic complexes with large β.

Table 1.12. Molecular second-order NLO measurements for bimetallic complexes.

Complex	Solvent	β^a (10^{-30} esu)	λ_{max} (nm)	β_o (10^{-30} esu)	Technique	Fund. (μm)	Ref.
[FcC≡C(η^7-C_7H_6)Cr(CO)$_3$]	CH_2Cl_2	570	600	105	HRS	1.06	106
[Fc-(*E*)-CH=CH(η^7-C_7H_6)Cr(CO)$_3$]	CH_2Cl_2	320	670	113	HRS	1.06	106
[Fc(η^6-BC_5H_5)Co(η^5-C_5H_5)]	CH_2Cl_2		370,410(sh),650	90 ± 30	HRS	1.06	108
[Fc-(*E*)-CH=CHB(mes)$_2$]	$CHCl_3$	-24	336		EFISH	1.91	109
[FcC≡CB(mes)$_2$]	$CHCl_3$	4.4	336		EFISH	1.91	109
[FcCH=C(SCH$_2$Ph)C=NCMe$_2$CH$_2$O -*N*,*S*-NiCl$_2$]	$CHCl_3$	10.3	500	3.92	EFISH	1.34	112,113
[FcCH=C(SCH$_2$Ph)C=NCMe$_2$CH$_2$O -*N*,*S*-NiBr$_2$]	$CHCl_3$	7.14	511	2.55	EFISH	1.34	112,113
[FcCH=C(SCH$_2$Ph)C=NCMe$_2$CH$_2$O -*N*,*S*-PdCl$_2$]	$CHCl_3$	12.2	530	4.13	EFISH	1.34	111-113
	$CHCl_3$	9	530	6	EFISH	1.91	112,113
[FcCH=C(SCH$_2$Ph)C=NCMe$_2$CH$_2$O -*N*,*S*-PtCl$_2$]	$CHCl_3$	16	523	5.2	EFISH	1.34	112,113
[FcCH=C{S(O)CH$_2$Ph}C=NCMe$_2$CH$_2$O -*N*,*S*-NiCl$_2$]	$CHCl_3$	15.8	498	6.0	EFISH	1.34	112,113
[FcCH=C{S(O)CH$_2$Ph}C=NCMe$_2$CH$_2$O -*N*,*S*-NiBr$_2$]	$CHCl_3$	5.85	494	2.3	EFISH	1.34	112,113
[FcCH=C{S(O)CH$_2$Ph}C=NCMe$_2$CH$_2$O -*N*,*S*-PdCl$_2$]	$CHCl_3$	30.2	540	7.6	EFISH	1.34	111-113
[FcCH=C{S(O)CH$_2$Ph}C=NCMe$_2$CH$_2$O -*N*,*S*-PtCl$_2$]	$CHCl_3$	28.0	548	7.7	EFISH	1.34	112,113
[Fc-(*E*)-CH=CHCH=C(SCH$_2$Ph)C=NCMe$_2$CH$_2$O -*N*,*S*-PdCl$_2$]	$CHCl_3$	58	567	14	EFISH	1.34	112,113
	$CHCl_3$	18.2	567	10.8	EFISH	1.91	112,113
[Fc-(*E*)-CH=CHCH=C{S(O)CH$_2$Ph}C=NCMe$_2$CH$_2$O -*N*,*S*-PdCl$_2$]	$CHCl_3$	123.5	602	19	EFISH	1.34	112,113

Table 1.12. (continued) Molecular second-order NLO measurements for bimetallic complexes.

Complex	Solvent	β^a (10^{-30} esu)	λ_{max} (nm)	β_o (10^{-30} esu)	Technique	Fund. (μm)	Ref.
$[FcC{\equiv}CCH{=}C(SCH_2Ph)\overline{C{=}NCMe_2CH_2O}\text{-}N,S\text{-}PdCl_2]$	$CHCl_3$	33.6	558	8.5	EFISH	1.34	112,113
$[Fc\text{-}2\text{-}C_4H_3S\{Mn(CO)_3\}][BF_4]$	CH_3NO_2	260	514	13	HRS	1.06	110
$[Fc\text{-}(E)\text{-}CH{=}CH\text{-}2\text{-}C_4H_3S\{Mn(CO)_3\}][BF_4]$	CH_3NO_2	670	536	-8	HRS	1.06	110
$[Fc\text{-}((E)\text{-}CH{=}CH)_2\text{-}2\text{-}C_4H_3S\{Mn(CO)_3\}][BF_4]$	CH_3NO_2	771	548	-34	HRS	1.06	110
$[Fc\text{-}(E)\text{-}CH{=}CH\text{-}3\text{-}C_4H_3S\{Mn(CO)_3\}][BF_4]$	CH_3NO_2	305	480	45	HRS	1.06	110
$[FcCH_2\text{-}2\text{-}C_4H_3S\{Mn(CO)_3\}][BF_4]$	CH_3NO_2	220			HRS	1.06	110
$[Ru\{C{\equiv}NRu(NH_3)_5\}(PPh_3)_2(\eta^5\text{-}C_5H_5)][CF_3SO_3]_3$	H_2O	1080[b]	~700		HRS	1.06	138
	CH_3NO_2	157	716	69	HRS	1.06	141
	MeOH	33			HRS	1.06	139
$[Ru\{C{\equiv}NOs(NH_3)_5\}(PPh_3)_2(\eta^5\text{-}C_5H_5)]^{3+}$	dmso	65	440	16	HRS	1.06	141
$[Mo\{C{\equiv}NRu(NH_3)_5\}(CO)_5]^{2+}$	acetone	225	693	90	HRS	1.06	141
$[W\{C{\equiv}NRu(NH_3)_5\}(CO)_5]^{2+}$	acetone	130	708	56	HRS	1.06	141
$[Ru\{C{\equiv}NCr(CO)_5\}(PPh_3)_2(\eta^5\text{-indenyl})]$	CH_2Cl_2	25	392	10	HRS	1.06	105,123,124
$[Ru\{C{\equiv}NW(CO)_5\}(PPh_3)_2(\eta^5\text{-indenyl})]$	CH_2Cl_2	40	392	15	HRS	1.06	105,123,124
$[Ru\{C{\equiv}NRu(NH_3)_5\}(PPh_3)_2(\eta^5\text{-indenyl})]^{3+}$	acetone	108	621	26	HRS	1.06	105,123,124
$[Ru\{C{\equiv}C\text{-}(E)\text{-}CH{=}CHC_6H_4\text{-}4\text{-}C{\equiv}NCr(CO)_5\}(PPh_3)_2(\eta^5\text{-indenyl})]$	CH_2Cl_2	465	442	119	HRS	1.06	105,123,124
$[Ru\{C{\equiv}C\text{-}(E)\text{-}CH{=}CHC_6H_4\text{-}4\text{-}C{\equiv}NW(CO)_5\}(PPh_3)_2(\eta^5\text{-indenyl})]$	CH_2Cl_2	700	456	150	HRS	1.06	105,123,124
$[Ru\{C{\equiv}C\text{-}(E)\text{-}CH{=}CHC_6H_4\text{-}4\text{-}C{\equiv}NRu(NH_3)_5\}(PPh_3)_2(\eta^5\text{-indenyl})]^{3+}$	acetone	315	442	80	HRS	1.06	105,123,124

[a] Uncertainty of ±10% except where indicated. [b] No uncertainty reported.

Table 1.13. contains data for organometallic complexes not falling into one of the categories above. The nonlinearities of the chloro complexes were used in conjunction with those of terminal acetylenes to demonstrate the importance of electronic comunication between ligated metal and acetylide ligand in derivative metal acetylide complexes formed from combining these precursors.[126,134,135] Evaluation of vinylidene, as with sesquifulvalene and carbene, is only experimentally straightforward following metal complexation. The vinylidene cation $[Ru(C{=}CHC_6H_4\text{-}4\text{-}NO_2)(PPh_3)_2(\eta^5\text{-indenyl})]^+$ can be directly compared to its parent acetylide complex $[Ru(C{\equiv}CC_6H_4\text{-}4\text{-}NO_2)(PPh_3)_2(\eta^5\text{-indenyl})]$; the corrected nonlinearity of the vinylidene is large, but less than half that of the acetylide. While the ligated metal centre in the acetylide complex is the donor in a classical donor-bridge-acceptor composition, the vinylidene metal-bound carbon is electron deficient, and the complex cation therefore has two potential acceptors. To assess the merit of vinylidene complexes as NLO materials, evaluation of a complex bearing an electron-donating phenylvinylidene ligand would be of interest.

The 16 electron square planar palladium and platinum complexes show low responses. The reported figures suggest that: (i) the platinum complex has a larger nonlinearity than its palladium analogue, (ii) the triphenylphosphine ligand leads to higher nonlinearities than triethylphosphine (consistent with results above for ruthenium acetylides bearing PPh_3 or PMe_3 ligands), (iii) the nitro group, not surprisingly, leads to higher nonlinearities than the formyl group which is a much poorer acceptor, and (iv) the iodo ligand leads to lower nonlinearities than the bromo ligand. As the measured nonlinearities are all low, conclusions from this series of complexes should be viewed as tentative.

Table 1.13. Molecular second-order NLO measurements for other complexes.

Complex	Solvent	β^a (10^{-30} esu)	λ_{max}	β_0 (10^{-30} esu)	Technique	Fund. (μm)	Ref.
$[NiCl(PPh_3)(\eta^5\text{-}C_5H_5)]$	thf	89	263,330	45	HRS	1.06	135
$[RuCl(PPh_3)_2(\eta^5\text{-}C_5H_5)]$	thf	< 7	357	< 4	HRS	1.06	127
$[Ru(C{\equiv}N)(PPh_3)_2(\eta^5\text{-indenyl})]$	CH_2Cl_2	13	396	5	HRS	1.06	105,123,124
$[Ru(C{=}CHC_6H_4\text{-}4\text{-}NO_2)(PPh_3)_2(\eta^5\text{-indenyl})]^+$	CH_2Cl_2	116	379	50	HRS	1.06	105,123,124
$[Ru\{C{=}C{=}C(2,7\text{-dimethyl-}4,5\text{-benzocycloheptatrienylidene})_2\}(PPh_3)_2(\eta^5\text{-}C_5H_5)][PF_6]$	CH_3CN	120	590	19	HRS	1.06	131
trans-$[PdI(C_6H_4\text{-}4\text{-}NO_2)(PEt_3)_2]$	$CHCl_3$	0.5			EFISH	1.91	99
trans-$[PdI(C_6H_4\text{-}4\text{-}NO_2)(PPh_3)_2]$	$CHCl_3$	1.5			EFISH	1.91	99
trans-$[PtBr(C_6H_4\text{-}4\text{-CHO})(PEt_3)_2]$	$CHCl_3$	2.1			EFISH	1.91	99
trans-$[PtBr(C_6H_4\text{-}4\text{-}NO_2)(PEt_3)_2]$	$CHCl_3$	3.8			EFISH	1.91	99
trans-$[PtI(C_6H_4\text{-}4\text{-}NO_2)(PEt_3)_2]$	$CHCl_3$	1.7			EFISH	1.91	99

[a] Uncertainty of ±10%.

1.5. ORGANOMETALLICS FOR THIRD-ORDER NONLINEAR OPTICS

The Tables in this Section contain data from approximately 40 research papers that have mostly employed THG, DFWM or Z-scan techniques to measure the third-order hyperpolarizabilities of organometallic complexes.

The first investigation of the third-order nonlinearity of an organotransition metal complex was of ferrocene, and functionalized and polymeric metallocenes continue to attract interest (Table 1.14.). Metallocenes were studied originally due to the belief that interaction of an organic π-electron system with a metal would cause distortion of the π-electron system and influence the nonlinearity. With this idea in mind, the archetypical metallocene ferrocene has been measured a number of times. The earliest values obtained by optical power limiting (OPL) measurements[142] are very high compared to subsequent measurements performed by DFWM (and THG on the dibutylated ferrocene $[Fe(\eta^5\text{-}C_5H_4Bu^n)_2]$);[143] these disparities in data are perhaps a function of the measurement technique, as OPL is carried out on a nanosecond time-scale and the higher nonlinearity which was observed may include a contribution from thermal effects. Unlike the other class of complex studied intensively (acetylides: see below), results with the ferrocenyl complexes show no significant imaginary contribution, and the real part of γ is positive.[144]

Organic substitution on the ferrocene cyclopentadienyl rings invariably increases the observed nonlinearity. The styrylferrocene complex has a much larger γ than the sum of its component molecules, ferrocene and styrene ($16.9 \pm 0.8 \times 10^{-36}$ esu),[144] suggesting that electronic communication between these components is important for optical nonlinearity. A significant increase in γ is observed on formylation of the ring remote from the chromophore for ferrocenyl complexes, but permethylation of the remote ring in $[Ru(\eta^5\text{-}C_5R_5)(\eta^5\text{-}C_5H_4\text{-}(E)\text{-}CH{=}CHC_6H_4\text{-}4\text{-}NO_2)]$ or replacement of a vinylic proton by a cyano group leads only to minor or no variation in γ.

Large nonlinearities with monomeric ferrocenes has led some investigators to examine oligomeric and polymeric ferrocenes. However, the nonlinearity of the oligomer incorporating 6-8 ferrocenyl groups is not significantly larger than that of the corresponding dimer. In this system, the increased π-electron conjugation in the oligomer has not significantly enhanced the nonlinearity, suggesting that the ferrocenyl linking groups are not effectively coupling the organic components. These results are similar to those seen in second-order nonlinear optical studies which were rationalized as arising from poor coupling between the metal centre and the substituent. The dominant contribution to

the third-order nonlinearity in ferrocene comes not from the lowest lying *d-d* transition, but from a combination of d-π^* and π-π^* levels;[144] the π-geometry of the metal-cyclopentadienyl interaction decreases the contribution of the metal to the nonlinearity.[98]

The effect of metal replacement has not been established with certainty. Direct comparison of ferrocene complexes with analogous ruthenocene complexes is only possible for the parent compounds, with ruthenocene having a slightly larger cubic nonlinearity.[145,146] This result needs to be treated cautiously, as the technique employed (OPL) is susceptible to thermal contributions (see above), and the low nonlinearities of the complexes induce substantial errors. The differing fundamental frequencies employed in the metallocenyl complex measurements further complicates the results, necessitating caution when carrying out comparisons.

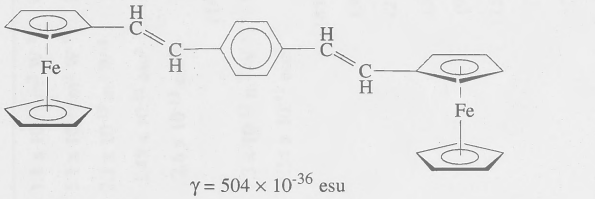

$\gamma = 504 \times 10^{-36}$ esu

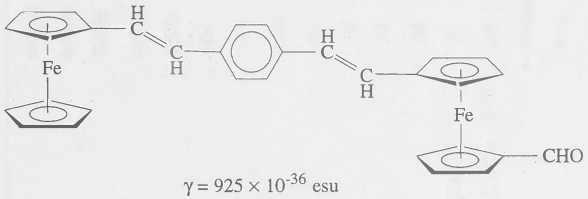

$\gamma = 925 \times 10^{-36}$ esu

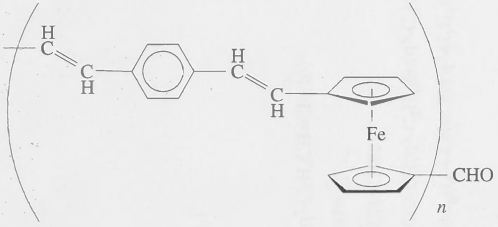

$\gamma = 1550 \times 10^{-36}$ esu

Figure 1.16. Ferrocenyl complexes with large γ.

Table 1.14. Third-order NLO measurements of ferrocenyl and ruthenocenyl complexes.

Complex	Solvent	n_2	γ	λ_{max} (nm)	Technique	Fund. (μm)	Ref.
[FcH]	molten	1.1×10^{-17} m^2 W^{-1}	4.4×10^{-45} m^5 V^{-2}	*a*	OPL	1.06	142
	molten	1.1×10^{-17} m^2 W^{-1}	2.9×10^{-45} m^5 V^{-2}	*a*	OPL	1.06	145
	EtOH	2.1×10^{-19} m^2 W^{-1}	3.9×10^{-45} m^5 V^{-2}	*a*	OPL	1.06	142
	molten	1.48×10^{-11} esu[b]	3.9×10^{-32} esu	*a*	OPL	1.06	146
	EtOH	2.6×10^{-13} esu[b]	1.2×10^{-32} esu	*a*	OPL	1.06	146
	thf		$(16.1 \pm 1.8) \times 10^{-36}$ esu	439.6	DFWM	0.60	144
[Fe(η^5-$C_5H_4SiMe_3$)$_2$]	neat	1.3×10^{-17} m^2 W^{-1}	5.5×10^{-45} m^5 V^{-2}	*a*	OPL	1.06	142,145
	neat	1.51×10^{-11} esu[b]	6.4×10^{-32} esu	*a*	OPL	1.06	146
[FcCH=CHPh)]	thf		$(85.5 \pm 19.8) \times 10^{-36}$ esu	445	DFWM	0.60	144
[Fe(η^5-C_5H_4CHO)(η^5-C_5H_4CH=CHPh)][c]	thf		$(305 \pm 36) \times 10^{-36}$ esu	462.4	DFWM	0.60	144
[Fe(η^5-C_5H_4CH=CHPh)$_2$][c]	thf		$(270 \pm 26) \times 10^{-36}$ esu	460.8	DFWM	0.60	144
[FcCH=CHC_6H_4-4-CH=CHFc][c]	thf		$(504 \pm 52) \times 10^{-36}$ esu	451.8	DFWM	0.60	144
[FcCH=CHC_6H_4-4-CH=CH(η^5-C_5H_4)Fe(η^5-C_5H_4CHO)][c]	thf		$(925 \pm 86) \times 10^{-36}$ esu	454.8	DFWM	0.60	144
[Fe(η^5-C_5H_4CH=CHC_6H_4-4-CH=CH)(η^5-C_5H_4)]$_n$CHO n = 6-8[c]	thf		$(1550 \pm 270) \times 10^{-36}$ esu	451.5	DFWM	0.60	144
[FcCOCH$_3$]	*p*-dioxane		$(27 \pm 3) \times 10^{-36}$ esu	*a*	THG	1.91	73,99
[Fe(η^5-$C_5H_4Bu^n$)$_2$]	neat		$(25 \pm 4) \times 10^{-36}$ esu	*a*	THG	1.91	143
[FcC≡CC≡CC≡CFc]	$CHCl_3$		110×10^{-36} esu	*a*	THG	1.91	147

Table 1.14. (continued) Third-order NLO measurements of ferrocenyl and ruthenocenyl complexes.

Complex	Solvent	n_2	γ	λ_{max} (nm)	Technique	Fund. (μm)	Ref.
$[Ru(\eta^5\text{-}C_5H_5)_2]$	molten	3.3×10^{-11} esu	3.9×10^{-45} m^5 V^{-2}		OPL	1.06	146
	molten	2.2×10^{-17} m^2 W^{-1}	3.9×10^{-45} m^5 V^{-2}		OPL	1.06	145
$[Ru(\eta^5\text{-}C_5H_5)(\eta^5\text{-}C_5H_4\text{-}(E)\text{-}CH{=}CHC_6H_4\text{-}4\text{-}NO_2)]$	*p*-dioxane		$(114 \pm 11) \times 10^{-36}$ esu	350, 390	THG	1.91	73,99
$[Ru(\eta^5\text{-}C_5Me_5)(\eta^5\text{-}C_5H_4\text{-}(E)\text{-}CH{=}CHC_6H_4\text{-}4\text{-}NO_2)]$	*p*-dioxane		$(140 \pm 14) \times 10^{-36}$ esu	370, 424	THG	1.91	73,99
$[Ru(\eta^5\text{-}C_5Me_5)\{\eta^5\text{-}C_5H_4\text{-}(E)\text{-}CH{=}C(CN)C_6H_4\text{-}4\text{-}NO_2\}]$	*p*-dioxane		$(105 \pm 11) \times 10^{-36}$ esu	370, 443	THG	1.91	99

[a] Not reported. [b] n_2 related to the electric field; see reference 146. [c] Stereochemistry not specified.

The group 4 metallocenes in Table 1.15. are formally d^0 16 electron complexes; the most important contributor to optical nonlinearity is therefore the LMCT transition.[143] For the halide complexes, the lowest energy transition is due to cyclopentadienyl to metal charge transfer. Compared to ferrocene, these complexes have very low nonlinearities (even when the cyclopentadienyl rings are methylated). Introduction of a metal-bound vinyl or acetylide ligand results in enhanced π-conjugation involving the cyclopentadienyl-metal bonding network and orbitals of like symmetry on the vinyl/acetylide ligands;[143,148] this has the effect of increasing the nonlinearity significantly. This is not simply an additive effect, the resultant nonlinearities being greater than the sum of those of the precursor chlorides and terminal alkynes.[143] Similarly, the nonlinearity for $[Ti(C{\equiv}CPh)_2(\eta^5\text{-}C_5H_5)_2]$ is three times that of $[Ti(C{\equiv}CPh)Cl(\eta^5\text{-}C_5H_5)_2]$. The divinylbenzene-linked bimetallics $[\{ZrCl(\eta^5\text{-}C_5H_5)_2\}_2(\mu\text{-}(E)\text{-}CH{=}CHC_6H_4\text{-}n\text{-}(X)\text{-}CH{=}CH)]$ ($n = 3$, $X = Z$; $n = 4$, $X = E$) exhibit reasonably large nonlinearities; deconvolution of the contributions to enhancing γ in progressing from *Z* to *E* stereochemistry or 3- to 4-aryl ring substitution in this system requires additional data.

The effect of metal replacement has been probed. Increased γ is observed on progressing up the group, corresponding to increased electron accepting ability of the metal;[143] for d^0 group 4 metals, this has been rationalized by assuming that mixing of titanium orbitals with those of the ligand is more effective than mixing of zirconium or hafnium with the ligand based orbitals.[143]

Tris(cyclopentadienyl) rare earth complexes ($[M(\eta^5\text{-}C_5H_5)_3]$; M = Er, Nd, Pr, Yb) have been measured by DFWM at a fundamental frequency corresponding to $\lambda = 1064$ nm.[151] They possess moderate nonlinearities despite having electronic transitions in the range 800-1550 nm which might have been expected to result in dispersively enhanced values. Solution $\chi^{(3)}{}_{1111}$ for $[Yb(\eta^5\text{-}C_5H_5)_3]$ [the largest nonlinearity of the series, and the complex with λ_{max} (1030 nm) closest to ω] is only about half that of CS_2.

A range of thiophenyl and isobenzothiophenyl group 10 metal complexes have been examined by four-wave mixing at 1064 nm (see Table 1.16.).[152-154] The linear and nonlinear optical properties are highly dependent on the metal; both the wavelength of the optical transition and the magnitude of the second hyperpolarizability decrease on progressing down the group,[154] a trend which mirrors that observed in group 10 metal alkynyl complexes (see below). Although no multiphoton absorption is observed, the magnitudes of the imaginary components are large; for conjugated systems where the degree of polarization is large, appreciable imaginary components resulting from electronic lattice coupling can be observed. Progressing from thiophenyl to the related fused ring isobenzothiophenyl palladium and platinum complexes results in an increased third-order

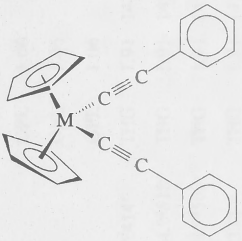

M = Ti: $\gamma = 92 \times 10^{-36}$ esu
= Zr: $\gamma = 58 \times 10^{-36}$ esu
= Hf: $\gamma = 51 \times 10^{-36}$ esu

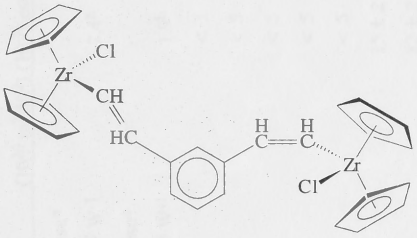

$\gamma = 68 \times 10^{-36}$ esu

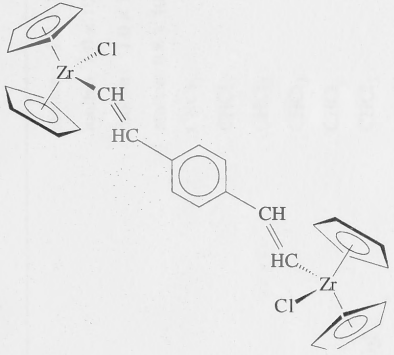

$\gamma = 154 \times 10^{-36}$ esu

Figure 1.17. Group four metallocene complexes with large γ.

Table 1.15. Third-order NLO measurements of other metallocene complexes and tris(cyclopentadienyl) rare earth complexes.

Complex	Solvent	n_2	$\chi^{(3)}$ (10^{20} m^2 V^{-2})	γ (10^{-36} esu)	λ_{max} (nm)	Technique	Fund. (μm)	Ref.
$[HfCl_2(\eta^5\text{-}C_5H_5)_2]$	molten	1.3×10^{-11} esu[a]				OPL	1.06	146
	molten	1.0×10^{-17} m^2 W^{-1}		2.4[b]		OPL	1.06	145
$[ZrCl_2(\eta^5\text{-}C_5H_5)_2]$	molten	1.0×10^{-11} esu[a]				OPL	1.06	146
	molten	0.8×10^{-17} m^2 W^{-1}		1.9[b]		OPL	1.06	145
$[TiF_2(\eta^5\text{-}C_5H_4Me)_2]$	$CHCl_3$			< 3	284,[c]324,[cd]414[e]	THG	1.91	143,148,149
$[TiCl_2(\eta^5\text{-}C_5H_4Me)_2]$	$CHCl_3$			< 5	274,[c]388,[e]394,[cd]518[e]	THG	1.91	143,148,149
$[TiBr_2(\eta^5\text{-}C_5H_4Me)_2]$	$CHCl_3$			< 5	276,[c]328,[c]428,[cd]568[e]	THG	1.91	143,148,149
$[ZrCl_2(\eta^5\text{-}C_5H_5)_2]$	$CHCl_3$			< 5	294,[c]334,[e]338[cd]	THG	1.91	143,148,149
$[HfCl_2(\eta^5\text{-}C_5H_5)_2]$	$CHCl_3$			< 5	306	THG	1.91	148
$[Ti(C{\equiv}CBu^n)_2(\eta^5\text{-}C_5H_4Me)_2]$	$CHCl_3$			15 ± 2		THG	1.91	149
$[Ti(C{\equiv}CBu^n)_2(\eta^5\text{-}C_5H_5)_2]$	$CHCl_3$			12 ± 2	390	THG	1.91	148
$[Ti(C{\equiv}CPh)_2(\eta^5\text{-}C_5H_5)_2]$	thf			92 ± 14	410,[d]416[e]	THG	1.91	143,148
$[Zr(C{\equiv}CPh)_2(\eta^5\text{-}C_5H_5)_2]$	thf			58 ± 9	370,[e]390[d]	THG	1.91	143,148
$[Hf(C{\equiv}CPh)_2(\eta^5\text{-}C_5H_5)_2]$	thf			51 ± 8	358,[e]390[d]	THG	1.91	143,148
$[Ti(C{\equiv}CPh)Cl(\eta^5\text{-}C_5H_5)_2]$	thf			31 ± 5	402,510(sh)	THG	1.91	143,148
$[Zr(CPh{=}CPh{=}CPh{=}CPh(\eta^5\text{-}C_5H_5)_2]$	thf			47 ± 7	370,474	THG	1.91	148
$[ZrCl(CH{=}CHC_6H_4Me)(\eta^5\text{-}C_5H_5)_2)]$[f]	thf			24 ± 4	356	THG	1.91	148

Table 1.15. (continued) Third-order NLO measurements of other metallocene complexes and tricyclopentadienyl rare earth complexes.

Complex	Solvent	n_2	$\chi^{(3)}$ (10^{20} m^2 V^{-2})	γ (10^{-36} esu)	λ_{max} (nm)	Technique	Fund. (μm)	Ref.
[{ZrCl(η^5-C_5H_5)$_2$}$_2$(-μ-(*E*)-CH=CHC_6H_4-3-(*Z*)-CH=CH)]	thf			68 ± 10	356	THG	1.91	148
[{ZrCl(η^5-C_5H_5)$_2$}$_2$(-μ-(*E*)-CH=CHC_6H_4-4-(*E*)-CH=CH)]	thf			154 ± 23	380	THG	1.91	148
[{ZrCl(η^5-C_5H_5)$_2$}$_2$O]	thf			10 ± 2	282	THG	1.91	148
[Yb(η^5-C_5H_5)$_3$]	thf	4.3-4.5 × 10^{-11} esu			1030	OPL	1.06	150
	thf		1.3		1030	DFWM	1.06	151
[Nd(η^5-C_5H_5)$_3$]	thf		0.43		910	DFWM	1.06	151
[Dy(η^5-C_5H_5)$_3$]	thf		0.19		1260	DFWM	1.06	151
[Er(η^5-C_5H_5)$_3$]	thf		< 0.1		660	DFWM	1.06	151
[Pr(η^5-C_5H_5)$_3$]	thf		< 0.1		1395	DFWM	1.06	151

[a] n_2 related to the electric field; see reference 146. [b] Units are 10^{-45} V^{-2} m^5. [c] Reference 149. [d] Reference 143. [e] Reference 148. [f] Geometry not specified.

Table 1.16. Third-order NLO measurements of thiophenyl and isobenzothiophenyl complexes.

Complex	Solvent	λ_{max} (nm)	Re γ (10^{-46} m^5 V^{-2})	|Im γ| (10^{-46} m^5 V^{-2})	|γ| (10^{-46} m^5 V^{-2})	Technique	Fund. (μm)	Ref.
$[Ni(2\text{-}C_4H_3S)_2(PEt_3)_2]$	$CHCl_3$	374	-5.1	4.6	6.8	DFWM	1.06	152-154
$[Pd(2\text{-}C_4H_3S)_2(PEt_3)_2]$	$CHCl_3$	330	-0.69	1.3	1.5	DFWM	1.06	152-154
$[Pt(2\text{-}C_4H_3S)_2(PEt_3)_2]$	$CHCl_3$	320	-0.25	0.60	0.65	DFWM	1.06	152-154
$[Ni(2\text{-}C_8H_5S)_2(PBu^n{}_3)_2]$	$CHCl_3$	388	-2 - -1	3-10	3-10	DFWM	1.06	152-154
$[Ni(2\text{-}C_8H_5S)_2(PEt_3)_2]$	$CHCl_3$	370	-2.8	1.5	3.1	DFWM	1.06	153
$[Pd(2\text{-}C_8H_5S)_2(PEt_3)_2]$	$CHCl_3$	370	-2.1	0.34	2.1	DFWM	1.06	153
$[Pt(2\text{-}C_8H_5S)_2(PEt_3)_2]$	$CHCl_3$	332	-1.1	0.22	1.1	DFWM	1.06	153
$[Ni(2\text{-}C_4H_2S)_2(PBu^n{}_3)_2]_n$	$CHCl_3$	515	-140 - -170	170-200	220-260	DFWM	1.06	152-154
$[Ni(2\text{-}C_8H_4S)_2(PBu^n{}_3)_2]_n$ $n_{av} = 9.5$	$CHCl_3$	580	-20 - -30	10-20	20-30	DFWM	1.06	152-154

nonlinearity, suggesting that the response is dominated by the MLCT transition. The converse trend is observed with the nickel complexes. The presence of the ligated metal centre is important in enhancing the response; the magnitudes of the nonlinearities are significantly larger than that for an organic analogue, terthiophene.[154]

Polymers are of interest for eventual device fabrication. Polymeric and oligomeric analogues of these *C*-coordinated thiophenyl group 10 complexes show a substantial increase (1-2 orders of magnitude) in nonlinearity over the corresponding monomers discussed above. Comparison to a related organic polymer, poly{3-butyl(thiophene)} ($|\gamma| = 10 \times 10^{-46}$ m^5 V^{-2}), reveals that the presence of the nickel enhances the nonlinearity despite a lower λ_{max}, a transparency/optical nonlinearity gain. The isobenzothiophene oligomer has a much smaller nonlinearity than the thiophene polymer, due to the decreased polymer chain length.

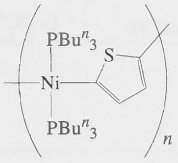

$\gamma = 220\text{-}260 \times 10^{-46}$ m^5 V^{-2}

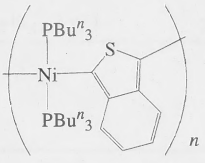

$\gamma = 20\text{-}30 \times 10^{-46}$ m^5 V^{-2}

Figure 1.18. Nickel thiophenyl and isobenzothiophenyl polymers with large γ.

The carbonyl complexes listed in Table 1.17. are of two types: tricarbonylchromium η^6-arene π-complexes and pentacarbonyltungsten σ-pyridine complexes, with both complex types having relatively low γ. Nonlinearities increase on arene or pyridine π-system lengthening, and on proceeding from acceptor to donor substituent on the tricarbonylchromium-coordinated arene ring. Relative magnitudes and trends thus mirror those observed with quadratic nonlinearities of these complexes.

Table 1.17. Third-order NLO measurements of carbonyl complexes.

Complex	Solvent	γ ($\times 10^{-36}$ esu)	λ_{max} (nm)	Technique	Fund. (μm)	Ref.
$[W(CO)_5(NC_5H_4\text{-}4\text{-}NH_2)]$	dmso	15	290	THG	1.91	99
$[W(CO)_5(NC_5H_4\text{-}4\text{-}Bu^n)]$	*p*-dioxane	15	328	THG	1.91	99
$[W(CO)_5(NC_5H_5)]$	toluene	8	332	THG	1.91	99
$[W(CO)_5(NC_5H_4\text{-}4\text{-}Ph)]$	$CHCl_3$	12	330-340	THG	1.91	99
$[W(CO)_5(NC_5H_4\text{-}4\text{-}COMe)]$	$CHCl_3$	14	420-440	THG	1.91	99
$[Cr(CO)_3(\eta^6\text{-}C_6H_6)]$	toluene	2	310	THG	1.91	99
$[Cr(CO)_3(\eta^6\text{-}C_6H_5OMe)]$	toluene	3	310	THG	1.91	99
$[Cr(CO)_3(\eta^6\text{-}C_6H_5NH_2)]$	*p*-dioxane	12	313	THG	1.91	99
$[Cr(CO)_3(\eta^6\text{-}C_6H_5NMe_2)]$	toluene	10	318	THG	1.91	99
$[Cr(CO)_3(\eta^6\text{-}C_6H_5COOMe)]$	toluene	6	318	THG	1.91	99
$[Cr(CO)_3(\eta^6\text{-}C_6H_5\text{-}(E)\text{-}CH{=}CHPh)]$	*p*-dioxane	21	410	THG	1.91	99
$[Mo_2OsSe(CO)_7(\eta^5\text{-}C_5H_5)_2]$	*n*-hexane	-2.2×10^{-12} cm^2 W^{-1}		Z-scan	0.53	155

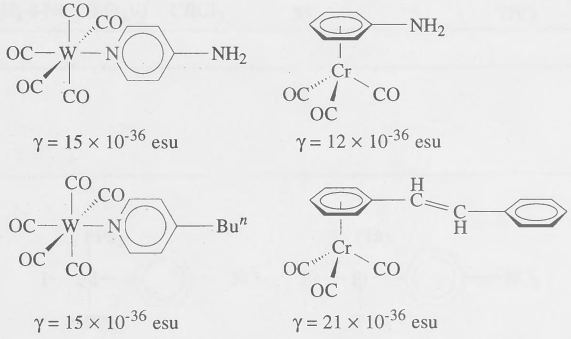

Figure 1.19. Carbonyl complexes of chromium and tungsten with large γ.

A systematically varied series of 16 electron square-planar arylpalladium and arylplatinum complexes have been examined by THG at 1.91 μm (see Table 1.18.), with the focus on assessing the importance of halo or phosphine co-ligands, or of 4-aryl substituents; metal replacement for the complexes *trans*-[MI(C_6H_4-4-NO_2)(PEt_3)$_2$] (M = Pd, Pt) had no effect on nonlinearity. All complexes have significantly larger γ than the carbonyl complexes above, but values are still low in absolute terms (as expected for small molecules with little conjugation). Replacement of iodo by bromo results in a 50 % increase in nonlinearity, and proceeding from triethylphosphine to triphenylphosphine co-ligand affords a similar increase in cubic NLO response, as does replacing a 4-formyl by a 4-nitro substituent on the σ-bound aryl ring. Following this prescription, the most efficient complexes in this systematically varied series should be *trans*-[MBr(C_6H_4-4-NO_2)(PPh_3)$_2$] (M = Pd, Pt) but these were not examined.

Table 1.18. Third-order NLO measurements of square-planar platinum and palladium complexes.

Complex	Solvent	γ (× 10^{-36} esu)	λ_{max} (nm)	Technique	Fund. (μm)	Ref.
trans-[PtBr(C_6H_4-4-CHO)(PEt_3)$_2$]	$CHCl_3$	37	[a]	THG	1.91	99
trans-[PdI(C_6H_4-4-NO_2)(PEt_3)$_2$]	$CHCl_3$	36	[a]	THG	1.91	99
trans-[PdI(C_6H_4-4-NO_2)(PPh_3)$_2$]	$CHCl_3$	50	[a]	THG	1.91	99
trans-[PtI(C_6H_4-4-NO_2)(PEt_3)$_2$]	$CHCl_3$	36	[a]	THG	1.91	99
trans-[PtBr(C_6H_4-4-NO_2)(PEt_3)$_2$]	$CHCl_3$	55	[a]	THG	1.91	99

[a] Not reported.

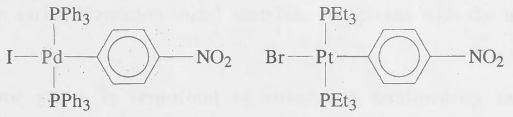

$\gamma = 50 \times 10^{-36}$ esu $\gamma = 55 \times 10^{-36}$ esu

Figure 1.20. Square-planar platinum and palladium complexes with large γ.

Investigations of the third-order nonlinearities of a systematically varied series of ruthenium acetylides established the significance of (i) phosphine ligand substitution (replacement of PPh_3 by PMe_3 resulted in only a small change), (ii) variation in phenylacetylide substituent (replacing 4-H by 4-Br resulted in no change, but introduction of 4-NO_2 resulted in an appreciable increase), and (iii) chain lengthening (progression from one-ring to biphenyl to ene-linked and yne-linked two-ring to imino-linked two-ring resulted in increasing nonlinearity). Negative nonlinearities were observed for all the nitro-containing complexes; thermal lensing was rejected as the cause of negative γ, and two-photon dispersion was deemed likely, but a negative static hyperpolarizability could not be ruled out.[126,156] *Trans*-bis(acetylide)bis(diphosphine)ruthenium complexes were investigated as monomeric models of polymers; they have nonlinearities with very large imaginary components implying significant two-photon absorption exists. The same acetylide ligands were coupled to ligated gold centres. Values for some of the gold complexes are larger than those of their ruthenium analogues, the opposite trend to that observed with β, emphasizing that enhancing cubic optical nonlinearities of organometallic complexes does not simply involve increasing quadratic NLO merit. Cubic nonlinearities for [Au(C≡CC_6H_4-4-C≡CC_6H_4-4-NO_2)(PPh_3)] and [Au(C≡CC_6H_4-4-(*E*)-CH=CHC_6H_4-4-NO_2)(PPh_3)] are the largest values for any of the complexes in the ruthenium, gold, and nickel systems (and in fact the largest for monomeric organometallic acetylide complexes), despite the gold complexes having the lower valence electron count.[157] Data for the nickel complexes are, within the error margins, equivalent to those of the ruthenium complexes, although the ruthenium complexes possess a more easily oxidizable metal and greater delocalization possibilities with the extra phosphine co-ligand, indicating that these variables are not critical for enhancing nonlinearity in these complexes.[135] This metal replacement (ruthenium vs nickel) may have a more subtle impact on nonlinearity which is not apparent with the large errors. It is clear, though, that the later transition metal ruthenium, nickel and gold complexes with the ligated metal acting as a donor group have significantly larger nonlinearities than earlier transition metal acetylide complexes with the metal acting as an acceptor moiety.

The nitro acceptor group is important in enhancing nonlinearity in these acetylide complexes. The mono- and di-metallic platinum and palladium acetylide complexes which lack nitro acceptor groups have much lower nonlinearities than the gold, ruthenium and nickel complexes containing the acceptor nitro substituent, but have nonlinearities which are comparable in magnitude to those of the group 4 metal, ruthenium, nickel and gold acetylides lacking this group.

Table 1.19. Third-order NLO measurements of acetylide and bis(acetylide) complexes.

Complex	Solvent	Re γ (10^{-36} esu)	Im γ (10^{-36} esu)	γ (10^{-36} esu)	λ_{max} (nm)	Technique	Fund. (μm)	Ref.
$[Ti(C{\equiv}CBu^n)_2(\eta^5\text{-}C_5H_4Me)_2]$	$CHCl_3$			15 ± 2	*d*	THG	1.91	149
$[Ti(C{\equiv}CBu^n)_2(\eta^5\text{-}C_5H_5)_2]$	$CHCl_3$			12 ± 2	390	THG	1.91	148
$[Ti(C{\equiv}CPh)_2(\eta^5\text{-}C_5H_5)_2]$	thf			92 ± 14	410,[a]416[b]	THG	1.91	143,148
$[Zr(C{\equiv}CPh)_2(\eta^5\text{-}C_5H_5)_2]$	thf			58 ± 9	370,[b]390[a]	THG	1.91	143,148
$[Hf(C{\equiv}CPh)_2(\eta^5\text{-}C_5H_5)_2]$	thf			51 ± 8	358,[b]390[a]	THG	1.91	143,148
$[Ti(C{\equiv}CPh)Cl(\eta^5\text{-}C_5H_5)_2]$	thf			31 ± 5	402,510(sh)	THG	1.91	143,148
$[Ru(C{\equiv}CPh)(PPh_3)_2(\eta^5\text{-}C_5H_5)]$	thf	≤ 150			311	Z-scan	0.80	156
$[Ru(C{\equiv}CC_6H_4\text{-}4\text{-}Br)(PPh_3)_2(\eta^5\text{-}C_5H_5)]$	thf	≤ 150			325	Z-scan	0.80	156
$[Ru(C{\equiv}CC_6H_4\text{-}4\text{-}NO_2)(PPh_3)_2(\eta^5\text{-}C_5H_5)]$	thf	-210 ± 50	≤ 10		461	Z-scan	0.80	156
	thf	-260 ± 60			461	DFWM	0.80	156
$[Ru(C{\equiv}CC_6H_4\text{-}4\text{-}NO_2)(PMe_3)_2(\eta^5\text{-}C_5H_5)]$	thf	-230 ± 70	74 ± 30		480	Z-scan	0.80	156
$[Ru(C{\equiv}CC_6H_4\text{-}4\text{-}C_6H_4\text{-}4\text{-}NO_2)(PPh_3)_2(\eta^5\text{-}C_5H_5)]$	thf	-380 ± 200	320 ± 160		310,448	Z-scan	0.80	126
$[Ru(C{\equiv}CC_6H_4\text{-}4\text{-}(E)\text{-}CH{=}CHC_6H_4\text{-}4\text{-}NO_2)(PPh_3)_2(\eta^5\text{-}C_5H_5)]$	thf	-450 ± 100	210 ± 100		346,476	Z-scan	0.80	156
$[Ru(C{\equiv}CC_6H_4\text{-}4\text{-}C{\equiv}CC_6H_4\text{-}4\text{-}NO_2)(PPh_3)_2(\eta^5\text{-}C_5H_5)]$	thf	-450 ± 100	≤ 20		346,447	Z-scan	0.80	156
$[Ru(C{\equiv}CC_6H_4\text{-}4\text{-}N{=}CHC_6H_4\text{-}4\text{-}NO_2)(PPh_3)_2(\eta^5\text{-}C_5H_5)]$	thf	-850 ± 300	360 ± 200		298,496	Z-scan	0.80	126
trans-$[RuCl(C{\equiv}CC_6H_4\text{-}4\text{-}NO_2)(dppm)_2]$	CH_2Cl_2	170 ± 34	230 ± 46		466	Z-scan	0.80	157
trans-$[RuCl(C{\equiv}CC_6H_4\text{-}4\text{-}C_6H_4\text{-}4\text{-}NO_2)(dppm)_2]$	CH_2Cl_2	140 ± 28	64 ± 13		448	Z-scan	0.80	157
trans-$[RuCl(C{\equiv}CC_6H_4\text{-}4\text{-}(E)\text{-}CH{=}CHC_6H_4\text{-}4\text{-}NO_2)(dppm)_2]$	CH_2Cl_2	200 ± 40	1100 ± 220		471	Z-scan	0.80	157
trans-$[Ru(C{\equiv}CC_6H_4\text{-}4\text{-}NO_2)_2(dppm)_2]$	CH_2Cl_2	300 ± 60	490 ± 98		474	Z-scan	0.80	157
trans-$[Ru(C{\equiv}CC_6H_4\text{-}4\text{-}C_6H_4\text{-}4\text{-}NO_2)_2(dppm)_2]$	CH_2Cl_2	≤ 800	2500 ± 500		453	Z-scan	0.80	157

Table 1.19. (continued) Third-order NLO measurements of acetylide and bis(acetylide) complexes.

Complex	Solvent	Re γ (10^{-36} esu)	Im γ (10^{-36} esu)	γ (10^{-36} esu)	λ_{max} (nm)	Technique	Fund. (μm)	Ref.
trans-[Ru(C≡CC_6H_4-4-(*E*)-CH=CHC_6H_4-4-NO_2)$_2$(dppm)$_2$]	CH_2Cl_2	≤ 1100	3400 ± 680		367	Z-scan	0.80	157
[Au(C≡CPh)(PPh_3)]	thf	39 ± 20			268,282,296	Z-scan	0.80	158
[Au(C≡CC_6H_4-4-NO_2)(PPh_3)]	thf	120 ± 40	20 ± 15		338	Z-scan	0.80	158
[Au(C≡CC_6H_4-4-C_6H_4-4-NO_2)(PPh_3)]	thf	540 ± 150	120 ± 50		274,287,350	Z-scan	0.80	158
[Au(C≡CC_6H_4-4-(*E*)-CH=CHC_6H_4-4-NO_2)(PPh_3)]	thf	1200 ± 200	470 ± 150		303,386	Z-scan	0.80	158
[Au(C≡CC_6H_4-4-(*Z*)-CH=CHC_6H_4-4-NO_2)(PPh_3)]	thf	420 ± 150	92 ± 30		298,362	Z-scan	0.80	158
[Au(C≡CC_6H_4-4-C≡CC_6H_4-4-NO_2)(PPh_3)]	thf	1300 ± 400	560 ± 150		301,362	Z-scan	0.80	158
[Au(C≡CC_6H_4-4-N=CHC_6H_4-4-NO_2)(PPh_3)]	thf	130 ± 30	330 ± 60		297,392	Z-scan	0.80	158
[Ni(C≡CPh)(PPh_3)(η^5-C_5H_5)]	thf	15 ± 10	< 10		307	Z-scan	0.80	135
[Ni(C≡CC_6H_4-4-NO_2)(PPh_3)(η^5-C_5H_5)]	thf	-270 ± 100	70 ± 50		368,439	Z-scan	0.80	135
[Ni(C≡CC_6H_4-4-C_6H_4-4-NO_2)(PPh_3)(η^5-C_5H_5)]	thf	-580 ± 200	300 ± 60		263,310,413	Z-scan	0.80	135
[Ni(C≡CC_6H_4-4-(*E*)-CH=CHC_6H_4-4-NO_2)(PPh_3)(η^5-C_5H_5)]	thf	-420 ± 100	480 ± 150		313,437	Z-scan	0.80	135
[Ni(C≡CC_6H_4-4-(*Z*)-CH=CHC_6H_4-4-NO_2)(PPh_3)(η^5-C_5H_5)]	thf	-230 ± 50	160 ± 80		307,417	Z-scan	0.80	135
[Ni(C≡CC_6H_4-4-C≡CC_6H_4-4-NO_2)(PPh_3)(η^5-C_5H_5)]	thf	-640 ± 300	720 ± 300		313,417	Z-scan	0.80	135
[Ni(C≡CC_6H_4-4-N=CHC_6H_4-4-NO_2)(PPh_3)(η^5-C_5H_5)]	thf	< 120	360 ± 100		282,448	Z-scan	0.80	135

Table 1.19. (continued) Third-order NLO measurements of acetylide and bis(acetylide) complexes.

Complex	Solvent	Re γ (10^{-36} esu)	Im γ (10^{-36} esu)	γ (10^{-36} esu)	λ_{max} (nm)	Technique	Fund. (μm)	Ref.
cis-[PtCl(PBu$^n_3$)$_2$(-μ-C≡CC$_6$H$_4$-4-C≡C)PtCl(PBu$^n_3$)$_2$]	thf	11 ± 25%	224 ± 25%		*d*	OKG/IDS	1.06/0.53	160
trans-[PtCl(PBu$^n_3$)$_2$(-μ-C≡CC$_6$H$_4$-4-C≡C)PtCl(PBu$^n_3$)$_2$]	thf	19 ± 25%	827 ± 25%		*d*	OKG/IDS	1.06/0.53	160
trans-[PtCl(PBu$^n_3$)$_2$(-μ-C≡CC$_6$H$_4$-4-C≡C)Pt(PBu$^n_3$)$_2$(-μ-C≡CC$_6$H$_4$-4-C≡C)PtCl(PBu$^n_3$)$_2$]	thf	45 ± 25%	1196 ± 25%		*d*	OKG/IDS	1.06/0.53	160
trans-[PtCl(PBu$^n_3$)$_2$(C≡CC$_6$H$_4$-4-C≡CC≡CC$_6$H$_4$-4-C≡C)PtCl(PBu$^n_3$)$_2$]	thf	88 ± 25%	2167 ± 25%		*d*	OKG/IDS	1.06/0.53	160
trans-[Pt(C≡CC$_6$H$_4$-4-C≡CH)$_2$(PBu$^n_3$)$_2$]	thf	53 ± 25%	759 ± 25%		*d*	OKG/IDS	1.06/0.53	160
trans-[Pt(C≡CC$_6$H$_4$-4-C≡CH)(PBu$^n_3$)$_2$(-μ-C≡CC$_6$H$_4$-4-C≡C)Pt(C≡CC$_6$H$_4$-4-C≡CH)(PBu$^n_3$)$_2$]	thf	66 ± 25%	1328 ± 25%		*d*	OKG/IDS	1.06/0.53	160
trans-[Pt(NCS)(PBu$^n_3$)$_2$(-μ-C≡CC$_6$H$_4$-4-C≡C)Pt(NCS)(PBu$^n_3$)$_2$]	thf	30 ± 25%	1134 ± 25%		*d*	OKG/IDS	1.06/0.53	160
trans-[PtCl(PBu$^n_3$)$_2$(-μ-C≡CC$_6$H$_4$-4-C≡C){PtCl(PBu$^n_3$)$_2$]	*d*			350[c]	*d*	FWM	0.63	159
cis-[Pt(C≡CC$_6$H$_4$-4-C≡CH)$_2$(PBu$^n_3$)$_2$]	*d*	230[c]	260[c]	290[c]	*d*	FWM	0.63	159
trans-[Pd(C≡CPh)$_2$(PBu$^n_3$)$_2$]	*d*			110[c]	*d*	FWM	0.63	159

[a] Reference 143. [b] Reference 148. [c] Error not quoted. [d] Not reported.

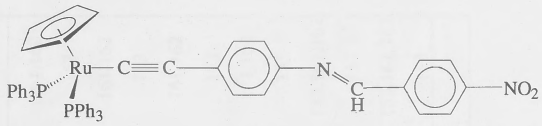

$Re\gamma = -850 \times 10^{-36}$ esu; $Im\gamma = 360 \times 10^{-36}$ esu

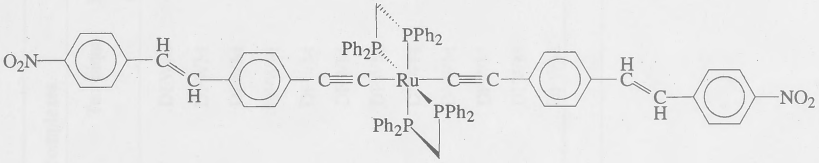

$Re\gamma \leq 1100 \times 10^{-36}$ esu; $Im\gamma = 3400 \times 10^{-36}$ esu

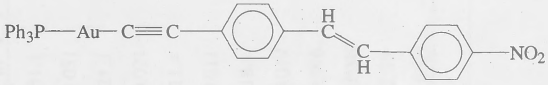

$Re\gamma = 1200 \times 10^{-36}$ esu; $Im\gamma = 470 \times 10^{-36}$ esu

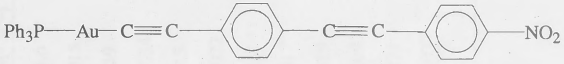

$Re\gamma = 1300 \times 10^{-36}$ esu; $Im\gamma = 560 \times 10^{-36}$ esu

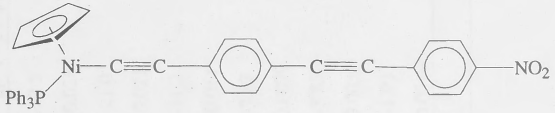

$Re\gamma = -640 \times 10^{-36}$ esu; $Im\gamma = 720 \times 10^{-36}$ esu

Figure 1.21. Acetylide and bis(acetylide) complexes with large γ.

Measurements made by DFWM on group 10 metal bis(acetylide) complexes are listed in Table 1.20. Although results cannot be directly compared to those above, internal comparisons within the series are valid. These reveal that hyperpolarizability decreases progressing down the group for phenylacetylide examples [as observed with other acetylide complexes: (see above)], but that larger nonlinearities are observed for butadiynide complexes of the heavier metals. The complexes exhibit a high-order intensity dependence, characteristic of multiphoton resonant enhancement; for these complexes this is possibly due to three-photon resonant enhancement, as λ_{max} is, in all cases, close to 3ω.

Table 1.20. Third-order NLO measurements of Group 10 metal bis(acetylide) complexes.

Complex	Solvent	Re γ (10^{-44} m^5 V^{-2})	Im γ (10^{-44} m^5 V^{-2})	$\lvert\gamma\rvert$ (10^{-44} m^5 V^{-2})	λ_{max} (nm)	Technique	Fund. (μm)	Ref.
trans-[Ni(C≡CPh)$_2$(PEt$_3$)$_2$]	$CHCl_3$	-27.5	14.6	31.1	370	DFWM	1.06	161,162
	[a]	-0.028	0.015	0.031	370	DFWM	1.06	153
trans-[Pd(C≡CPh)$_2$(PEt$_3$)$_2$]	$CHCl_3$	-21.0	3.39	21.3	370	DFWM	1.06	161,162
	[a]	-0.021	0.0034	0.021	370	DFWM	1.06	153
trans-[Pt(C≡CPh)$_2$(PEt$_3$)$_2$]	$CHCl_3$	-11.2	2.15	11.4	332	DFWM	1.06	161,162
	[a]	-0.011	0.0022	0.011	332	DFWM	1.06	153
trans-[Ni(C≡CC≡CH)$_2$(PEt$_3$)$_2$]	$CHCl_3$	-7.87	17.2	18.9	336	DFWM	1.06	161,162
	[a]	-0.0079	0.017	0.019	336	DFWM	1.06	153
trans-[Pd(C≡CC≡CH)$_2$(PEt$_3$)$_2$]	$CHCl_3$	-3.85	0.919	0.396	290	DFWM	1.06	153,161,162
	[a]	-0.0039	0.00092	0.0040	290	DFWM	1.06	153
trans-[Pt(C≡CC≡CH)$_2$(PEt$_3$)$_2$]	$CHCl_3$	-1.93	0.771	2.08	318	DFWM	1.06	153,161,162
	[a]	-0.0019	0.00077	0.0021	318	DFWM	1.06	153

[a] Not reported.

Table 1.21. Third-order NLO measurements of bis(acetylide) complexes.

Complex	Solvent	n_2 ($\times 10^{-18}$ m^2 W^{-1})	Technique	Fund. (μm)	Ref.
trans-[Pd(C≡CPh)$_2$(PBu$^n_3$)$_2$]	thf	-0.5 ± 0.1	Z-scan	0.53	163
trans-[Pt(C≡CPh)$_2$(PBu$^n_3$)$_2$]	thf	-3.0 ± 0.1	Z-scan	0.53	163
trans-[Ni(C≡CPh)$_2$(PBu$^n_3$)$_2$]	thf	-16 ± 5	Z-scan	0.53	163
trans-[Pd(C≡CC$_6$H$_4$-4-C≡CPh)$_2$(PBu$^n_3$)$_2$]	thf	-25 ± 3	Z-scan	0.53	163
trans-[Pt(C≡CC$_6$H$_4$-4-C≡CPh)$_2$(PBu$^n_3$)$_2$]	thf	-209 ± 27	Z-scan	0.53	163

The data in Table 1.21. are given as nonlinear refractive indices n_2; other experimental parameters are needed to derive γ values which are required for comparison to the results above. As with the data in Table 1.20., results in Table 1.21. permit internal conclusions to be drawn; the resultant trends can then be compared to those above. The data here are consistent with increased nonlinearity upon chromophore chain-lengthening (as observed with acetylide complexes above), and with a metal efficiency series nickel > platinum > palladium.

In the acetylide polymers of square-planar nickel, palladium and platinum listed in Table 1.22., the imaginary part of the nonlinearity is the major contributor, implying significant two-photon absorption. Some of the polymers have nonlinearities which are significantly larger than related monometallic acetylide complexes. There does not seem to be a consistent trend in nonlinearity upon increasing polymer size. Although it is hard to compare the data across metal (because the polymers vary in length as well as composition), the platinum polymers are in many cases more efficient than the analogous palladium polymers. The nonlinearities of these polymers do not depend dramatically upon aromatic ring substitution, but increasing the number of diethynylarenes in the repeat unit from one to two increases the nonlinearity.[160]

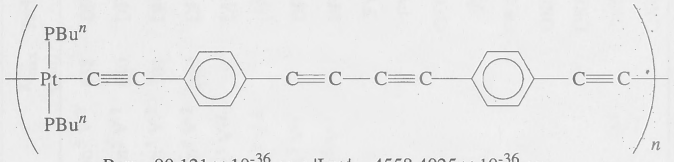

Reγ = 90,121 × 10^{-36} esu; |Imγ| = 4558,4025 × 10^{-36} esu

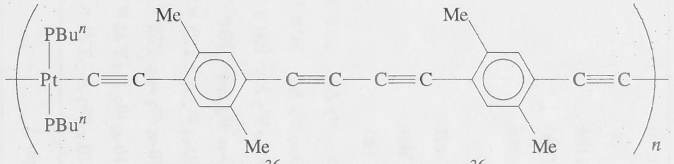

Reγ = 120 × 10^{-36} esu; |Imγ| = 5400 × 10^{-36} esu

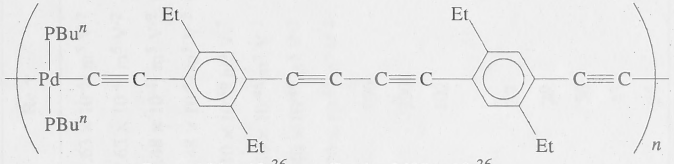

Reγ = 106 × 10^{-36} esu; |Imγ| = 3490 × 10^{-36} esu

Figure 1.22. Acetylide polymer complexes with large γ.

Table 1.22. Third-order NLO measurements of acetylide polymer complexes.[a]

Complex	Solvent	Re γ	Im γ	$\lvert\gamma\rvert$	λ_{max} (nm)	Technique	Fund. (μm)	Ref.
$[Ni(C{\equiv}CC{\equiv}C)(PBu^n_3)_2]_n$	$CHCl_3$	-2.63×10^{-42} m^5 V^{-2}	-2.41×10^{-42} m^5 V^{-2}	3.57×10^{-42} m^5 V^{-2}	412	DFWM	1.06	161,162,164
	[b]	-2.63×10^{-45} m^5 V^{-2}	-2.41×10^{-45} m^5 V^{-2}	3.57×10^{-45} m^5 V^{-2}	410	DFWM	1.06	153
$[Pt(C{\equiv}CC{\equiv}C)(PBu^n_3)_2]_n$	$CHCl_3$	-1.48×10^{-42} m^5 V^{-2}	1.74×10^{-42} m^5 V^{-2}	2.28×10^{-42} m^5 V^{-2}	364	DFWM	1.06	161,162,164
	[b]	-1.48×10^{-45} m^5 V^{-2}	1.74×10^{-45} m^5 V^{-2}	2.28×10^{-45} m^5 V^{-2}	360	DFWM	1.06	153
$[Ni(C{\equiv}CC_6H_4\text{-}4\text{-}C{\equiv}C)(PBu^n_3)_2]_n$	$CHCl_3$	-10×10^{-46} m^5 V^{-2}	20×10^{-46} m^5 V^{-2}	20×10^{-46} m^5 V^{-2}		DFWM	1.06	164
$[Ni(C{\equiv}CC_6H_4\text{-}4\text{-}C{\equiv}C)(POc^n_3)_2]_n$	$CHCl_3$	-40×10^{-46} m^5 V^{-2}	100×10^{-46} m^5 V^{-2}	100×10^{-46} m^5 V^{-2}		DFWM	1.06	164
$[Ni(C{\equiv}CC{\equiv}C)\{P(C_8H_{17})_3)\}]_n$	$CHCl_3$	-40×10^{-46} m^5 V^{-2}	30×10^{-46} m^5 V^{-2}	50×10^{-46} m^5 V^{-2}		DFWM	1.06	164
$[Pd_2(C{\equiv}CC_6H_4\text{-}4\text{-}C{\equiv}C)(\mu\text{-dppm})_2]_n$	$CHCl_3$	-20×10^{-46} m^5 V^{-2}	20×10^{-46} m^5 V^{-2}	20×10^{-46} m^5 V^{-2}		DFWM	1.06	164
$[Pt(C{\equiv}CC_6H_4\text{-}4\text{-}C{\equiv}C)(PBu^n_3)_2]_n$	[b]	890	130	1450		FWM	0.63	159
$[Pd(C{\equiv}CC_6H_4\text{-}4\text{-}C{\equiv}C)(PBu^n_3)_2]_n$	[b]	390	380	490		FWM	0.63	159
$[Pd(C{\equiv}CC_6H_4\text{-}4\text{-}C{\equiv}C)(PBu^n_3)_2]_n$ n = 112	thf	102	3401			OKG/IDA	1.06/0.53	165
$[Pt(C{\equiv}CC_6H_4\text{-}4\text{-}C{\equiv}C)(PBu^n_3)_2]_n$ ~32 000 amu	benzene			1470		THG	1.06	166
$[Pt(C{\equiv}CC_6H_4\text{-}4\text{-}C{\equiv}C)(PBu^n_3)_2]_n$ n = 112	thf	37	1906			OKG/IDA	1.06/0.53	160
$[Pt(C{\equiv}CC_6H_2\text{-}2,5\text{-}Me_2\text{-}4\text{-}C{\equiv}C)(PBu^n_3)_2]_n$ n = 26	thf	29	1200			OKG/IDA	1.06/0.53	160
	thf	56	1199			OKG/IDA	1.06/0.53	167
$[Pt(C{\equiv}CC_6H_2\text{-}2,5\text{-}Et_2\text{-}4\text{-}C{\equiv}C)(PBu^n_3)_2]_n$ n = 15	thf	43	956			OKG/IDA	1.06/0.53	160
$[Pt(C{\equiv}CC_6H_3\text{-}3\text{-}F\text{-}4\text{-}C{\equiv}C)(PBu^n_3)_2]_n$ n = 18	thf	56	1260			OKG/IDA	1.06/0.53	160

Table 1.22. (continued) Third-order NLO measurements of acetylide polymer complexes.[a]

Complex	Solvent	Re γ	|Im γ|	Technique	Fund. (μm)	Ref.
$[Pt(C{\equiv}CC_6H_2\text{-}2,5\text{-}(OMe)_2\text{-}4\text{-}C{\equiv}C)(PBu^n{}_3)_2]_n$ n = 111, 105, 62	thf	48,65,43	1724,1330,1586	OKG/IDA	1.06/0.53	160
$[Pt(C{\equiv}CC_6Me_4\text{-}4\text{-}C{\equiv}C)(PBu^n{}_3)_2]_n$ oligomer	thf	28	1324	OKG/IDA	1.06/0.53	160
$[Pt(C{\equiv}CC_6H_3\text{-}3\text{-}NH_2\text{-}4\text{-}C{\equiv}C)(PBu^n{}_3)_2]_n$ n = 76	thf	18	1342	OKG/IDA	1.06/0.53	160
$[Pt(C{\equiv}CC_6H_3\text{-}3\text{-}CF_3\text{-}4\text{-}C{\equiv}C)(PBu^n{}_3)_2]_n$ n = 44	thf	34	2148	OKG/IDA	1.06/0.53	160
$[Pt\{C{\equiv}C(1\text{-naphthyl})\text{-}4\text{-}C{\equiv}C\}(PBu^n{}_3)_2]_n$ n = 62	thf	19	2474	OKG/IDA	1.06/0.53	160
$[Pt\{3\text{-}C{\equiv}C(C_5H_3N)\text{-}2\text{-}C{\equiv}C\}(PBu^n{}_3)_2]_n$ n = 47, 35	thf	33	2263	OKG/IDA	1.06/0.53	160
$[Pd(C{\equiv}CC_6H_2\text{-}2,5\text{-}Me_2\text{-}4\text{-}C{\equiv}C)(PBu^n{}_3)_2]_n$ n = 4	thf	19	1169	OKG/IDA	1.06/0.53	160
$[Pd(C{\equiv}CC_6H_3\text{-}3\text{-}NH_2\text{-}4\text{-}C{\equiv}C)(PBu^n{}_3)_2]_n$ n = 12	thf	15	1753	OKG/IDA	1.06/0.53	160
$[Pd(C{\equiv}CC_6H_2\text{-}2,5\text{-}(OMe)_2\text{-}4\text{-}C{\equiv}C)(PBu^n{}_3)_2]_n$ n = 67	thf	22	2432	OKG/IDA	1.06/0.53	160
$[Pt(C{\equiv}CC_6H_4\text{-}4\text{-}C{\equiv}CC{\equiv}CC_6H_4\text{-}4\text{-}C{\equiv}C)(PBu^n{}_3)_2]_n$ n = 223, 97	thf	90,121	4558,4025	OKG/IDA	1.06/0.53	160
$[Pt(C{\equiv}CC_6H_4\text{-}4\text{-}C{\equiv}CC{\equiv}CC_6H_4\text{-}4\text{-}C{\equiv}C)(PBu^n{}_3)_2]_n$ n > 144	thf	856	3570	OKG/IDA	1.06/0.53	165
$[Pt(C{\equiv}CC_6H_2\text{-}2,5\text{-}Me_2\text{-}4\text{-}C{\equiv}CC{\equiv}CC_6H_2\text{-}2,5\text{-}Me_2\text{-}4\text{-}C{\equiv}C)(PBu^n{}_3)_2]_n$ n = 52,38	thf	116	2432	OKG/IDA	1.06/0.53	160
$[Pt(C{\equiv}CC_6H_2\text{-}2,5\text{-}Me_2\text{-}4\text{-}C{\equiv}CC{\equiv}CC_6H_2\text{-}2,5\text{-}Me_2\text{-}4\text{-}C{\equiv}C)(PBu^n{}_3)_2]_n$ n = 52	thf	181	4366	OKG/IDA	1.06/0.53	165,168
	thf	120 ± 30	5400 ± 500	OKG	0.53	165
$[Pt(C{\equiv}CC_6H_2\text{-}2,5\text{-}Et_2\text{-}4\text{-}C{\equiv}CC{\equiv}CC_6H_2\text{-}2,5\text{-}Et_2\text{-}4\text{-}C{\equiv}C)(PBu^n{}_3)_2]_n$ n = 146	thf	79	4933	OKG/IDA	1.06/0.53	160
$[Pd(C{\equiv}CC_6H_4\text{-}4\text{-}C{\equiv}CC{\equiv}CC_6H_4\text{-}4\text{-}C{\equiv}C)(PBu^n{}_3)_2]_n$ oligomer, 5, 2	thf	66	2094	OKG/IDA	1.06/0.53	160
$[Pd(C{\equiv}CC_6H_2\text{-}2,5\text{-}Et_2\text{-}4\text{-}C{\equiv}CC{\equiv}CC_6H_2\text{-}2,5\text{-}Et_2\text{-}4\text{-}C{\equiv}C)(PBu^n{}_3)_2]_n$ n = 16	thf	106	3490	OKG/IDA	1.06/0.53	160
$[Pt(C{\equiv}CC_6H_4\text{-}4\text{-}C{\equiv}C)(PBu^n{}_3)_2Pt(C{\equiv}CC_6H_4C_6H_4\text{-}4\text{-}C{\equiv}C)(PBu^n{}_3)_2]_n$ n = 66	thf		4466	OKG/IDA	1.06/0.53	160

[a] Units of 10^{-36} esu except where indicated. [b] Not reported.

Third-order measurements of fullerene derivatives are given in Table 1.23. The organometallic fullerene derivative $[(\eta^2\text{-}C_{60})Pt(PPh_3)_2]$ was measured by Z-scan using both circular and linear polarized light.[169] Different selection rules allowing two-photon absorption exist when considering different polarizations of light. The two-photon absorption contribution to nonlinearities is substantial here, confirmed by a significant difference in the result obtained by using circular polarized light. These measurements are complicated because of the comparatively large nonlinearity of the solvent toluene (the complex was insufficiently soluble in thf). A broad electron absorption band which tails out at ~800 nm renders extraction of the off-resonance nonlinearity impossible because of the fundamental frequencies employed. This contributes to making comparison of results very difficult. Comparison with the free fullerene reveals that coordination to the ligated platinum centre significantly increased nonlinear absorption (this is an order of magnitude greater in $[(\eta^2\text{-}C_{60})Pt(PPh_3)_2]$ than in C_{60}).

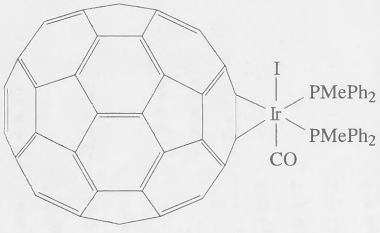

$Im(\chi^{(3)}) = 4.14 \times 10^{-17}\ m^2\ V^{-2}$

Figure 1.23. $[(\eta^2\text{-}C_{60})IrI(CO)(PMePh_2)_2]$.

The imaginary components of the third-order nonlinear susceptibility of palladium and iridium complexes of C_{60} and C_{70} were determined using saturation spectroscopy. In all cases, $Im(\chi^{(3)})$ values are smaller than those of uncomplexed C_{60} ($1.78 \times 10^{-16}\ m^2\ V^{-2}$) or C_{70} ($7.55 \times 10^{-17}\ m^2\ V^{-2}$), a result explained by decreased conjugation in the molecule and consequent decreased electron delocalization, although differing photodynamics were not excluded.

Table 1.23. Third-order NLO measurements of fullerene derivatives.

Complex	Re($\chi^{(3)}$)	Im($\chi^{(3)}$)	Re γ (esu)	Im γ (esu)	Conc. (g/L)	Technique	Polarization	τ (ps)	Fund. (μm)	Ref.
$[(\eta^2\text{-}C_{60})Pt(PPh_3)_2]^b$			1.4×10^{-30}	3.4×10^{-30}	0.35	Z-scan	linear	10	0.53	169
	1.7×10^{-12} esu	7.8×10^{-13} esu	6.9×10^{-31}*a*	1.3×10^{-30}	0.35	Z-scan	linear	10	0.53	169,170
	3.2×10^{-12} esu	2.0×10^{-12} esu	1.4×10^{-30}*a*	3.4×10^{-30}	0.35	Z-scan	circular	10	0.53	169,170
	-	1.32×10^{-16} m^2 V^{-2}			2	IDA		500	0.59	171
$[(FcH)_2C_{60}]^b$	1.2×10^{-12} esu	7.7×10^{-13} esu	-2.4×10^{-32}*a*	1.8×10^{-31}	2	Z-scan	linear		0.53	170
		2.4×10^{-12} esu		5.6×10^{-31}	2	Z-scan	circular		0.53	170
$[Co(\eta^5\text{-}C_5H_5)_2C_{60}]^c$	1.8×10^{-13} esu		-1.9×10^{-30}		0.068	Z-scan	linear		0.53	170
	3.4×10^{-13} esu		-3.6×10^{-30}		0.068	Z-scan	circular		0.53	170
	6.8×10^{-14} esu		1.3×10^{-31}*a*		0.068	Z-scan	linear		1.06	170
$[(\eta^2\text{-}C_{60})Pd(PPh_3)_2]^b$		1.55×10^{-17} m^2 V^{-2}			2	IDA		500	0.59	171
$[(\eta^2\text{-}C_{70})Pd(PPh_3)_2]^b$		5.78×10^{-17} m^2 V^{-2}			2	IDA		500	0.59	171
$[(\eta^2\text{-}C_{60})IrI(CO)(PMePh_2)_2]^b$		4.14×10^{-17} m^2 V^{-2}			2	IDA		500	0.59	171
$[(\eta^2\text{-}C_{70})IrI(CO)(PMePh_2)_2]^b$		2.64×10^{-17} m^2 V^{-2}			2	IDA		500	0.59	171

a Authors note that values are less than or comparable to the total experimental error, and may not be reliable. *b* As a solution in toluene. *c* As a solution in THF.

Two (cyclopentadienyl)bis(phosphine)ruthenium chloride complexes have been investigated; the nonlinearities are low. These results have been used in conjunction with measured nonlinearities of acetylenes and acetylide complexes to demonstrate that values for the latter are not simply the sum of the molecular components (see above). An example of a metal alkyl, $[Pd_2(\mu\text{-dppm})_2Me_2]$ has also been measured; given the lack of a π-system for efficient electron delocalization, the nonlinearity is not surprisingly low. The only (isonitrile)ruthenium complex examined has a planar ruthenaphthalocyanine axially ligated by 1,4-diisocyanobenzene to form an oligomer. THG measurements of $\chi^{(3)}(-3\omega;\omega,\omega,\omega)$ of a film of this complex (3.7×10^{-12} esu; Table 1.25.) are significantly less than $\chi^{(3)}(-\omega;\omega,\omega,-\omega)$ obtained by DFWM (Table 1.23.). A difference of four orders of magnitude was also found with the cubic molecular nonlinearities of the mixed cobalt-iron cluster $[CoFe_2(\mu_3\text{-}S)(\mu_3\text{-}Se)(CO)_6(\eta^5\text{-}C_5H_5)]$, a significant frequency dependence; as λ_{max} is at ~550 nm, the larger value is likely to be significantly resonance enhanced.

A range of organometallic films (organotransition metal complexes doped into organic polymer hosts) has been examined for their bulk NLO response; results are listed in Table 1.24. Third-order nonlinear susceptibilities of a ferrocene-containing polyazine have been measured in the wavelength region 1.0 to 1.95 μm.[155] When the ferrocene unit is replaced by a pyridine linkage, the nonlinearity of the polymer is reduced by more than a third. Nalwa suggests that the larger nonlinearity in the ferrocene-containing complex arises from metal-ligand bonding, with extended conjugation being precluded from the polymer by symmetry considerations and lack of orbital overlap. Third-harmonic nonlinearities $\chi^{(3)}(-3\omega:\omega,\omega,\omega)$ for some (cyclopentadienyl)bis(phosphine)ruthenium complexes containing *p*-substituted benzonitrile ligands in a polymethylmethacrylate host polymer were determined by THG. These give moderate nonlinearities that are not ascribed to three-photon resonance. Comparison of the results for $[Ru(N{\equiv}CC_6H_4\text{-}4\text{-}C_6H_4\text{-}4\text{-}NO_2)(dppe)(\eta^5\text{-}C_5H_5)]^+$ with those for oligomers of poly(thiophenevinylene) of similar size using the same technique suggests that γ is four times larger for the organometallic; this is explained in terms of reduced bond-alternation in $[Ru(N{\equiv}CC_6H_4\text{-}4\text{-}C_6H_4\text{-}4\text{-}NO_2)(dppe)(\eta^5\text{-}C_5H_5)]^+$, for which π-back donation enhances the delocalized π-electron system. Variations in the counter-ion ($[BPh_4]^-$, $[PF_6]^-$, $[CF_3SO_3]^-$, $[MeC_6H_4\text{-}4\text{-}SO_3]^-$) or phosphine (dppe, (+)-diop) had minimal effect on the nonlinearity for these complexes.

Table 1.24. Third-order NLO measurements of other complexes.

Complex	Solvent	Quantity Measured	value	λ_{max}	Technique	Fund. (μm)	Ref.
$[RuCl(PPh_3)_2(\eta^5\text{-}C_5H_5)]$	thf	Re γ	$150 \pm 100 \times 10^{-36}$ esu	348	Z-scan	0.80	156
	thf	Re γ	$50 \pm 20 \times 10^{-36}$ esu	348	DFWM	0.80	156
$[RuCl(PMe_3)_2(\eta^5\text{-}C_5H_5)]$	thf	Re γ	$\leq 80 \times 10^{-36}$ esu	346	Z-scan	0.80	156
	thf	Re γ	$80 \pm 30 \times 10^{-36}$ esu	346	DFWM	0.80	156
$[Pd_2(\mu\text{-dppm})_2Me_2]$	$CHCl_3$	Re γ	-1×10^{-46} m^5 V^{-2}		DFWM	1.06	164
	$CHCl_3$	Im γ	2×10^{-46} m^5 V^{-2}		DFWM	1.06	164
	$CHCl_3$	γ	2×10^{-46} m^5 V^{-2}		DFWM	1.06	164
$[(^tBu_4\text{-phthalocyaninato})Ru(4\text{-}CNC_6H_4NC)]_n$	$CHCl_3$	$\chi^{(3)}(-\omega;\omega,\omega,-\omega)$	$0\text{-}11.5 \times 10^{-8}$ esu		DFWM	0.50-0.80	172
$[Ir(CHCHCMeNHEt)\{HB(dmpz)_3\}]$	CH_2Cl_2	n_2	$-6.6 \pm 0.7 \times 10^{-11}$ cm^2 W^{-1}		Z-scan	0.53	173
$[CoFe_2(\mu_3\text{-}S)(\mu_3\text{-}Se)(CO)_6(\eta^5\text{-}C_5H_5)]$		γ	2.7×10^{-14} m^2 W^{-1}	~550	Z-scan	0.53	174
		γ	-5.8×10^{-18} m^2 W^{-1}	~550	Z-scan	1.06	174

Table 1.25. Third-order measurements on organometallic films and composites.

Material	Film Thickness (nm)	$\chi^{(3)}$ (10^{-12} esu)	γ (10^{-36} esu)	Technique	Fund. (μm)	Ref.
$[Fe\{\eta^5\text{-}C_5H_3(C_6H_{13})\text{-}2\text{-}(E)\text{-}CH{=}CH\}_2]_n$		1-4		THG	1.0-2.4	175
$[(N{=}CMe\text{-}\eta^5\text{-}C_5H_4)Fe\{\eta^5\text{-}C_5H_4CMe{=}NN{=}CMeC(CH_2CH_2CH_3){=}N\}]_n$	190	9.43		THG	1.05	155
	190	12.0		THG	1.2	155
	190	19.8		THG	1.5	155
	190	22.3		THG	1.8	155
	190	21.1		THG	1.95	155
$[Ru(N{\equiv}CC_6H_4\text{-}4\text{-}NO_2)(dppe)(\eta^5\text{-}C_5H_5)][BPh_4]^a$	200-400	0.07	230	THG	1.06	176
$[Ru(N{\equiv}CC_6H_4\text{-}4\text{-}NO_2)(dppe)(\eta^5\text{-}C_5H_5)][PF_6]^a$	200-400	0.17	470	THG	1.06	176
$[Ru(N{\equiv}CC_6H_4\text{-}4\text{-}NO_2)(dppe)(\eta^5\text{-}C_5H_5)][CF_3SO_3]^a$	200-400	0.23	510	THG	1.06	176
$[Ru(N{\equiv}CC_6H_4\text{-}4\text{-}NO_2)(dppe)(\eta^5\text{-}C_5H_5)][MeC_6H_4\text{-}4\text{-}SO_3]^a$	200-400	0.23	630	THG	1.06	176
$[Ru(N{\equiv}CC_6H_4\text{-}4\text{-}NO_2)(dppe)(\eta^5\text{-}C_5H_5)][BF_4]^a$	200-400	0.27	690	THG	1.06	176
$[Ru(N{\equiv}CC_6H_4\text{-}4\text{-}NO_2)((+)\text{-}diop)(\eta^5\text{-}C_5H_5)][PF_6]^a$	200-400	0.24	720	THG	1.06	176
$[Ru(N{\equiv}CC_6H_4\text{-}4\text{-}NO_2)((+)\text{-}diop)(\eta^5\text{-}C_5H_5)][CF_3SO_3]^a$	200-400	0.21	650	THG	1.06	176
$[Ru(N{\equiv}CC_6H_4\text{-}4\text{-}NO_2)((+)\text{-}diop)(\eta^5\text{-}C_5H_5)][MeC_6H_4\text{-}4\text{-}SO_3]^a$	200-400	0.10	320	THG	1.06	176
$[Ru(N{\equiv}CC_6H_4\text{-}4\text{-}NMe_2)(dppe)(\eta^5\text{-}C_5H_5)][PF_6]^a$	200-400	0.21	590	THG	1.06	176
$[Ru(N{\equiv}CC_6H_4\text{-}4\text{-}Ph)(dppe)(\eta^5\text{-}C_5H_5)][PF_6]^a$	200-400	0.24	660	THG	1.06	176
$[Ru(N{\equiv}C\text{-}(E)\text{-}CH{=}CHC_6H_4\text{-}4\text{-}NO_2)(dppe)(\eta^5\text{-}C_5H_5)][PF_6]^a$	200-400	0.36	1020	THG	1.06	176
$[Ru(N{\equiv}CC_6H_4\text{-}4\text{-}C_6H_4\text{-}4\text{-}NO_2)(dppe)(\eta^5\text{-}C_5H_5)][PF_6]^a$	200-400	0.76	2280	THG	1.06	176
$[Fc((E)\text{-}CH{=}CH)_3Fc]^b$	1000-2000	0.029		DFWM	0.53	177
$[(^tBu_4\text{-phthalocyaninato})Ru(4\text{-}CNC_6H_4NC)]_n^c$	160	3.7 ± 1.5	-	THG	1.06	172

[a] As a polymethyl methacrylate composite, ca 10% by mass. [b] As a polystyrene composite, ca 2.5% by mass. [c] As a spin-cast film.

1.6. Optical limiting properties of organometallic complexes

The optical limiting properties of metal cluster compounds and some fullerene complexes have been studied by reverse saturable absorption (RSA), with some of the results reviewed.[178] Table 1.26. contains optical limiting data for the cluster and fullerene complexes investigated.

Cyclopentadienyliron carbonyl tetramer ($[Fe(CO)(\eta^5\text{-}C_5H_5)]_4$, King's complex) has been shown to exhibit RSA on picosecond timescales.[179] The cross section of the singlet excited state is about twice that of the ground state, much too small to explain the degree of RSA observed on nanosecond timescales.[179] Subsequently, cross sections for ground and first excited state absorptions, first excited state lifetime and an upper limit on the second excited state lifetime were determined.[180] The contribution of intersystem crossing to the triplet state has been assessed; from the picosecond measurements, it seems that the majority of molecules relax directly from the first excited singlet state to the ground state with minimal population in the triplet excited state.

Parameters gained from the picosecond measurements have been used in conjunction with the five level model to attempt to predict the response observed on the nanosecond timescale; however, the nanosecond response was too strong to be modelled by the excited state parameter extracted from the picosecond experiments. In order to explain the difference between the picosecond and nanosecond responses, further experiments with varying laser fluences (where fluence is the energy of the laser per unit of area) and delay times between pump and probe beams were performed, which suggested that the large nanosecond responses had significant thermally induced scattering (this thermal effect is too slow to affect the picosecond measurements at fluences used to obtain previous data). In order to eliminate this thermally induced scattering, nanosecond measurements were perfomed on King's complex embedded in a solid host, resulting in much better agreement with the five level model using picosecond parameters but even better agreement with a three level model (i.e. ignoring triplet absorption).[180] It seems then that triplet absorption plays a very minor role in RSA of King's complex.

The ground to first excited state transition has been ascribed to electron transfer from a *d*-orbital of the metal to an antibonding orbital.[181] To determine the origin of the excited state absorption responsible for RSA in King's complex, several derivatives of this complex were prepared and RSA measurements performed on a picosecond timescale,[181] with $[Fe(CO)(\eta^5\text{-}C_5H_4Me)]_4$, $[Fe(COAlEt_3)(\eta^5\text{-}C_5H_5)]_4$ and King's complex affording virtually

the same response.[181] Both LMCT and MLCT transitions have therefore been rejected as the source of the excited state absorption, as these cluster modifications impact on charge transfer transitions involving carbonyl ($[Fe(COAlEt_3)(\eta^5\text{-}C_5H_5)]_4$) and cyclopentadienyl ($[Fe(CO)(\eta^5\text{-}C_5H_4Me)]_4$) ligands. The measured excited state cross section in King's complex and its methylcyclopentadienyl analogue showed no solvent dependence for solvents dichloromethane, thf and toluene; the excited state transition responsible has therefore been tentatively assigned to a second *d-d* transition within the metal core.

A series of iron-cobalt mixed-metal clusters were examined to probe the effect of ligand variation (CO to PMe_3 to PPh_3) and removal of hydride ligand ([cluster]H versus [cluster]$^-$) on the RSA response.[182,183] It was found that the RSA response varies little upon hydride removal, but that ligand substitution strongly affects optical limiting performance;[182] significantly, although replacing PMe_3 by PPh_3 produces large changes in the optical limiting response, no change was observed in the ground state UV-vis spectrum.

Fullerene derivatives have also been investigated. Complexation of both C_{60} and C_{70} modifies the absorption spectra significantly, with large shifts (50-100 nm) in absorption maxima. The first excited state cross sections σ_{01} of the complexes are all larger than those of the non-ligated fullerenes (C_{60}: 1.45×10^{-18} cm^2; C_{70} 2.94×10^{-18} cm^2), and the σ_{12}/σ_{01} ratios for the non-ligated fullerenes (C_{60}: 4.16; C_{70} 2.74) are larger than those for the fullerene complexes with the exception of the C_{60}-chromium complexes measured by Song *et al.* Inclusion of the metal fragment in the latter complex improves the optical limiting properties compared to C_{60}. Each of the other complexes in Table 1.26. are poorer optical limiters than the free fullerenes.

Table 1.26. Optical limiting data.

Complex	Solvent	λ (nm)	Pulse Width	σ_{01} (10^{-18} cm^2)	σ_{12} (10^{-18} cm^2)	τ_{10}	τ_{21} (ps)	Ref.
$[Fe(CO)(\eta^5\text{-}C_5H_5)]_4$	CH_2Cl_2	532	25 ps	4.1	7.8 ± 0.8	120 ± 5 ps	< 1	179-181
$[FeMe(CO)(\eta^5\text{-}C_5H_4Me)]_4$	CH_2Cl_2	532	25 ps	4.7	9.1 ± 0.9	120 ± 5 ps		181
$[Fe(COAlEt_3)(\eta^5\text{-}C_5H_5)]_4$	CH_2Cl_2	532	25 ps	4.9	7.3 ± 1.4	120 ± 5 ps		181
$[HFeCo_3(CO)_{12}]$	CH_2Cl_2	532	8 ns					182,183
$[NEt_4][FeCo_3(CO)_{12}]$	CH_2Cl_2	532	8 ns					182,183
$[HFeCo_3(CO)_{10}(PMe_3)_2]$	CH_2Cl_2	532	8 ns			~115 ns		182,183
$[HFeCo_3(CO)_{10}(PPh_3)_2]$	CH_2Cl_2	532	8 ns			~115 ns		182,183
$[(\eta^2\text{-}C_{60})Pt(PPh_3)_2]$	toluene	588	500 ps	11.4	16.4			171
$[(\eta^2\text{-}C_{60})Pd(PPh_3)_2]$	toluene	588	500 ps	5.61	9.09			171
$[(\eta^2\text{-}C_{70})Pd(PPh_3)_2]$	toluene	588	500 ps	11.6	14.2			171
$[(\eta^2\text{-}C_{60})IrI(CO)(PMePh_2)_2]$	toluene	588	500 ps	2.56	7.11			171
$[(\eta^2\text{-}C_{70})IrI(CO)(PMePh_2)_2]$	toluene	588	500 ps	3.46	8.93			171
$[(\eta^2\text{-}C_{60})Cr(CO)_3(dppe)]$	CH_2Cl_2	532	21 ps	7.5	350			184

1.7. Conclusion

The studies summarized above have begun to establish structure/NLO property relationships for organometallic systems, but a great deal of work investigating variation in metal, charge-transfer ligands, oxidation state, co-ligands, and geometry remains to be done. The molecular nonlinearities obtained for some of the complexes are extremely large, suggesting that the potential for application of organometallics remains.

In the current work, the results of studies addressing some of the points mentioned above are presented, namely, the effect of metal variation (Chapter 2), charge-transfer ligands (Chapter 3) and molecular geometry (Chapter 4) upon the optical nonlinearities.

1.8. References

(1) Nie, W. *Adv. Mater.* **1993**, *5*, 520.

(2) Allen, S. *New Scientist* **1989**, *1 July*, 31.

(3) *Nonlinear Optical Properties of Organic and Polymeric Materials*; Williams, D. J., Ed. American Chemical Society: Washington, D.C., 1983; Vol. 233.

(4) *Nonlinear Optical Properties of Organic Molecules and Crystals I*; Chemla, D. S. and Zyss, J., Eds.; Academic Press: Orlando, 1987.

(5) *Nonlinear Optical Properties of Organic Molecules and Crystals II*; Chemla, D. S. and Zyss, J., Eds.; Academic Press: Orlando, 1987.

(6) *Nonlinear Optical Properties of Polymers*; Heeger, A. J., Orenstein, J. and Ulrich, D. R., Eds.; Materials Research Society: Pittsburgh, 1988.

(7) *Organic Materials for Non-linear Optics*; Hann, R. A. and Bloor, D., Eds.; Royal Society of Chemistry: London, 1989.

(8) *Nonlinear Optical Effects in Organic Polymers*; Messier, J., Kajzar, F., Prasad, P. and Ulrich, D., Eds.; Kluwer Academic Publishers: Dordrecht, 1989; Vol. E162.

(9) *Nonlinear Optics of Organics and Semiconductors*; Kobayashi, T., Ed. Springer-Verlag: Berlin, 1989.

(10) *Materials for Non-linear and Electro-optics 1989*; Lyons, M. H., Ed. Institute of Physics: Bristol, 1989.

(11) *Materials for Nonlinear Optics, Chemical Perspectives*; Marder, S. R., Sohn, J. E. and Stucky, G. D., Eds.; American Chemical Society: Washington DC, 1991.

(12) *Organic Materials for Non-linear Optics II*; Hann, R. A. and Bloor, D., Eds.; Royal Society of Chemistry: London, 1991.

(13) *Organic Molecules for Nonlinear Optics and Photonics*; Messier, J., Kajzar, F. and Prasad, P., Eds.; Kluwer: Dordrecht, 1991.

(14) *Organic Materials for Non-linear Optics III*; Ashwell, G. J. and Bloor, D., Eds.; Royal Society of Chemistry: Cambridge, 1993.

(15) Williams, D. J. *Angew. Chem., Int. Ed. Engl.* **1984**, *23*, 690.

(16) Garito, A.; Fang Shi, R.; Wu, M. *Physics Today* **1994**, *May*, 51.

(17) Marder, S. R.; Perry, J. W.; Bourhill, G.; Gorman, C. B.; Tiemann, B. G.; Mansour, K. *Science* **1993**, *261*, 186.

(18) Nalwa, H. S. *Adv. Mater.* **1993**, *5*, 341.

(19) Zyss, J. *Nonlinear Opt.* **1991**, *1*, 3.

(20) Nalwa, H. S. *Appl. Organomet. Chem.* **1991**, *5*, 349.

(21) Marder, S. R. In *Inorganic Materials*; Bruce, D. W. and O'Hare, D., Eds.; Wiley: Chichester, 1992, p 116.

(22) Long, N. J. *Angew. Chem., Int. Ed. Engl.* **1995**, *34*, 21.

(23) Nalwa, H. S.; Watanabe, T.; Miyata, S. *Adv. Mater.* **1995**, *7*, 754.

(24) Kanis, D. R.; Ratner, M. A.; Marks, T. J. *Chem. Rev.* **1994**, *94*, 195.

(25) Shen, Y. R. *The Principles of Nonlinear Optics*; Wiley: New York, 1984.

(26) Butcher, P. N.; Cotter, D. *The Elements of Nonlinear Optics*; Cambridge University Press: New York, 1990.

(27) Boyd, R. W. *Nonlinear Optics*; Academic Press: New York, 1992.

(28) Sutherland, R. L. *Handbook of Nonlinear Optics*; Marcel Dekker: New York, 1996.

(29) Zyss, J.; Chemla, D. S. In *Nonlinear Optical Properties of Organic Molecules and Crystals I*; Chemla, D. S. and Zyss, J., Eds.; Academic Press: New York, 1987, p 23.

(30) Kurtz, S. K.; Perry, T. T. *J. Appl. Phys.* **1968**, *39*, 3798.

(31) Bosshard, C.; Knöpfle, G.; Prêtre, P.; Günter, P. *J. Appl. Phys.* **1992**, *71*, 1594.

(32) Paley, M. S.; Harris, J. M.; Looser, H.; Baumert, J. C.; Bjorklund, G. C.; Jundt, D.; Twieg, R. J. *J. Org. Chem.* **1989**, *54*, 3774.

(33) Lequan, M.; Lequan, R. M.; Ching, K. C. *J. Mater. Chem.* **1991**, *1*, 997.

(34) Maker, P. D.; Terhune, R. W.; Nisenoff, M.; Savage, C. M. *Phys. Rev. Lett.* **1962**, *8*, 21.

(35) Chemla, D. S.; Oudar, J. L.; Jerphagnon, J. *Phys. Rev. B* **1975**, *12*, 4534.

(36) Clays, K.; Persoons, A. *Phys. Rev. Lett.* **1991**, *66*, 2980.

(37) Clays, K.; Persoons, A. *Rev. Sci. Instrum.* **1992**, *63*, 3285.

(38) Hendrickx, E.; Dehu, C.; Clays, K.; Brédas, J. L.; Persoons, A. In *Polymers for Second-Order Nonlinear Optics*; Lindsay, G. A. and Singer, K. D., Eds.; American Chemical Society: Washington, DC, 1995, p 82.

(39) Sheik-Bahae, M.; Said, A. A.; Wei, T.; Hagan, D. J.; van Stryland, E. W. *IEEE J. Quantum Electr.* **1990**, *26*, 760.

(40) Marder, S. R.; Perry, J. W.; Schaefer, W. P. *Science* **1989**, *245*, 626.

(41) Yamazaki, Y.; Hosono, K.; Matsuda, H.; Minami, N.; Asai, M.; Nakanishi, H. *Biotechnol. Bioeng.* **1991**, *38*, 1218.

(42) Marder, S. R.; Perry, J. W.; Tiemann, B. G.; Schaefer, W. P. *Organometallics* **1991**, *10*, 1896.

(43) Marder, S. R.; Tiemann, B. G.; Perry, J. W.; Cheng, L. T.; Tam, W.; Schaefer, W. P.; Marsh, R. E. In *Materials for Nonlinear Optics: Chemical Perspectives*; Marder, S. R., Sohn, J. E. and Stucky, G. D., Eds.; American Chemical Society: Washington, DC, 1991; Vol. 455, p 187.

(44) Marder, S. R.; Perry, J. W.; Schaefer, W. P.; Tiemann, B. G.; Groves, P. C.; Perry, K. J. *Proc. SPIE-Int. Soc. Opt. Eng.* **1989**, *1147*, 108.

(45) Marder, S. R.; Perry, J. W.; Schaefer, W. P.; Ginsburg, E. J.; Gorman, C. B.; Grubbs, R. H. *Mat. Res. Soc. Symp. Proc.* **1990**, *175*, 101.

(46) Green, M. L. H.; Marder, S. R.; Thompson, M. E.; Bandy, J. A.; Bloor, D.; Kolinsky, P. V.; Jones, R. J. *Nature* **1987**, *330*, 360.

(47) Bunting, H. E.; Green, M. L. H.; Marder, S. R.; Thompson, M. E.; Bloor, D.; Kolinsky, P. V.; Jones, R. J. *Polyhedron* **1992**, *11*, 1489.

(48) Bandy, J. A.; Bunting, H. E.; Green, M. L. H.; Marder, S. R.; Thomson, M. E.; Bloor, D.; Kolinsky, P. V.; Jones, R. J. In *Organic Materials for Nonlinear Optics*; Hann, R. A. and Bloor, D., Eds.; Royal Society of Chemistry: London, 1989; Vol. 69, p 219.

(49) Green, M. L. H.; Qin, J.; O'Hare, D.; Bunting, H. E.; Thompson, M. E.; Marder, S. R.; Chatakondu, K. *Pure Appl. Chem.* **1989**, *61*, 817.

(50) Tiemann, B. G.; Marder, S. R.; Perry, J. W.; Cheng, L.-T. *Chem. Mater.* **1990**, *2*, 690.

(51) Balavoine, G. G. A.; Daran, J.-C.; Iftime, G.; Lacroix, P. G.; Manoury, E.; Delaire, J. A.; Maltey-Fanton, I.; Nakatani, K.; Bella, S. D. *Organometallics* **1999**, *18*, 21.

(52) Bandy, J. A.; Bunting, H. E.; Garcia, M.-H.; Green, M. L. H.; Marder, S. R.; Thompson, M. E.; Bloor, D.; Kolinsky, P. V.; Jones, R. J.; Perry, J. W. *Polyhedron* **1992**, *11*, 1429.

(53) Coe, B. J.; Kurek, S. S.; Rowley, N. M.; Foulon, J. D.; Hamor, T. A.; Harman, M. E.; Hursthouse, M. B.; Jones, C. J.; McCleverty, J. A.; Bloor, D. *Chemtronics* **1991**, *5*, 23.

(54) Coe, B. J.; Jones, C. J.; McCleverty, J. A.; Bloor, D.; Kolinsky, P. V.; Jones, R. J. *J. Chem. Soc., Chem. Commun.* **1989**, 1485.

(55) Coe, B. J.; Foulon, J. D.; Hamor, T. A.; Jones, C. J.; McCleverty, J. A.; Bloor, D.; Cross, G. H.; Axon, T. L. *J. Chem. Soc., Dalton Trans.* **1994**, 3427.

(56) Coe, B. J.; Hamor, T. A.; Jones, C. J.; McCleverty, J. A.; Bloor, D.; Cross, G. H.; Axon, T. L. *J. Chem. Soc., Dalton Trans.* **1995**, 673.

(57) Anderson, A. G.; Calabrese, J. C.; Tam, W.; Williams, I. D. *Chem. Phys. Lett.* **1987**, *134*, 392.

(58) Eaton, D. F.; Anderson, A. G.; Tam, W.; Wang, Y. In *Polymers for High Technology: Electronics and Photonics*; Bowden, M. J. and Turner, S. R., Eds.; American Chemical Society: Washington, DC, 1987; Vol. 346, p 381.

(59) Eaton, D. F.; Anderson, A. G.; Tam, W.; Wang, Y. *J. Am. Chem. Soc.* **1987**, *109*, 1886.

(60) Tam, W.; Eaton, D. F.; Calabrese, J. C.; Williams, I. D.; Wang, Y.; Anderson, A. G. *Chem. Mater.* **1989**, *1*, 128.

(61) Tam, W.; Calabrese, J. C. *Chem. Phys. Lett.* **1988**, *144*, 79.

(62) Tam, W.; Wang, Y.; Calabrese, J. C.; Clement, R. A. *Proc. SPIE-Int. Soc. Opt. Eng.* **1988**, *971*, 107.

(63) Dias, A. R.; Garcia, M. H.; Robalo, M. P.; Green, M. L. H.; Lai, K. K.; Pulham, A. J.; Klueber, S. M.; Balavoine, G. *J. Organomet. Chem.* **1993**, *453*, 241.

(64) Dias, A. R.; Garcia, M. H.; Rodrigues, J. C.; Green, M. L. H.; Kuebler, S. M. *J. Organomet. Chem.* **1994**, *475*, 241.

(65) Whittall, I. R.; Humphrey, M. G.; Samoc, M.; Luther-Davies, B.; Hockless, D. C. R. *J. Organomet. Chem.* **1997**, *544*, 189.

(66) Meredith, G. R. In *Nonlinear Optical Properties of Organic and Polymeric Materials*; Williams, D. J., Ed.; American Chemical Society: Washington, DC, 1983, p 27.

(67) Frazier, C. C.; Harvey, M. A.; Cockerham, M. P.; Hand, H. M.; Chauchard, E. A.; Lee, C. H. *J. Phys. Chem.* **1986**, *90*, 5703.

(68) Kobayashi, T. *IEICE Trans. Electron.*, **1992**, *E75*, 36.

(69) Bandy, J. A.; Bunting, H. E.; Garcia, M.-H.; Green, M. L. H.; Marder, S. R.; Thompson, M. E.; Bloor, D.; Kolinsky, P. V.; Jones, R. J. In *Organic Materials for Nonlinear Optics*; Hann, R. A. and Bloor, D., Eds.; Royal Society of Chemistry: London, 1989; Vol. 69, p 225.

(70) Whittall, I. R.; Cifuentes, M. P.; Costigan, M. J.; Humphrey, M. G.; Goh, S. C.; Skelton, B. W.; White, A. H. *J. Organomet. Chem.* **1994**, *471*, 193.

(71) Houlton, A.; Miller, J. R.; Silver, J.; Jassim, N.; Ahmet, M. J.; Axon, T. L.; Bloor, D.; Cross, G. H. *Inorg. Chim. Acta* **1993**, *205*, 67.

(72) Coe, B. J.; Jones, C. J.; McCleverty, J. A.; Bloor, D.; Cross, G. *J. Organomet. Chem.* **1994**, *464*, 225.

(73) Calabrese, J. C.; Tam, W. *Chem. Phys. Lett.* **1987**, *133*, 244.

(74) Kimura, M.; Abdel-Halim, H.; Robinson, D. W.; Cowan, D. O. *J. Organomet. Chem.* **1991**, *403*, 365.

(75) Pollagi, T. P.; Stoner, T. C.; Dallinger, R. F.; Gilbert, T. M.; Hopkins, M. D. *J. Am. Chem. Soc.* **1991**, *113*, 703.

(76) Benito, A.; Cano, J.; Martinez-Manez, R.; Paya, J.; Soto, J.; Julve, M.; Lloret, F.; Marcos, M. D.; Sinn, E. *J. Chem. Soc., Dalton Trans.* **1993**, 1999.

(77) Marder, T. B.; Lesley, G.; Yuan, Z.; Fyfe, H. B.; Chow, P.; Stringer, G.; Jobe, I. R.; Taylor, N. J.; Williams, I. D.; Kurtz, S. K. In *Materials for Nonlinear Optics: Chemical Perspectives*; Marder, S. R., Sohn, J. E. and Stucky, G. D., Eds.; American Chemical Society: Washington, DC, 1991; Vol. 455, p 605.

(78) Fyfe, H. B.; Mlekuz, M.; Stringer, G.; Taylor, N. J.; Marder, T. B. In *Inorganic and Organometallic Polymers with Special Properties*; Laine, R. M., Ed.; Kluwer: Dordrecht, 1992; Vol. 206, p 331.

(79) Coe, B. J.; Jones, C. J.; McCleverty, J. A. *Polyhedron* **1994**, *13*, 2107.

(80) O'Reilly, S. A.; White, P. S.; Templeton, J. L. *Chem. Mater.* **1996**, *8*, 93.

(81) Copley, R. C. B.; Lambeth, C.; Machell, J.; Mingos, D. M.; Murphy, D. M.; Powell, H. *J. Mater. Chem.* **1991**, *1*, 583.

(82) Wu, X.; Qin, J.; Liu, D.; Wu, B.; Chen, C. *Nonlinear Optics* **1994**, *7*, 153.

(83) Lesley, G.; Yuan, Z.; Stringer, G.; Jobe, I. R.; Taylor, N. J.; Koch, L.; Scott, K.; Marder, T. B. In *Organic Materials for Non-linear Optics II*; Hann, R. A. and Bloor, D., Eds.; Royal Society of Chemistry: London, 1991, p 197.

(84) Eaton, D. F.; Anderson, A. G.; Tam, W.; Wang, Y. *J. Am. Chem. Soc.* **1987**, *109*, 1886.

(85) Wright, M. E.; Cochran, B. B.; Toplikar, E. G.; Lackritz, H. S.; Kerney, J. T. In *Inorganic and Organometallic Polymers II: Advanced Materials and Intermediates*;

Wisian-Neilson, P., Allcock, H. R. and Wynne, K. J., Eds.; American Chemical Society: Washington, DC, 1994; Vol. 572, p 456.

(86) Wright, M. E.; Toplikar, E. G.; Lackritz, H. S.; Kerney, J. T. *Macromolecules* **1994**, *27*, 3016.

(87) Lacroix, P. G.; Lin, W.; Wong, G. K. *Chem. Mater.* **1995**, *7*, 1293.

(88) Corriu, R. J. P.; Douglas, W. E.; Yang, Z.; Karakus, Y.; Cross, G. H.; Bloor, D. *J. Organomet. Chem.* **1993**, *455*, 69.

(89) Wang, K. Z.; Huang, C. H.; Zhou, D. J.; Xu, G. X.; Xu, Y.; Liu, Y. Q.; Zhu, D. B.; Zhao, X. S.; Xie, X. M. *Solid State Commun.* **1995**, *93*, 189.

(90) Gao, L. H.; Wang, K. Z.; Huang, C. H.; Zhao, X. S.; Xia, X. H.; Xu, J. M.; Li, T. K. *Chem. Lett.* **1995**, *11*, 1049.

(91) Kezhi, W.; Chunhui, H.; Guangxian, X.; Xinsheng, Z.; Xiaoming, X.; Lingge, X.; Tiankai, L. *Thin Solid Films* **1994**, *247*, 1.

(92) Chai, X. D.; Yang, W. S.; Lu, R.; Cao, Y. W.; Lu, N.; Jiang, Y. S.; Bai, Y. B.; Li, T. J. *Supramol. Sci.* **1998**, *5*, 679.

(93) Cao, Y. W.; Chai, X. D.; Yang, W. S.; Lu, R.; Jiang, Y. S.; Li, T. J.; Blanchard-Desce, M.; Lehn, J. M. *Thin Solid Films* **1996**, *285*, 859.

(94) Richardson, T.; Roberts, G. G.; Polywka, M. E. C.; Davies, S. G. *Thin Solid Films* **1988**, *160*, 231.

(95) López-Garabito, C.; Campo, J. A.; Heras, J. V.; Cano, M.; Rojo, G.; Agulló-López, F. *J. Phys. Chem. B.* **1998**, *102*, 10698.

(96) Campo, J. A.; Cano, M.; Heras, J. V.; Lopez-Garabito, C.; Pinilla, E.; Torres, R.; Rojo, G.; Agullo-Lopez, F. *J. Mater. Chem.* **1999**, *9*, 899.

(97) Wright, M. E.; Toplikar, E. G.; Kubin, R. F.; Seltzer, M. D. *Macromolecules* **1992**, *25*, 1838.

(98) Calabrese, J. C.; Cheng, L.-T.; Green, J. C.; Marder, S. R.; Tam, W. *J. Am. Chem. Soc.* **1991**, *113*, 7227.

(99) Cheng, L. T.; Tam, W.; Meredith, G. R.; Marder, S. R. *Mol. Cryst. Liq. Cryst.* **1990**, *189*, 137.

(100) Marder, S. R.; Beratan, D. N.; Tiemann, B. G.; Cheng, L. T.; Tam, W. In *Organic Materials for Nonlinear Optics II*; Hann, R. A. and Bloor, D., Eds.; Royal Society of Chemistry: London, 1991; Vol. 91, p 165.

(101) Cheng, L.-T. In *Organic Molecules for Nonlinear Optics and Photonics*; Messier, J., Kajzar, F. and Prasad, P., Eds.; Kluwer: Dordrecht, 1991; Vol. 194, p 121.

(102) Mata, J.; Uriel, S.; Peris, E.; Llusar, R.; Houbrechts, S.; Persoons, A. *J. Organomet. Chem.* **1998**, *562*, 197.

(103) Herrmann, R.; Pedersen, B.; Wagner, G.; Youn, J.-H. *J. Organomet. Chem.* **1998**, *571*, 261.

(104) Alagesan, K.; Ray, P. C.; Das, P. D.; Samuelson, A. G. *Curr. Sci.* **1996**, *70*, 69.

(105) Cadierno, V.; Conejero, S.; Gamasa, M. P.; Gimeno, J.; Asselberghs, I.; Houbrechts, S.; Clays, K.; Persoons, A.; Borge, J.; Garcia-Granda, S. *Organometallics* **1999**, *18*, 582.

(106) Behrens, U.; Brussaard, H.; Hagenau, U.; Heck, J.; Hendrickx, E.; Kornich, J.; van der Linden, J. G. M.; Persoons, A.; Spek, A. L.; Veldman, N.; Voss, B.; Wong, H. *Chem. Eur. J.* **1996**, *2*, 98.

(107) Briel, O.; Suenkel, K.; Krossing, I.; Noeth, H.; Schmaelzlin, E.; Meerholz, K.; Braeuchle, C.; Beck, W. *Eur. J. Inorg. Chem.* **1999**, 483.

(108) Hagenau, U.; Heck, J.; Hendrickx, E.; Persoons, A.; Schuld, T.; Wong, H. *Inorg. Chem.* **1996**, *35*, 7863.

(109) Yuan, Z.; Taylor, N. J.; Sun, Y.; Marder, T. B. *J. Organomet. Chem.* **1993**, *449*, 27.

(110) Lee, I. S.; Seo, H.; Chung, Y. K. *Organometallics* **1999**, *18*, 1091.

(111) Doisneau, G.; Balavoine, G.; Fillebeen-Khan, T.; Clinet, J.; Delaire, J.; Ledoux, I.; Loucif, R.; Puccetti, G. *J. Organomet. Chem.* **1991**, *421*, 299.

(112) Loucif-Saibi, R.; Delaire, J. A.; Bonazzola, L.; Doisneau, G.; Balavoine, G.; Fillebeen-Khan, T.; Ledoux, I.; Puccetti, G. *Chem. Phys.* **1992**, *167*, 369.

(113) Ledoux, I. *Synth. Met.* **1993**, *54*, 123.

(114) Alain, V.; Blanchard-Desce, M.; Chen, C.-T.; Marder, S. R.; Fort, A.; Barzoukas, M. *Synth. Met.* **1996**, *81*, 133.

(115) Blanchard-Desce, M.; Runser, C.; Fort, A.; Barzoukas, M.; Lehn, J.-M.; Bloy, V.; Alain, V. *Chem. Phys.* **1995**, *199*, 253.

(116) Alain, V.; Fort, A.; Barzoukas, M.; Chen, C.-T.; Blanchard-Desce, M.; Marder, S. R.; Perry, J. W. *Inorg. Chim. Acta* **1996**, *242*, 43.

(117) Wu, Z.; Ortiz, R.; Fort, A.; Barzoukas, M.; Marder, S. R. *J. Organomet. Chem.* **1997**, *528*, 217.

(118) Cheng, L.-T.; Tam, W.; Eaton, D. F. *Organometallics* **1990**, *9*, 2856.

(119) Tam, W.; Cheng, L. T.; Bierlein, J. D.; Cheng, L. K.; Wang, Y.; Feiring, A. E.; Meredith, G. R.; Eaton, D. F.; Calabrese, J. C.; Rikken, G. L. J. A. In *Materials for Nonlinear Optics: Chemical Perspectives*; Marder, S. R., Sohn, J. E. and Stucky, G. D., Eds.; American Chemical Society: Washington, DC, 1991; Vol. 455, p 158.

(120) Maiorana, S.; Papagni, A.; Licandro, E.; Persoons, A.; Clay, K.; Houbrechts, S.; Porzio, W. *Gazz. Chim. Ital.* **1995**, *125*, 377.

(121) Roth, G.; Fischer, H.; Meyer-Friedrichsen, T.; Heck, J.; Houbrechts, S.; Persoons, A. *Organometallics* **1998**, *17*, 1511.

(122) Bruce, D. W.; Thorton, A. *Mol. Cryst. Liq. Cryst.* **1993**, *231*, 253.

(123) Houbrechts, S.; Clays, K.; Persoons, A.; Cadierno, V.; Gamasa, M. P.; Gimeno, J.; Whittall, I. R.; Humphrey, M. G. *Proc. SPIE-Int. Soc. Opt. Eng.* **1996**, *2852*, 98.

(124) Houbrechts, S.; Clays, K.; Persoons, A.; Cadierno, V.; Gamasa, M. P.; Gimeno, J. *Organometallics* **1996**, *15*, 5266.

(125) Tamm, M.; Grzegorzeweski, A.; Steiner, T.; Jentzsch, T.; Werncke, W. *Organometallics* **1996**, *15*, 4984.

(126) Whittall, I. R.; Humphrey, M. G.; Cifuentes, M. P.; Samoc, M.; Luther-Davies, B.; Persoons, A.; Houbrechts, S.; Heath, G. A.; Hockless, D. C. R. *J. Organomet. Chem.* **1997**, *549*, 127.

(127) Whittall, I. R.; Humphrey, M. G.; Persoons, A.; Houbrechts, S. *Organometallics* **1996**, *15*, 1935.

(128) Wu, I.-Y.; Lin, J. T.; Luo, J.; Li, C.-S.; Tsai, C.; Wen, Y. S.; Hsu, C.-C.; Yeh, F.-F.; Liou, S. *Organometallics* **1998**, *17*, 2188.

(129) Naulty, R. H.; Cifuentes, M. P.; Humphrey, M. G.; Houbrechts, S.; Boutton, C.; Persoons, A.; Heath, G. A.; Hockless, D. C. R.; Luther-Davies, B.; Samoc, M. *J. Chem. Soc., Dalton Trans.* **1997**, 4167.

(130) Wu, I.-Y.; Lin, J. T.; Luo, J.; Sun, S.-S.; Li, C.-S.; Lin, K. J.; Tsai, C.; Hsu, C.-C.; Lin, J.-L. *Organometallics* **1997**, *16*, 2038.

(131) Tamm, M.; Jentzsch, T.; Werncke, W. *Organometallics* **1997**, *16*, 1418.

(132) Naulty, R. H.; McDonagh, A. M.; Whittall, I. R.; Cifuentes, M. P.; Humphrey, M. G.; Houbrechts, S.; Maes, J.; Persoons, A.; Heath, G. A.; Hockless, D. C. R. *J. Organomet. Chem.* **1998**, *563*, 137.

(133) Whittall, I. R.; Humphrey, M. G.; Houbrechts, S.; Maes, J.; Persoons, A.; Schmid, S.; Hockless, D. C. R. *J. Organomet. Chem.* **1997**, *544*, 277.

(134) Whittall, I. R.; Humphrey, M. G.; Houbrechts, S.; Persoons, A.; Hockless, D. C. R. *Organometallics* **1996**, *15*, 5738.

(135) Whittall, I. R.; Cifuentes, M. P.; Humphrey, M. G.; Luther-Davies, B.; Samoc, M.; Houbrechts, S; Persoons, A.; Heath, G. A.; Bogsanyi, D. *Organometallics* **1997**, *16*, 2631.

(136) Whitaker, C. M.; Patterson, E. V.; Kott, K. L.; McMahon, R. J. *J. Am. Chem. Soc.* **1996**, *118*, 9966.

(137) Wenseleers, W.; Gerbrandij, A. W.; Goovaerts, E.; Garcia, M. H.; Robalo, M. P.; Mendes, P. J.; Rodrigues, J. C.; Dias, A. R. *J. Mater. Chem.* **1998**, *8*, 925.

(138) Laidlaw, W. M.; Denning, R. G.; Verbiest, T.; Chauchard, E.; Persoons, A. *Nature* **1993**, *363*, 58.

(139) Morrison, I. D.; Denning, R. G.; Laidlaw, W. M.; Stammers, M. A. *Rev. Sci. Instrum.* **1996**, *67*, 1445.

(140) Dias, A. R.; Garcia, M. H.; Mendes, P.; Fatima, M.; Piedade, M.; Duarte, M. T.; Calhorda, M. J.; Mealli, C.; Wenseleers, W.; Gerbrandij, A. W.; Goovaerts, E. *J. Organomet. Chem.* **1998**, *553*, 115.

(141) Laidlaw, W. M.; Denning, R. G.; Verbiest, T.; Chauchard, E.; Persoons, A. *Proc. SPIE-Int. Soc. Opt. Eng.* **1994**, *2143*, 14.

(142) Winter, C. S.; Oliver, S. N.; Rush, J. D. *Optics Commun.* **1988**, *69*, 45.

(143) Myers, L. K.; Langhoff, C.; Thompson, M. E. *J. Am. Chem. Soc.* **1992**, *114*, 7560.

(144) Ghosal, S.; Samoc, M.; Prasad, P. N.; Tufariello, J. T. *J. Phys. Chem.* **1990**, *94*, 2847.

(145) Winter, C. S.; Oliver, S. N.; Rush, J. D. In *Organic Materials for Nonlinear Optics*; Hann, R. A. and Bloor, D., Eds.; Royal Society of Chemistry: London, 1989; Vol. 69, p 232.

(146) Winter, C. S.; Oliver, S. N.; Rush, J. D. In *Nonlinear Optical Effects in Organic Polymers*; Messier, J., Kajzar, F., Prasad, P. and Ulrich, D., Eds.; Kluwer: Dordrecht, 1989; Vol. 162, p 247.

(147) Yuan, Z.; Stringer, G.; Jobe, I. R.; Kreller, D.; Scott, K.; Koch, L.; Taylor, N. J.; Marder, T. B. *J. Organomet. Chem.* **1993**, *452*, 115.

(148) Myers, L. K.; Ho, D. M.; Thompson, M. E.; Langhoff, C. *Polyhedron* **1995**, *14*, 57.

(149) Thompson, M. E.; Chiang, W.; Myers, L. K.; Langhoff, C. *Proc. SPIE-Int. Soc. Opt. Eng.* **1991**, *1497*, 423.

(150) Winter, C. S.; Oliver, S. N.; Rush, J. D.; Manning, R. J.; Hill, C.; Underhill, A. In *Materials for Nonlinear Optics: Chemical Perspectives*; Marder, S. R., Sohn, J. E. and Stucky, G. D., Eds.; American Chemical Society: Washington, DC, 1991; Vol. 455, p 616.

(151) Oliver, S. N.; Winter, C. S.; Rush, J. D.; Underhill, A. E.; Hill, C. *Proc. SPIE-Int. Soc. Opt. Eng.* **1990**, *1337*, 81.

(152) Blau, W. J.; Cardin, C. J.; Cardin, D. J.; Davey, A. P. In *Organic Materials for Nonlinear Optics III*; Ashwell, G. J. and Bloor, D., Eds.; Royal Society of Chemistry: Cambridge, 1993, p 124.

(153) Davey, A. P.; Page, H.; Blau, W. *Synth. Met.* **1993**, *55-57*, 3980.

(154) Davey, A. P.; Byrne, H. J.; Page, H.; Blau, W.; Cardin, D. J. *Synth. Met.* **1993**, *58*, 161.

(155) Nalwa, H. S. *Mater. Lett.* **1997**, *33*, 23.

(156) Whittall, I. R.; Humphrey, M. G.; Samoc, M.; Swiatkiewicz, J.; Luther-Davies, B. *Organometallics* **1995**, *14*, 5493.

(157) Whittall, I. R.; Humphrey, M. G.; Samoc, M.; Luther-Davies., B. *Angew. Chem., Int. Ed. Engl.* **1997**, *36*, 370.

(158) McDonagh, A. M.; Cifuentes, M. P.; Whittall, I. R.; Humphrey, M. G.; Samoc, M.; Luther-Davies, B.; Hockless, D. C. R. *J. Organomet. Chem.* **1996**, *526*, 99.

(159) Frazier, C. C.; Chauchard, E. A.; Cockerham, M. P.; Porter, P. L. *Mater. Res. Soc. Symp. Proc.* **1988**, *109*, 323.

(160) Porter, P. L.; Guha, S.; Kang, K.; Frazier, C. C. *Polymer* **1991**, *32*, 1756.

(161) Blau, W. J.; Byrne, H. J.; Cardin, D. J.; Davey, A. P. *J. Mater. Chem.* **1991**, *1*, 245.

(162) Davey, A. P.; Cardin, D. J.; Byrne, H. J.; Blau, W. In *Organic Molecules for Nonlinear Optics and Photonics*; Messier, J., Kajzar, F. and Prasad, P., Eds.; Kluwer: Dordrecht, 1991; Vol. 194, p 391.

(163) Haub, J.; Johnson, M.; Orr, B.; Woodruff, M.; Crisp, G., presented at *CLEO/QUELS '91*; Baltimore, 1991.

(164) Page, H.; Blau, W.; Davey, A. P.; Lou, X.; Cardin, D. J. *Synth. Met.* **1994**, *63*, 179.

(165) Guha, S.; Kang, K.; Porter, P.; Roach, J. F.; Remy, D. E.; Aranda, F. J.; Rao, D. V. G. L. N. *Opt. Lett.* **1992**, *17*, 264.

(166) Frazier, C. C.; Guha, S.; Chen, W. P.; Cockerham, M. P.; Porter, P. L.; Chauchard, E. A.; Lee, C. H. *Polymer* **1987**, *28*, 553.

(167) Guha, S.; Frazier, C. C.; Porter, P. L.; Kang, K.; Finberg, S. E. *Opt. Lett.* **1989**, *14*, 952.

(168) Guha, S.; Frazier, C. C.; Chen, W. P.; Porter, P.; Kang, K.; Finberg, S. E. *Proc. SPIE-Int. Soc. Opt. Eng.* **1989**, *1105*, 14.

(169) Ergorov, A. N.; Mavritsky, O. B.; Petrovsky, A. N.; Yakubovsky, K. V. *Laser Phys.* **1995**, *5*, 1006.

(170) Mavritsky, O. B.; Egorov, A. N.; Petrovsky, A. N.; Yakubovsky, K. V.; Blau, W. J.; Weldon, D. N.; Henary, F. Z. *Proc. SPIE-Int. Soc. Opt. Eng.* **1996**, *2854*, 254.

(171) Callaghan, J.; Weldon, D. N.; Henari, F. Z.; Blau, W.; Cardin, D. J. In *Electronic Properties of Fullerenes*; Kuzmany, H., Fink, J., Mehing, M. and Roth, S., Eds.; Springer: Berlin, 1993, p 307.

(172) Grund, A.; Kaltbeitzel, A.; Mathy, A.; Schwarz, R.; Bubeck, C. *J. Phys. Chem* **1992**, *96*, 7450.

(173) Hernandez, F. E.; Marcano, A. O.; Alvarado, Y.; Biondi, A.; Maillotte, H. *Opt. Commun.* **1998**, *152*, 77.

(174) Banerjee, S.; Kumar, G. R.; Mathur, P.; Sekar, P. *J. Chem. Soc., Chem. Commun.* **1997**, 299.

(175) Itoh, T.; Saitoh, H.; Iwatsuki, S. *J. Polym. Sci. Part A: Polym. Chem.* **1995**, *33*, 1589.

(176) Dias, A. R.; Garcia, M. H.; Rodrigues, J. C.; Petersen, J. C.; Bjornholm, T.; Geisler, T. *J. Mater. Chem.* **1995**, *5*, 1861.

(177) Sachtleben, M. L.; Spangler, C. W.; Tang, N.; Hellwarth, R.; Dalton, L. In *Organic Materials for Non-linear Optics III*; Ashwell, G. J. and Bloor, D., Eds.; Royal Society of Chemistry: London, 1993, p 231.

(178) Tutt, L. W.; Boggess, T. F. *Prog. Quant. Electr.* **1993**, *17*, 299.

(179) Allan, G. R.; Labergerie, D. R.; Rychnovsky, S. J.; Boggess, T. F.; Smirl, A. L.; Tutt, L. *J. Phys. Chem.* **1992**, *96*, 6313.

(180) Boggess, T. F.; Allan, G. R.; Rychnovsky, S. J.; Labergerie, D. R.; Venzke, C. H.; Smirl, A. L.; Tutt, L. W.; Kost, A. R.; McCahon, S. W.; Klein, M. B. *Opt. Eng.* **1993**, *32*, 1063.

(181) Allan, G. R.; Rychnovsky, S. J.; Venzke, C. H.; Boggess, T. F. *J. Phys. Chem.* **1994**, *98*, 216.

(182) Tutt, L. W.; McCahon, S. W. *Opt. Lett.* **1990**, *15*, 700.

(183) Tutt, L. W.; McCahon, S. W.; Klein, M. B. *Proc. SPIE-Int. Soc. Opt. Eng.* **1990**, *1307*, 315.

(184) Song, Y.; Fang, G.; Wang, Y.; Liu, S.; Li, C.; Song, L.; Zhu, Y.; Hu, Q. *Appl. Phys. Lett.* **1999**, *74*, 332.

Chapter 2

Acetylide Complexes of Iron, Ruthenium and Osmium, and Some of Their Nonlinear Optical Properties

Contents

Chapter 2

Acetylide Complexes of Iron, Ruthenium and Osmium and Some of Their Nonlinear Optical Properties

2.1. Introduction

Chapter 1 contains many examples of transition metal acetylide complexes possessing extremely large second-order nonlinearities. These complexes generally contain an electron donating species linked by a π-conjugated system to an electron accepting moiety. While there are many reports describing the effects of variation of donor and acceptor groups, modification of conjugated linkages, and ligand variation about the metal centres, few reports of the systematic variation of metals within a group exist.

While the current work was in progress, Wenseleers *et al*[1] prepared a series of cationic nitrile complexes (see Figure 2.1.(a) and Table 1.11.) and found that the trend in β_{HRS} for metal variation was iron > ruthenium > nickel > cobalt. They suggested a correlation between the N≡C stretching frequency and β.

Earlier studies of some metallocenyl complexes revealed larger values of β for ferrocenyl complexes than for the homologous ruthenocenyl examples.[2-5] In this group of complexes, the metal does not lie in the plane of the π-conjugation; rather, it is orthogonal to it (see Figure 2.1.(b); it has been suggested that this geometry may reduce the effectiveness of the metal as a donor in these molecules.[5]

Reports of second-order optical nonlinearities of several series of early transition metal complexes of chromium, molybdenum and tungsten[4,6-10] show that, for some examples, there is little difference upon metal replacement,[9] but with others significant differences are observed.[10] In any case, the metal variation in these complexes occurs at the group 6 metal centre (see Figure 2.1.1.(c)) which is acting as an electron acceptor, in contrast to the group

8 complexes targeted for investigation in this project in which the ligated metal is a donor group.

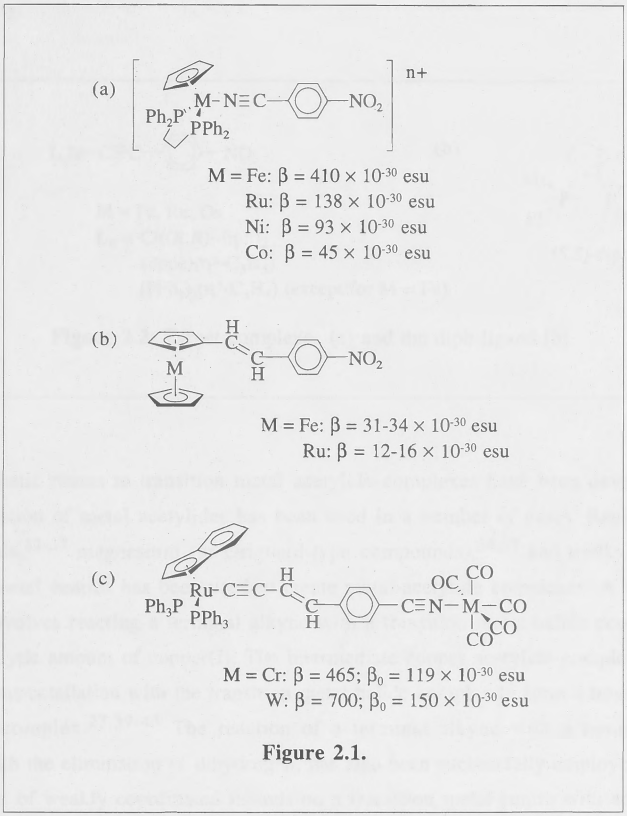

Figure 2.1.

The aim of the work presented in this Chapter is to examine the effect of metal variation upon the second-order optical nonlinearity of several series of group 8 transition metal acetylide complexes. The target complexes are shown in Figure 2.2.(a). In these complexes, the metal lies in the same plane as the alkynyl ligand π system and should therefore act as an effective electron donor. The alkynyl ligand $C{\equiv}CC_6H_4$-4-NO_2 was chosen because i) the nitro group acts as an effective electron acceptor, ii) the phenylethynyl moiety provides a system of π-delocalized electrons linking the donor to the acceptor, iii) the associated alkyne is straightforward to prepare, and iv) previous studies have shown that transition metal complexes incorporating this ligand have high molecular second-order optical

nonlinearities.[11] The optically active ligand 1,2-bis(methylphenylphosphino)benzene, henceforth referred to as diph (see Figure 2.2.(b)), was used in one series of complexes to ensure non-centrosymmetric packing in the solid state, a prerequisite for bulk second-order NLO activity.

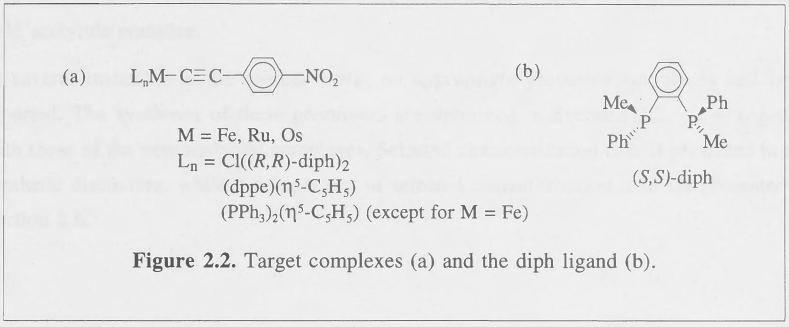

Figure 2.2. Target complexes (a) and the diph ligand (b).

Many synthetic routes to transition metal acetylide complexes have been developed. The transmetallation of metal acetylides has been used in a number of cases. Replacement of alkali metals,[12-33] magnesium (in Grignard-type compounds),[34,35] and trialkyltin[36-38] by transition metal centres has been used to create metal-acetylide complexes. A variation of this idea involves reacting a terminal alkyne with a transition metal halide complex along with a catalytic amount of copper(I). The intermediate copper acetylide complex may then undergo transmetallation with the transition metal halide complex to form a transition metal acetylide complex.[23,39-43] The reaction of a terminal alkyne with a transition metal hydride, with the elimination of dihydrogen, has also been successfully employed.[44-52] The replacement of weakly coordinated ligands on a transition metal centre with acetylide has been reported.[42,53-62] Oxidative addition of an alkyne to a transition metal centre is another proven synthetic procedure.[63-70] The synthetic approach used in the current work is based on literature procedures[71-81] that involve the formation of an intermediate vinylidene complex by reacting a terminal alkyne with a ligated transition metal halide (see Scheme 2.1).

$$[L_nMX] + HC{\equiv}CR \rightarrow [L_nM{=}C{=}CHR]^+X^- \xrightarrow{Base^-} [L_nMC{\equiv}CR] + BaseH + X^-$$

Scheme 2.1.

In some instances the vinylidene complex may be isolated, whereas in other cases it is preferable to perform the deprotonation step *in situ*. The deprotonation of the β-carbon of the vinylidene complex proceeds rapidly upon the addition of a base (such as methoxide ion) to yield the desired acetylide complex. A variation on this procedure involves including base in the reaction mixture, thereby deprotonating the vinylidene as soon as it is formed.[82-86] This method is used in the work presented in Chapter 3 for the formation of a gold acetylide complex.

In several instances in the current work, no appropriate precursor complexes had been reported. The syntheses of these precursors are described in Sections 2.2. - 2.4. together with those of the new acetylide complexes. Selected characterization data is presented in the synthetic discussion, while a comparison of selected characterization data are presented in Section 2.6.

2.2. Synthesis of Iron Complexes

2.2.1. Synthesis of $(-)_{436}$-trans-[Fe(4-C≡CC$_6$H$_4$NO$_2$)Cl((*R,R*)-diph)$_2$]

The new complex $(-)_{436}$-*trans*-[Fe(4-C≡CC$_6$H$_4$NO$_2$)Cl((*R,R*)-diph)$_2$] was prepared from its dichloro precursor, the latter prepared by extending the literature procedures for the preparation of [FeCl$_2$(diphos)$_2$][87] [where diphos = 1,2-bis(dimethylphosphino)benzene]. The acetylide complex was then synthesized by modifications to the procedure described for the synthesis of *trans*-[Ru(C≡CPh)Cl(dppe)$_2$].[80] An outline of the procedure is shown in Scheme 2.2.

The new iron dichloride complex $(-)_{589}$-*trans*-[FeCl$_2$((*R,R*)-diph)$_2$] was obtained in excellent yield by stirring two equivalents of the diph ligand with [FeCl$_2$·1.5THF][88] in refluxing methanol for 30 min. Performing the reaction at this temperature avoids racemization of the free diph ligand which ensues at temperatures approaching 80 °C. The complex was characterized by ^{1}H and ^{31}P NMR spectroscopy, microanalyses, FAB mass spectrometry and optical rotation measurements.

The *trans* geometry of the complex was established by ^{31}P NMR spectroscopy, a broad singlet at 67.7 ppm being observed. The optical activity of the complex was confirmed by optical rotation measurements. The complex has a large specific rotation at 589 nm with $[\alpha]_D$ = –1760 (*c* 0.101, CH_2Cl_2). The UV-vis spectrum contains overlapping bands at 37400 and 34700 cm^{-1}, characteristic of phenyl substituents on the phosphine,[11] together with a much weaker band at 26400 cm^{-1}.

Preparation of the complex $(-)_{436}$-*trans*-[Fe(4-C≡CC$_6$H$_4$NO$_2$)Cl((*R,R*)-diph)$_2$] (Figure 2.1.) proceeded in two steps. In the first step, a cationic vinylidene of the form [Fe(C=CHC$_6$H$_4$-4-NO$_2$)Cl((*R,R*)-diph)$_2$]$^+$ was formed by stirring *trans*-[FeCl$_2$((*R,R*)-diph)$_2$], 4-HC≡CC$_6$H$_4$NO$_2$ and sodium hexafluorophosphate in refluxing dichloromethane for 2 h. The hexafluorophosphate counterion stabilizes the above-mentioned vinylidene (both the sodium and ammonium salts of the hexafluorophosphate anion are used throughout this work, the use of a particular salt being determined by availability in the laboratory). The vinylidene complex is air sensitive, attempts at collection by filtration in air leading to significant decomposition. If the vinylidene was not isolated from any unreacted acetylene before addition of base (to form the acetylide complex), then two difficulties arose: i) separation of the acetylide product and any unreacted acetylene was extremely difficult, and ii) small quantities of bis-acetylide complex formed. Furthermore, if an excess of the acetylene was not used, yields were substantially reduced. The vinylidene was

therefore isolated by precipitation from a dichloromethane / petroleum spirit mixture using Schlenk techniques and the excess acetylene (still in solution) removed by filter-tipped cannula. In the second step, the vinylidene complex was deprotonated with sodium methoxide in an oxygen-free environment to yield the acetylide complex in 54 % yield. The acetylide is air stable [samples have shown no noticeable degradation (monitoring by NMR spectroscopy) over a period of months when kept in vials under air]. The complex was characterized by ^{1}H and ^{31}P NMR spectroscopy, satisfactory microanalysis, IR and UV-vis spectroscopy, FAB mass spectrometry and optical rotation measurements.

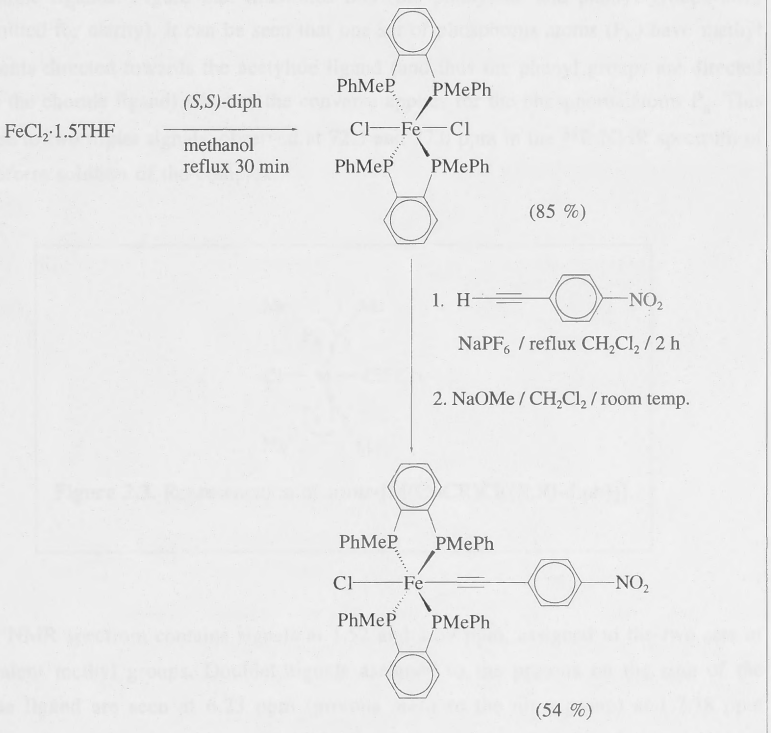

Scheme 2.2. Synthesis of $(-)_{589}$-*trans*-[$FeCl_2$((*R,R*)-diph)$_2$] and $(-)_{436}$-*trans*-[Fe(4-C≡C$C_6H_4NO_2$)Cl((*R,R*)-diph)$_2$]

The FAB mass spectrum contains signals due to the molecular ion, with bandshapes consistent with those predicted from their isotope composition. Fragmentation of the molecular ion by competitive loss of the chloride, acetylide, and diphosphine ligands is observed. The UV-vis spectrum of a tetrahydrofuran solution of this complex has bands at 37 400 and 36 400 cm^{-1}, similar to the parent dichloride, but also contains a weak band at 29 400 cm^{-1} and a more intense one at 18 400 cm^{-1}, the latter assigned to a MLCT transition from the metal to the acetylide ligand. The IR spectrum of a dichloromethane solution of the complex shows a characteristic $\nu(C{\equiv}C)$ at 2043 cm^{-1}.

The ^{31}P NMR spectrum is useful in confirming the *trans* geometry of the complex. There are two sets of inequivalent phosphorus centres in this molecule because of the chiral diphosphine ligands. Figure 2.3. illustrates this (the phenylene and phenyl groups have been omitted for clarity). It can be seen that one set of phosphorus atoms (P_b) have methyl substituents directed towards the acetylide ligand (and thus the phenyl groups are directed towards the choride ligand) whereas the converse applies for the phosphorus atoms P_a. This gives rise to two triplet signals, observed at 72.3 and 77.0 ppm in the ^{31}P NMR spectrum of a chloroform solution of the complex.

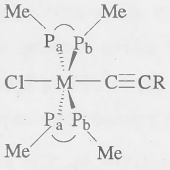

Figure 2.3. Representation of *trans*-[M(C≡CR)Cl((*R,R*)-diph)$_2$].

The ^1H NMR spectrum contains signals at 1.52 and 1.59 ppm, assigned to the two sets of inequivalent methyl groups. Doublet signals assigned to the protons on the ring of the acetylide ligand are seen at 6.23 ppm (protons *meta* to the nitro group) and 7.78 ppm (protons *ortho* to the nitro group). Multiple signals assigned to the phenyl and phenylene groups of the diphosphine ligand are located between 7.23 and 7.52 ppm.

Measurement of the optical rotation at the frequently used sodium 'D' line (589 nm) was not possible using the apparatus available because of strong absorption at this wavelength. The

measurement was made at 436 nm where absorption was weaker, a specific optical rotation of $[\alpha]_{436}$ = –3820 (*c* 0.022, CH_2Cl_2) being recorded.

2.2.2. Synthesis of [Fe(4-C≡CC$_6$H$_4$NO$_2$)(dppe)(η^5-C$_5$H$_5$)]

The new complex [Fe(4-C≡CC$_6$H$_4$NO$_2$)(dppe)(η^5-C$_5$H$_5$)] was prepared by extending the literature procedure for the preparation of [Fe(C≡CBu^t)(dppe)(η^5-C$_5$H$_5$)] to include 4-ethynylnitrobenzene.[62] A mixture of [FeCl(dppe)(η^5-C$_5$H$_5$)],[89] 4-HC≡CC$_6$H$_4$NO$_2$ and ammonium hexafluorophosphate were stirred in refluxing methanol to yield the vinylidene complex [Fe(C=CHC$_6$H$_4$-4-NO$_2$)(dppe)(η^5-C$_5$H$_5$)][PF$_6$] which was deprotonated *in situ* using sodium methoxide. The acetylide complex thus formed was characterized by IR, UV-vis, ^{1}H and ^{31}P NMR spectroscopy, satisfactory microanalysis, and FAB mass-spectrometry.

The FAB mass spectrum contains signals due to the molecular ion, with bandshapes consistent with those predicted from their isotope composition. Fragmentation of the molecular ion is observed with peaks indicating competitive loss of the chloride and acetylide ligands. The UV-vis spectrum of this complex has bands at 31 500 and 20 000 cm^{-1}, the latter being assigned to a MLCT transition from the metal to the acetylide ligand. The IR spectrum shows a characteristic ν(C≡C) at 2044 cm^{-1}. The ^{1}H NMR spectrum contains resonances at 2.23 and 2.55 ppm, assigned to the two sets of inequivalent ethylene protons of the diphosphine ligand, a singlet assigned to the cyclopentadienyl ring at 4.29 ppm, and a signal assigned to the protons *meta* to the nitro group on the ring of the acetylide ligand at 6.25 ppm. The protons *ortho* to the nitro group are obscured by multiple signals assigned to the phenyl groups of the diphosphine ligand, located between 7.20 and 7.84 ppm. The ^{31}P NMR spectrum contains one broad singlet at 106.2 ppm.

2.2.3. Attempted synthesis of [Fe(4-C≡CC$_6$H$_4$NO$_2$)(dppm)(η^5-C$_5$H$_5$)]

It was originally planned to synthesize the complex [Fe(4-C≡CC$_6$H$_4$NO$_2$)(dppm)(η^5-C$_5$H$_5$)], rather than the dppe analogue, simply because of availability of the diphosphine in the laboratory. However, this was not achieved by either of the two methods trialed. The first method involved preparing the complex [FeCl(dppm)(η^5-C$_5$H$_5$)] and proceeding in an analogous fashion to that utilized with the dppe-containing complex (described above). Several attempts to prepare [FeCl(dppm)(η^5-C$_5$H$_5$)] by the photolysis of [FeCl(CO)$_2$(η^5-C$_5$H$_5$)] in the presence of the diphosphine[89] (the same method that was successfully used to prepare [FeCl(dppe)(η^5-C$_5$H$_5$)]) yielded only the mono-substituted complex [FeCl(CO)(η^1–dppm)(η^5-C$_5$H$_5$)]. The second method involved preparing the carbonyl acetylide complex [Fe(4-C≡CC$_6$H$_4$NO$_2$)(CO)$_2$(η^5-C$_5$H$_5$)] and then reacting this with dppm under photolytic conditions using the method of Gamasa *et al* [23](used to prepare the complexes [Fe(C≡CR)(dppm)(η^5-C$_5$H$_5$)] where R = SiMe$_3$, CO$_2$Me, Bu^t, Ph). The carbonyl acetylide complex was easily prepared by the method of Bruce *et al*[43] but photolysis in the

presence of dppm gave only unidentified decomposition products. At this stage, the decision was taken to use the dppe ligand, which was successfully used as described in Section 2.2.2. A decision was also made not to attempt the synthesis of the bis-triphenylphosphine analogue because i) a search of the Chemical Abstracts database failed to find reports of the parent complex $[FeCl(PPh_3)_2(\eta^5\text{-}C_5H_5)]$ or related acetylide complexes, the inference being that the cone angle of triphenylphosphine is too large for a di-substituted iron cyclopentadienyl halide or acetylide complex, and ii) the synthesis using the dppe ligand was successful.

2.3. Synthesis of Ruthenium Complexes

2.3.1. Synthesis of $(-)_{589}$-trans-[Ru(4-C≡$CC_6H_4NO_2$)Cl((R,R)-diph)$_2$]

The new complex $(-)_{589}$-*trans*-[Ru(4-C≡$CC_6H_4NO_2$)Cl((*R,R*)-diph)$_2$] was prepared by extending literature procedures for the preparation of *cis*-[$RuCl_2$(dppm)$_2$][90] and *trans*-[Ru(4-C≡$CC_6H_4NO_2$)Cl(dppm)$_2$][76,81] to the diph-containing analogues. The synthetic procedure is outlined in Scheme 2.3.

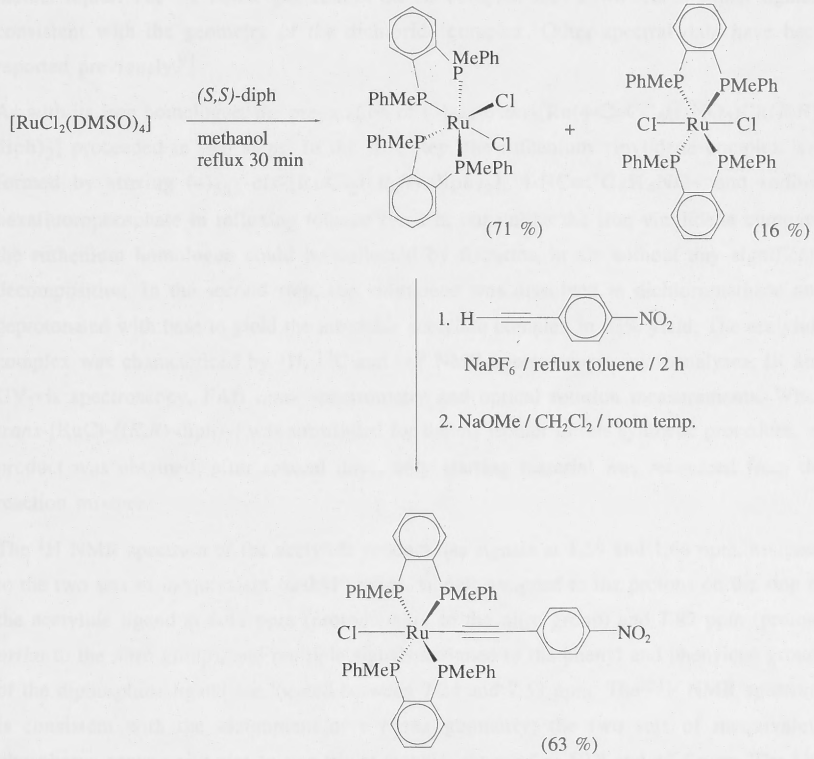

Scheme 2.3. Synthesis of *cis* / *trans*-[$RuCl_2$((*R,R*)-diph)$_2$] and $(-)_{589}$-*trans*-[Ru(4-C≡$CC_6H_4NO_2$)Cl((*R,R*)-diph)$_2$]

The complex $(-)_{589}$-*cis*-[$RuCl_2$((*R,R*)-diph)$_2$] has been prepared previously by Grocott and Wild.[91] In their preparation, the complex *trans*-[$RuCl_2$((*R,R*)-diph)$_2$] is prepared from $RuCl_3 \cdot nH_2O$ which has been reduced to Ru^{II} *in situ* by hydrogen gas, by addition of the diphosphine ligand in a boiling methanol / formaldehyde mixture. The *trans* complex is then isomerized to the *cis* complex by treatment with triethylaluminium at 75 °C for 2 h. An adaptation[92] of the procedure for the preparation of *cis*-[$RuCl_2$(dppm)$_2$][90] achieved a more convenient synthesis. The easily prepared [$RuCl_2(DMSO)_4$] complex[93] (where DMSO = dimethylsulfoxide) and the diphosphine ligand were stirred in refluxing methanol for 30 min. After recrystallization, the complex $(-)_{589}$-*cis*-[$RuCl_2$((*R,R*)-diph)$_2$] was obtained in good yield (71 %) and a small amount (16 %) of the *trans* isomer was isolated from the mother liquor. The ^{31}P NMR spectrum of the *cis* complex shows two sets of triplet signals, consistent with the geometry of the dichloride complex. Other spectral data have been reported previously.[91]

As with its iron homologue, the preparation of $(-)_{589}$-*trans*-[Ru(4-C≡C$C_6H_4NO_2$)Cl((*R,R*)-diph)$_2$] proceeded in two steps. In the first step, the ruthenium vinylidene complex was formed by stirring $(-)_{589}$-*cis*-[$RuCl_2$((*R,R*)-diph)$_2$], 4-HC≡C$C_6H_4NO_2$ and sodium hexafluorophosphate in refluxing toluene for 2 h, but unlike the iron vinylidene complex, the ruthenium homologue could be collected by filtration in air without any significant decomposition. In the second step, the vinylidene was dissolved in dichloromethane and deprotonated with base to yield the air-stable acetylide complex in 63% yield. The acetylide complex was characterized by ^1H, ^{13}C and ^{31}P NMR spectroscopy, microanalyses, IR and UV-vis spectroscopy, FAB mass spectrometry and optical rotation measurements. When *trans*-[$RuCl_2$((*R,R*)-diph)$_2$] was substituted for the *cis* isomer in this synthetic procedure, no product was obtained; after several days, only starting material was recovered from the reaction mixture.

The ^1H NMR spectrum of the acetylide product has signals at 1.59 and 1.64 ppm, assigned to the two sets of inequivalent methyl groups, signals assigned to the protons on the ring of the acetylide ligand at 6.41 ppm (protons *meta* to the nitro group) and 7.82 ppm (protons *ortho* to the nitro group), and multiple signals assigned to the phenyl and phenylene groups of the diphosphine ligand are located between 7.24 and 7.53 ppm. The ^{31}P NMR spectrum is consistent with the assignment of a *trans* geometry; the two sets of inequivalent phosphorus centres give rise to two triplet signals, observed at 50.4 and 54.4 ppm. The ^{13}C NMR spectrum shows two multiplets at 12.4 and 14.9 ppm, which may be assigned to the two inequivalent methyl groups of the diph ligand which couple to the phosphorus atoms. A singlet signal at 111.6 ppm may be assigned to the β-carbon of the acetylide ligand (no signal from the α-carbon was found). A multitude of resonances are observed between

123.4 and 147.4 ppm and are assigned to the carbon atoms of aromatic rings of the diph and acetylide ligands. The FAB mass spectrum contains signals due to the molecular ion, with bandshapes consistent with those predicted from their isotope composition. Fragmentation of the molecular ion occurs by loss of the chloride, acetylide, and diphosphine ligands. The UV-vis spectrum of this complex is similar to that of the *trans*-dichloride complex, with bands at 39 800 and 41 200 cm^{-1}, but also a band at 21 400 cm^{-1} which may be assigned to a MLCT transition from the metal to the acetylide ligand. The IR spectrum contains a characteristic ν(C≡C) at 2057 cm^{-1}; this corresponds to a blue shift of more than 10 cm^{-1} compared to the analogous band for the iron homologue. A dichloromethane solution of the complex at the sodium 'D' line (589 nm) revealed a specific optical rotation of $[\alpha]_D = -504$ (*c* 0.145, CH_2Cl_2).

2.3.2 Synthesis of [Ru(4-C≡CC$_6$H$_4$NO$_2$)(dppe)(η^5-C$_5$H$_5$)]

The new complex [Ru(4-C≡C$C_6H_4NO_2$)(dppe)(η^5-C_5H_5)] was prepared by modifications to the procedures used for the preparation of $(-)_{589}$-*trans*-[Ru(4-C≡C$C_6H_4NO_2$)Cl((*R,R*)-diph)$_2$]. A mixture of [RuCl(dppe)(η^5-C_5H_5)],[55] 4-HC≡C$C_6H_4NO_2$ and ammonium hexafluorophosphate was stirred in refluxing methanol for 1 h. The vinylidene complex is air stable and it was isolated in air, before deprotonation to form the desired acetylide complex. The acetylide complex was characterized by ^{1}H and ^{31}P NMR, FAB mass spectrometry, satisfactory microanalysis, IR and UV-vis spectroscopy.

The ^{1}H NMR spectrum contains signals at 2.30 and 2.57 ppm, assigned to the ethylene bridge of the diphosphine ligand, a singlet at 4.79 ppm, assigned to the cyclopentadienyl ligand, and at 6.31 ppm signal assigned to the protons *meta* to the nitro group at 6.31 ppm. The protons *ortho* to the nitro group are obscured by signals assigned to the phenyl groups of the diphosphine ligand, located between 7.26 and 7.87 ppm. The ^{31}P NMR spectrum has the expected single resonance at 86.2 ppm. The FAB mass spectrum contains signals due to the molecular ion, with a bandshape consistent with that predicted from the isotope composition. Fragmentation of the molecular ion occurs by the loss of the acetylide ligand. The IR spectrum shows the expected ν(C≡C) at 2056 cm^{-1}, a a shift of more than 10 cm^{-1} towards the higher energy end of the spectrum compared to the analogous absorption for the iron homologue. The UV-vis spectrum of this complex contains a band at 22 200 cm^{-1}, assigned to the MLCT transition from the metal to the acetylide ligand.

2.4. Synthesis of Osmium Complexes

2.4.1 Synthesis of $(-)_{365}$-*trans*-[Os(C≡CC_6H_4R)Cl((*R,R*)-diph)$_2$]

The synthesis of $(-)_{365}$-*trans*-[Os(4-C≡C$C_6H_4NO_2$)Cl((*R,R*)diph)$_2$] posed a greater challenge than that of its iron or ruthenium homologues. Established methodologies for synthesis of analogous bis(diphosphine) complexes are not satisfactory for the preparation of the acetylide precursor *cis*-[$OsCl_2$((*R,R*)-diph)$_2$]; some methods require elevated temperatures[94,95] which racemize the uncoordinated optically active diphosphine ligand, while others yielded little or no product when trialed with the diph ligand.[96,97] A new route was therefore developed (see Scheme 2.4.) and is discussed below.

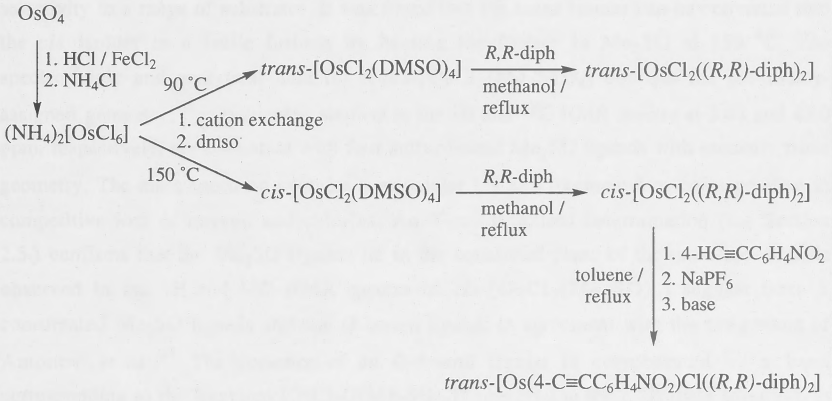

Scheme 2.4. Synthesis of osmium complexes.

Ammonium hexachloroosmate may be prepared from the commercially available osmium tetroxide using the method of Dwyer and Hogarth[98] and converted to hexachloroosmic acid by cation exchange chromatography. Antonov *et al.* have reported that [$OsCl_2$(DMSO)$_4$] can be prepared directly from hexachloroosmic acid,[99] and although the syntheses[93,100-102] and structural characterization[100,103,104] of ruthenium sulfoxide

complexes have been the subjects of many reports, only two studies of the osmium analogues have appeared.[99,105] Because the osmium dimethylsulfoxide complexes were little studied, an investigation into this area was undertaken.

Antonov *et al* spectroscopically identified two isomers as *trans*-[$OsCl_2(Me_2SO)_4$] and *cis*-[$OsCl_2(Me_2SO)_3(Me_2SO)$] (where Me_2SO and Me_2SO are *S* and *O*-bound dimethylsulfoxide ligands, respectively) but no structural or reactivity studies of these complexes were reported prior to the current work. Reaction of hexabromoosmate with Me_2SO is reported to afford *trans*-[$OsBr_2(Me_2SO)_4$].[106] The analogous reaction with hexachloroosmate was trialed but reaction of the ammonium or potassium salts of hexachloroosmate with Me_2SO in the presence of $SnCl_2.2H_2O$ at temperatures between 110 and 180 °C did not afford any of the desired product. The *trans* isomer was therefore prepared by cation exchange of the ammonium complex, followed by heating the resultant hexachloroosmic acid in DMSO at 90°C. Routes into the *cis* as well as *trans* isomer are of interest, as the homologous ruthenium examples show differing reactivity and product selectivity to a range of substrates. It was found that the *trans* isomer can be converted into the *cis* isomer in a facile fashion by heating the former in Me_2SO at 150 °C. The spectroscopic and analytical data for *trans*-[$OsCl_2(Me_2SO)_4$] confirm the previously-assigned geometry;[99] in particular, singlets in the ^1H and ^{13}C NMR spectra at 3.44 and 42.0 ppm, respectively, are consistent with four sulfur-bound Me_2SO ligands with mutually *trans* geometry. The mass spectrum contains a molecular ion and fragment ions corresponding to competitive loss of oxygen and chlorine. An X-ray structural determination (see Section 2.5.) confirms that the Me_2SO ligands lie in the equatorial plane of the molecule. Signals observed in the ^1H and ^{13}C NMR spectra of *cis*-[$OsCl_2(Me_2SO)_4$] suggest three *S* coordinated Me_2SO ligands and one *O* bound ligand, in agreement with the assignment of Antonov *et al*.[99] The presence of an *O*-bound ligand is corroborated by a band corresponding to the fragment $[OsCl_2O(Me_2SO)_2]^+$ observed in the FAB mass spectrum, in addition to bands corresponding to the molecular ion and competitive fragmentation of O and Cl as observed with the *trans* isomer. The UV-vis spectrum of the *trans* isomer is readily distinguishable from that of the *cis* isomer due to the presence of a weak low-energy absorption at 28 460 cm^{-1}. In addition to resonances corresponding to *cis*-[$OsCl_2(Me_2SO)_3$ (Me_2SO)], the ^1H NMR spectrum also contain small singlets at 3.48 and 3.64 ppm (ratio 1:1), assigned to a 10% abundant minor isomer. A crystal grown from the mixture was structurally characterized by X-ray diffraction as the all *S*-bound *cis*-isomer (see Section 2.5.).

Preparation of *cis*-[$OsCl_2((R,R)$-diph)$_2$] involves reacting (*S,S*)-diph with *cis*-[$OsCl_2(DMSO)_4$] in refluxing methanol. Reaction at this temperature avoids the rapid racemization which ensues at temperatures approaching 80 °C (refluxing benzene or

ethanol). No *trans* isomer was detected in the product, indicating that the stereochemistry at the metal was retained. Preparation of *trans*-[$OsCl_2$((*R,R*)-diph)$_2$] involves reacting the diph ligand with *trans*-[$OsCl_2(DMSO)_4$] using the same procedure. Stereochemistry at the metal was again retained with no *cis* isomer detected.

The *cis* and *trans* isomers are readily distinguished by their ^{31}P NMR spectra, which show a pair of triplets at 10.6 and 16.3 ppm for the former and a singlet at 18.1 ppm for the latter.

A crystal of the *trans* complex was structurally characterized by X-ray diffraction and confirms retention of both stereochemistry at metal and configuration of the diphosphine ligand (see Section 2.5.). This is the first structural study of an osmium complex incorporating the diph ligand, although a number of examples of ruthenium complexes with this ligand have been reported previously.[107-110] Typical barriers to inversion of alkyldiarylphosphines lie in the range 120-130 kJ mol^{-1} [111]; the present procedure provides a facile synthesis of both *cis*- and *trans*- isomers of chiral-at-phosphorus bis(diphosphine) osmium complexes, which could also be used for other chiral-at-phosphorus bis(diphosphine) ligands.

Once the synthesis of *cis*-[$OsCl_2$((*R,R*)-diph)$_2$] was achieved, the preparation of $(-)_{365}$-*trans*-[Os(4-C≡C$C_6H_4NO_2$)Cl((*R,R*)-diph)$_2$] was straightforward, the procedure being identical to that used for the ruthenium homologue, with similar yields obtained. As with the ruthenium complex preparation, it was found that *trans*-[$OsCl_2$((*R,R*)-diph)$_2$] was unreactive towards the acetylene ligand in the presence of hexafluorophosphate, even under quite forcing conditions (refluxing decalin, 24 h).

The acetylide complex was characterized by a combination of ^1H, ^{13}C and ^{31}P NMR spectroscopy, satisfactory microanalyses, IR and UV-vis spectroscopy, FAB mass spectrometry and optical rotation measurements. As with its iron homologue, the absorption of the osmium acetylide complex at 589 nm was too strong to allow a measurement of the optical rotation using the available apparatus. The optical rotation was therefore measured at 365 nm, with a specific rotation of $[\alpha]_{365} = -2730$ (*c* 0.0495, CH_2Cl_2) being recorded.

2.4.2. Synthesis of [Os(4-C≡C$C_6H_4NO_2$)(L_n)(η^5-C_5H_5)] (n = 1, L = dppe; n = 2, L = PPh_3)

The acetylide complexes were prepared from the corresponding halide complexes, [OsBr(dppe)(η^5-C_5H_5)][55] and [OsBr(PPh_3)$_2$(η-C_5H_5)],[112] by similar methods to the literature procedure.[79] Stirring the halide complex in refluxing methanol with the acetylene and ammonium hexafluorophosphate gave the vinylidene complexes which were deprotonated *in situ* to yield the desired acetylide complexes. The latter were characterized

by ^{1}H and ^{31}P NMR spectroscopy, microanalyses, IR and UV-vis spectroscopy and FAB mass spectrometry.

The ^{1}H NMR spectrum of $[Os(4\text{-}C{\equiv}CC_6H_4NO_2)(PPh_3)_2(\eta^5\text{-}C_5H_5)]$ contains a singlet at 4.43 ppm assigned to the cyclopentadienyl ligand, signals at 6.98 and 8.00 ppm assigned to the protons *meta* and *ortho* to the nitro group, respectively, and signals located between 7.05 and 7.35 ppm assigned to the phenyl groups of the diphosphine ligand. The ^{31}P NMR spectrum has the expected singlet resonance at 2.8 ppm. The FAB mass spectrum contains signals due to the molecular ion, with a bandshape consistent with that predicted from the isotope composition. The IR spectrum shows the expected $\nu(C{\equiv}C)$ at 2054 cm^{-1}. The UV-vis spectrum of this complex contains a band at 21000 cm^{-1}, assigned to the MLCT transition from the metal to the acetylide ligand, as well as higher energy bands associated with the phosphine ligands.

The ^{1}H NMR spectrum of $[Os(4\text{-}C{\equiv}CC_6H_4NO_2)(dppe)(\eta^5\text{-}C_5H_5)]$ contains a multiplet centred at 2.50 ppm assigned to the ethylene bridge of the diphosphine ligand, a singlet at 4.78 ppm assigned to the cyclopentadienyl ligand, and a signal at 6.25 ppm assigned to the protons *meta* to the nitro group at 6.31 ppm. The resonance assigned to the protons *ortho* to the nitro group is at 7.72 ppm, and lies amongst the signals assigned to the phenyl groups of the diphosphine ligand, located between 7.17 and 7.85 ppm. The ^{31}P NMR spectrum has the expected singlet resonance at 46.7 ppm. The FAB mass spectrum contains signals due to the molecular ion, with a bandshape consistent with that predicted from the isotope composition. Fragmentation of the molecular ion occurs by the loss of the acetylide ligand. The IR spectrum shows the expected $\nu(C{\equiv}C)$ at 2055 cm^{-1}. The UV-vis spectrum of this complex contains a band at 21 600 cm^{-1}, assigned to the MLCT transition from the metal to the acetylide ligand, as well as higher energy bands associated with the diphosphine ligands.

2.5. X-ray Structural Studies of Some Osmium Complexes

2.5.1. trans- and cis-[$OsCl_2(Me_2SO)_4$]

Single crystal X-ray diffraction studies on *trans*-[$OsCl_2(Me_2SO)_4$] and *cis*-[$OsCl_2(Me_2SO)_4$] have been performed by collaborators at the Australian National University. Crystal data are collected in Table 2.1., the atomic coordinates are listed in Tables 2.2. and 2.4., and important bond lengths and angles gathered in Table 2.3. (*cis*-[$OsCl_2(Me_2SO)_4$]) and Table 2.5. (*trans*-[$OsCl_2(Me_2SO)_4$], together with those of its ruthenium homologue and their bromo analogues). ORTEP plots are displayed in Figures 2.4. and 2.5.

The structural study of *trans*-[$OsCl_2(Me_2SO)_4$] confirms the molecular geometry inferred from the spectral data, while that of *cis*-[$OsCl_2(Me_2SO)_4$] reveals the presence of a previously unheralded isomeric form. The disorder inherent in the structural determination of *trans*-[$OsCl_2(Me_2SO)_4$] renders the intraligand geometries associated with the minor component of disorder unreliable. The major component, however, is in excellent agreement with expected values. In *trans*-[$OsCl_2(Me_2SO)_4$], the Os-Cl distance [2.415(5) Å] is similar to those previously reported for *trans*-disposed chlorines in osmium(II) complexes [2.431(1) - 2.448(2) Å].[113-115] The Os-S parameter [2.342(4) Å] is experimentally indistinguishable from the only previously reported Os(II)-S datum [2.351(2) Å in [$OsBr_2(Me_2SO)_4$]].[106] The crystal of *trans*-[$OsCl_2(Me_2SO)_4$] is isomorphous with that of its ruthenium homologue,[100,116] and their bromo analogues,[106,117] affording the opportunity to assess the effect of metal and halogen replacement on bond parameters. The bond length and angle data reveal that geometric parameters are crystallographically equivalent (within 3σ) across the two chloro-containing structures. Comparison of important data for the bromo-containing complexes is consistent with a marginal lengthening of M-Br in proceeding from Ru to Os, with other significant parameters experimentally indistinguishable. Assessment of the impact of halo replacement for the osmium complexes reveals only the expected Os-X contraction on proceeding from bromo to chloro-containing complexes. In contrast, comparison of the ruthenium data (utilizing the better-defined structure in reference 100) reveals the expected decrease in Ru-X parameter on proceeding from bromo to chloro, together with marginal decreases in Ru-S distance and contraction in Ru-S-C angle.

Three structural modifications of *cis*-[$RuCl_2(Me_2SO)_4$] have been reported previously, all of which contain three *S*-bound and one *O*-bound Me_2SO ligands.[103,104,116] In contrast,

the structural determination of *cis*-$[OsCl_2(Me_2SO)_4]$ reveals four *S*-coordinated Me_2SO ligands. The Os-Cl distances for chloro ligands *trans* to Me_2SO [2.424(1), 2.427(1) Å] are similar to previously reported data for mutually *trans* chlorines (see above). Mutually *trans* Os-S vectors [2.349(1), 2.355(1) Å] are not unusual, being comparable to literature precedents (see above). Os-S distances for Me_2SO ligands *trans* to chloro groups [2.275(1), 2.277(1) Å] are significantly shorter than those for mutually *trans* Me_2SO, possibly a result of enhanced π-back-bonding when the Me_2SO ligands are *trans* to the π-donor chloro ligands. Bond lengths and angles within the Me_2SO ligands are unexceptional.

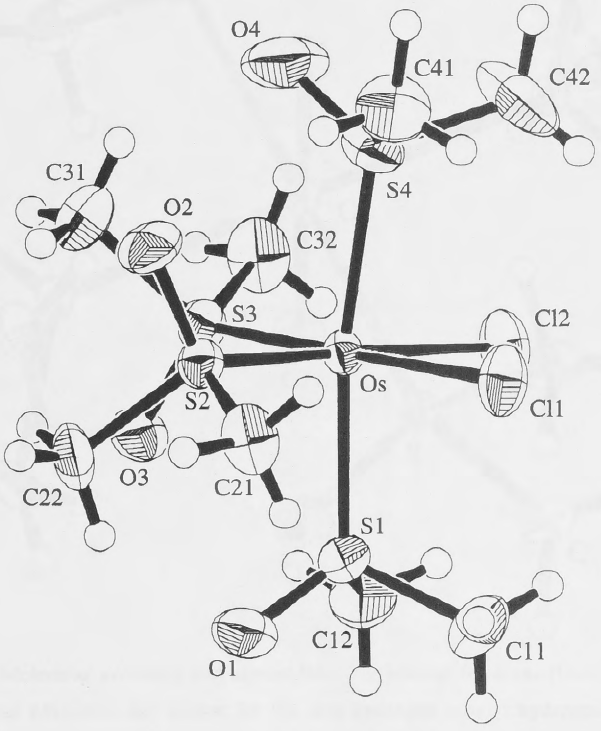

Figure 2.4. Molecular geometry and atomic labelling scheme for *cis*-$[OsCl_2(Me_2SO)_4]$. 50 % thermal ellipsoids are shown for the non-hydrogen atoms; hydrogen atoms have arbitrary radii.

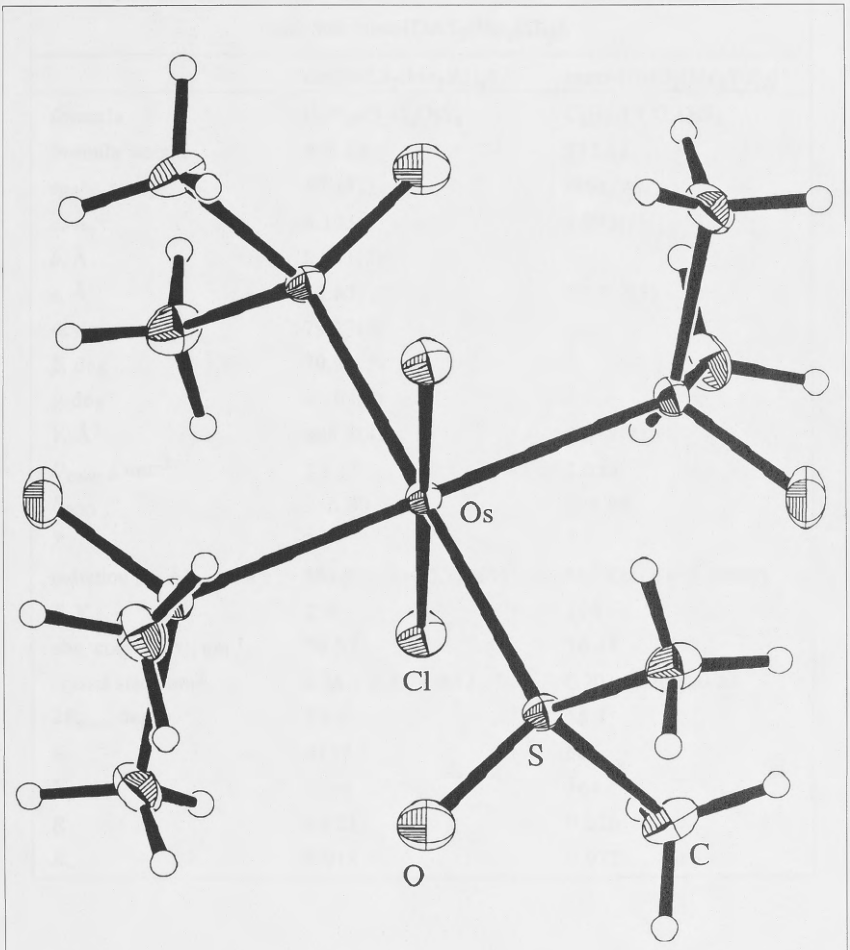

Figure 2.5. Molecular geometry and atomic labelling scheme for *trans*-$[OsCl_2(Me_2SO)_4]$. 50 % thermal ellipsoids are shown for the non-hydrogen atoms; hydrogen atoms have arbitrary radii.

Table 2.1. Experimental Parameters for the X-ray Diffraction Studies of *cis*- and *trans*-$[OsCl_2(Me_2SO)_4]$.

	cis-$[OsCl_2(Me_2SO)_4]$	*trans*-$[OsCl_2(Me_2SO)_4]$
formula	$C_8H_{24}Cl_2O_4OsS_4$	$C_8H_{24}Cl_2O_4OsS_4$
formula weight	573.62	573.62
space group	$P\bar{1}$ (#2)	$I4/m$ (#87)
a, Å	8.193(2)	9.092(2)
b, Å	8.941(3)	
c, Å	13.837(3)	11.212(3)
α, deg	79.77(2)	
β, deg	79.91(2)	
γ, deg	65.03(2)	
V, Å^3	898.5(4)	926.8(2)
D_{calc}, g cm^{-3}	2.120	2.055
F_{000}	556.00	556.00
Z	2	2
radiation (λ, Å)	Mo Kα (λ = 0.71069)	Mo Kα (λ = 0.71069)
T, K	296	296
abs. coeff.(Kα), cm^{-1}	78.57	76.18
crystal size, mm^3	0.36 x 0.20 x 0.12	0.20 x 0.20 x 0.20
$2\theta_{max}$, deg	55.1	55.1
N	4152	566
N_0	3669	564
R	0.021	0.026
R_w	0.018	0.032

Table 2.2. Atomic Coordinates and Equivalent Isotropic Thermal Parameters for *cis*-$[OsCl_2(Me_2SO)_4]$.

atom	x	y	z	B
Os	0.15776(2)	0.23741(2)	0.24249(1)	2.048(4)
Cl(1)	–0.0197(2)	0.3251(2)	0.10411(9)	3.74(3)
Cl(2)	–0.0753(1)	0.1477(2)	0.32977(9)	3.74(3)
S(1)	0.2989(2)	–0.0320(1)	0.19499(9)	3.26(3)
S(2)	0.3693(1)	0.3234(1)	0.15258(8)	2.56(2)
S(3)	0.3125(1)	0.1522(1)	0.37749(8)	2.68(2)
S(4)	–0.0229(2)	0.5060(2)	0.2872(1)	3.72(3)
O(1)	0.4880(4)	–0.0914(4)	0.1486(3)	5.0(1)
O(2)	0.3585(4)	0.4857(4)	0.1713(2)	4.18(9)
O(3)	0.4692(4)	–0.0105(4)	0.3756(2)	3.76(8)
O(4)	0.0293(5)	0.5605(5)	0.3664(3)	6.5(1)
C(11)	0.1746(7)	–0.0585(7)	0.1103(4)	5.1(2)
C(12)	0.2859(7)	–0.1915(6)	0.2915(4)	4.7(1)
C(21)	0.3698(6)	0.3357(6)	0.0234(3)	3.8(1)
C(22)	0.6008(6)	0.1810(6)	0.1599(4)	3.9(1)
C(31)	0.3952(7)	0.2929(6)	0.4074(4)	4.3(1)
C(32)	0.1749(6)	0.1401(7)	0.4905(3)	4.3(1)
C(41)	–0.0618(7)	0.6664(6)	0.1872(4)	5.2(1)
C(42)	–0.2532(7)	0.5364(7)	0.3217(5)	7.2(2)

Table 2.3. Selected Bond Distances (Å) and Angles (deg.) for *cis*-$[OsCl_2(Me_2SO)_4]$.

Os-Cl(1)	2.424(1)	Os-Cl(2)	2.427(1)
Os-S(1)	2.349(1)	Os-S(2)	2.275(1)
Os-S(3)	2.277(1)	Os-S(4)	2.355(1)
S(1)-O(1)	1.474(3)	S(2)-O(2)	1.483(3)
S(3)-O(3)	1.479(3)	S(4)-O(4)	1.467(4)
S(1)-C(11)	1.785(5)	S(1)-C(12)	1.798(5)
S(2)-C(21)	1.771(5)	S(2)-C(22)	1.791(4)
S(3)-C(31)	1.794(5)	S(3)-C(32)	1.776(5)
S(4)-C(41)	1.771(5)	S(4)-C(42)	1.777(5)
Cl(1)-Os-Cl(2)	85.42(4)	Cl(1)-Os-S(1)	89.42(4)
Cl(1)-Os-S(2)	91.39(4)	Cl(1)-Os-S(3)	176.99(4)
Cl(1)-Os-S(4)	85.03(4)	Cl(2)-Os-S(1)	84.75(4)
Cl(2)-Os-S(2)	176.74(4)	Cl(2)-Os-S(3)	91.60(4)
Cl(2)-Os-S(4)	88.80(5)	S(1)-Os-S(2)	94.58(4)
S(1)-Os-S(3)	90.70(4)	S(1)-Os-S(4)	171.81(4)
S(2)-Os-S(3)	91.60(4)	S(2)-Os-S(4)	91.58(4)
S(3)-Os-S(4)	94.54(4)	Os-S(1)-O(1)	119.2(1)
Os-S(1)-C(11)	110.9(2)	Os-S(1)-C(12)	114.1(2)
O(1)-S(1)-C(11)	105.3(2)	O(1)-S(1)-C(12)	106.7(2)
C(11)-S(1)-C(12)	98.4(2)	Os-S(2)-O(2)	116.1(1)
Os-S(2)-C(21)	113.1(2)	Os-S(2)-C(22)	115.9(2)
O(2)-S(2)-C(21)	106.2(2)	O(2)-S(2)-C(22)	105.9(2)
C(21)-S(2)-C(22)	97.5(2)	Os-S(3)-O(3)	115.2(1)
Os-S(3)-C(31)	116.2(2)	Os-S(3)-C(32)	113.5(2)
O(3)-S(3)-C(31)	105.9(2)	O(3)-S(3)-C(32)	106.5(2)
C(31)-S(3)-C(32)	97.9(2)	Os-S(4)-O(4)	118.1(2)
Os-S(4)-C(41)	114.6(2)	Os-S(4)-C(42)	112.0(2)
O(4)-S(4)-C(41)	107.1(2)	O(4)-S(4)-C(42)	106.1(3)
C(41)-S(4)-C(42)	96.6(3)		

Table 2.4. Atomic Coordinates and Equivalent Isotropic Thermal Parameters for *trans*-$[OsCl_2(Me_2SO)_4]$.

atom	x	y	z	B(eq)	occ
Os	0.0000	0.0000	0.5000	1.85(1)	1/8
Cl	0.0000	0.0000	0.2846(4)	3.13(2)	1/4
S	0.2550(2)	0.0365(2)	0.5000	2.29(4)	0.405
S′	0.195(1)	0.168(1)	0.5000	3.8(2)	0.095
O	0.3404(6)	−0.1053(7)	0.5000	5.2(2)	1/2
C	0.3239(6)	0.1417(7)	0.3780(5)	3.8(1)	

Table 2.5. Selected Bond Distances (Å) and Angles (deg.) for *trans*-$[MX_2(Me_2SO)_4]$ (M = Os, X = Cl, Br; M = Ru, X = Cl, Br).

	M = Os X = Cl[a]	M = Ru X = Cl[100]	M = Ru X = Cl[116]	M = Os, X = Br[106]	M = Ru X = Br[117]
M-X	2.414(2)	2.432(1)	2.402(2)	2.555(1)	2.540(1)
M-S	2.342(2)	2.3534(9)	2.352(2)	2.351(2)	2.360(1)
M-S′	2.34(1)				
S-O	1.505(6)[b]	1.492(4)	1.491(5)	1.487(6)	1.484(3)
S′-O	1.77(1)[b]				
S-C	1.783(6)[b]	1.800(4)	1.780(5)	1.784(6)	1.789(3)
S′-C	1.817(9)[b]				
M-S-O	112.9(3)[b]	112.9(1)	112.5(2)	113.5(2)	112.5(1)
M-S′-O	103.3(5)[b]				
M-S-C	115.0(4)[b]	115.1(1),	115.4(2)	115.8(2)	116.0(1)
M-S′-C	113.8(4)[b]				
O-S-C	106.2(3)[b]	106.0(2)	106.0(2)	105.2(3)	105.7(1)
O-S′-C	114.5(5)[b]				
C-S-C	100.2(4)[b]	100.5(3)	100.3(2)	99.8(5)	99.6(2)
C-S′-C	96.6(6)[b]				

[a]This work. [b]Unreliable data: see discussion.

2.5.2. $(-)_{589}$-*trans*-[$OsCl_2$((*R,R*)-diph)$_2$]

A crystal of $(-)_{589}$-*trans*-[$OsCl_2$((*R,R*)-diph)$_2$] was structurally characterized by X-ray diffraction. Selected bond distances and angles are listed in Table 2.6., crystal data are collected in Table 2.7., and an ORTEP plot is displayed in Figure 2.6.. This is the first structural study of an osmium complex incorporating the diph ligand, although a number of examples of ruthenium complexes with this ligand have been reported previously.[107-110] This study confirms the retention of both stereochemistry at metal and configuration of the diphosphine ligand. Intraligand bond lengths are not unusual, while comparison to the analogous ruthenium complex[107] reveals similar M-P distances [2.304(1), 2.321(1), 2.338(1), 2.354(1) Å, M = Ru versus 2.310(2), 2.328(2), 2.337(2), 2.349(2) Å, M = Os] and a marginal lengthening of M-Cl distances [2.426(1), 2.432(1) Å, M = Ru versus 2.441(2), 2.445(2) Å, M = Os].

Table 2.6. Selected Bond Distances (Å) and Angles (deg.) for *trans*-[$OsCl_2$((*R,R*)-diph)$_2$].

Os-Cl(1)	2.445(2)	Os-P(2)	2.310(2)
Os-Cl(2)	2.441(2)	Os-P(3)	2.349(2)
Os-P(1)	2.328(2)	Os-P(4)	2.337(2)
Cl(1)-Os-Cl(2)	171.77(9)	P(1)-Os-P(2)	84.25(8)
Cl(1)-Os-P(1)	82.41(8)	P(1)-Os-P(3)	171.38(7)
Cl(1)-Os-P(2)	87.18(7)	P(1)-Os-P(4)	97.26(8)
Cl(1)-Os-P(3)	88.97(8)	P(2)-Os-P(3)	95.37(7)
Cl(1)-Os-P(4)	96.34(7)	P(2)-Os-P(4)	176.32(8)
Cl(2)-Os-P(1)	90.23(8)	P(3)-Os-P(4)	83.65(7)
Cl(2)-Os-P(2)	88.43(7)	Os-P(1)-C(101)	118.4(3)
Cl(2)-Os-P(3)	98.37(7)	Os-P(1)-C(111)	121.4(3)
Cl(2)-Os-P(4)	88.20(8)	Os-P(1)-C(121)	108.5(3)

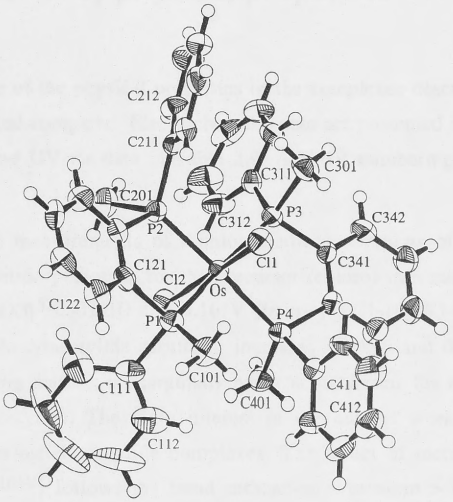

Figure 2.6. ORTEP drawing of *trans*-[$OsCl_2$((*R*,*R*)-diph)$_2$].

Table 2.7. Experimental Parameters for the X-ray Diffraction Study of *trans*-[$OsCl_2$((*R*,*R*)-diph)$_2$].

formula	$C_{40}H_{40}Cl_2OsP_4$	Z	4
formula weight	905.76	radiation (λ, Å)	Mo Kα (λ = 0.71069)
crystal system	orthorhombic	T, K	296
space group	$P2_12_12_1$ (#19)	abs. coeff.(Kα), cm^{-1}	37.20
a, Å	11.642(3)	crystal size, mm^3	0.20 x 0.16 x 0.16
b, Å	12.237(5)	$2\theta_{max}$, deg	50.1
c, Å	26.463(3)	N	3778
V, $Å^3$	3770(2)	N_0	3095
D_{calc}, g cm^{-3}	1.596	R, R_w	0.025, 0.023
F(000)	1800.00		

2.6. *Comparisons of physical properties*

In this Section, some of the physical properties of the complexes described in Sections 2.2. - 2.4. are collected and compared. Electrochemical data are presented in Table 2.8., and ^{1}H and ^{31}P NMR, IR and UV-vis data in Table 2.9. A NMR numbering scheme is shown in Figure 2.7.

Cyclic voltammetric measurements of dichloromethane solutions of selected complexes were recorded. Oxidation potentials for the precursor (chloro) iron complexes are found at 0.13 V ([FeCl(dppe)(η^5-C_5H_5)]) and 0.16 V (*trans*-[$FeCl_2$((*R,R*)-diph)$_2$]). Replacing chloride by *p*-nitrophenylacetylide results in increases of 0.16 and 0.1 V in E^0 ($Fe^{II/III}$), respectively, indicating that Cl^- is marginally better at stabilizing the higher oxidation state than *p*-nitrophenylacetylide. The main interest in the current work lies in comparison between homologous metal acetylide complexes. The effect of metal variation upon E^0 ($M^{II/III}$) and E^0 ($M^{III/IV}$) follows the trend ruthenium > osmium > iron, not unexpected given that previous reports of Group 8 metal bis(diphosphine) complexes[87,95] and metallocenes[118] show the same trend. Thus, the redox behaviour of these complexes is that predicted based on literature precedents.

Table 2.8. Cyclic voltametric data.[a]

Compound	$E^0(M^{II/III})$ (V)	$E^0(M^{III/IV})$ (V)	$E^0(NO_2^{0/-I})$ (V)
[FeCl(dppe)(η^5-C_5H_5)]	0.13		
[Fe(4-C≡C$C_6H_4NO_2$)(dppe)(η^5-C_5H_5)]	0.29	1.63	–1.13
trans-[$FeCl_2$((*R,R*)-diph)$_2$]	0.16	1.49	
trans-[Fe(4-C≡C$C_6H_4NO_2$)Cl((*R,R*)-diph)]$_2$	0.26	1.44	–1.15
trans-[Ru(4-C≡C$C_6H_4NO_2$)Cl((*R,R*)-diph)]$_2$	0.74	1.63	–1.13
trans-[Os(4-C≡C$C_6H_4NO_2$)Cl((*R,R*)-diph)]$_2$	0.52	1.51	–1.15

[a] Scan rates were 100 mV s^{-1}. Values are referenced to ferrocene (E^0 0.56 V).

Selected ^{1}H NMR data are shown in Table 2.9. and a brief numbering scheme is shown in Figure 2.7. Inspection of the chemical shifts of the methyl groups of the complexes *trans*-[M(4-C≡C$C_6H_4NO_2$)Cl((*R,R*)-diph)$_2$] reveals a very small downfield shift of this resonance on progressing from M = Fe to Ru and then Os. For complexes containing the cyclopentadienyl group, the trend in chemical shift of the Cp ring protons is (in terms of ppm) Os ≥ Ru > Fe.

Table 2.9. ^{1}H and ^{31}P NMR, IR and UV-vis data.

Compound	^{1}H NMR resonances[a] (ppm (J_{HH} (Hz)))				^{31}P resonances[a] (ppm (J_{PP} (Hz)))	$\nu(C\equiv C)$[b] (cm^{-1})	$\bar{\nu}_{max}$[c] (cm^{-1}) (ε (10^4 M^{-1} cm^{-1}))
	CH_3 (triplet)	H_4 (doublet)	H_5 (doublet)	η^5-C_5H_5			
trans-[Fe(4-C≡C$C_6H_4NO_2$)Cl((*R,R*)-diph)]$_2$	1.52 (4)	6.23 (9)	7.78. (9)		72.3 (triplet, 43)	2043	18400 (1.7)
	1.59 (4)				77.0 (triplet, 43)		
trans-[Ru(4-C≡C$C_6H_4NO_2$)Cl((*R,R*)-diph)]$_2$	1.59 (3)	6.41 (9)	7.82 (9)		50.4 (triplet, 22)	2057	21400 (2.1)
	1.64 (3)				54.4 (triplet, 22)		
trans-[Os(4-C≡C$C_6H_4NO_2$)Cl((*R,R*)-diph)]$_2$	1.62 (4)	6.38 (9)	7.82 (9)		18.9 (triplet, 13)	2052	20400 (1.8)
	1.71 (4)				23.0 (triplet, 13)		
[Fe(4-C≡C$C_6H_4NO_2$)(dppe)(η^5-C_5H_5)]		6.25 (9)	obscured	4.29	106.2	2044	20000 (1.3)
[Ru(4-C≡C$C_6H_4NO_2$)(dppe)(η^5-C_5H_5)]		6.31 (9)	obscured	4.79	86.2	2056	22200 (1.8)
[Os(4-C≡C$C_6H_4NO_2$)(dppe)(η^5-C_5H_5)]		6.25 (9)	7.72 (9)	4.78	46.7	2055	21600 (1.7)
[Ru(4-C≡C$C_6H_4NO_2$)(PPh_3)$_2$(η^5-C_5H_5)]		7.03 (9)	8.00 (9)	4.36	50.9	2053	21800 (1.1)
[Os(4-C≡C$C_6H_4NO_2$)(PPh_3)$_2$(η^5-C_5H_5)]		6.98 (9)	8.00 (9)	4.43	2.8	2054	21000 (2.2)
[Fe(4-C≡C$C_6H_4NO_2$)(CO)$_2$(η^5-C_5H_5)]		7.34 (9)	8.05 (9)	5.08		2104	27000 (1.3)
[Ru(4-C≡C$C_6H_4NO_2$)(CO)$_2$(η^5-C_5H_5)]		7.35 (9)	8.03 (9)	5.45		2108	26900 (1.6)

[a] In chloroform. [b] In dichloromethane. [c] In tetrahydrofuran.

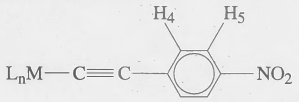

Figure 2.7. NMR numbering scheme.

Inspection of chemical shifts of the H_4 protons reveals no apparent trend on varying the metal, while keeping the ligand environment unchanged. Variation of co-ligand for a specific alkynylmetal combination reveals the trend (in terms of ppm) CO > PPh_3 > dppe > diph. This may be a reflection of the electron donating capacity of ligands, the phosphine ligands being able to donate more electron density to the metal, resulting in a more shielded environment for the H_4 protons. No trends are apparent in the chemical shifts for the H_5 protons, presumably as they are too remote from the metal.

The ^{31}P NMR data reveals the chemical shift sequence iron > ruthenium > osmium (in terms of ppm), not unexpected, as reports of Group 3[119] and Group 8[120] complexes show similar trends in ^{31}P chemical shifts. Where ^{31}P-^{31}P NMR coupling exists, the coupling constants follow the expected sequence[120] (in terms of Hz) iron > ruthenium > osmium.

The ν(C≡C) frequencies in the IR spectrum follow the trend iron < ruthenium ≈ osmium, probably resulting from greater electron back-donation from the metal to the acetylide ligand for the iron complex than for the heavier homologues. Ligand variation affords the trend in ν(C≡C) CO >> phosphine, again readily explained by back-bonding (the carbonyl ligands are more strongly π-electron withdrawing than the phosphine ligands, leading to less electron density at the metal centre and thus less electron back-donation to the acetylide ligand).

The MLCT transitions in the UV-vis spectra follow the sequence (in terms of energy), ruthenium > osmium > iron (with the exception of the carbonyl complexes for which Ru ≈ Fe). The UV-vis spectra for the complexes *trans*-[M(4-C≡C$C_6H_4NO_2$)Cl((*R,R*)-diph)]$_2$ (M = Fe, Ru, Os) are shown in Figure 2.8. The trend in absorption maxima mirrors the trend found for the metal redox potentials. Comparison of the energies of MLCT transition of carbonyl-containing complexes with those of their phosphine-containing analogues reveals the trend CO >> phosphine.

In summary, variation in metal or ligand afford the expected change in the measured electrochemical and spectroscopic properties.

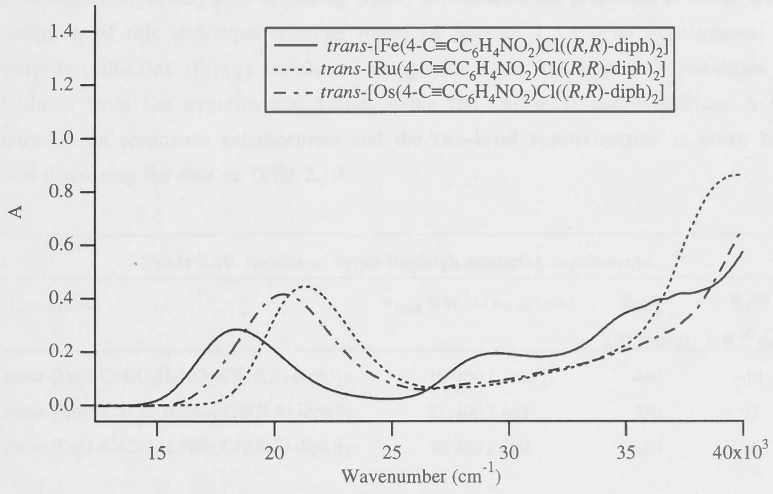

Figure 2.8. UV-vis spectra of [M(4-C≡CC$_6$H$_4$NO$_2$)Cl((*R,R*)-diph)2] (M = Fe, Ru, Os).

2.7. *Nonlinear optical investigations*

2.7.1. Molecular quadratic nonlinear optical measurements by hyper-Rayleigh scattering

The results of hyper-Rayleigh scattering (HRS) experiments are presented in Table 2.10. A description of this technique may be found in Section 1.3.5. The experimental first hyperpolarizabilities (β_{HRS}) are shown along with static first hyperpolarizabilities (β_0) calculated from the experimental values using the two-level approximation. A brief discussion on resonance enhancement and the two-level approximation is given below before discussing the data in Table 2.10.

Table 2.10. Results of hyper-Rayleigh scattering experiments.

Compound	$\tilde{\nu}_{max}$ (cm^{-1}) / λ_{max} (nm)	β_{HRS} [a] (10^{-30} esu)	β_0 [a,b] (10^{-30} esu)
trans-[Fe(4-C≡C$C_6H_4NO_2$)Cl((*R,R*)-diph)]$_2$	18 400 / 543	440	–14
trans-[Ru(4-C≡C$C_6H_4NO_2$)Cl((*R,R*)-diph)]$_2$	21 400 / 467	530	97
trans-[Os(4-C≡C$C_6H_4NO_2$)Cl((*R,R*)-diph)]$_2$	20 400 / 490	620	74
[Fe(4-C≡C$C_6H_4NO_2$)(dppe)(η^5-C_5H_5)]	20 000 / 498	665	64
[Ru(4-C≡C$C_6H_4NO_2$)(dppe)(η^5-C_5H_5)]	22 200 / 447	665	161
[Os(4-C≡C$C_6H_4NO_2$)(dppe)(η^5-C_5H_5)]	21 600 / 461	930	188
[Ru(4-C≡C$C_6H_4NO_2$)(PPh_3)$_2$(η^5-C_5H_5)] [c]	21 800 / 459	510	105
[Os(4-C≡C$C_6H_4NO_2$)(PPh_3)$_2$(η^5-C_5H_5)]	21 000 / 474	1050	174
[Fe(4-C≡C$C_6H_4NO_2$)(CO)$_2$(η^5-C_5H_5)]	27 000 / 370	50	22
[Ru(4-C≡C$C_6H_4NO_2$)(CO)$_2$(η^5-C_5H_5)]	26 900 / 372	58 [d]	27

[a] Error ±10%. [b] Static first hyperpolarizabilities calculated from the experimental values using the two-level approximation with $\beta_o = \beta[1-(2\lambda_{max}/1064)^2][1-(\lambda_{max}/1064)^2]$; damping factors not included. [c] HRS measurements have been previously reported[121] and agree within experimental error. [d] From reference 122.

The following representation of the ideas behind resonance enhancement is based on a description given by Boyd in reference 123. Figure 2.9.(i) depicts the second-harmonic generation process whereby two photons of frequency ω are simultaneously converted to

one photon of energy 2ω. The ground state of the system is represented by the solid line and the dashed lines represent virtual levels. If a real energy level is nearly coincident with one of the virtual levels (as depicted in Figure 2.9.(ii) and (iii)) then coupling between the radiation and the molecular system is strong, and the nonlinear optical process becomes enhanced.

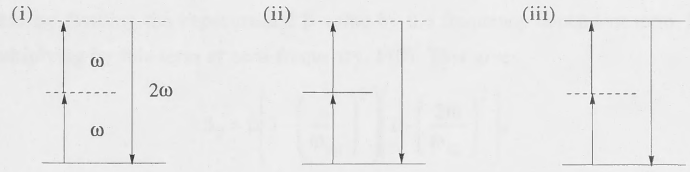

Figure 2.9. Depiction of the second-harmonic generation process.

The laser used for the HRS apparatus in the current work operates at a wavelength of 1064 nm (or 9400 cm^{-1}). Although the complexes shown in Table 2.10. are transparent at this wavelength (i.e. there is no energy level near the fundamental wavelength as depicted in Figure 2.9.(ii)), the UV-vis spectra shown in Figure 2.8 reveal appreciable absorption at the second-harmonic wavelength of 532 nm (or 18 800 cm^{-1}). This is similar to the situation depicted in Figure 2.9.(iii) and leads to resonance enhancement of the second-harmonic signal and hence β.

In order to compare data that contain significant resonance enhancement, a method was developed whereby β values are calculated for the zero-frequency case (i.e. with a static applied field present). A model that assumes that the dominant contributor to β influenced by resonance effects is a charge-transfer transition between the ground state and a single low-lying excited state (the two-level model) was tested on second-order NLO data of nitroanilines by Oudar and Chemla.[124] They found that the charge-transfer transition associated with some nitroaniline derivatives gave rise to large β values, and that the two-level model described this with good accuracy. The term associated with the charge-transfer, β_{CT}, may be written:[124]

$$\beta_{CT} = \frac{3e^2\hbar}{2m} \frac{\omega_{eg} f \Delta\mu}{\left(\omega_{eg}^2 - \omega^2\right)\left(\omega_{eg}^2 - (2\omega)^2\right)} \qquad (1)$$

where e is the electronic charge, m is the rest mass of an electron, ω_{eg} is the frequency of the optical transition, f is the oscillator strength, $\Delta\mu$ is the difference between the ground and excited state dipole moment, and ω is the frequency of the exciting radiation. This equation may be expressed as,

$$\beta_{CT=}\frac{3e^2\hbar\omega_{eg}f\Delta\mu}{2m}\times F(\omega), \text{ where } F(\omega)=\frac{1}{\left(\omega_{eg}^2-\omega^2\right)\left(\omega_{eg}^2-(2\omega)^2\right)}$$

The approximated zero-frequency (or static) second-order hyperpolarizability, β_0, may be calculated by dividing the experimental β value by the frequency dependent term, $F(\omega)$ and then multiplying by this term at zero-frequency, F(0). This gives

$$\beta_0=\beta\left(1-\left(\frac{\omega}{\omega_{eg}}\right)^2\right)\left(1-\left(\frac{2\omega}{\omega_{eg}}\right)^2\right),$$

or it may be expressed in terms of the wavelength of maximum absorption of the CT transition, λ_{max} as,

$$\beta_0=\beta\left(1-\left(\frac{\lambda_{max}}{\lambda}\right)^2\right)\left(1-\left(\frac{2\lambda_{max}}{\lambda}\right)^2\right) \qquad (2)$$

where λ is the wavelength of the exciting radiation.

It should be mentioned that this method of calculating static β values has some shortcomings. The assumption that only one transition is dominant with respect to β might not always be true. Computational studies by Kanis *et al*[125] using the ZINDO routine showed that in some systems (including organometallic molecules), the contribution to the two-level calculated β that comes from the first excited state may be as low as 60 %. They also found that the inclusion of a second excited state (a three-level model) revealed significant contributions to β associated with the additional transition. A study by van Walree *et al*[126] suggested that three-level terms may also be important contributors to β in studies of stilbenyl-type compounds. Furthermore, in the above zero-frequency method, no allowance for the effect of damping has been made. Damping occurs when energy absorbed by the system is dissipated in addition to being emitted as radiation. Inspection of equation (1) shows that when ω_{eg} approaches ω or 2ω, β tends to infinity. This unrealistic result arises because of the neglect of damping. A treatment to include damping into such an expression by treating the transition frequency as a complex quantity may be found in reference 123, although it produces more complicated equations. Nevertheless, use of (2) to calculate static first hyperpolarizabilities appears to be widespread and may give some qualitative insights into β measurements affected by resonance enhancement.

A comparison of the β_{HRS} values for the metal acetylide complexes (Table 2.10.) indicates that the iron-containing complexes have the lowest responses. This is in contrast to the trend reported for donor-acceptor nitrile[1] and metallocenyl complexes[2-5] discussed in Section 2.1. In the current work, the iron acetylide complexes have absorption bands closer to the second harmonic wavelength of 532 nm (or 18800 cm^{-1}) than either the ruthenium or osmium homologues (with the exception of the iron and ruthenium carbonyl complexes), suggesting that the β_{HRS} values for the iron complexes contain a larger resonance contribution than those of the ruthenium and osmium homologues.

The β_{HRS} values for the osmium acetylide complexes are in each case greater than the values for the ruthenium-containing complexes. Absorption bands for the osmium complexes are closer to the second-harmonic than are those of the ruthenium homologues. For the cyclopentadienyl complexes, if static β values are calculated from the experimental β_{HRS} values using a two-level model (see above for a discussion of this approximation), then the trend remains the same as for the experimental values. The values for the complexes containing the diph ligand show that ruthenium has the higher calculated static value. While this suggests some ambiguity, the two-level model may have limited applicability with organometallic complexes of this type. It is therefore be likely that the β_{HRS} values for this type of complex follow the ordering; iron < ruthenium < osmium.

Comparison of the β_{HRS} values for $[M(4\text{-}C{\equiv}CC_6H_4NO_2)(dppe)(\eta^5\text{-}C_5H_5)]$ and $[M(4\text{-}C{\equiv}CC_6H_4NO_2)(CO)_2(\eta^5\text{-}C_5H_5)]$ (M = Fe, Ru) illustrate the effect of varying co-ligands. Replacement of the electron donating diphosphine ligand with the relatively strongly electron withdrawing carbonyls results in a significant reduction of the second-order NLO response. This is readily rationalized as the amount of electron density available to the donating metal centre, and hence its donor strength, is reduced on replacing diphosphine by two carbonyl groups.

Correlating readily accessible spectroscopic parameters with NLO properties would, if successful, afford information about the NLO response of complexes without recourse to less readily-available NLO measurements. While connections between linear optical properties and nonlinear optical properties have been probed significantly,[125] attempts to find relationships between other physical data (e.g. redox potentials and NMR resonances) and the quadratic hyperpolarizability should be made with caution. The series $[M(C{\equiv}CC_6H_4NO_2)Cl((R,R)\text{-diph})_2]$ (M = Fe, Ru, Os) suggests a relationship between the ^{31}P NMR chemical shifts and β_{HRS} values, a relationship which appears to hold upon introduction of data from the series $[M(C{\equiv}CC_6H_4NO_2)(dppe)(\eta^5\text{-}C_5H_5)]$ (M = Fe, Ru, Os). When all the data available are examined, however, this trend does not persist. It was suggested by Wenseleers *et al*[1] that there may be a correlation between $\nu(N{\equiv}C)$ and β_{HRS}

for the nitrile complexes $[M(N{\equiv}CC_6H_4\text{-}4\text{-}R)(dppe)(\eta^5\text{-}C_5H_5)]^+$ (where M = Fe, Ru, R = Ph, NMe_2, NO_2, $C_6H_4NO_2$)], for which a lower energy stretch would correspond to a larger optical nonlinearity. This trend is not reproduced in the current work with acetylide ligands, making such claims tenuous.

2.7.2. Second-harmonic generation in bulk samples

Experiments to detect a bulk second-order response were performed on selected samples using the Kurtz powder technique,[127] the results being presented in Table 2.12.

Table 2.12. Kurtz powder measurement results.

Complex	SHG vs Urea
trans-$[Fe(4\text{-}C{\equiv}CC_6H_4NO_2)Cl((R,R)\text{-diph})]_2$	~ 2
trans-$[Ru(4\text{-}C{\equiv}CC_6H_4NO_2)Cl((R,R)\text{-diph})]_2$	None detected
trans-$[Os(4\text{-}C{\equiv}CC_6H_4NO_2)Cl((R,R)\text{-diph})]_2$	« 1

These crude experiments were performed by directing a laser beam onto a powder sample and detecting any emitted light at the second-harmonic wavelength. The intensity of the measured SHG was compared to that of urea, a common standard. The bulk second-order measurements show that complexes of this type are, in some instances, capable of second-harmonic generation. These experiments were not designed to elucidate any detailed information about the bulk responses of the samples (e. g. phase matchability), and may not be used to compare the efficiency of the various metal centres. By comparison with some of the values shown in Chapter 1, the new data are quite modest, but the non-zero responses for the iron- and osmium-containing complexes confirm the ability of the diph ligand to force non-centrosymmetric packing and permit a bulk second-order NLO response.

2.8. Conclusions

The aim of the work presented in this Chapter is to examine the effect of metal variation upon the second-order optical nonlinearity of several series of group 8 transition metal acetylide complexes. A comparison of the values of β_{HRS} for the metal acetylide complexes shows that the iron-containing complexes have the lowest responses and are also the most resonance enhanced. The β_{HRS} values for the osmium acetylide complexes are in each case greater than the values for the ruthenium-containing complexes but have absorption bands closer to the second-harmonic wavelength than are those of the ruthenium homologues. If a two-level model is used to calculate static β values (β_0) from the β_{HRS} values, then the β_0 values are greater for the osmium complexes than the ruthenium complexes, with the exception of the diph-containing complexes. It may therefore be suggested that the trend in β_{HRS} values for this type of complex follows the order: iron < ruthenium < osmium.

Previously reported trends in β values versus transition metal[1-5] are not reproduced in the current work. It is likely that other factors play a more dominant role in determining the optical nonlinearity. The predictive merit of a few physical properties on optical nonlinearities may be of little value.

Experiments to detect a bulk second-order response show that complexes of this type are, in some instances, capable of second-harmonic generation. They confirm the ability of the optically-active diph ligand to permit a bulk second-order NLO response.

From a synthetic perspective, two series of homologous iron / ruthenium / osmium acetylide complexes were prepared. One series incorporated the optically active diph ligand, and included the first examples of such iron and osmium complexes. A synthetic route into *cis* and *trans* isomers of $[OsCl_2(diph)_2]$ was developed to facilitate the preparation of the osmium diph acetylide complex.

A structural study of *trans*-$[OsCl_2(Me_2SO)_4]$ confirmed the spectroscopically assigned all-S-bound Me_2SO configuration and a crystallographic determination of the *cis* isomer revealed a previously unreported all-S-bound Me_2SO geometry. A structural study of *trans*-$[OsCl_2\{(R,R)\text{-diph})\}_2]$ confirmed the retention of both stereochemistry at metal and configuration at phosphorus in proceeding from the dimethylsulfoxide precursor to the new bis(diphosphine) complex.

2.9. Experimental

2.9.1. General Conditions, Reagents and Instruments

General Conditions

All reactions were performed under a nitrogen atmosphere with the use of Schlenk techniques unless otherwise stated. Dichloromethane was dried by distilling over CaH_2, methanol was dried by distilling over Mg/I_2, toluene was dried by distilling over sodium / benzophenone, and other solvents were used as received. "Pet. spirit" refers to a fraction of petroleum ether of boiling range 60-80 °C. Cation exchange resin was Dowex 50W-X2, 50-100 mesh.

Reagents

The following were prepared by literature methods: $[FeCl_2 \cdot 1.5THF]$,[88] *(S,S)*-1,2-bis(methylphenylphosphino)benzene (diph),[128] 4-$HC{\equiv}CC_6H_4NO_2$,[129] $[Fe(4\text{-}C{\equiv}CC_6H_4NO_2)(CO)_2(\eta^5\text{-}C_5H_5)]$,[43] $[FeCl(dppe)(\eta^5\text{-}C_5H_5)]$,[89] $[RuCl_2(DMSO)_4]$,[93] $[RuCl(dppe)(\eta^5\text{-}C_5H_5)]$,[55] $[Ru(4\text{-}C{\equiv}CC_6H_4NO_2)(dppe)(\eta^5\text{-}C_5H_5)]$,[130] $(NH_4)_2[OsCl_6]$,[98] $[OsBr(dppe)(\eta^5\text{-}C_5H_5)]$.[55] The literature procedure for the preparation of $[OsBr(PPh_3)_2(\eta^5\text{-}C_5H_5)]$[112] was modified in the following way: methanol was substituted for ethanol as solvent, reaction time was reduced from 12 h to 30 min, diethyl ether was substituted for benzene as the eluant for column chromatography. Ammonium hexafluorophosphate (Aldrich), anhydrous magnesium sulfate (Aldrich) and stannous chloride dihydrate (Unilab) were used as received. Sodium hexafluorophosphate (Aldrich) was recrystallized from acetonitrile before use. Sodium methoxide solutions were prepared by the slow addition of sodium to dry methanol.

Instruments

Mass spectra were recorded using a VG ZAB 2SEQ instrument (30 kV Cs^+ ions, current 1 mA, accelerating potential 8 kV, 3-nitrobenzyl alcohol matrix) at the Research School of Chemistry, Australian National University; peaks are reported as *m/z* (assignment, relative intensity). Microanalyses were carried out at the Research School of Chemistry, Australian National University. Electrochemical measurements were recorded using a MacLab 400 interface and MacLab potentiostat from AD Instruments (using a glassy carbon disc working, Pt auxiliary and Ag-AgCl reference mini-electrodes from Cypress Systems). Scan rates were 100 mV s^{-1}. Electrochemical solutions contained 0.1 M $(NBu_4)[PF_6]$ and ca. 10^{-3} M complex in dichloromethane. Solutions were purged and maintained under an atmosphere of nitrogen. All values are referenced to an internal sample reference of

ferrocene (E^0 0.56 V). Infrared spectra were recorded as dichloromethane solutions using a Perkin-Elmer System 2000 FT-IR. ^1H, ^{13}C and ^{31}P NMR spectra were recorded using a Varian Gemini-300 FT NMR spectrometer and are referenced to residual $CHCl_3$ (7.24 ppm), $CDCl_3$ (77.0 ppm) or external 85% H_3PO_4 (0.0 ppm), respectively. NMR assignments follow the numbering scheme shown in Figure 2.7. UV-vis spectra were recorded using a Cary 5 spectrophotometer as solutions in tetrahydrofuran in 1 cm cells. Optical rotations were measured at 20 °C on a Perkin-Elmer model 241 polarimeter.

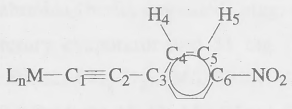

Figure 2.7. NMR numbering scheme.

2.9.2. Synthesis of Iron Complexes

$(-)_{589}$-*trans*-[$FeCl_2$((*R,R*)-diph)$_2$]

A mixture of $FeCl_2$.1.5THF (145 mg, 0.62 mmol) and *(S,S)*-diph (400 mg, 1.24 mmol) was stirred in methanol (10 mL) for 45 min at reflux. A lime green precipitate formed. The mixture was allowed to cool to room temperature and then cooled in an ice bath for 15 min. The precipitate was collected by filtration in air and washed with pet. spirit (2 x 30 mL). It was then dissolved in dichloromethane and passed through a plug of Celite to remove any residual Fe^0. Pet. spirit (30 mL) was added to the filtrate and the solvent was removed on a rotary evaporator. The lime green powder was collected and dried *in vacuo*. Yield was 405 mg (85 %). $[\alpha]_D$: –1760 (*c* 0.101, CH_2Cl_2). MS: 770 ($[M]^+$, 20), 735 ($[M - Cl]^+$, 20), 700 ($[Fe(diph)_2]^+$, 5), 413($[FeCl(diph)]^+$, 50), 322 ($diph^+$, 45). Anal. Calcd for $C_{40}H_{40}Cl_2FeP_4$: C 62.28, H 5.23 %. Found: C 61.89, H 5.18 %. UV-vis ($\bar{\nu}_{max}$, cm^{-1} (ε, M^{-1} cm^{-1})): 15 260 (70), 21 900 (sh, 370), 26 410 (1310), 34 670 (sh, 11 300), 37 370 (23 200). ^1H NMR: (δ, 300 MHz, $CDCl_3$); 1.24 (s(br), 12H, Me), 7.27 to 7.46 (m, 28H, Ph). ^{31}P NMR: (δ, 121 MHz, $CDCl_3$); 67.7 (s (br)).

$(-)_{436}$-*trans*-[Fe(4-C≡C$C_6H_4NO_2$)Cl((*R,R*)-diph)$_2$]

A mixture of $(-)_{589}$-*trans*-[$FeCl_2$((*R,R*)-diph)$_2$] (50 mg, 0.065 mmol), 4-HC≡C$C_6H_4NO_2$ (20 mg, 0.14 mmol) and sodium hexafluorophosphate (20 mg, 0.12 mmol) was stirred in dichloromethane (5 mL) for 2 h at reflux. The mixture was allowed to cool to room temperature and then 12 mL of pet. spirit added. A brown precipitate formed. The solvent and excess acetylene were removed by filter-tipped cannula under nitrogen. The remaining solid was dissolved in dichloromethane and sodium methoxide solution (1mL, 0.3 M solution in methanol) was added with stirring. The mixture immediately turned a deep purple in colour. The solvent was then removed *in vacuo*. The residue extracted into diethyl ether and passed through an alumina (basic, ungraded) plug, eluting with diethyl ether. The solvent was removed on a rotary evaporator and 31 mg (54 %) of purple powder was collected. $[\alpha]_{436}$ = –3180 (*c* 0.022, CH_2Cl_2). MS: 881 ([M]$^+$, 100), 846 ([M - Cl]$^+$, 15), 735 ([FeCl(diph)$_2$]$^+$, 20), 700 ([Fe(diph)$_2$]$^+$, 5), 559 ([Fe(4-C≡C$C_6H_4NO_2$)Cl(diph)]$^+$, 35), 413 ([FeCl(diph)]$^+$, 50). Anal. Calcd for $C_{48}H_{44}ClNO_2P_4Ru$: C 65.36, H 5.03, N 1.59 %. Found: C 64.41, H 5.39, N 1.78 %. UV-vis ($\tilde{\nu}_{max}$, cm^{-1} (ε, M^{-1} cm^{-1})): 18 400 (16 500), 29 400 (11 300), 36 400 (22 500) 37 300 (24 100). IR (cm^{-1}): 2043 ν(C≡C). ^{1}H NMR: (δ, 300 MHz, $CDCl_3$); 1.52 (t, J_{HH} = 4 Hz, 6H, Me), 1.59 (t, J_{HH} = 4 Hz, 6H, Me), 6.23 (d, J_{HH} = 9 Hz, 2H, H_4), 7.23 to 7.53 (m, 28H, Ph), 7.78 (d, J_{HH} = 9 Hz, 2H, H_5). ^{31}P NMR: (δ, 121 MHz, $CDCl_3$); 72.3 (t, J_{PP} = 43 Hz, 2P), 77.0 (t, J_{PP} = 43 Hz, 2P).

[Fe(4-C≡C$C_6H_4NO_2$)(dppe)(η^5-C_5H_5)]

A mixture of [FeCl(dppe)(η^5-C_5H_5)] (200 mg, 0.36 mmol), 4-HC≡C$C_6H_4NO_2$ and ammonium hexafluorophosphate was stirred in methanol (40 mL) for 90 min at reflux. The mixture was allowed to cool to room temperature and then 2 mL of sodium methoxide solution (0.33 M in methanol) was added with stirring. The solvent was removed *in vacuo* and residue was absorbed onto alumina (basic, ungraded) and placed atop an alumina column. Excess acetylene was eluted using 3:7 dichloromethane / pet. spirit and the product was eluted using 3:5 dichloromethane / pet. spirit. The volume was reduced to ~10 mL whereupon the product precipitated and was collected by filtration in air and washed with pet. spirit. Yield was 75 mg (31 %). MS: 665 ([M]$^+$, 65), 649 ([Fe(4-C≡CC_6H_4NO)(dppe)(η^5-C_5H_5)]$^+$, 7), 519 ([Fe(dppe)(η^5-C_5H_5)]$^+$, 100). Anal. Calcd for $C_{39}H_{33}FeNO_2P_2$: C 70.39, H 5.00, N 2.10 %. Found: C 70.37, H 5.10, N 2.30 %. IR (cm^{-1}): 2044 (νC≡C). UV-vis ($\tilde{\nu}_{max}$, cm^{-1} (ε, M^{-1} cm^{-1})): 20 000 (13 300), 31 490 (9800). ^{1}H NMR: (δ, 300 MHz, $CDCl_3$); 2.23 (m, 2H, CH_2), 2.55 (m, 2H, CH_2), 4.29 (s, 5H, C_5H_5), 6.25 (m, 2H, H_4), 7.20 to 7.84 (m, 22H, Ph). ^{31}P NMR: (δ, 121 MHz, $CDCl_3$); 106.2 (s (br), PPh_2).

2.9.3. Synthesis of Ruthenium Complexes

cis- and trans-[$RuCl_2$((R,R)-diph)$_2$]

A mixture of [$RuCl_2(DMSO)_4$] (375 mg, 0.77 mmol) and *(S,S)*-diph (500 mg, 1.56 mmol) was stirred in methanol (15 mL) for 30 min at reflux. The mixture was allowed to cool to room temperature. The yellow precipitate that formed was filtered off. The filtrate was reduced to a viscous oil on a rotary evaporator and water (5 mL) was added. A yellow precipitate formed and was collected by filtration, dissolved in dichloromethane and then dried over anhydrous magnesium sulfate. This mixture was filtered and the yellow solution was reduced to dryness on a rotavap and the yellow powder collected. Both samples of yellow solid contained *cis* and *trans* isomers and so they were combined to give 572 mg (90 %). The *cis/trans* isomers were cleanly separated by fractional crystallization. The mixture of isomers (572 mg) was dissolved in dichloromethane (10 mL) and pet. spirit (65 mL) was slowly added. Upon standing, the *cis* isomer crystallized and was collected by filtration to give 450 mg (71 %) of lemon yellow crystals. $[\alpha]_D$ –25.8° (*c* 0.42, CH_2Cl_2). MS: 816 ($[M]^+$, 60), 781 ($[M - Cl]^+$, 100), 745 ($[Ru((RR)\text{-diph})_2]^+$, 25), 423 ($[Ru((RR)\text{-diph})]^+$, 27). ^1H NMR: (δ, 300 MHz, $CDCl_3$); 1.63 (m, 6H, Me), 2.31 (m, 6H, Me), 6.55 to 7.68 (28H, Ph). ^{31}P NMR: (δ, 121 MHz, $CDCl_3$); 55.1 (t, J_{PP} = 22 Hz, 2P), 47.5 (t, J_{PP} = 22 Hz, 2P).

The volume of the filtrate was reduced to ~10 mL and, upon standing, the *trans* isomer precipitated. This was collected by filtration to yield 100 mg (16 %) of golden yellow microcrystals. ^1H NMR: (δ, 300 MHz, $CDCl_3$); 1.55 (br s, 12H, Me), 6.60 to 7.49 (28H, Ph). ^{31}P NMR: (δ, 121 MHz, $CDCl_3$); 52.0 (s).

$(-)_{589}$-trans-[Ru(4-C≡C$C_6H_4NO_2$)Cl((R,R)-diph)$_2$]

cis-[$RuCl_2$((*R,R*)-diph)$_2$] (50 mg, 0.061 mmol), 4-HC≡$CC_6H_4NO_2$ (20 mg, 0.14 mmol) and sodium hexafluorophosphate (25 mg, 0.15 mmol) were stirred in toluene (5 mL) at reflux for 2 h. A light brown precipitate formed. This was collected by filtration in air and then dissolved in dichloromethane. Sodium methoxide (1 mL, 0.2 M solution in methanol) was added with stirring. The solvent was removed on a rotavap and the residue extracted into dichloromethane (~10 mL). The mixture was filtered, pet. spirit (about 5 mL) was added and the solution taken to dryness to yield 36 mg of red powder (63 %). $[\alpha]_D$ = –504 (*c* 0.145, CH_2Cl_2). MS: 927 ($[M]^+$, 100), 892 ($[M - Cl]^+$, 20), 745 ($[Ru(diph)_2]^+$, 28), 423 ($[Ru(diph)]^+$, 26). Anal. Calcd for $C_{48}H_{44}ClNO_2P_4Ru$: C 62.17, H 4.78, N 1.51 %. Found: C 61.97, H 4.89, N 1.37 %. UV-vis ($\bar{\nu}_{max}$, cm^{-1} (ε, M^{-1} cm^{-1})): 21 400 (20 700), 39 800 (40 000), 41 200 (sh, 47 500). IR (cm^{-1}): 2057 ν(C≡C). ^1H NMR: (δ, 300 MHz, $CDCl_3$); 1.59 (t, J_{HH} = 3 Hz, 6H, Me), 1.64 (t, J_{HH} = 3 Hz, 6H, Me), 6.41 (d, J_{HH} = 9 Hz, 2H, H_4), 7.24 to 7.53 (m, 28H, Ph), 7.82 (d, J_{HH} = 9 Hz, 2H, H_5). ^{31}P NMR: (δ, 121 MHz, $CDCl_3$); 50.4 (t,

J_{PP} = 22 Hz, 2P), 54.4 (t, J_{PP} = 22 Hz, 2P). ^{13}C NMR: (δ, 75 MHz, $CDCl_3$); 12.4 (t, J_{CP} = 16 Hz, Me), 14.9 (t, J_{CP} = 16 Hz, Me), 111.6 (s, C_2), 123.4 to 147.4 (Ph).

[Ru(4-C≡C$C_6H_4NO_2$)(dppe)(η^5-C_5H_5)]

A mixture of [RuCl(dppe)(η^5-C_5H_5)] (250 mg, 0.35 mmol), 4-HC≡C$C_6H_4NO_2$ (130 mg, 0.88 mmol) and ammonium hexafluorophosphate (150 mg, 0.92 mmol) was stirred in methanol (40 mL) for 1 h at reflux. The mixture was allowed to cool to room temperature, dichloromethane (40 mL) was added and the mixture filtered. Pet. spirit (~20 mL) was added and the volume reduced *in vacuo* until the vinylidene complex precipitated. It was collected by filtration in air and then dissolved in dichloromethane. To this solution was added 10 mL of sodium methoxide solution (0.1 M in methanol) with stirring. The solvent was removed and the product purified by column chromatography on alumina, eluting with 65 % dichloromethane / 35 % pet. spirit. Yield was 75 mg (30 %). MS: 711 ([M]$^+$, 100), 565 ([Ru(dppe)(η^5-C_5H_5)]$^+$. Anal. Calcd for $C_{39}H_{33}NO_2P_2Ru$: C 65.91, H 4.68, N 1.97 %. Found: C 65.91, H 4.60, N 1.79 %. IR (cm^{-1}): 2056 ν(C≡C). UV-vis ($\tilde{\nu}_{max}$, cm^{-1} (ε, M^{-1} cm^{-1})): 22 200 (17 800). ^1H NMR: (δ, 300 MHz, $CDCl_3$); 2.30 (m, 2H, CH_2), 2.57 (m, 2H, CH_2), 4.79 (s, 5H, C_5H_5), 6.31 (d, J_{HH} = 7 Hz, 2H, H_4), 7.26 to 7.87 (m, 22H, Ph). ^{31}P NMR: (δ, 121 MHz, $CDCl_3$); 86.2 (s, PPh_2).

2.9.4. Syntheses of Osmium Complexes

trans-[$OsCl_2$(DMSO)$_4$]

An aqueous solution of $(NH_4)_2[OsCl_6]$ (500 mg, 1.14 mmol) was passed through a cation exchange column in the protic form, eluting with H_2O, after which the solvent was removed from the eluate using a rotary evaporator. The residue was dissolved in dimethylsulfoxide (4 mL), $SnCl_2.2H_2O$ (400 mg, 1.78 mmol) was added and the resultant solution heated at 90 °C for 1 h. The yellow precipitate that formed was collected by filtration and washed with acetone (2 x 15 mL) and ether (2 x 15 mL), yielding 300 mg (46 %) as a yellow solid. MS: 574 ([M]$^+$, 32), 558 ([M - O]$^+$, 29), 539 ([M - Cl]$^+$, 7), 497 ([M – Me_2SO]$^+$, 15). Anal. Calcd for $C_8H_{24}Cl_2O_4OsS_4$: C 16.75, H 4.22 %. Found: C 16.43, H 4.10 %. ^1H NMR: (δ, 300 MHz, $CDCl_3$); 3.44 (s, Me). UV-vis ($\tilde{\nu}_{max}$, cm^{-1} (ε, M^{-1} cm^{-1})): 28 460 (50), 37 290 (sh, 920), 40 000 (1760). ^1H NMR: (δ, 300 MHz, $CDCl_3$); 3.44 (s, Me). ^{13}C NMR: (δ, 75 MHz, $CDCl_3$); 42.0 (Me). A crystal suitable for X-ray diffraction study was grown by liquid diffusion from $CHCl_3$ / hexane at room temperature.

cis-[$OsCl_2$(DMSO)$_4$]

An aqueous solution of $(NH_4)_2[OsCl_6]$ (250 mg, 0.57 mmol) was passed through a cation exchange column in the protic form, eluting with H_2O, after which the solvent was removed

from the eluate using a rotary evaporator. The residue was transferred to a Schlenk tube as a solution in methanol and the solvent removed *in vacuo*. The red/black residue was then dissolved in dimethylsulfoxide (1 mL), $SnCl_2.2H_2O$ (200 mg, 0.89 mmol) was added and the mixture was stirred under N_2 for 0.5 h at 120 °C, over which time a precipitate formed. The temperature was increased to 150 °C and stirring continued for 0.5 h. The mixture was cooled to room temperature and acetone (7 mL) was added. It was then allowed to stand overnight under N_2 whereupon a light grey precipitate formed which was collected and washed with acetone and ether. Recrystallization from $CHCl_3$ / ether afforded 110 mg as white microcrystals (34 %). MS: 575 ($[M]^+$, 83), 558 ($[M - O]^+$, 8), 539 ($[M - Cl]^+$, 100), 434 ($[OsCl_2O(Me_2SO)_2]^+$, 81). Anal. Calcd for $C_8H_{24}Cl_2O_4OsS_4$: C 16.75, H 4.22 %. Found: C 16.67, H 3.87 %. UV-vis ($\tilde{\nu}_{max}$, cm^{-1} (ε, $M^{-1}\,cm^{-1}$)): 34 390 (550), 40 330 (sh, 950). ^1H NMR: (δ, 300 MHz, $CDCl_3$); 2.75 (s, 6H, Me), 3.41 (s, 6H, Me), 3.52 (s, 6H, Me), 3.56 (s, 6H, Me). ^{13}C NMR: (δ, 75 MHz, $CDCl_3$); 38.4 (Me), 45.0 (Me), 47.7 (Me), 47.9 (Me). The complex was also synthesized by stirring *trans*-$[OsCl_2(DMSO)_4]$ (100 mg, 0.17 mmol), prepared as above, in 5 mL of DMSO at 150 °C for 1 h. Evaporation of the DMSO *in vacuo* and washing of the resultant white powder with 1 : 1 acetone / ether (2 x 4 mL), and then ether (2 x 4 mL) yielded 78 mg (78 %) of the *cis* product. A crystal suitable for X-ray diffraction study was grown by liquid diffusion from chloroform / diethyl ether at room temperature.

$(+)_{589}$-cis-$[OsCl_2((R,R)$-diph$)_2]$

A mixture of *cis*-$[OsCl_2(DMSO)_4]$ (100 mg, 0.17 mmol) and (*S,S*)-diph (112 mg, 0.35 mmol) was stirred in refluxing methanol (5 mL) for 5 h. The mixture was allowed to cool to room temperature and the resultant pale yellow precipitate was collected, washed with ether and dried *in vacuo*. 56 mg of powder was collected and a further 20 mg of product was obtained by removing the solvent *in vacuo*, dissolving the residue in dichloromethane and then precipitating with pet. spirit. Yield 76 mg (48 %). $[\alpha]_D$: +9.0 (*c* 0.22, CH_2Cl_2). MS: 906 ($[M]^+$). Anal. Calcd for $C_{40}H_{40}Cl_2OsP_4$: C 53.04, H 4.45 %. Found: C 52.84, H 4.36 %. ^1H NMR: (δ, 300 MHz, $CDCl_3$); 1.76 (m, 6H, Me), 2.23 (t, J = 4 Hz, 6H, Me), 5.99 - 7.80 (m, 28H, Ph). ^{31}P NMR: (δ, 121 MHz, $CDCl_3$); 10.6 (t, J_{PP} = 9 Hz, 2P), 16.3 (t, J_{PP} = 9 Hz, 2P).

$(-)_{589}$-trans-$[OsCl_2((R,R)$-diph$)_2]$

A mixture of *trans*-$[OsCl_2(DMSO)_4]$ (100 mg, 0.17 mmol) and (*S,S*)-diph (118 mg, 0.36 mmol) was stirred in refluxing methanol (10 mL) for 18 h, and then allowed to cool to room temperature. The yellow microcrystals that formed were collected, washed with pet. spirit and dried *in vacuo* (104 mg, 66 %). $[\alpha]_D$: –397.5 (*c* 0.20, CH_2Cl_2). MS: 906 ($[M]^+$). Anal. Calcd for $C_{40}H_{40}Cl_2OsP_4$: C 53.04, H 4.45 %. Found: C 52.61, H 4.31 %. ^1H NMR:

(δ, 300 MHz, $CDCl_3$); 1.54 (s, 12H, Me), 7.23 to 7.37 (m, 28H, Ph). ^{31}P NMR: (δ, 121 MHz, $CDCl_3$); 18.1. A crystal suitable for X-ray diffraction study was grown from dichloromethane / methanol.

$(-)_{365}$-trans-[Os(4-C≡C$C_6H_4NO_2$)Cl((R,R)-diph)$_2$]:

A mixture of *$(+)_{589}$-cis-[$OsCl_2$((R,R)-diph)$_2$]* (50 mg, 0.055 mmol), 4-HC≡C$C_6H_4NO_2$ (20 mg, 0.14 mmol) and sodium hexafluorophosphate (20 mg, 0.12 mmol) was stirred in toluene (5 mL) for 2 h at reflux. The mixture was allowed to cool to room temperature and the brown precipitate that formed was collected by filtration in air and washed with pet. spirit. It was then dissolved in dichloromethane and 1 mL of sodium methoxide solution (0.3 M in methanol) was added with stirring. The mixture immediately turned deep red in colour. The solvent was removed *in vacuo*. The residue was extracted into dichloromethane and filtered. Pet. spirit was added to filtrate and the solvent was removed on a rotary evaporator and 33 mg (59 %) of dark red powder was collected. $[\alpha]_{365}$ = –2730 (*c* 0.0495, CH_2Cl_2). MS: 1017 ($[M]^+$, 100). Anal. Calcd for $C_{48}H_{44}ClNO_2OsP_4$: C 56.72, H 4.36, N 1.38 %. Found: C 57.31, H 4.80, N 1.65 %. IR (cm^{-1}): 2052 ν(C≡C). UV-vis ($\bar{\nu}_{max}$, cm^{-1} (ε, M^{-1} cm^{-1})): 20 400 (18 200), 40 900 (sh, 35 200). ^1H NMR: (δ, 300 MHz, $CDCl_3$); 1.62 (t, J_{HH} = 4 Hz, 6H, Me), 1.71 (t, J_{HH} = 4 Hz, 6H, Me), 6.38 (d, J_{HH} = 9 Hz, 2H, H_4), 7.22 to 7.48 (m, 28H, Ph), 7.82 (d, J_{HH} = 9 Hz, 2H, H_5). ^{31}P NMR: (δ, 121 MHz, $CDCl_3$); 18.9 (t, J_{PP} = 13 Hz, 2P), 23.0 (t, J_{PP} = 13 Hz, 2P). ^{13}C NMR: (δ, 75 MHz, $CDCl_3$); 10.7 (t, J_{CP} = 20 Hz, Me), 13.7 (t, J_{CP} = 20 Hz, Me), 109.7 (C_2), 123.4 to 147.4 (Ph).

[Os(4-C≡C$C_6H_4NO_2$)(PPh_3)$_2$(η^5-C_5H_5)]

A mixture of [OsBr(PPh_3)$_2$(η^5-C_5H_5)] (250 mg, 0.29 mmol), 4-HC≡C$C_6H_4NO_2$ (130 mg, 0.88 mmol) and ammonium hexafluorophosphate (150 mg, 0.92 mmol) was stirred in methanol (40 mL) for 3 h at reflux. The mixture was allowed to cool to room temperature and then 2 mL of sodium methoxide solution (0.3 M in methanol) was added with stirring. The solvent was removed and the product purified by column chromatography on alumina eluting firstly with 30 % dichloromethane / 70 % pet. spirit to remove any excess acetylene, and then with 60 % dichloromethane / 40 % pet. spirit to remove the product. The solvent was removed and the product was collected to yield 210 mg (78 %) of dark red microcrystals. MS: 927 ($[M + H]^+$, 100), 781 ($[Os(PPh_3)_2(\eta\text{-}C_5H_5)]^+$, 10), 664 ($[M - PPh_3]^+$, 35). Anal. Calcd for $C_{49}H_{39}NO_2OsP_2$: C 63.56, H 4.25, N 1.51 %. Found: C 63.55, H 4.42, N 1.61 %. IR (cm^{-1}): 2054 ν(C≡C). UV-vis ($\bar{\nu}_{max}$, cm^{-1} (ε, M^{-1} cm^{-1})): 21 000 (22 300), 36 400 (sh, 16 000). ^1H NMR: (δ, 300 MHz, $CDCl_3$); 4.43 (s, 5H, C_5H_5), 6.98 (d, J_{HH} = 9 Hz, 2H, H_4), 7.05 to 7.35 (m, 30H, Ph), 8.00 (d, J_{HH} = 9 Hz, 2H, H_5). ^{31}P NMR: (δ, 121 MHz, $CDCl_3$); 2.8 (s, PPh_3).

[Os(4-C≡CC$_6$H$_4$NO$_2$)(dppe)(η^5-C$_5$H$_5$)]

A mixture of [OsBr(dppe)(η^5-C$_5$H$_5$)] (160 mg, 0.22 mmol), 4-HC≡CC$_6$H$_4$NO$_2$ (50 mg, 0.34 mmol) and ammonium hexafluorophosphate (75 mg, 0.46 mmol) was stirred in methanol (30 mL) for 65 h at reflux. The solvent was removed *in vacuo* and the residue extracted into dichloromethane (10 mL) and filtered through a sintered glass funnel. Diethyl ether (50 mL) was added to the filtrate and 100 mg of yellow powder was collected. This was dissolved in dichloromethane (10 mL) and 2 mL of sodium methoxide solution (0.3 M in methanol) was added with stirring. The solvent was removed and the product purified by column chromatography on alumina eluting with dichloromethane. The solvent was removed and the product was collected to yield 30 mg (17 %) of dark red powder. MS: 802 ([M]$^+$, 100), 655 ([Os(dppe)(η^5-C$_5$H$_5$)]$^+$, 25). Anal. Calcd for C$_{39}$H$_{33}$NO$_2$OsP$_2$: C 58.57, H 4.16, N 1.75 %. Found: C 58.40, H 4.11, N 1.57 %. IR (cm^{-1}): 2055 ν(C≡C). UV-vis ($\bar{\nu}_{max}$, cm^{-1} (ε, M^{-1} cm^{-1})): 21 600 (16 900) 36 800 (sh, 10 400). ^{1}H NMR: (δ, 300 MHz, CDCl$_3$); 2.42 (m, 4H, CH$_2$), 4.78 (s, 5H, C$_5$H$_5$), 6.25 (d, J_{HH} = 9 Hz, 2H, H$_4$), 7.17 to 7.38 (m, 20H, Ph), 7.72 (d, J_{HH} = 9 Hz, 2H, C$_5$), 7.85 (m, 4H, Ph). ^{31}P NMR: (δ, 121 MHz, CDCl$_3$); 46.7 (s, PPh$_2$).

2.9.5. X-ray structure determinations

Unique diffractometer data sets were obtained using the ω-2θ scan technique and yielded N independent reflections, N_o of these with $I \geq 3.00\sigma(I)$ being considered "observed" and used in full matrix least squares refinement; an empirical psi-type absorption correction was applied in each case. Anisotropic thermal parameters were refined for the non-hydrogen atoms; $(x, y, z, U_{iso})_H$ were included constrained at estimated values. For the complex *trans*-[OsCl$_2$(DMSO)$_4$], disorder was modelled with the S atom occupying two sites with occupancies summing to 0.5. Conventional residuals R and R_w on $|F|$ are given; the weighting function $w = 4F_o^2/\sigma^2(F_o^2)$ where $\sigma^2(F_o^2) = [S^2(C + 4B) + (pF_o^2)^2]/Lp^2$ (S = scan rate, C = peak count, B = background count, $p = p$ factor determined experimentally from standard reflections) was employed. Computation used the teXsan package.[131] Specific data collection, solution and refinement parameters are given in the Tables in Section 2.5.

2.9.6. Nonlinear optical measurements

Hyper-Rayleigh scattering

An injection-seeded Nd:YAG laser (Q-switched Nd:YAG Quanta Ray GCR5, 1064 nm, 8 ns pulses, 10 Hz) was focussed into a cylindrical cell (7 mL) containing the sample. The intensity of the incident beam was varied by rotation of a half-wave plate placed between crossed polarizers. Part of the laser pulse was sampled by a photodiode to measure the

vertically polarized incident light intensity. The frequency doubled light was collected by an efficient condenser system and detected by a photomultiplier. The harmonic scattering and linear scattering were distinguished by appropriate filters; gated integrators were used to obtain intensities of the incident and harmonic scattered light. All measurements were performed in tetrahydrofuran using *p*-nitroaniline ($\beta = 21.4 \times 10^{-30}$ esu)[132] as a reference. Further details of the experimental procedure have been reported in the literature.[133,134]

Powder SHG measurements

Samples were ungraded powders placed in the circular cavity (10 mm diameter x 0.5 mm depth) of a microscope slide with a cover slip. Powder SHG efficiencies were measured using the Kurtz technique.[127] The fundamental output of a Q-switched Quanta-Ray GC-130 Nd:YAG laser was directed onto the sample (spot size ~ 5 mm; energy per pulse: up to 20 mJ). A collecting lens (orthogonally placed with respect to the fundamental beam) focussed the backscattered second harmonic light through an infrared absorbing filter and a 532 nm interference filter onto a photodiode detector, which was connected to a HP digital 54510A oscilloscope. Measurements thus made were compared with a urea powder sample.

2.10. References

(1) Wenseleers, W.; Gerbrandij, A. W.; Goovaerts, E.; Garcia, M. H.; Robalo, M. P.; Mendes, P. J.; Rodrigues, J. C.; Dias, A. R. *J. Mater. Chem.* **1998**, *8*, 925.

(2) Marder, S. R.; Tiemann, B. G.; Perry, J. W.; Cheng, L. T.; Tam, W.; Schaefer, W. P.; Marsh, R. E. In *Materials for Nonlinear Optics: Chemical Perspectives*; Marder, S. R., Sohn, J. E. and Stucky, G. D., Eds.; American Chemical Society: Washington, DC, 1991; Vol. 455, p 187.

(3) Calabrese, J. C.; Cheng, L.-T.; Green, J. C.; Marder, S. R.; Tam, W. *J. Am. Chem. Soc.* **1991**, *113*, 7227.

(4) Cheng, L. T.; Tam, W.; Meredith, G. R.; Marder, S. R. *Mol. Cryst. Liq. Cryst.* **1990**, *189*, 137.

(5) Marder, S. R.; Beratan, D. N.; Tiemann, B. G.; Cheng, L. T.; Tam, W. In *Organic Materials for Nonlinear Optics II*; Hann, R. A. and Bloor, D., Eds.; Royal Society of Chemistry: London, 1991; Vol. 91, p 165.

(6) Houbrechts, S.; Clays, K.; Persoons, A.; Cadierno, V.; Gamasa, M. P.; Gimeno, J. *Organometallics* **1996**, *15*, 5266.

(7) Houbrechts, S.; Clays, K.; Persoons, A.; Cadierno, V.; Gamasa, M. P.; Gimeno, J.; Whittall, I. R.; Humphrey, M. G. *Proc. SPIE-Int. Soc. Opt. Eng.* **1996**, *2852*, 98.

(8) Tam, W.; Cheng, L. T.; Bierlein, J. D.; Cheng, L. K.; Wang, Y.; Feiring, A. E.; Meredith, G. R.; Eaton, D. F.; Calabrese, J. C.; Rikken, G. L. J. A. In *Materials for Nonlinear Optics: Chemical Perspectives*; Marder, S. R., Sohn, J. E. and Stucky, G. D., Eds.; American Chemical Society: Washington, DC, 1991; Vol. 455, p 158.

(9) Cheng, L.-T.; Tam, W.; Eaton, D. F. *Organometallics* **1990**, *9*, 2856.

(10) Maiorana, S.; Papagni, A.; Licandro, E.; Persoons, A.; Clay, K.; Houbrechts, S.; Porzio, W. *Gazz. Chim. Ital.* **1995**, *125*, 377.

(11) Naulty, R. H.; McDonagh, A. M.; Whittall, I. R.; Cifuentes, M. P.; Humphrey, M. G.; Houbrechts, S.; Maes, J.; Persoons, A.; Heath, G. A.; Hockless, D. C. R. *J. Organomet. Chem.* **1998**, *563*, 137.

(12) Sun, Y.; Taylor, N. J.; Carty, A. J. *Organometallics* **1992**, *11*, 4293.

(13) Wakatsuki, Y.; Satoh, M.; Yamazaki, H. *Chem. Lett.* **1989**, 1585.

(14) Chakravarty, A. R.; Cotton, F. A. *Inorg. Chim. Acta* **1986**, *113*, 19.

(15) Li, Y.; Han, B.; Kadish, K. M.; Bear, J. L. *Inorg. Chem.* **1993**, *32*, 4175.

(16) Bear, J. L.; Han, B.; Huang, S. *J. Am. Chem. Soc.* **1993**, *115*, 1175.

(17) Sun, Y.; Taylor, N. J.; Carty, A. J. *J. Organomet. Chem.* **1992**, *423*, C43.

(18) Albertin, G.; Antoniutti, S.; Bordignon, E.; Cazzaro, F.; Ianelli, S.; Pelizzi, G. *Organometallics* **1995**, *14*, 4114.

(19) Janssen, M. D.; Herres, M.; Zsolnai, L.; Grove, D. M.; Spek, A. L.; Lang, H.; van Koten, G. *Organometallics* **1995**, *14*, 1098.

(20) Yao, C.; Park, K. H.; Khokar, A. R.; Jun, M.; Bear, J. L. *Inorg. Chem.* **1990**, *29*, 4033.

(21) Calvin, G.; Coates, G. E.; Dixson, P. S. *Chem. Ind. (London)* **1959**, 1628.

(22) Akita, M.; Terada, M.; Oyama, S.; Moro-oka, Y. *Organometallics* **1990**, *9*, 816.

(23) Gamasa, M. P.; Gimeno, J.; Lastra, E.; Lanfranchi, M.; Tiripicchio, A. *J. Organomet. Chem.* **1991**, *405*, 333.

(24) Manna, J.; Geib, S. J.; Hopkins, M. D. *J. Am. Chem. Soc.* **1992**, *114*, 9199.

(25) Wing-Wah Yam, V.; Chor-Yue Lau, V.; Cheung, K. *Organometallics* **1995**, *14*, 2749.

(26) Evans, W. J.; Bloom, I.; Doedens, R. J. *J. Organomet. Chem* **1984**, *265*, 249.

(27) Schubert, U.; Köhler, F. H.; Prößdorf, W. *Cryst. Struct. Comm.* **1981**, *10*, 245.

(28) Köhler, F. H.; Prössdorf, W.; Schubert, U.; Neugebauer, D. *Angew. Chem. Int. Ed. Engl.* **1978**, *17*, 850.

(29) Erker, G.; Frömberg, W.; Benn, R.; Mynott, R.; Angermund, K.; Krüger, C. *Organometallics* **1989**, *8*, 911.

(30) Ramsden, J. A.; Weng, W.; Arif, A. M.; Gladysz, J. A. *J. Am. Chem. Soc.* **1992**, *114*, 5890.

(31) Weigand, W.; Robl, C. *Chem. Ber.* **1993**, *126*, 1807.

(32) Stoner, T. C.; Gieb, S. J.; Hopkins, M. D. *J. Am. Chem. Soc.* **1992**, *114*, 4201.

(33) Stoner, T. C.; Dallinger, R. F.; Hopkins, M. D. *J. Am. Chem. Soc.* **1990**, *112*, 5651.

(34) Giese, B.; Zehnder, M.; Neuburger, M.; Trach, F. *J. Organomet. Chem.* **1991**, *412*, 415.

(35) Goddard, R.; Howard, J.; Woodward, P. *J. Chem. Soc. Dalton Trans.* **1974**, 2025.

(36) Atherton, Z.; Faulkner, C. W.; Ingham, S. L.; Kakkar, A. K.; Khan, M. S.; Lewis, J.; Long, N. J.; Raithby, P. R. *J. Organomet. Chem.* **1993**, *462*, 265.

(37) Faulkner, C. W.; Ingham, S. L.; Khan, M. S.; Lewis, J.; Long, N. J.; Raithby, P. R. *Organometallics* **1994**, *482*, 139.

(38) Faust, R.; Diederich, F.; Gramlich, V.; Seiler, P. *Chem. Eur. J.* **1995**, *1*, 111.

(39) Sonogashira, K.; Yatake, T.; Tohda, Y.; Takahashi, S.; Hagihara, N. *J. Chem. Soc., Chem. Commun.* **1977**, 291.

(40) Russo, M. V.; Furlani, A.; Licoccia, S.; Paolesse, R.; Villa, A. C.; Guastini, C. *J. Organomet. Chem.* **1994**, *469*, 245.

(41) Ogawa, H.; Onitsuka, K.; Joh, T.; Takahashi, S. *Organometallics* **1988**, *7*, 2257.

(42) Bruce, M. I.; Hinterding, P.; Tiekink, E. R. T.; Skelton, B. W.; White, A. H. *J. Organomet. Chem.* **1993**, *450*, 209.

(43) Bruce, M. I.; Humphrey, M. G.; Matisons, J. G.; Roy, S. K.; Swincer, A. G. *Aust. J. Chem.* **1984**, *37*, 1955.

(44) Jia, G.; Rhiengold, A. L.; Meek, D. W. *Organometallics* **1989**, *8*, 1378.

(45) Jia, G.; Gallucci, J. C.; Rheingold, A. L.; Haggerty, B. S.; Meek, D. W. *Organometallics* **1991**, *10*, 3459.

(46) Echavarren, A. M.; López, J.; Santos, A.; Romero, A.; Hermoso, J. A.; Vegas, A. *Organometallics* **1991**, *10*, 2371.

(47) Torres, M. R.; Santos, A.; Ros, J.; Solans, X. *Organometallics* **1987**, *6*, 1091.

(48) Werner, H.; Höhn, A.; Shultz, M. *J. Chem. Soc. Dalton Trans.* **1991**, 777.

(49) Werner, H.; Baum, M.; Schneider, D.; Windmüller, B. *Organometallics* **1994**, *13*, 1089.

(50) Field, L. D.; George, A. V.; Malouf, E. Y.; Slip, I. H. M.; Hambley, T. W. *Organometallics* **1991**, *10*, 3842.

(51) Hills, A.; Hughes, D. L.; Jiminez-Tenorio, M.; Leigh, G. J. *J. Organomet. Chem.* **1990**, *391*, C41.

(52) Espuelas, J.; Esteruelas, M. A.; Lahoz, F. J.; Oro, L. A.; Valero, C. *Organometallics* **1993**, *12*, 663.

(53) Fernández, M. J.; Esteruelas, M. A.; Covarrubias, M.; Oro, L. A.; Apreda, M.; Foces-Foces, C.; Cano, F. H. *Organometallics* **1989**, *8*, 1158.

(54) Kaharu, T.; Ishii, R.; Adachi, T.; Yoshida, T.; Takahashi, S. *J. Mater. Chem.* **1995**, *5*, 687.

(55) Ashby, G. S.; Bruce, M. I.; Tomkins, I. B.; Wallis, R. C. *Aust. J. Chem.* **1979**, *32*, 1003.

(56) Bianchini, C.; Laschi, F.; Masi, D.; Ottaviani, F. M.; Pastor, A.; Peruzzini, M.; Zanello, P.; Zanobini, F. *J. Am. Chem. Soc.* **1993**, *115*, 2723.

(57) Hughes, D. L.; Leigh, G. J.; Jimenez-Tenorio, M.; Rowley, A. T. *J. Chem. Soc. Dalton Trans.* **1993**, 75.

(58) Klien, H.; Beck, H.; Hammerschmitt, B.; Koch, U.; Koppert, S.; Cordier, G.; Paulus, H. *Z. Naturforsch.* **1991**, *46 b*, 147.

(59) Buang, N. A.; Hughes, D. L.; Kashef, N.; Richards, R. L.; Pombeiro, A. J. L. *J. Organomet. Chem.* **1987**, *323*, C47.

(60) Pombeiro, A. J. L.; Hills, A.; Hughes, D. L.; Richards, R. L. *J. Organomet. Chem.* **1990**, *398*, C15.

(61) Touchard, D.; Guesmi, S.; Le Pichon, L.; Daridor, A.; Dixneuf, P. H. *Inorg. Chim. Acta* **1998**, *280*, 118.

(62) Bitcon, C.; Whiteley, M. W. *J. Organomet. Chem.* **1987**, *336*, 385.

(63) Garcia Basallote, M.; Hughes, D. L.; Jiménez-Tenorio, M.; Leigh, G. J.; Puerta Vizcaíno, M. C.; Valerga Jiménez, P. *J. Chem. Soc., Dalton Trans.* **1993**, 1841.

(64) Rappert, T.; Nürnberg, O.; Mahr, N.; Wolf, J.; Werner, H. *Organometallics* **1992**, *11*, 4156.

(65) Bianchini, C.; Masi, D.; Meli, A.; Peruzzini, M.; Ramirez, J. A.; Vacca, A.; Zanobini, F. *Organometallics* **1989**, *8*, 2179.

(66) Bianchini, C.; Peruzzini, M.; Vacca, A.; Zanobini, F. *Organometallics* **1991**, *10*, 3697.

(67) Fyfe, H. B.; Mlekuz, M.; Zargarian, D.; Taylor, N. J.; Marder, T. B. *J. Chem. Soc., Chem. Commun.* **1991**, 188.

(68) Chow, P.; Zargarian, D.; Taylor, N. J.; Marder, T. B. *J. Chem. Soc., Chem. Commun.* **1989**, 1545.

(69) Marder, T. B.; Zargarian, D.; Calabrese, J. C.; Herskovitz, T. H.; Milstein, D. *J. Chem. Soc., Chem. Commun.* **1987**, 1484.

(70) Bianchini, C.; Mealli, C.; Peruzzini, M.; Vizza, F.; Zanobini, F. *J. Organomet. Chem.* **1988**, *346*, C53.

(71) Wisner, J. M.; Bartczak, T. J.; Ibers, J. A. *Inorg. Chim. Acta* **1985**, *100*, 115.

(72) Lemke, F. R.; Szalda, D. J.; Bullock, R. M. *J. Am. Chem. Soc.* **1991**, *113*, 8466.

(73) Sato, M.; Shintate, H.; Kawata, Y.; Sekino, M. *Organometallics* **1994**, *13*, 1956.

(74) Touchard, D.; Morice, C.; Cadierno, V.; Haquette, P.; Toupet, L.; Dixneuf, P. H. *J. Chem. Soc., Chem. Commun.* **1994**, 859.

(75) Touchard, D.; Haquette, P.; Pirio, N.; Toupet, L.; Dixneuf, P. H. *Organometallics* **1993**, *12*, 3132.

(76) Hodge, A. J.; Ingham, S. L.; Kakkar, A. K.; Khan, M. S.; Lewis, J.; Long, N. J.; Parker, D. G.; Raithby, P. R. *J. Organomet. Chem.* **1995**, *488*, 205.

(77) Haquette, P.; Pirio, N.; Touchard, D.; Toupet, L.; Dixneuf, P. H. *J. Chem. Soc., Chem. Commun.* **1993**, 163.

(78) Field, L. D.; George, A. V.; Hambley, T. W. *Inorg. Chem.* **1990**, *29*, 4565.

(79) Bruce, M. I.; Wallis, R. C. *Aust. J. Chem.* **1979**, *32*, 1471.

(80) Touchard, D.; Haquette, P.; Guesmi, S.; LePichon, L.; Daridor, A.; Toupet, L.; Dixneuf, P. H. *Organometallics* **1997**, *16*, 3640.

(81) McDonagh, A. M.; Whittall, I. R.; Humphrey, M. G.; Skelton, B. W.; White, A. H. *J. Organomet. Chem.* **1996**, *519*, 229.

(82) Jia, G.; Puddephatt, R. J.; Scott, J. D.; Vittal, J. J. *Organometallics* **1993**, *12*, 3565.

(83) Jia, G.; Puddephatt, R. J.; Vittal, J. J.; Payne, N. C. *Organometallics* **1993**, *12*, 263.

(84) Cross, R.; Davidson, M. F.; McLennan, A. J. *J. Organomet. Chem.* **1984**, *265*, C37.

(85) Bruce, M. I.; Horn, E.; Matisons, J. G.; Snow, M. R. *Aust. J. Chem.* **1984**, *37*, 1163.

(86) Lavastre, O.; Even, M.; Dixneuf, P. H.; Pacreau, A.; Vairon, J. P. *Organometallics* **1996**, *15*, 1530.

(87) Warren, L. F.; Bennett, M. A. *Inorg. Chem.* **1976**, *15*, 3126.

(88) Aresta, M.; Nobile, C. F.; Petruzzelli, D. *Inorg. Chem.* **1977**, *16*, 1817.

(89) King, R. B.; Houk, L. W.; Pannell, K. H. *Inorg. Chem.* **1969**, *8*, 1042.

(90) Chaudret, B.; Commenges, G.; Poilblanc, R. *J. Chem. Soc., Dalton Trans.* **1984**, 1635.

(91) Grocott, S. C.; Wild, S. B. *Inorg. Chem.* **1982**, *21*, 3526.

(92) McDonagh, A. M., *Honours thesis*, Australian National University, **1995**.

(93) Evans, I. P.; Spencer, A.; Wilkinson, G. *J. Chem. Soc., Dalton Trans.* **1973**, 204.

(94) Chatt, J.; Hayter, R. G. *J. Chem. Soc.* **1961**, 896.

(95) Sullivan, B. P.; Meyer, T. J. *Inorg. Chem.* **1982**, *21*, 1037.

(96) Bressan, M.; Ettorre, R.; Rigo, P. *Inorg. Chim. Acta* **1977**, *24*, L57.

(97) Chakravarty, A. R.; Cotton, F. A.; Schwotzer, W. *Inorg. Chim. Acta* **1984**, *84*, 179.

(98) Dwyer, F. P.; Hogarth, J. W. *Inorg. Synth.* **1957**, *5*, 206.

(99) Antonov, P. G.; Kukushkin, Y. N.; Konnov, V. I.; Kostikov, Y. P. *Koord. Khim.* **1980**, *6*, 1585.

(100) Jaswal, J. S.; Rettig, S. J.; James, B. R. *Can. J. Chem.* **1990**, *68*, 1808.

(101) James, B. R.; Ochiai, E.; Rempel, G. L. *Inorg. Nucl. Chem. Lett.* **1971**, *7*, 781.

(102) Tokunoh, R.; Sodeoka, M.; Aoe, K.; Shibasaki, M. *Tetrahedron Lett.* **1995**, *36*, 8035.

(103) Attia, W. M.; Calligaris, M. *Acta Cryst.* **1987**, *C43*, 1426.

(104) Mercer, A.; Trotter, J. *J. Chem. Soc., Dalton Trans.* **1975**, 2480.

(105) Antonov, P. G.; Amantova, I. A. *J. Gen. Chem.* **1988**, *58*, 2245.

(106) Robinson, P. D.; Hinckley, C. C.; Ikuo, A. *Acta Cryst.* **1989**, *C45*, 1079.

(107) Hockless, D. C. R.; Wild, S. B.; McDonagh, A. M.; Whittall, I. R.; Humphrey, M. G. *Acta Cryst.* **1996**, *C52*, 1639.

(108) Grocott, S. C.; Skelton, B. W.; White, A. H. *Aust. J. Chem.* **1983**, *36*, 259.

(109) Grocott, S. C.; Skelton, B. W.; White, A. H. *Aust. J. Chem.* **1983**, *36*, 267.

(110) Grocott, S. C.; Skelton, B. W.; White, A. H. *Aust. J. Chem.* **1983**, *36*, 271.

(111) Mislow, K. *Trans. N.Y. Acad. Sci.* **1973**, *35*, 227.

(112) Jia, G.; Ng, W. S.; Yao, J.; Lau, C. P.; Chen, Y. *Organometallics* **1996**, *15*, 5039.

(113) Cotton, F. A.; Diebold, M. P.; Matusz, M. *Polyhedron* **1987**, *6*, 1131.

(114) Levason, W.; Champness, N. R.; Webster, M. *Acta Cryst.* **1993**, *C49*, 1884.

(115) Blake, A. J.; Champness, N. R.; Forder, R. J.; Frampton, C. S.; Frost, C. A.; Reid, G.; Simpson, R. H. *J. Chem. Soc., Dalton. Trans.* **1994**, 3377.

(116) Alessio, E.; Mestroni, G.; Nardin, G.; Attia, W. M.; Calligaris, M.; Sava, G.; Zorzet, S. *Inorg. Chem.* **1988**, *27*, 4099.

(117) Oliver, J. D.; Riley, D. P. *Inorg. Chem.* **1984**, *23*, 156.

(118) Gubin, S. P.; Smirnova, S. A.; Denisovich, L. I.; Lubovich, A. A. *J. Organomet. Chem.* **1971**, *30*, 243.

(119) Pregosin, P. S.; Kunz, R. W. *^{31}P and ^{13}C NMR of Transition Metal Phosphine Complexes*; Diehl, P., Fluck, E. and Kosfeld, R., Eds.; Springer: Berlin, 1979.

(120) Crumbliss, A. L.; Topping, R. J. In *Phosphorus-31 NMR Spectroscopy in Stereochemical Analysis*; Verkade, J. G. and Quin, L. D., Eds.; VCH: Deerfield Beach, FL, 1987; Vol. 8, p 531.

(121) Whittall, I. R.; Cifuentes, M. P.; Humphrey, M. G.; Luther-Davies, B.; Samoc, M.; Houbrechts, S.; Persoons, A.; Heath, G. A.; Hockless, D. C. R. *J. Organomet. Chem.* **1997**, *549*, 127.

(122) Cifuentes, M. P. *Personal communication*.

(123) Boyd, R. W. *Nonlinear Optics*; Academic Press: New York, 1992.

(124) Oudar, J. L.; Chemla, D. S. *J. Chem. Phys.* **1977**, *66*, 2664.

(125) Kanis, D. R.; Ratner, M. A.; Marks, T. J. *Chem. Rev.* **1994**, *94*, 195.

(126) van Walree, C. A.; Franssen, O.; Marsman, A. W.; Flipse, M. C.; Jennekens, L. W. *J. Chem. Soc., Perkin Trans. 2* **1997**, 799.

(127) Kurtz, S. K.; Perry, T. T. *J. Appl. Phys.* **1968**, *39*, 3798.

(128) Roberts, N. K.; Wild, S. B. *J. Am. Chem. Soc.* **1979**, *101*, 6254.

(129) Takahashi, S.; Kuroyama, Y.; Sonogashira, K.; Hagihara, N. *Synthesis* **1980**, 627.

(130) Whittall, I. R.; Humphrey, M. G.; Hockless, D. C. R.; Skelton, B. W.; White, A. H. *Organometallics* **1995**, *14*, 3970.

(131) teXsan: *Single Crystal Structure Analysis Software, Version 1.7-3*, Molecular Structure Corporation, The Woodlands, TX (1995).

(132) Stähelin, M.; Burland, D. M.; Rice, J. E. *Chem. Phys. Lett.* **1992**, *191*, 245.

(133) Clays, K.; Persoons, A. *Rev. Sci. Instrum.* **1992**, *63*, 3285.

(134) Houbrechts, S.; Clays, K.; Persoons, A.; Pikramenou, Z.; Lehn, J.-M. *Chem. Phys. Lett.* **1996**, *258*, 485.

Chapter 3

Transition Metal Complexes with Acetylide Ligands Containing Nitrogen Linkages and Some of Their Nonlinear Optical Properties

Contents

Chapter 3

Transition Metal Complexes with Acetylide Ligands Containing Nitrogen Linkages and Some of Their Nonlinear Optical Properties

3.1. Introduction

In this chapter, the preparation and characterization of transition metal complexes with acetylide ligands that contain nitrogen linkages, and an examination of their molecular second-order optical nonlinearities, is presented.

Studies of organic compounds with donor and acceptor substituents linked by a system of π-conjugation have shown that variation of the length and composition of the π-system leads to marked variations of their molecular NLO properties.[1-6] One area of interest is the effect of incorporating nitrogen into the π-conjugated system and, in particular, incorporating nitrogen into the linkages between arylene units. The results from several computational investigations have been reported,[7-13] data from which are collected in Table 3.1. The results of these studies are varied, with contradictory trends being seen. It is difficult to draw any solid conclusions about the effect of this bridging group variation on the optical nonlinearity.

Few experimental investigations have been undertaken in this area. Two reports[14,15] (see Table 3.2.) only provide a comparison of the *trans*-CH=CH with the N=CH linkages, with the former having larger β values in both cases. While the current work was in progress, a report[16] on the nonlinearities of organic stilbene, benzylideaniline and azobenzene derivatives measured by EFISH (Table 3.2.) stated that the first hyperpolarizabilities of

Table 3.1. Computational first hyperpolarizabilities for donor-acceptor compounds with an unsaturated X = Y linkage (X, Y = CH or N).

Compound	R					
	NH_2			NMe_2		Ph_3P Ru C≡C PPh_3
	$\beta_{CNDO/S}$[a] (10^{-30} esu)	$\beta_{6\text{-}31G}$[b] (10^{-30} esu)	β_{PPP}[c] (10^{-30} esu)	$\beta_{0\ CNDO/VSB}$[d] (10^{-30} esu)	β (β_0) $_{CNDO/VSB}$[e] (10^{-30} esu)	β_{ZINDO}[f] (10^{-30} esu)
R–⟨⟩–CH=CH–⟨⟩–NO_2	202.8		248.0	42.7	109.6 (50.3)	45
R–⟨⟩–CH=N–⟨⟩–NO_2	135.3		371.0	28.1	57.4 (31.1)	52
R–⟨⟩–N=CH–⟨⟩–NO_2	31.8		77.0	38.9	113.6 (50.6)	55
R–⟨⟩–N=N–⟨⟩–NO_2	132.0			59.6	128.2 (55.5)	89
R–CH=CH–CH=CH–CH=CH–NO_2		17.78				
R–CH=CH–CH=N–CH=CH–NO_2		16.91				
R–CH=CH–N=CH–CH=CH–NO_2		12.40				
R–CH=CH–N=N–CH=CH–NO_2		12.90				

[a] Zero-field first hyperpolarizabilities calculated using the CNDO/S method.[7,8] [b] Zero-field first hyperpolarizabilities calculated using the *ab initio* CPHF method.[9] [c] Zero-field first hyperpolarizabilities calculated using the PPP method.[10] [d] Zero-field first hyperpolarizabilities calculated using the CNDO/VSB method.[11] [e] First hyperpolarizabilities calculated at 1.36 μm and at zero-field using the CNDO/VSB method.[12] [f] First hyperpolarizabilities calculated at 1.91 μm using the ZINDO method.[15]

Table 3.2. Experimental first hyperpolarizabilities for donor-acceptor compounds with an unsaturated X=Y linkage (X,Y = CH or N).

Compound	R		
	NMe_2	$Ph_3P(Ru)(C\equiv C-)PPh_3$	NMe_2
	β_{EFISH} (β_0) [a] (10^{-30} esu)	β_{HRS} (β_0) [b] (10^{-30} esu)	$\beta_{0\ EFISH}$ [c] (10^{-30} esu)
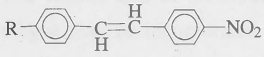	105 (52)	1455 (232)	56
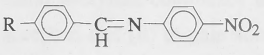			35
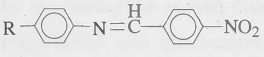	77 (37)	840 (86)	44
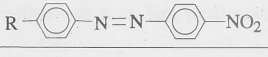			58

[a] First hyperpolarizabilities measured at 1.36 μm using the EFISH technique (β_{EFISH}) and static first hyperpolarizabilities calculated using the two-level approximation (β_0).[14] [b] First hyperpolarizabilities measured at 1.06 μm using the HRS technique (β_{HRS})and static first hyperpolarizabilities calculated using the two-level approximation (β_0).[15] [c] Static first hyperpolarizabilities calculated using the two-level approximation from experimental values measured at 1.91 μm using the EFISH technique.[16]

trans-CH=CH and N=N bridged donor-acceptor compounds are of comparable magnitude and that the substitution of one carbon by a nitrogen atom reduces the second-order NLO activity. This report finds the same trend between the *trans*-CH=CH and N=CH linkages as do the previous two reports but in addition suggests that N=N linked compounds are worthy of further investigation. No reports of NLO studies on transition metal azo-linked acetylide complexes are extant. Whittall *et al*[17] reported that attempts to prepare the terminal alkyne (*E*)-4,4´-$HC\equiv CC_6H_4N=NC_6H_4$-$NO_2$ had failed, but attempts were not exhaustive.

The first aim of the studies described in this Chapter is to fill this gap in the current knowledge about the preparation and NLO properties of donor-acceptor substituted azo-bridged complexes. The preparation and characterization of (*E*)-4,4´-$HC\equiv CC_6H_4N=NC_6H_4NO_2$ and derivative ruthenium and gold acetylide complexes are presented in this Chapter, together with second-order NLO data.

NLO studies on donor-acceptor substituted indoanilines have been reported.[18,19] These compounds have an arylene group connected to a quinonal group *via* a nitrogen atom. Experimentally determined values of β for some of these indoaniline derivatives are significant: see Table 3.3. In the ground state, there is one aromatic ring and one quinonal ring. Upon excitation, this system compensates for the loss of aromaticity with the aromatic ring by the gain of aromaticity with the quinonal ring (see Figure 3.1.). Marder *et al*[18] have suggested that this tends to assist in charge polarization and favourably influences the second-order NLO activity. To date, no synthetic or NLO investigations of transition metal complexes bearing this type of substituent have been reported.

The second aim of the studies described in this Chapter is (i) to determine if a terminal alkyne may be incorporated into this type of compound and hence to prepare some novel metal acetylide complexes that contain an imino bridging group with a quinonal oxygen acceptor, and (ii) to gain some insight into the effect of this substituent on NLO properties by measuring the second-order NLO responses of these complexes. This Chapter details the preparation and characterization of 4-HC≡CC$_6$H$_4$N=CCH=CBu^{t}C(O)CBu^t=CH and ruthenium acetylide derivatives, together with their second-order NLO data.

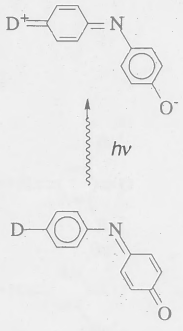

Figure 3.1. Ground and CT excited states of donor(D)-acceptor substituted indoaniline compounds.

Table 3.3. First hyperpolarizabilities of some indoaniline derivatives.[a]

Compound	β_{EFISH} [b]	β_0 [c]
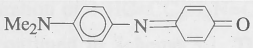	190	106
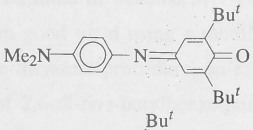	78	47
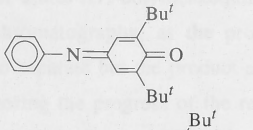	5.9	4.5
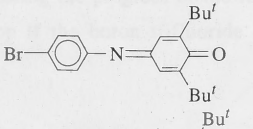	13	9.9
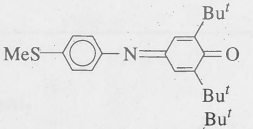	16	11
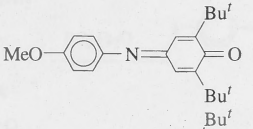	17	12
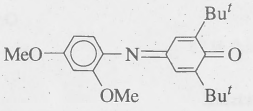	19	13
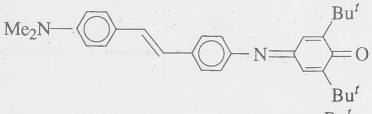	116	77
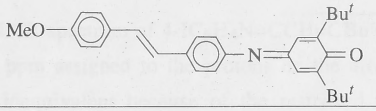	48	33

[a] References 18,19. [b] First hyperpolarizability measured by EFISH at 1.91 μm.

[c] Static first hyperpolarizability calculated using the two-level approximation.

3.2. Syntheses of terminal alkynes

3.2.1. 4-HC≡CC$_6$H$_4$N=CCH=CBu^{t}C(O)CBu^t=CH (1)

The preparation of 4-HC≡CC$_6$H$_4$N=CCH=CBu^{t}C(O)CBu^t=CH (**1**) was achieved using the synthesis outlined in Scheme 3.1. The iodide 4-IC$_6$H$_4$N=CCH=CBu^{t}C(O)CBu^t=CH was obtained in good yield using a modification to the literature procedure of Figueras *et al.*[20] Unlike the literature procedure, an excess of 4-iodoaniline was used to ensure the complete reaction of 2,6-di-*tert*-butylbenzoquinone. This aided in the purification of the product by column chromatography, as the product and 2,6-di-*tert*-butylbenzoquinone were quite difficult to separate but the product and 4-iodoaniline were readily separated. It was found (by monitoring the progress of the reaction with ^{1}H NMR spectroscopy) that the reaction would stop if the boron trifluoride catalyst was not replenished over the course of the reaction.

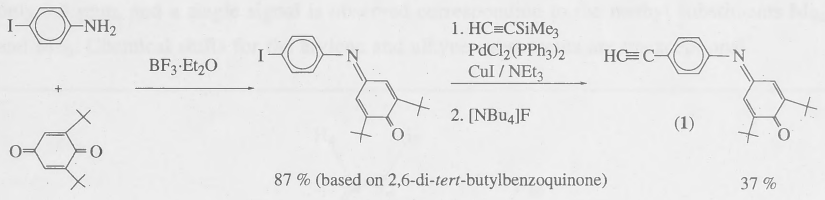

Scheme 3.1. Synthesis of **1**.

The ^{1}H NMR spectrum of 4-IC$_6$H$_4$N=CCH=CBu^{t}C(O)CBu^t=CH contains signals at 7.69 and 6.63 ppm assigned to the protons on the aromatic ring. The protons of the quinone ring are inequivalent because of the restricted rotation about the double bond to the nitrogen atom. This inequivalence is reflected in the ^{1}H NMR spectrum, which contains two doublet signals at 7.01 and 6.74 ppm corresponding to the protons attached to the quinonal ring, and two singlet signals at 1.30 and 1.18 ppm assigned to the *tert*-butyl groups. No attempt was made to assign individual signals to the protons of the quinone ring. The identity of this compound was further confirmed by high-resolution mass spectrometry.

The coupling reaction of Sonogashira *et al*[21] was utilized to obtain the terminal alkyne **1** from the aryl iodide 4-$IC_6H_4N{=}\overline{CCH{=}CBu^tC(O)CBu^t{=}CH}$ in moderate yield (see Scheme 3.1). No advantage (in terms of purity or yield of the final product) was gained by isolating the intermediate trimethylsilyl-protected alkyne. Compound **1** was characterized by EI mass spectrometry, satisfactory microanalysis, UV-vis and IR spectroscopy, and ^1H and ^{13}C NMR spectroscopy. The UV-vis spectrum contains bands at 34 900 and 39 400 cm^{-1}, assigned to $\pi{\rightarrow}\pi^*$ transitions, and a much weaker band at 22 300 cm^{-1}, assigned to an $n{\rightarrow}\pi^*$ transition. The IR spectrum contains a strong band at 1633 cm^{-1} which may be assigned to the C=O stretching mode. The ^1H NMR spectrum is similar to that of the starting material, with no change in the chemical shifts of the signals assigned to the substituents on the quinone ring; in contrast, the signals assigned to the protons of the arylene ring are 0.4 ppm closer together. A signal assigned to the proton of the terminal alkyne is observed at 3.10 ppm. The inequivalence of each of the carbon atoms associated with the quinone ring is reflected in the ^{13}C NMR spectrum (see Figure 3.2. for the NMR numbering scheme). The carbon atoms C_{10} and C_{14} have signals 13 ppm apart (at 134.3 and 121.3 ppm, respectively), atoms C_{11} and C_{13}, which are one bond further from the nitrogen centre are separated by ~ 5 ppm, while atoms C_{15} and C_{16}, which are another bond further removed, are separated by only 0.4 ppm, and a single signal is observed corresponding to the methyl substituents Me_a and Me_b. Chemical shifts for the arylene and alkyne substituents are unexceptional.

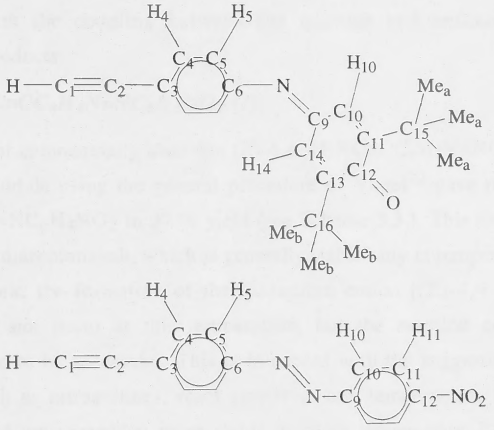

Figure 3.2. NMR numbering schemes.

An alternative synthetic route to **1** was trialed (see Scheme 3.2.) in which trimethylsilyl acetylene was coupled to 4-iodoaniline (using the method of Sonogashira *et al*[21]) and the product, 4-trimethylsilylethynylaniline, was then reacted with 2,6-di-*tert*-butylbenzoquinone under similar conditions to those described above, before deprotection of the alkyne with tetrabutylammonium fluoride.

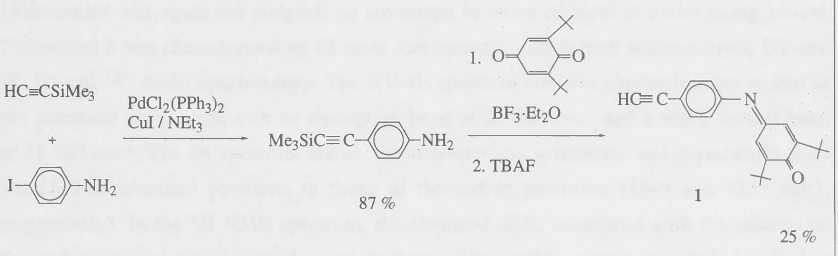

Scheme 3.2. Alternative synthesis of **1**.

The desired product was prepared, but the overall yield was inferior and the work-up less time-efficient, with the coupling between the quinone and aniline yielding several unidentified by-products.

3.2.2. (E)-4,4´-HC≡CC$_6$H$_4$N=NC$_6$H$_4$NO$_2$ (2)

The diazotization of commercially available (*E*)-4,4´-$H_2NC{\equiv}CC_6H_4N{=}NC_6H_4NO_2$ followed by reaction with iodide using the general procedure of Vogel[22] gave the aryl iodide (*E*)-4,4´-$IC{\equiv}CC_6H_4N{=}NC_6H_4NO_2$ in 37 % yield (see Scheme 3.3.). This method first requires the formation of a diazonium salt, which is generally stable only at temperatures below 5 °C. In the current work, the formation of the diazonium cation $[(E)$-4,4´-$N{\equiv}NC_6H_4N{=}NC_6H_4NO_2]^+$ did not occur at this temperature, but the reaction conducted at room temperature proved to be successful. This is in accord with the suggestion of Vogel[22] that some amines, such as nitroanilines, react slowly at low temperatures but the diazonium compounds formed are somewhat more stable at room temperature. The reaction of the diazonium salt with potassium iodide proceeded rapidly to yield the desired aryl iodide. This compound was characterized by high resolution mass spectrometry, UV-vis, IR spectroscopy and ^{1}H NMR spectroscopy. The UV-vis spectrum shows an absorption band at

28 300 cm^{-1}, assigned to a $\pi \rightarrow \pi^*$ transition, with a much weaker band at 21 400 cm^{-1}, assigned to a $n \rightarrow \pi^*$ transition. Characteristic symmetric and asymmetric N=O stretches are observed in the IR spectrum at 1347 and 1527 cm^{-1}, respectively. The ^1H NMR spectrum contains four sets of doublets with assignments as follows (see Figure 3.2. for numbering scheme); 7.68 (H_4), 7.90 (H_5), 8.02 (H_{10}), 8.37 (H_{11}).

The coupling reaction of Sonogashira *et al*[21] was again utilized to prepare the terminal alkyne **2** from the aryl iodide (see Scheme 3.3.). The trimethylsilyl-protected alkyne intermediate was again not isolated, no advantage in terms of yield or purity being gained. Compound **2** was characterized by EI mass spectrometry, satisfactory microanalysis, UV-vis, IR, ^1H and ^{13}C NMR spectroscopy. The UV-vis spectrum contains similar features to that of the precursor aryl iodide with an absorption band at 28 400 cm^{-1} and a much weaker band at 21 700 cm^{-1}. The IR spectrum shows the characteristic symmetric and asymmetric N=O stretches in identical positions to those of the iodide precursor (1346 and 1527 cm^{-1}, respectively). In the ^1H NMR spectrum, the chemical shifts associated with the protons on the arylene groups are almost identical to those of the iodide starting material. A signal at 3.27 ppm is assigned to the proton of the terminal alkyne.

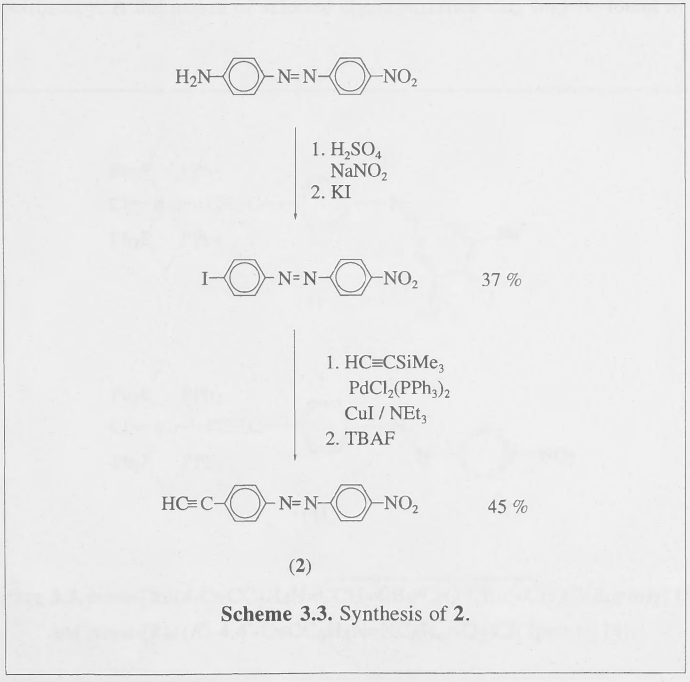

Scheme 3.3. Synthesis of **2**.

3.3. Syntheses of metal acetylide complexes

3.3.1. *trans*-[Ru(4-C≡CC_6H_4NR)Cl(dppm)$_2$] (R = $\overline{CCH=CBu^tC(O)CBu^t=CH}$ (3), $NC_6H_4NO_2$ (4))

The preparation of the new acetylide complexes **3** and **4**, incorporating the *trans*-bis(dppm)chlororuthenium unit, follows the literature procedure of Touchard *et al*[23] for the preparation of the phenylacetylide analogue. This reaction is described in more detail in Chapter 2. Reaction of *cis*-[$RuCl_2(dppm)_2$], sodium hexafluorophosphate and a terminal alkyne (the syntheses of which are described in 3.2.) in dichloromethane at room temperature afforded vinylidene complexes of the type *trans*-[Ru(C=CH-4-C_6H_4NR)Cl(dppm)$_2$]PF_6 (where R = $\overline{CCH=CBu^tC(O)CBu^t=CH}$ and $NC_6H_4NO_2$). These were deprotonated with base *in situ* before work-up, to afford the desired acetylide complex (see Figure 3.3.) in good yields (65 and 62 %, respectively). Both triethylamine and a methanolic solution of sodium methoxide were found to be satisfactory for the deprotonation step. The new acetylide complexes were characterized by FAB mass spectrometry, satisfactory microanalyses, UV-vis and IR spectroscopy, ^1H, ^{31}P and ^{13}C NMR spectroscopy. A discussion of selected characterization data may be found in Section 3.3.4.

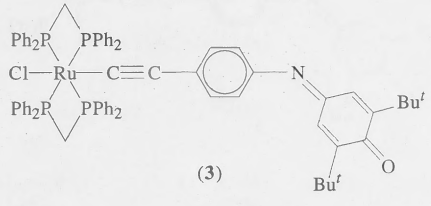

(**3**)

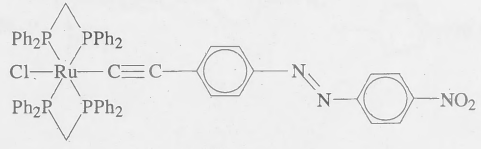

(**4**)

Figure 3.3. *trans*-[Ru(4-C≡CC_6H_4N=$\overline{CCH=CBu^tC(O)CBu^t=CH}$)Cl(dppm)$_2$] (**3**) and *trans*-[Ru((*E*)-4,4′-C≡CC_6H_4N=N$C_6H_4NO_2$)Cl(dppm)$_2$] (**4**).

3.3.2. *[Ru(C≡CC$_6$H$_4$NR)(PPh$_3$)$_2$(η^5-C$_5$H$_5$)] (R = CCH=CBu^{t}C(O)CBu^t=CH (5), NC$_6$H$_4$NO$_2$ (6))*

The preparation of the new (cyclopentadienyl)bis(triphenylphosphine)ruthenium acetylide complexes follows the literature procedure of Bruce *et al*[24] for the preparation of the phenylacetylide analogue. Reaction of [RuCl(PPh$_3$)$_2$(η^5-C$_5$H$_5$)] with terminal alkyne in refluxing methanol afforded vinylidene complexes of the type *trans*-[Ru(C=CHC$_6$H$_4$NR)(PPh$_3$)$_2$(η^5-C$_5$H$_5$)]$^+$ (where R = CCH=CBu^{t}C(O)CBu^t=CH and NC$_6$H$_4$NO$_2$). Unlike their bis(dppm)-containing analogues described in Section 3.2.1, no addition of counter-ions (such as hexafluorophosphate) was required to stabilize the vinylidene complexes, the displaced chloride presumably being sufficient. The vinylidene complexes were deprotonated with base *in situ* to afford the desired acetylide complexes (see Figure 3.4.) in 32 and 51 % yield, respectively. The new acetylide complexes were characterized by FAB mass spectrometry, satisfactory microanalyses, UV-vis and IR spectroscopy, ^{1}H, ^{31}P and ^{13}C NMR spectroscopy. A discussion of the characterization data may be found in Section 3.3.4.

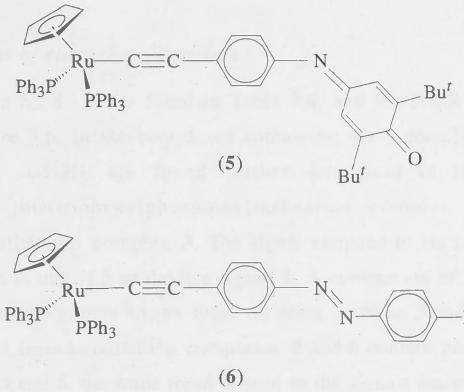

Figure 3.4. [Ru(4-C≡CC$_6$H$_4$N=CCH=CBu^{t}C(O)CBu^t=CH)(PPh$_3$)$_2$(η^5-C$_5$H$_5$)] (**5**) and [Ru((*E*)-4,4′-C≡CC$_6$H$_4$N=NC$_6$H$_4$NO$_2$)(PPh$_3$)$_2$(η^5-C$_5$H$_5$)] (**6**).

3.3.3. [Au((E)-4,4′-C≡CC$_6$H$_4$N=NC$_6$H$_4$NO$_2$)(PPh$_3$)] (7)

The preparation of this acetylide complex is based on the literature procedure of Whittall *et al.*[25] A mixture of (triphenylphosphine)gold chloride, (*E*)-4,4′-HC≡CC$_6$H$_4$N=NC$_6$H$_4$NO$_2$ and sodium methoxide solution was stirred in dichloromethane for 18 h to give [Au((*E*)-4,4′-C≡CC$_6$H$_4$N=NC$_6$H$_4$NO$_2$)(PPh$_3$)] (see Figure 3.5.) in 71 % yield. The complex was characterized by FAB mass spectrometry, satisfactory microanalysis, UV-vis and IR spectroscopy, ^{1}H, ^{31}P and ^{13}C NMR spectroscopy. A discussion of selected characterization data may be found in Section 3.3.4.

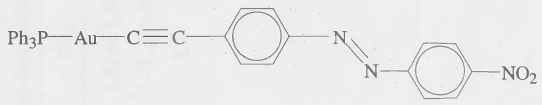

(**7**)

Figure 3.5. [Au((*E*)-4,4′-C≡CC$_6$H$_4$N=NC$_6$H$_4$NO$_2$)(PPh$_3$)]

3.3.4. Comparisons of characterization data

The ^{1}H NMR data for **1** - **7** are listed in Table 3.4. and the NMR numbering scheme is displayed in Figure 3.6. In the complexes containing the indoaniline ligand, the signals assigned to H_4 and H_5 are found further downfield in the spectrum of the (cyclopentadienyl)bis(triphenylphosphine)ruthenium complex **5** than in that of the chlorobis(dppm)ruthenium complex **3**. The signal assigned to H_4 is further upfield in the spectrum of **3** than in that of **5** or the free ligand **1**. A comparison of the signals assigned to the phenyl and methyl groups shows little variation between **3** and **5**. The spectra of the azo-linked alkynyl ligand-containing complexes **4** and **6** contain phenyl resonances in the same region. For **4** and **6**, the same trend is seen in the signals assigned to H_4 and H_5 as is observed with **3** and **5**, with those of **4** found upfield compared with those of **6** or the free ligand **2**. The H_{10} and H_{11} signals are relatively invariant for complexes **4** and **6** and the free ligand. Comparing spectra for the two sets of complexes bearing the same phosphine ligand but different acetylide ligands, H_4 is invariant for the complexes with the dppm ligands (**3** and **4**), but H_5 is significantly upfield for complexes with the indoaniline acetylide compared to those with the N=N linked acetylide. The methylene signals are

Table 3.4. ^{1}H NMR data for complexes **1**-**7**[a].

Compound	Chemical shift in ppm (J_{HH} in Hz (all doublets))										
	HC≡C	H_4	H_5	H_{10}	H_{11}	H_{14}	Me_a	Me_b	CH_2	Phenyl	C_5H_5
1	3.10	6.82 (8)	7.50 (8)	6.72 (3) or 7.00 (3)		6.72 (3) or 7.00 (3)	1.17 or 1.31	1.17 or 1.31			
3		6.04 (8)	6.53 (8)	6.94 (3) or under Ph		6.94 (3) or under Ph	1.27 or 1.31	1.27 or 1.31	4.91 (m)	7.02 - 7.43	
5		6.77 (8)	under Ph	under Ph		under Ph	1.24	1.32		7.01 - 7.48	4.32
2	3.27	7.65 (9)	7.92 (9)	8.02 (9)	8.38 (9)						
4		6.06 (9)	7.53 (9)	7.92 (9)	8.33 (9)				4.93 (m)	7.06 - 7.43	
6		under Ph	7.80 (8)	7.96 (9)	8.34 (9)					7.07 - 7.47	4.36
7		7.64 (8)	7.87 (8)	7.98 (9)	8.35 (9)					7.42 - 7.57	

[a] Referenced to residual $CHCl_3$ (7.24 ppm).

invariant. For the complexes bearing triphenylphosphine ligands (**5** and **6**), comparison is difficult because signals arising from the phenylene groups of the acetylide ligands are obscured by signals from the phenyl groups. The signals assigned to the cyclopentadienyl substituents have the same chemical shift in both complexes. The gold complex **7** has resonances assigned to the acetylide ligand at similar chemical shifts as those of the free ligand **2**.

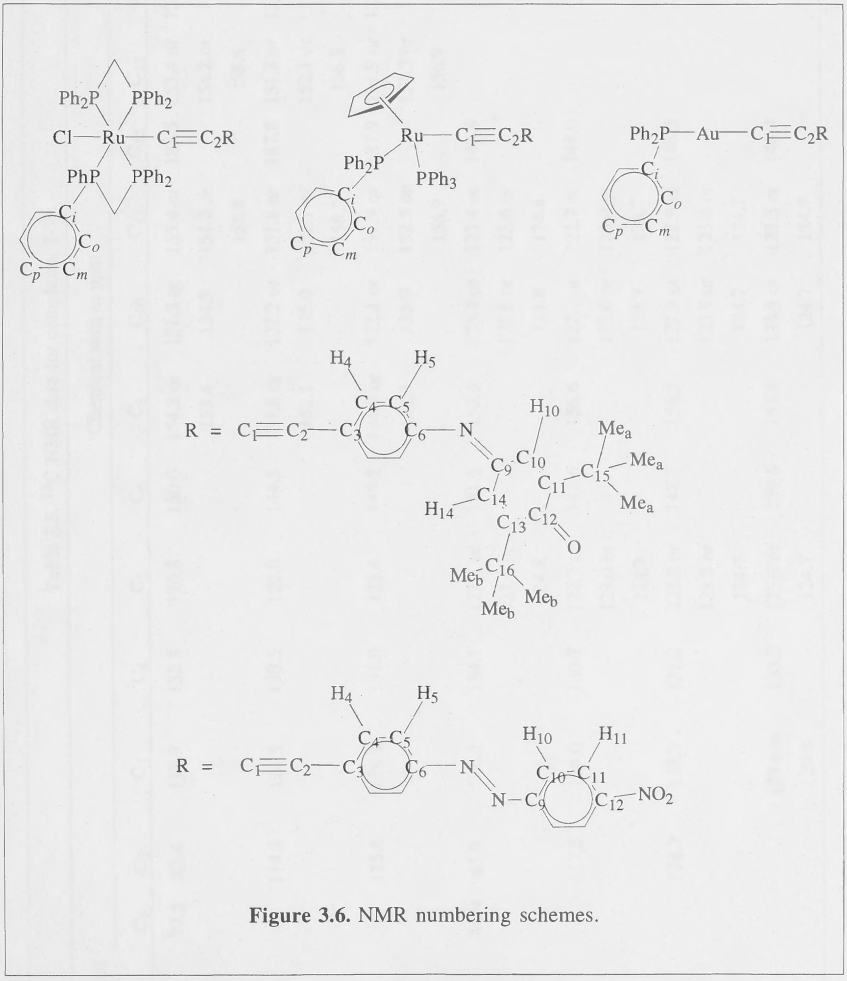

Figure 3.6. NMR numbering schemes.

Table 3.5. ^{13}C NMR data for complexes **1-7**[a].

Compound	Chemical shift in ppm														
	C_1	C_2	C_3	C_4	C_5	C_6	C_9	C_{10}	C_{11}	C_{12}	C_{13}	C_{14}	C_{15}	C_{16}	Me_a / Me_b
1	77.5	83.4	118.9	132.8	120.8	150.0	154.2 or 153.4	121.3 or 134.3	153.4 or 154.2 or 158.8	187.5	153.4 or 154.2 or 158.8	121.3 or 134.3	35.4 or 35.8	35.4 or 35.8	29.4
3		114.2	128.5	130.5	122.0	144.5	151.8 or 152.1	122.2 or 135.0	151.8 or 152.1 or 156.5	187.8	151.8 or 152.1 or 156.5	122.2 or 135.0	35.3 or 35.7	35.3 or 35.7	29.4
5		115.6	129.1	131.0	122.4	145.2	151.9 or 152.5	122.1 or 135.0	151.9 or 152.5 or 156.9	187.9	151.9 or 152.5 or 156.9	122.1 or 135.0	35.3 or 35.7	35.3 or 35.7	29.5
2	80.4	83.0	126.2	133.1	123.4 or 123.6 or 124.8	151.8	155.5	123.4 or 123.6 or 124.8	123.4 or 123.6 or 124.8	148.8					
4		117.5	136.0	130.7	122.7 or 123.0 or 124.7	147.6	156.6	122.7 or 123.0 or 124.7	122.7 or 123.0 or 124.7	148.0					
6		118.7	135.7	131.2	122.9 or 123.8 or 124.7	147.7	156.5	122.9 or 123.8 or 124.7	122.9 or 123.8 or 124.7	148.5					
7			129.6 or 129.8	133.2	123.3 or 124.7	150.6	155.8	123.3 or 124.7	123.3 or 124.7	148.4					

Table 3.5. (continued) ^{13}C NMR data for complexes **1-7**.[a]

Compound	Chemical shift in ppm					
	CH_2	C_i	C_o	C_m	C_p	C_5H_5
3	50.3 (m)	134.5 (m, partially obscured by C_o)	133.3, 133.6	129.0, 129.3	127.5	-
4	50.2 (m)	134.3 (m, partially obscured by C_o)	133.2, 133.6	129.2, 129.4	127.6	-
5		138.7 (m)	133.8 (t, 5 Hz)	127.2 (t, 5 Hz)	128.4	85.3
6		138.5 (m)	133.7 (t, 5 Hz)	127.3 (t, 5 Hz)	128.6	85.6
7			134.2 (d, 14 Hz)	129.2 (d, 6 Hz)	131.6	-

[a] Referenced to $CDCl_3$ (77.0 ppm).

The ^{13}C NMR spectra of complexes **3** and **5** (Table 3.5.) have signals assigned to the C_2 carbon of the acetylide ligand at similar chemical shifts, with the shifts of the atoms further from the metal (C_9 to C_{16}) similar to those of the free ligand. The effect of ligation is reflected most in the chemical shifts of atoms C_2 and C_3, all substantially downfield of the equivalent carbon of the free ligand. The ^{13}C NMR spectra of the ruthenium complexes **4** and **6** also contain a resonance for the C_2 carbon of the acetylide ligand at similar chemical shifts; resonances for atoms C_9 to C_{12} are found at very similar chemical shifts to those of the free ligand. The chemical shifts of atoms C_2 and C_3 in **4** and **6** are substantially downfield of the equivalent carbons in the free ligand. Signals corresponding to C_1 were not detected. The signals assigned to the phosphine ligand carbon atoms resonate with similar chemical shifts when comparing the pairs of complexes **3** and **5**, and **4** and **6**. There are two sets of C_i, C_o and C_m signals associated with the dppm ligand (complexes **3** and **4**) but one signal for each of these carbon atoms for the triphenylphosphine ligand (complexes **5** and **6**). This difference arises because there are two inequivalent sets of phenyl groups in the dppm-containing acetylide complexes. Figure 3.7. shows how four of the phenyl groups are in the vicinity of the chloro ligand while the other four are closer to the acetylide ligand. It has been shown previously[26] that, in symmetrical bis-acetylide complexes of the type *trans*-$[Ru(C{\equiv}CR)_2(dppm)_2]$, a single set of signals is observed for each of C_i, C_o and C_m.

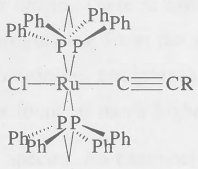

Figure 3.7. *trans*-$[Ru(C{\equiv}CR)Cl(dppm)_2]$ showing inequivalent phenyl groups.

The resonances corresponding to the acetylide ligand of the gold complex **7** occur at chemical shifts more similar to those of the free ligand than do those of the ruthenium analogues. The signals assigned to the carbon atoms associated with the phosphine ligand are unexceptional.

The ^{31}P NMR spectra of the ruthenium complexes were unremarkable, with similar shifts observed for complexes with a given phosphine ligand (–6.1, –6.3 for **3** and **4**, 50.7 for **5** and **6**, respectively).

Table 3.6. IR[a] and UV-vis[b] data for complexes **1-7**.

Compound	ν(C≡C) (cm^{-1})	$\bar{\nu}_{max}$. cm^{-1}(ε, M^{-1} cm^{-1})			
1		22 300 (4700)	34 900 (28 000)	39 400 (15 000)	
2		21 700 (860)	28 00 (27 200)		
3	2067	15 500 (8020)	31 300 (s, 18 100)	36 600 (29 600)	37 300 (29 400)
4	2061	17 100 (27 200)	27 300 (14 100)	37 400 (41 000)	
5	2061	16 000 (15 500)	31 500 (29 800)	41 800 (34 400)	
6	2054	17 700 (28 600)	28 800 (17 300)	34 400 (16 800)	39 900 (24 500)
7	2113	25 100 (32 800)	34 700, (14 600)	37 300 (17 400)	41 500 (32 000)

[a] In dichloromethane. [b] In tetrahydrofuran.

Table 3.6. contains selected IR and UV-vis data for **1-7**. The IR spectra of the ruthenium complexes shows some trends upon ligand variation. There is a decrease in the C≡C stretching frequency of about 6 cm^{-1} upon progressing from the indoaniline acetylide complexes (**3** and **5**) to the N=N linked acetylide complexes (**4** and **6**), suggesting that the nitro group of the azo-linked ligand may be a more effective electron withdrawing group than the oxygen of the indoaniline ligand. There is also a decrease in the C≡C stretching frequency of about 6 cm^{-1} upon progressing from the dppm-containing complexes (**3** and **4**) to the triphenylphosphine-containing complexes (**5** and **6**). The C≡C stretching frequency of the gold complex **7** is found at much higher energy.

Trends are also seen in the UV-vis spectra. An examination of the MLCT transition, seen at 15 500 to 17 700 cm^{-1} in the spectra of ruthenium complexes, reveals an increase of about 1600 cm^{-1} and a two to three-fold increase in the molar absorptivity upon proceeding from the indoaniline complexes to the azo-containing complexes. Spectra for the dppm-containing complexes have the MLCT band at energies ~ 500 cm^{-1} lower than those of their triphenylphosphine-containing analogues. The spectrum of the gold complex has the MLCT band at much higher energy (25 500 cm^{-1})

3.4. X-ray structural study of trans-[Ru((E)-4,4′-C≡CC$_6$H$_4$N=NC$_6$H$_4$NO$_2$)Cl(dppm)$_2$]

A single crystal X-ray diffraction study of *trans*-[Ru((*E*)-4,4′-C≡CC$_6$H$_4$N=NC$_6$H$_4$NO$_2$)Cl-(dppm)$_2$] has been performed by collaborators at the Australian National University. ORTEP plots are displayed in Figures 3.8. and 3.9., and selected bond lengths and angles are gathered in Table 3.7. A comparison of selected bond lengths and angles with those of related complexes appears in Table 3.8. and crystal data are collected in Table 3.9.

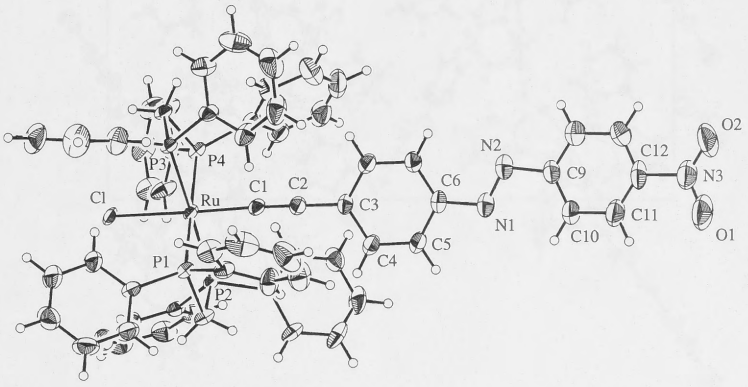

Figure 3.8. Molecular geometry and atomic labelling scheme for *trans*-[Ru((*E*)-4,4′-C≡CC$_6$H$_4$N=NC$_6$H$_4$NO$_2$)Cl(dppm)$_2$]. 30 % thermal ellipsoids are shown for the non-hydrogen atoms; hydrogen atoms are placed in calculated positions with arbitrary bond lengths of 0.95 Å.

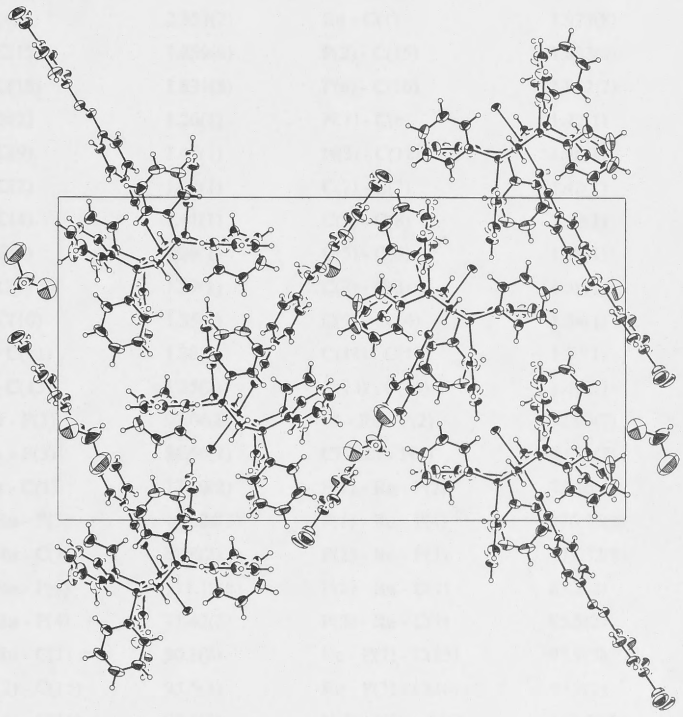

Figure 3.9. Cell packing diagram for

trans-[Ru((*E*)-4,4′-C≡CC_6H_4N=N$C_6H_4NO_2$)Cl(dppm)$_2$] viewed down the *a* axis.

Table 3.7. Selected bond distances (Å) and angles (deg) for *trans*-[Ru((*E*)-4,4′-C≡CC_6H_4N=N$C_6H_4NO_2$)Cl(dppm)$_2$].

Ru - Cl	2.510(2)	Ru - P(1)	2.319(2)
Ru - P(2)	2.352(2)	Ru - P(3)	2.348(2)
Ru - P(4)	2.353(2)	Ru - C(1)	1.977(8)
P(1) - C(15)	1.859(8)	P(2) - C(15)	1.833(9)
P(3) - C(16)	1.831(8)	P(4) - C(16)	1.842(7)
N(1) - N(2)	1.26(1)	N(1) - C(6)	1.42(1)
N(2) - C(9)	1.46(1)	N(3) - C(12)	1.48(1)
C(1) - C(2)	1.22(1)	C(2) - C(3)	1.42(1)
C(3) - C(4)	1.41(1)	C(3) - C(8)	1.39(1)
C(4) - C(5)	1.39(1)	C(5) - C(6)	1.37(1)
C(6) - C(7)	1.39(1)	C(7) - C(8)	1.38(1)
C(9) - C(10)	1.35(1)	C(9) - C(14)	1.34(1)
C(10) - C(11)	1.38(1)	C(11) - C(12)	1.32(1)
C(12) - C(13)	1.35(2)	C(13) - C(14)	1.40(1)
Cl - Ru - P(1)	97.06(8)	Cl - Ru - P(2)	92.96(7)
Cl - Ru - P(3)	86.66(7)	Cl - Ru - P(4)	84.31(7)
Cl - Ru - C(1)	173.0(2)	P(1) - Ru - P(2)	72.16(8)
P(1) - Ru - P(3)	105.24(8)	P(1) - Ru - P(4)	176.36(8)
P(1) - Ru - C(1)	88.8(2)	P(2) - Ru - P(3)	177.32(8)
P(2) - Ru - P(4)	111.19(8)	P(2) - Ru - C(1)	85.2(2)
P(3) - Ru - P(4)	71.42(8)	P(3) - Ru - C(1)	95.5(2)
P(4) - Ru - C(1)	90.1(2)	Ru - P(1) - C(15)	95.9(3)
Ru - P(2) - C(15)	95.5(3)	Ru - P(3) - C(16)	93.9(2)
Ru - P(4) - C(16)	93.4(3)	N(2) - N(1) - C(6)	113.4(9)
N(1) - N(2) - C(9)	111.6(9)	O(1) - N(3) - O(2)	125(1)
Ru - C(1) - C(2)	175.0(7)	C(1) - C(2) - C(3)	180(1)
C(2) - C(3) - C(8)	121.0(8)	C(2) - C(3) - C(4)	120.2(8)
C(3) - C(4) - C(5)	118.8(9)	C(4) - C(3) - C(8)	118.8(8)
N(1) - C(6) - C(5)	115.1(9)	C(4) - C(5) - C(6)	121.4(9)
C(5) - C(6) - C(7)	119.9(8)	N(1) - C(6) - C(7)	125.0(9)
C(3) - C(8) - C(7)	121.6(8)	C(6) - C(7) - C(8)	119.5(9)
N(2) - C(9) - C(14)	116(1)	N(2) - C(9) - C(10)	124(1)
C(9) - C(10) - C(11)	119(1)	C(10) - C(9) - C(14)	120(1)
C(11) - C(12) - C(13)	122(1)	C(10) - C(11) - C(12)	121(1)
C(9) - C(14) - C(13)	121(1)	C(12) - C(13) - C(14)	117(1)
P(3) - C(16) - P(4)	96.7(4)	P(1) - C(15) - P(2)	96.3(4)

Table 3.8. Comparison of selected bond distances (Å) and angles (deg) for *trans*-[Ru((*E*)-4,4′-C≡CC_6H_4N=N$C_6H_4NO_2$)Cl(dppm)$_2$] (**4**) and related complexes.

	4	*a*	*b*	*c*
Ru - Cl	2.510(2)	2.483(2)	2.499(1)	-
Ru - P(1)	2.319(2)	2.379(2)	2.350(1)	-
Ru - P(2)	2.352(2)	2.358(2)	2.361(1)	-
Ru - P(3)	2.348(2)	2.332(2)	2.330(1)	-
Ru - P(4)	2.353(2)	2.332(2)	2.3581)	-
Ru - C(1)	1.977(8)	1.998(7)	1.994(4)	2.008(6)
C(1) - C(2)	1.22(1)	1.190(8)	1.198(6)	1.199(7)
C(2) - C(3)	1.42(1)	1.428(8)	1.439(7)	1.438(8)
N(1) - N(2)	1.26(1)			
CH=CH				1.302(8)
Cl - Ru - C(1)	173.0(2)	177.7(2)	175.2(1)	-
Ru - C(1) - C(2)	175.0(7)	176.8(5)	177.9(4)	174.2(6)
C(1) - C(2) - C(3)	180(1)	168.4(7)	179.1(5)	177.6(7)
C(6) - CH=CH				129.1(7)
CH=CHC(9)				129.1(8)
C(6) - N(1) - N(2)	113.4(9)			
N(1)- N (2) - C(9)	111.6(9)			

[a] *trans*-[Ru(4-C≡C$C_6H_4NO_2$)Cl(dppm)$_2$].[27] [b] *trans*-[Ru(4,4′-C≡C$C_6H_4C_6H_4NO_2$)-Cl(dppm)$_2$].[28]
[c] [Ru((*E*)-4,4′-C≡CC_6H_4CH=CH$C_6H_4NO_2$)(PPh_3)$_2$(η^5-C_5H_5)].[13]

The structural study confirms the octahedral geometry at ruthenium and *trans*-disposed chloride and acetylide ligands, and shows the *E* stereochemistry about the azo-linkage. The molecular ORTEP diagram (Figure 3.8.) shows the two inequivalent sets of phenyl groups associated with the phosphine ligand as discussed in Section 3.3.4. Important bond lengths about the metal centre are similar to those of the related, structurally characterized donor-acceptor complexes *trans*-[Ru(4-C≡C$C_6H_4NO_2$)Cl(dppm)$_2$][27] and *trans*-[Ru(4,4′-C≡C$C_6H_4C_6H_4NO_2$)Cl(dppm)$_2$][28] (see Table 3.8.). The Cl-Ru-C(1) and Ru-C(1)-C(2) angles deviate slightly from the idealized 180°, presumably a result of packing effects. Distances and angles within the diphosphine ligands are unexceptional. A comparison of bond angles C(6)-X-X and X-X-C(9) (X = CH, N) between the *trans*-CH=CH linked ligand

and the N=N linked ligand shows that the azo linkage subtends more acute bond angles than does the *trans*-CH=CH linkage. The two phenylene units of the acetylide ligand are not co-planar, with the angle between the two planes being 16.9 degrees. The rotation from co-planarity of adjacent phenyl groups in *trans*-[Ru(4,4′-C≡C$C_6H_4C_6H_4NO_2$)Cl(dppm)$_2$] has been reported to have an effect on computationally-derived molecular NLO activity.[28] The centrosymmetric space group suggests that no bulk NLO response would be observed; the molecules have packed with dipoles aligned antiparallel in pairs, as discussed in Section 1.4.1.

Table 3.9. Experimental parameters for the X-ray diffraction studies of *trans*-[Ru((*E*)4,4′-C≡CC_6H_4N=N$C_6H_4NO_2$)Cl(dppm)$_2$].

formula	$C_{64}H_{52}ClN_3O_2P_4Ru.CH_2Cl_2$	Z	4
formula weight	1240.48	radiation (λ, Å)	Cu Kα (λ = 1.544178)
space group	$P2_1/n$ (#14)	T, K	296
a, Å	10.242(4)	abs. coeff.(Kα), cm^{-1}	47.30
b, Å	32.063(6)	crystal size, mm^3	0.40 x 0.10 x 0.05
c, Å	18.310(4)	$2\theta_{max}$, deg	120.1
β, deg	95.24(2)	N	9692
V, $Å^3$	5987(3)	N_0	9120
D_{calc}, g cm^{-3}	1.38	R	0.054
F_{000}	2544.00	R_w	0.059

3.5. *Nonlinear optical investigations*

3.5.1. Results of nonlinear optical measurements

Measurements of the second-order optical nonlinearities of the new metal acetylide complexes and the terminal alkyne ligands were performed at 1064 nm using the hyper-Rayleigh scattering technique by collaborators at the University of Leuven, Belgium. The data are presented in Table 3.10. Figures 3.10. and 3.11. show a comparison of the data for the ruthenium complexes with previously reported values for related ruthenium complexes, and Figure 3.12. shows a comparison of the data for the new gold complex with previously reported values for related gold complexes.

Table 3.10. Experimental quadratic nonlinear optical responses measured by HRS at 1064 nm.

Compound	β (10^{-30} esu)	($\bar{\nu}_{max}$, cm^{-1} (ε, M^{-1} cm^{-1})) / λ_{max} (nm)	β_0[a] (10^{-30} esu)
1	[b]	22 300 (4700) / 448	-
2	59	28 400 (27 200) / 381	29
3	417	15 500 (8020) / 645	124
5	658	16 000 (15 500) / 622	159
4	1649	17 100 (27 200) / 583	232
6	1627	17 700 (28 600) / 565	149
7	180	25 100 (32 800) / 399	68

[a] Static first hyperpolarizabilities calculated from the experimental values using the two-level approximation with $\beta_o = \beta[1-(2\lambda_{max}/1064)^2][1-(\lambda_{max}/1064)^2]$; damping factors not included.
[b] Too low to measure.

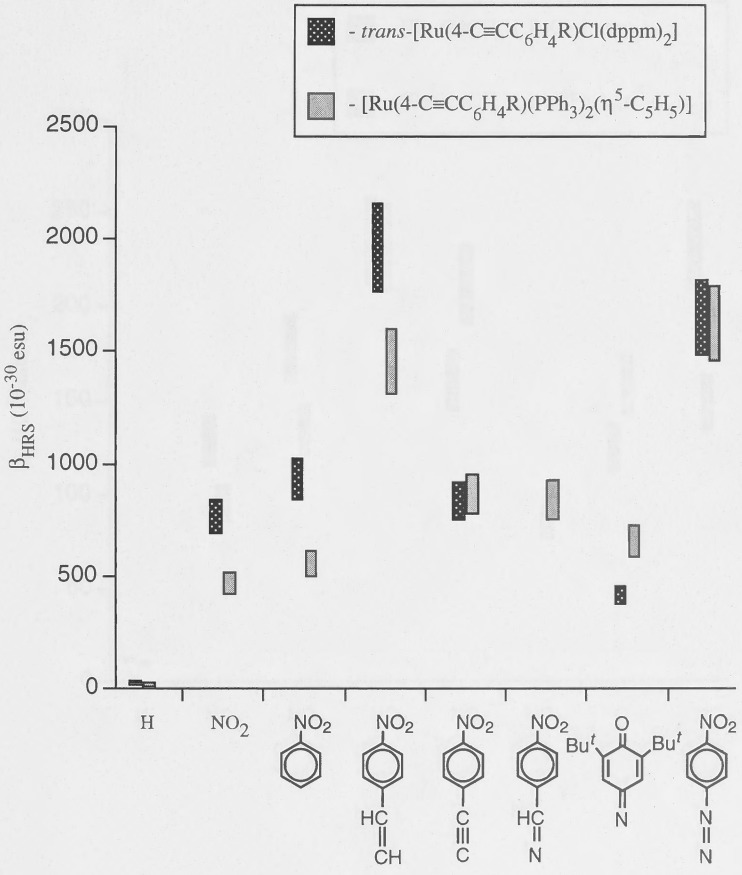

Figure 3.10. Experimental first hyperpolarizabilities (β_{HRS}) of the new ruthenium complexes and some previously reported complexes.[15] All measurement were made at 1064 nm using the same HRS apparatus. Range of error is ± 10%.

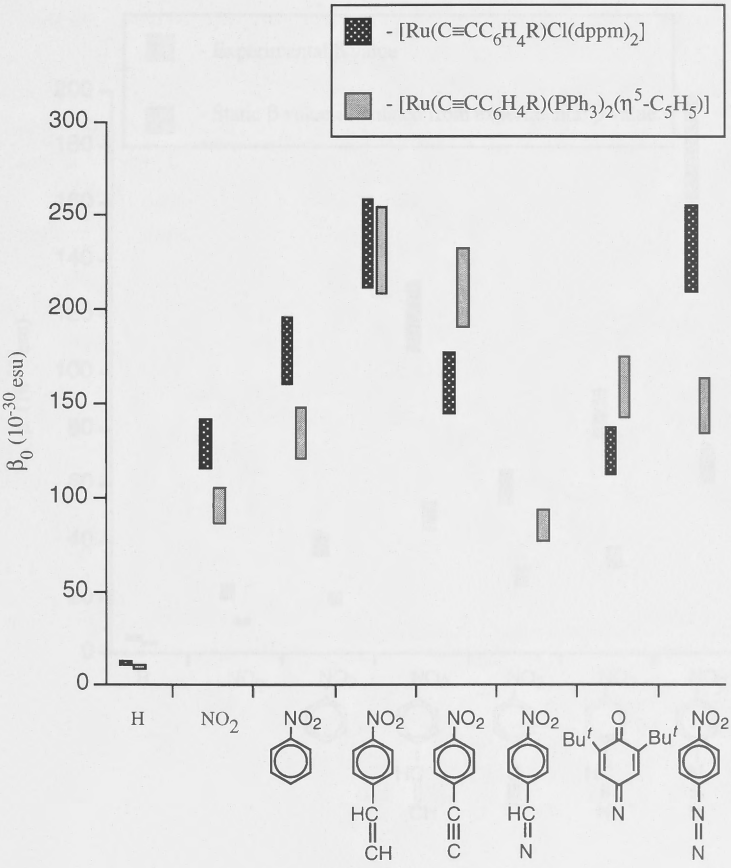

Figure 3.11. Static first hyperpolarizabilities (β_0) of the new ruthenium complexes and some previously reported complexes[15] calculated from the experimental values using the two-level model with $\beta_o = \beta[1-(2\lambda_{max}/1064)^2][1-(\lambda_{max}/1064)^2]$; damping factors not included. Range of error is ± 10%.

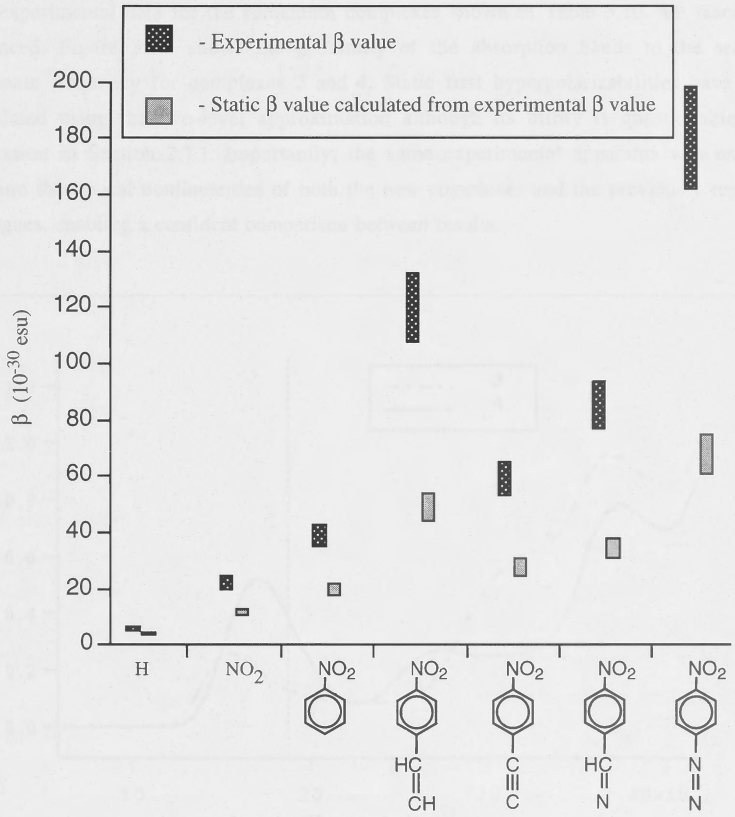

Figure 3.12. Experimental and static first hyperpolarizabilities for the new gold complex and some previously reported complexes.[25] Static values are calculated from the experimental values using the two-level model with $\beta_o = \beta[1-(2\lambda_{max}/1064)^2][1-(\lambda_{max}/1064)^2]$; damping factors not included. All measurements were made using the same HRS apparatus. Range of error is ± 10%.

3.5.2. Discussion

The experimental data for the ruthenium complexes shown in Table 3.10. are resonance enhanced. Figure 3.13. shows the proximity of the absorption bands to the second-harmonic frequency for complexes **3** and **4**. Static first hyperpolarizabilities have been calculated using the two-level approximation although its utility is questionable (see discussion in Section 2.7.). Importantly, the same experimental apparatus was used to measure the optical nonlinearities of both the new complexes and the previously reported analogues, enabling a confident comparison between results.

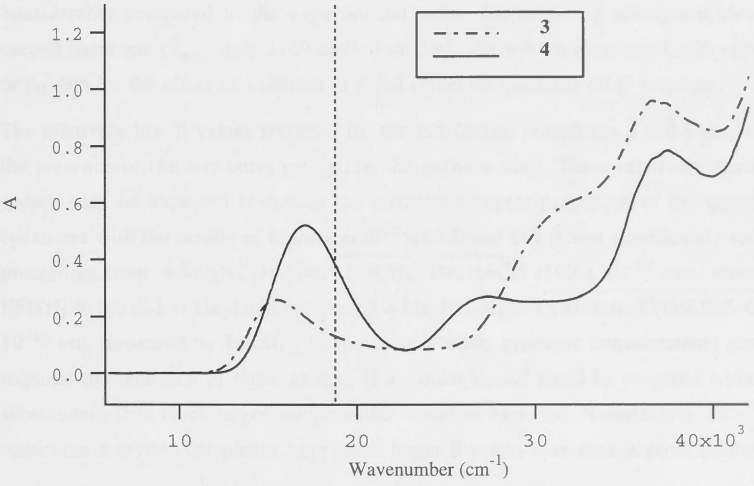

Figure 3.13. UV-vis spectra for **3** and **4**. The vertical dotted line indicates the second-harmonic frequency.

The experimental data for the ruthenium complexes shown in Figure 3.10. reveal conflicting trends for varying the ligands at the two different ligated ruthenium centres. The trend in β for the complexes of the type *trans*-[Ru(4-C≡CC_6H_4R)Cl(dppm)$_2$] is (in terms of R): (*E*)-4′-CH=C$HC_6H_4NO_2$ ≈ (*E*)-4′-N=N$C_6H_4NO_2$ > 4′-$C_6H_4NO_2$ ≈ 4′-C≡C$C_6H_4NO_2$ ≈ NO_2 > N=CCH=CBu^{t}C(O)CBu^t=CH > H. The trend in β values for complexes of the type [Ru(4-C≡CC_6H_4R)(PPh_3)$_2$(η^5-C_5H_5)] is (in terms of R): (*E*)-4′-CH=C$HC_6H_4NO_2$ ≈ (*E*)-

4′-N=NC$_6$H$_4$NO$_2$ > 4′-C≡CC$_6$H$_4$NO$_2$ ≈ 4′-N=CHC$_6$H$_4$NO$_2$ > N=CCH=CBu^{t}C(O)CBu^t=CH ≈ 4′-C$_6$H$_4$NO$_2$ ≈ NO$_2$ > H (with N=CCH=CBu^{t}C(O)CBu^t=CH > NO$_2$). For both groups of acetylide complexes, the β values for the N=N linked and the *trans*-CH=CH linked complexes are comparable and significantly larger than those of the other acetylide complexes.

The β_0 values reflect the trend found in the experimental data for the complexes containing the dppm ligand, with the exception of the indoaniline complex **3**. The β_0 values of the triphenylphosphine-containing complexes show a different trend to those of the experimental data, with the ordering being (in terms of R): (*E*)-4′-CH=CHC$_6$H$_4$NO$_2$ ≈ 4′-C≡CC$_6$H$_4$NO$_2$ > N=CCH=C(Bu^t)C(O)C(Bu^t)=CH ≈ (*E*)-4′-N=NC$_6$H$_4$NO$_2$ ≈ 4′-C$_6$H$_4$NO$_2$ > NO$_2$ ≈ 4′-N=CHC$_6$H$_4$NO$_2$ > H. The β_0 value of the N=N linked complex **6** is reduced considerably compared to the experimental value due to strong absorption close to the second harmonic ($\bar{\nu}_{max}$ only 1100 cm^{-1} from 2ω). There is no clear trend with either β_{HRS} or β_0 data for the effect of variation in metal centre on quadratic NLO response.

The relatively low β values recorded for the indoaniline complexes **3** and **5** may be due to the presence of the *tert*-butyl groups on the quinone ring. These relatively electron rich groups may be expected to reduce the electron acceptor properties of the quinone ring, consistent with the results of Marder *et al*[19] who found that β was significantly reduced on proceeding from 4-Me$_2$NC$_6$H$_4$N=CCH=CHC(O)CH=CH (190 x 10^{-30} esu, measured by EFISH) to the di-*tert*-butylated compound 4-Me$_2$NC$_6$H$_4$N=CCH=CBu^{t}C(O)CBu^t=CH (78 x 10^{-30} esu, measured by EFISH). In the current work, synthetic considerations have so far required the inclusion of these groups. If a similar ligand could be prepared without these substituents, then much larger nonlinearities would be expected. Nevertheless, all of the new ruthenium acetylide complexes have much larger β values than their organic analogues.

The experimental data for the gold acetylide complexes (see Figure 3.12.) show a clear trend in β_{HRS} upon alkynyl ligand variation: (*E*)-4′-N=NC$_6$H$_4$NO$_2$ > (*E*)-4′-CH=CHC$_6$H$_4$NO$_2$ > 4′-N=CHC$_6$H$_4$NO$_2$ > 4′-C≡CC$_6$H$_4$NO$_2$ > 4′-C$_6$H$_4$NO$_2$ > NO$_2$ > H, an ordering also clearly reflected in the β_0 data. These complexes have low absorption at the second-harmonic wavelength (see Figure 3.14. for the UV-vis spectrum of **7**) so resonance enhancement of β should be far less significant than for the ruthenium analogues, providing a clearer indication of the effect of ligand variation on β. These data provide further evidence that complexes bearing the N=N linked ligand have β values as large if not larger than complexes containing the *trans*-CH=CH linkage. A comparison of the β values of the gold complexes with those of the organic compounds reported by van Walree[16] (see Table 3.2.) suggests that the (triphenylphosphine)gold moiety acts as an electron donor of comparable efficiency to the NMe$_2$ group.

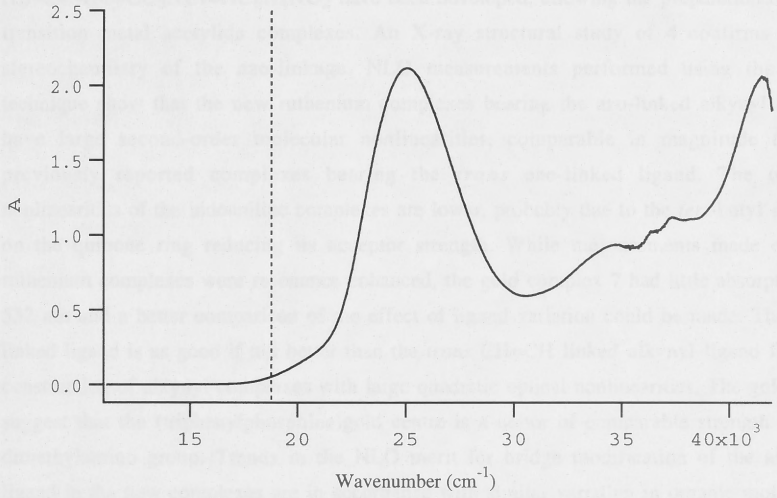

Figure 3.14. UV-vis spectrum of **7**. The vertical dotted line indicates the second-harmonic frequency.

3.6. Conclusions

Synthetic routes into the terminal alkynes 4-HC≡CC_6H_4N=CCH=$CBu^tC(O)CBu^t$=CH and (*E*)-4,4′-HC≡CC_6H_4N=$NC_6H_4NO_2$ have been developed, allowing the preparation of new transition metal acetylide complexes. An X-ray structural study of **4** confirms the *E* stereochemistry of the azo-linkage. NLO measurements performed using the HRS technique show that the new ruthenium complexes bearing the azo-linked alkynyl ligand have large second-order molecular nonlinearities, comparable in magnitude to the previously reported complexes bearing the *trans* ene-linked ligand. The optical nonlinearities of the indoaniline complexes are lower, probably due to the *tert*-butyl groups on the quinone ring reducing its acceptor strength. While measurements made on the ruthenium complexes were resonance enhanced, the gold complex **7** had little absorption at 532 nm and a better comparison of the effect of ligand variation could be made. The azo-linked ligand is as good if not better than the *trans* CH=CH linked alkynyl ligand for the construction of alkynyl complexes with large quadratic optical nonlinearities. The gold data suggest that the (triphenylphosphine)gold centre is a donor of comparable strength to the dimethylamino group. Trends in the NLO merit for bridge modification of the alkynyl ligand in the new complexes are in accordance with similar variation in organic molecules by van Walree *et al.*[16]

3.7. Experimental

3.7.1. General Conditions, Reagents and Instruments

General Conditions

All reactions were performed under a nitrogen atmosphere with the use of Schlenk techniques unless otherwise stated. Dichloromethane was dried by distilling over calcium hydride, methanol was dried by distilling over magnesium / iodine, tetrahydrofuran was dried by distilling over sodium / benzophenone; other solvents were used as received. "Pet. spirit" refers to a fraction of petroleum ether of boiling range 60-80 °C. Chromatography was on silica gel (230-400 mesh ASTM) or ungraded basic alumina.

Reagents

The following were prepared by literature procedures: $[RuCl(PPh_3)_2(\eta^5\text{-}C_5H_5)]$,[29] *cis*-$[RuCl_2(dppm)_2]$,[30] $[AuCl(PPh_3)]$.[31] Sodium methoxide solutions were prepared by dissolving sodium in dry methanol. Dichlorobis(triphenylphosphine)palladium(II) was prepared by stirring two equivalents of triphenylphosphine with palladium(II) chloride in dimethylformamide at reflux for 2 h. The resulting precipitate was collected and recrystallized from chloroform. Sodium hexafluorophosphate (Aldrich) was recrystallized from acetonitrile before use. 2,6-Di-*tert*-butyl-1,4-benzoquinone (Aldrich), 4-iodoaniline (Aldrich), boron trifluoride etherate (Aldrich), trimethylsilylacetylene (Aldrich), copper(I) iodide (Unilab), tetrabutylammonium fluoride (1 M solution in tetrahydrofuran) (Aldrich), sulfuric acid (98 %) (Univar), (*E*)-4,4´-$H_2NC_6H_4N{=}NC_6H_4NO_2$ (Disperse Orange 3 95 %) (Aldrich), sodium nitrite (M & B), potassium iodide (M & B) and anhydrous magnesium sulfate (Aldrich) were used as received.

Instruments

EI (electron impact) mass spectra (both unit resolution and high resolution (HR)) were recorded using a VG Autospec instrument (70 eV electron energy, 8 kV accelerating potential) and secondary ion mass spectra were recorded using a VG ZAB 2SEQ instrument (30 kV Cs^+ ions, current 1 mA, accelerating potential 8 kV, 3-nitrobenzyl alcohol matrix) at the Research School of Chemistry, Australian National University; peaks are reported as *m/z* (assignment, relative intensity). Microanalyses were carried out at the Research School of Chemistry, Australian National University. Infrared spectra were recorded as dichloromethane solutions using a Perkin-Elmer System 2000 FT-IR. ^1H, ^{13}C and ^{31}P NMR spectra were recorded using a Varian Gemini-300 FT NMR spectrometer and are referenced to residual chloroform (7.24 ppm), *d*-chloroform (77.0 ppm) or external 85%

H_3PO_4 (0.0 ppm), respectively. The assignments follow the numbering schemes shown in Figure 3.15. UV-Vis spectra of solutions in tetrahydrofuran in 1 cm cells were recorded using either a Cary 4 or Cary 5 spectrophotometer.

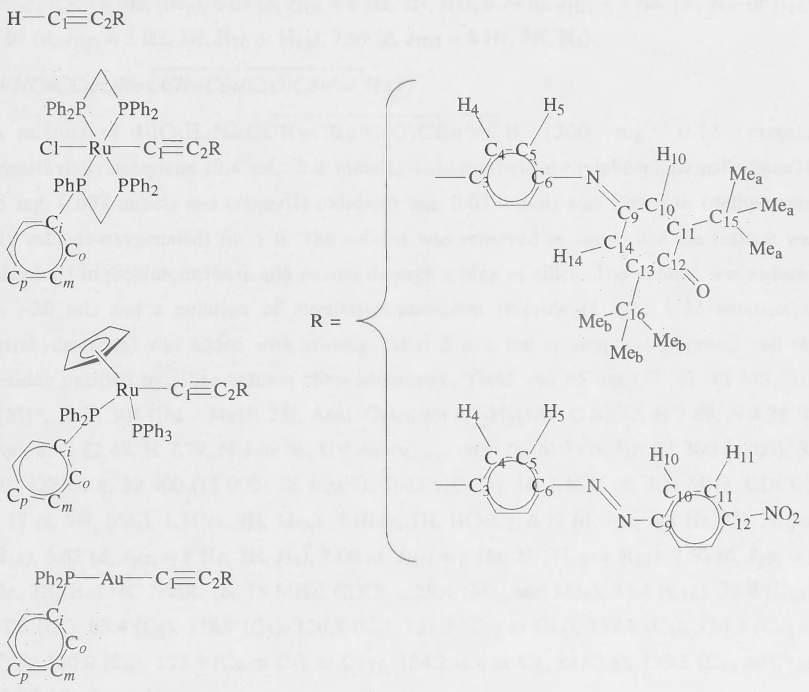

Figure 3.15. NMR numbering scheme.

3.7.2. Synthesis of ligands containing nitrogen bridges

4-IC$_6$H$_4$N=CCH=CBu^{t}C(O)CBu^t=CH

A mixture of 2,6-di-*tert*-butyl-1,4-benzoquinone (500 mg, 2.27 mmol), 4-iodoaniline (1400 mg, 6.39 mmol) and boron trifluoride etherate (30 μL, 0.16 mmol)) was stirred in tetrahydrofuran (30 mL) at reflux for 7 h, with a further six aliquots of boron trifluoride

etherate (30 μL) being added at hourly intervals. The mixture was then allowed to cool to room temperature and the solvent removed *in vacuo*. The residue was purified by silica column chromatography, with the product being eluted with 3:5 dichloromethane / pet. spirit. Yield was 800 mg (84 % based on di-*tert*-butylbenzoquinone). HR MS (EI) $C_{20}H_{24}INO$: calc. 421.0903, found 421.0906. ^1H NMR: (δ, 300 MHz, $CDCl_3$); 1.18 (s, 9H, Me_a), 1.30 (s, 9H, Me_b), 6.63 (d, J_{HH} = 8 Hz, 2H, H_5), 6.74 (d, J_{HH} = 3 Hz, 1H, H_{10} or H_{14}), 7.01 (d, J_{HH} = 3 Hz, 1H, H_{10} or H_{14}), 7.69 (d, J_{HH} = 8 Hz, 2H, H_4).

*4-HC≡CC$_6$H$_4$N=CCH=CBu^{t}C(O)CBu^t=CH (**1**)*

A mixture of 4-IC$_6$H$_4$N=CCH=CBu^{t}C(O)CBu^t=CH (300 mg, 0.71 mmol), trimethylsilylacetylene (0.4 mL, 2.8 mmol), dichlorobis(triphenylphosphine)palladium(II) (5 mg, 0.007 mmol) and copper(I) iodide (5 mg, 0.03 mmol) was stirred in triethylamine (10 mL, de-oxygenated) for 1 h. The solvent was removed *in vacuo* and the residue was dissolved in dichloromethane and passed through a plug of silica. The volume was reduced to ~20 mL and a solution of tetrabutylammonium fluoride (1 mL, 1 M solution in tetrahydrofuran) was added with stirring. After 5 min the solvent was removed and the residue purified by silica column chromatography. Yield was 85 mg (37 %). EI MS: 319 ([M]$^+$, 100), 304 ([M – Me]$^+$, 25). Anal. Calcd for $C_{22}H_{25}NO$: C 82.72, H 7.89, N 4.38 %. Found: C 82.48, H 7.79, N 3.89 %. UV-vis ($\tilde{\nu}_{max}$, cm^{-1} (ε, M^{-1} cm^{-1})): 22 300 (4700), 34 900 (28 000), 39 400 (15 000). IR (cm^{-1}): 1633 ν(C=O). ^1H NMR: (δ, 300 MHz, $CDCl_3$); 1.17 (s, 9H, Me_a), 1.31 (s, 9H, Me_b), 3.10 (s, 1H, HC≡C), 6.72 (d, J_{HH} = 3 Hz, 1H, H_{10} or H_{14}), 6.82 (d, J_{HH} = 8 Hz, 2H, H_4), 7.00 (d, J_{HH} = 3 Hz, 1H, H_{10} or H_{14}), 7.50 (d, J_{HH} = 8 Hz, 2H, H_5).^{13}C NMR: (δ, 75 MHz, $CDCl_3$); 29.4 (Me_a and Me_b), 35.4 (C_{16}), 35.8 (C_{15}), 77.5 (C_1), 83.4 (C_2), 118.9 (C_3), 120.8 (C_5), 121.3 (C_{10} or C_{14}), 132.8 (C_4), 134.3 (C_{10} or C_{14}), 150.0 (C_6), 153.4 (C_9 or C_{11} or C_{13}), 154.2 (C_9 or C_{11} or C_{13}), 158.8 (C_{11} or C_{13}), 187.5 (C_{12}).

(E)-4,4´-IC$_6$H$_4$N=NC$_6$H$_4$NO$_2$

No attempt to exclude air was made during this procedure. Concentrated sulfuric acid (2 mL) was added to water (250 mL) in a 500 mL round-bottomed flask. (*E*)-4,4´-$H_2NC{\equiv}CC_6H_4N{=}NC_6H_4NO_2$ (2.0 g, 8.3 mmol) was added and the mixture stirred until a fine suspension was formed (~ 10 min). Sodium nitrite (800 mg, 11.6 mmol) was added and the mixture stirred at room temperature for 1 h. The mixture was filtered through a plug of Celite and an aqueous solution of potassium iodide (2.5 g, 15 mmol, in 50 mL of water) was added to the filtrate with stirring, whereupon a precipitate formed. The mixture was extracted with dichloromethane, the organic phase separated and dried with magnesium sulfate, and the solvent removed on a rotary evaporator. The residue was then purified by

column chromatography on silica. Yield was 1.02 g (37 %) of an orange / brown powder. HR MS (EI) $C_{12}H_8IN_3O_2$: calc. 352.9661, found 352.9665. UV-vis ($\bar{\nu}_{max}$, cm^{-1} (ε, $M^{-1}\,cm^{-1}$)): 21 400 (1500), 28 300 (28 300). IR (cm^{-1}): 1527 ν_{as}(N=O), 1347 ν_s(N=O). ^1H NMR: (δ, 300 MHz, $CDCl_3$); 7.68 (d, J_{HH} = 9 Hz, 2H, H_4), 7.90 (d, J_{HH} = 9 Hz, 2H, H_5), 8.02 (d, J_{HH} = 9 Hz, 2H, H_{10}), 8.37 (d, J_{HH} = 9 Hz, 2H, H_{11}).

(E)-4,4´-HC≡CC$_6$H$_4$N=NC$_6$H$_4$NO$_2$ (2)

(*E*)-4,4´-IC$_6$H$_4$N=NC$_6$H$_4$NO$_2$ (250 mg, 0.71 mmol) and trimethylsilylacetylene (0.4 mL, 2.8 mmol) were dissolved in tetrahydrofuran (5 mL) with stirring. Triethylamine (2 mL) was added followed by dichlorobis(triphenylphosphine)palladium(II) (50 mg, 0.071 mmol) and copper (I) iodide (20 mg, 0.11 mmol), and the resultant mixture was stirred for 1 h. The mixture was then passed through a silica plug eluting with dichloromethane. The volume was reduced to ~40 mL on a rotary evaporator and a solution of tetrabutylammonium fluoride (1 mL, 1 M solution in tetrahydrofuran) was added without the exclusion of air. The mixture was stirred for 5 min. and then the solvent was removed on a rotary evaporator. The residue was purified by column chromatography on silica eluting with 1:1 dichloromethane / pet. spirit. Yield was 89 mg (45 %) of an orange powder. EI MS: 251 ([M]$^+$, 45), 150 ([$N_2C_6H_4NO_2$]$^+$, 5), 129 ([HC≡C$C_6H_4N_2$]$^+$, 35), 101 ([HC≡CC_6H_4]$^+$, 100). Anal. Calcd for $C_{14}H_9N_3O_2$: C 66.93, H 3.61, N 16.73 %. Found: C 66.03, H 3.48, N 16.04 %. UV-vis ($\bar{\nu}_{max}$, cm^{-1} (ε, $M^{-1}\,cm^{-1}$)): 21 700 (860), 28 400 (27 200). IR (cm^{-1}): 1527 ν_{as}(N=O), 1346 ν_s(N=O). ^1H NMR: (δ, 300 MHz, $CDCl_3$); 3.27 (s, 1H, HC≡C), 7.65 (d, 2H, J_{HH} = 9 Hz, H_4), 7. 92 (d, 2H, J_{HH} = 9 Hz, H_5), 8.02 (d, 2H, J_{HH} = 9 Hz, H_{10}), 8.38 (d, 2H, J_{HH} = 9 Hz, H_{11}). ^{13}C NMR: (δ, 75 MHz, $CDCl_3$); 80.4 (C_1), 83.0 (C_2), 123.4, 123.6, 124.8 (C_5, C_{10}, C_{11}), 126.2 (C_3), 133.1 (C_4), 148.8 (C_{12}), 151.8 (C_6), 155.5 (C_9).

3.7.3. Metal Acetylide Complexes

trans-[Ru(4-C≡CC$_6$H$_4$N=CCH=CBu^{t}C(O)CBu^t=CH)Cl(dppm)$_2$] (3)

cis-[$RuCl_2$(dppm)$_2$] (140 mg, 0.16 mmol), **1** (75 mg, 0.24 mmol) and sodium hexafluorophosphate (55 mg, 0.33 mmol) were stirred in dichloromethane (5 mL) for 5 h at room temperature. Triethylamine (1 mL) was added with stirring and after 1 min the solvent was removed *in vacuo*. The residue was absorbed onto basic alumina and placed atop an alumina column. Elution with 1:3 dichloromethane / pet. spirit removed any excess acetylene. The product was eluted with 4:1 dichloromethane / pet. spirit. Evaporation of the solvent on a rotary evaporator yielded 123 mg (65 %) of a deep blue powder. FAB MS: 1223 ([M]$^+$, 50), 1188 ([M – Cl]$^+$, 15), 905 ([RuCl(dppm)$_2$]$^+$, 20), 869 ([Ru(dppm)$_2$]$^+$, 100). Anal. Calcd for $C_{72}H_{68}ClNOP_4Ru$: C 70.67, H 5.60, N 1.14 %. Found: C 70.30, H

5.93, N 0.92 %. UV-vis ($\tilde{\nu}_{max}$, cm^{-1} (ε, M^{-1} cm^{-1})): 15 500 (8020), 31 300 (sh, 18 100), 36 600 (29 600), 37 300 (29 400). IR (cm^{-1}): 2067 ν(C≡C). ^{1}H NMR: (δ, 300 MHz, $CDCl_3$); 1.27 (s, 9H, Me_a or Me_b), 1.31 (s, 9H, Me_a or Me_b), 4.91 (m, 4H, CH_2), 6.04 (d, 2H, J_{HH} = 8 Hz, H_4), 6.53 (d, 2H, J_{HH} = 9 Hz, H_5), 6.94 (d, 2H, J_{HH} = 3 Hz, H_{10} or H_{14}), 7.02 to 7.43 (m, 41H, phenyl and H_{10} or H_{14}). ^{31}P NMR (δ, 121 MHz, $CDCl_3$): –6.1 (PPh_2). ^{13}C NMR: (δ, 75 MHz, $CDCl_3$); 29.4 (Me_a and Me_b), 35.3 (C_{15} or C_{16}), 35.7 (C_{15} or C_{16}), 50.3 (CH_2), 114.2 (C_2), 122.0 (C_5), 122.2 (C_{10} or C_{14}), 127.5 (C_p), 128.5 (C_3), 129.0, 129.3 (C_m), 130.5 (C_4), 133.3, 133.6 (C_o), 134.5 (m, partially obscured by C_o, C_i), 135.0 (C_{10} or C_{14}), 144.5 (C_6), 151.8, 152.1 (C_9, C_{11} or C_{13}), 156.5 (C_{11} or C_{13}), 187.8 (C_{12}).

*trans-[Ru((E)-4,4´-C≡CC_6H_4N=N$C_6H_4NO_2$)Cl(dppm)$_2$] (**4**)*

cis-[$RuCl_2$(dppm)$_2$] (90 mg, 0.096 mmol), **2** (30 mg, 0.12 mmol) and sodium hexafluorophosphate (40 mg, 0.24 mmol) were stirred in dichloromethane (10 mL) for 4 h at room temperature. A solution of sodium methoxide (1 mL, 0.3 M solution in methanol) was added with stirring. The mixture was passed through a plug of alumina eluting with dichloromethane, and the solvent was then removed on a rotary evaporator. The residue was recrystallized from dichloromethane / methanol to yield 75 mg (62 %) of dark purple microcrystals. A crystal suitable for X-ray diffraction studies was grown by the slow diffusion of methanol into a dichloromethane solution. FAB MS: 1155 ([M]$^+$, 40), 869 ([Ru(dppm)$_2$]$^+$, 20). Anal. Calcd for $C_{64}H_{52}ClN_3O_2P_4Ru$: C 66.52, H 4.54, N 3.64 %. Found: C 66.60, H 4.24, N 3.72 %. UV-vis ($\tilde{\nu}_{max}$, cm^{-1} (ε, M^{-1} cm^{-1})): 17 100 (27 200), 27 300 (14 000), 37 400 (41 000). IR (CH_2Cl_2): ν(C≡C) 2061 cm^{-1}. ^{1}H NMR: (δ, 300 MHz, $CDCl_3$); 4.93 (m, 4H, CH_2), 6.06 (d, 2H, J_{HH} = 9 Hz, H_4), 7.06 to 7.42 (m, 40H, Ph), 7.53 (d, 2H, J_{HH} = 9 Hz, H_5), 7.92 (d, 2H, J_{HH} = 9 Hz, H_{10}), 8.33 (d, 2H, J_{HH} = 9 Hz, H_{11}). ^{31}P NMR (δ, 121 MHz, $CDCl_3$): – 6.3 (PPh_2). ^{13}C NMR: (δ, 75 MHz, $CDCl_3$); 50.2 (CH_2), 117.5 (C_2), 122.7, 123.0, 124.7 (C_5, C_{10}, C_{11}), 127.6 (C_p), 129.2, 129.4 (C_m), 130.7 (C_4), 133.2, 133.4 (C_o), 134.3 (m, partially obscured by C_o, C_i) 136.0 (C_3), 147.6 (C_6), 148.0 (C_{12}), 156.6 (C_9).

*[Ru(4-C≡CC_6H_4N=$\overline{CCH=CBu^tC(O)CBu^t=CH}$)($PPh_3$)$_2$($\eta^5$-$C_5H_5$)] (**5**)*

[$RuCl(PPh_3)_2(\eta^5$-$C_5H_5)$] (90 mg, 0.12 mmol) and **1** (75 (50 mg, 0.16 mmol) were stirred in methanol (10 mL) at reflux for 45 min. The mixture was then cooled to room temperature and sodium methoxide solution (1 mL, 0.2 M solution in methanol) was added with stirring. The solvent was removed and the residue purified by column chromatography on silica. The product was then recrystallized from dichloromethane / pet. spirit affording 40 mg (32 %) of dark blue microcrystals. FAB MS: 1009 ([M]$^+$, 25), 746 ([M + H – PPh_3]$^+$, 30), 691 ([$Ru(PPh_3)_2(\eta^5$-$C_5H_5)$]$^+$, 25), 429 ([$Ru(PPh_3)(\eta^5$-$C_5H_5)$]$^+$, 100). Anal. Calcd for $C_{63}H_{59}NOP_2Ru$: C 74.98, H 5.89, N 1.39 %. Found: C 75.92, H 5.97, N 1.12 %.

UV-vis ($\tilde{\nu}_{max}$, cm^{-1} (ε, M^{-1} cm^{-1})): 16 000 (15 500), 31 500 (29 800), 41 800 (34 400). IR (cm^{-1}): 2061 ν(C≡C). ^{1}H NMR: (δ, 300 MHz, $CDCl_3$); 1.24 (s, 9H, Me_a), 1.32 (s, 9H, Me_b), 4.32 (s, 5H, η^5-C_5H_5), 6.77 (d, 2H, J_{HH} = 8 Hz, H_4), 7.01 to 7.48 (m, 34H, Ph). ^{31}P NMR: (δ, 121 MHz, $CDCl_3$); 50.7 (PPh_3). ^{13}C NMR: (δ, 75 MHz, $CDCl_3$); 29.5 (Me_a and Me_b), 35.3 (C_{15} or C_{16}), 35.7 (C_{15} or C_{16}), 85.3 (η^5-C_5H_5), 115.6 (C_2), 122.1 (C_{10} or C_{14}), 122.5 (C_5), 127.2 (t, J_{CP} = 5 Hz, C_m), 128.4 (C_p), 129.1 (C_3), 131.0 (C_4), 133.8 (t, J_{CP} = 5 Hz, C_o), 135.0 (C_{10} or C_{14}), 138.7 (m, C_i), 145.2 (C_6), 151.9 (C_9 or C_{11} or C_{13})), 152.5 (C_9 or C_{11} or C_{13})), 156.9 (C_{11} or C_{13}), 187.9 (C_{12}).

*[Ru((E)-4,4´-C≡CC_6H_4N=N$C_6H_4NO_2$)(PPh_3)$_2$(η^5-C_5H_5)] (**6**)*

[RuCl(PPh_3)$_2$(η^5-C_5H_5)] (170 mg, 0.23 mmol) and **2** (70 mg, 0.28 mmol) were stirred in methanol (10 mL) at reflux for 30 min. The mixture was then cooled to room temperature and sodium methoxide solution (2 mL, 0.2 M solution in methanol) was added with stirring. The solvent was removed and the residue passed through a silica column eluting first with 3:5 dichloromethane / pet. spirit to remove excess acetylene, and then with 1:20 acetone / dichloromethane. The solvent was removed from the second fraction and the residue purified by thin-layer chromatography to yield 112 mg (51 %) of dark purple microcrystals. FAB MS: 941 ([M]$^+$, 55), 691 ([Ru(PPh_3)$_2$(η^5-C_5H_5)]$^+$, 40), 429 ([Ru(PPh_3)(η^5-C_5H_5)]$^+$, 70). Anal. Calcd for $C_{55}H_{43}N_3O_2P_2Ru$: C 70.20, H 4.61, N 4.47 %. Found: C 69.37, H 4.60, N 4.62 %. UV-vis ($\tilde{\nu}_{max}$, cm^{-1} (ε, M^{-1} cm^{-1})): 17 700 (28 600), 28 800 (17 300), 34 400 (16 800), 39 900 (24 500). IR (cm^{-1}): 2054 ν(C≡C), 1342 ν_s(N=O). ^{1}H NMR: (δ, 300 MHz, $CDCl_3$); 4.36 (s, 5H, η^5-C_5H_5), 7.07 to 7.47 (m, 32H, Ph), 7.80 (d, 2H, J_{HH} = 8 Hz, H_5), 7.96 (d, 2H, J_{HH} = 9 Hz, H_{10}), 8.34 (d, 2H, J_{HH} = 9 Hz, H_{11}). ^{31}P NMR: (δ, 121 MHz, $CDCl_3$); 50.7 (PPh_3). ^{13}C NMR: (δ, 75 MHz, $CDCl_3$); 85.6 (η^5-C_5H_5), 118.7 (C_2), 122.9 (C_5 or C_{10} or C_{11}), 123.8 (C_5 or C_{10} or C_{11}), 124.7 (C_5 or C_{10} or C_{11}), 127.3 (t, J_{CP} = 5 Hz, C_m), 128.6 (C_p), 131.2 (C_4), 133.7 (t, J_{CP} = 5 Hz, C_o), 135.7 (C_3), 138.5 (m, C_i), 147.7 (C_6), 148.5 (C_{12}), 156.5 (C_9).

*[Au((E)-4,4´-C≡CC_6H_4N=N$C_6H_4NO_2$)(PPh_3)] (**7**)*

[AuCl(PPh_3)] (167 mg, 0.34 mmol), **2** (85 mg, 0.34 mmol) and sodium methoxide solution (1 mL, 0.5 M solution in methanol) were stirred in dichloromethane (5 mL) for 18 h. Methanol (10 mL) was then added and the volume reduced to ~ 10 mL whereupon the product precipitated. After filtration in air and washing with methanol (2 x 5 mL), 170 mg (71 %) of orange / brown microcrystals were collected. FAB MS: ([Au(PPh_3)$_2$]$^+$, 15), 459 ([Au(PPh_3)]$^+$, 95). Anal. Calcd for $C_{32}H_{23}N_3O_2PAu$: C 54.17, H 3.27, N 5.92 %. Found: C 54.07, H 3.18, N 6.12 %. UV-vis ($\tilde{\nu}_{max}$, cm^{-1} (ε, M^{-1} cm^{-1})): 25 100 (32 800), 34 700 (14 000), 37 300 (17 400), 41 500 (32 000). IR (cm^{-1}): 2113 ν(C≡C), 1345 ν_s(N=O). ^{1}H NMR: (δ, 300 MHz, $CDCl_3$); 7.42 to 7.57 (m, 15H, Ph), 7.64 (d, 2H, J_{HH} = 8 Hz, H_4), 7.87

(d, 2H, J_{HH} = 8 Hz, H_5), 7.98 (d, 2H, J_{HH} = 9 Hz, H_{10}), 8.35 d, 2H, J_{HH} = 9 Hz, H_{11}). ^{31}P NMR: (δ, 121 MHz, $CDCl_3$); 42.6 (PPh_3). ^{13}C NMR: (δ, 75 MHz, $CDCl_3$); 123.3 (C_5 or C_{10} or C_{11}), 124.7 (C_5 or C_{10} or C_{11}), 129.2 (d, J_{CP} = 6 Hz, C_m), 131.6 (C_p), 133.2 (C_4), 134.2 (d, J_{CP} = 14 Hz, C_o), 148.4 (C_{12}), 150.6 (C_6), 155.8 (C_9).

2.9.5. X-ray Structure Determination

A unique diffractometer data set was obtained using the ω-2θ scan technique and yielded 9692 independent reflections, 9120 of these with $I \geq 2.00\sigma(I)$ being considered "observed" and used in full matrix least squares refinement; an analytical absorption correction was applied. The structure was solved by direct methods (SIR92), and anisotropic thermal parameters were refined using full-matrix methods for the non-hydrogen atoms; $(x, y, z, U_{iso})_H$ were included constrained at estimated values. Conventional residuals R and R_w on $|F|$ are given; the weighting function $w = [\sigma_c^2(F_o) + (p^2/4)F_o^2]^{-1}$ (where $\sigma_2(F_o)$ = e.s.d. based on counting statistics and $p = p$ factor determined experimentally from standard reflections) was employed. Computation used the teXsan package.[32] Specific data collection, solution and refinement parameters are given in the tables in Section 3.4.

2.9.6. Hyper-Rayleigh scattering measurements

An injection-seeded Nd:YAG laser (Q-switched Nd:YAG Quanta Ray GCR5, 1064 nm, 8 ns pulses, 10 Hz) was focussed into a cylindrical cell (7 mL) containing the sample. The intensity of the incident beam was varied by rotation of a half-wave plate placed between crossed polarizers. Part of the laser pulse was sampled by a photodiode to measure the vertically polarized incident light intensity. The frequency doubled light was collected by an efficient condenser system and detected by a photomultiplier. The harmonic scattering and linear scattering were distinguished by appropriate filters; gated integrators were used to obtain intensities of the incident and harmonic scattered light. All measurements were performed in tetrahydrofuran using *p*-nitroaniline ($\beta = 21.4 \times 10^{-30}$ esu)[33] as a reference. Further details of the experimental procedure have been reported in the literature.[34,35]

3.8. References

(1) *Nonlinear Optical Properties of Organic and Polymeric Materials*; Williams, D. J., Ed.; American Chemical Society: Washington, D.C., 1983; Vol. 233.

(2) *Nonlinear Optical Properties of Organic Molecules and Crystals I*; Chemla, D. S. and Zyss, J., Eds.; Academic Press: Orlando, 1987.

(3) *Nonlinear Optical Properties of Organic Molecules and Crystals II*; Chemla, D. S. and Zyss, J., Eds.; Academic Press: Orlando, 1987.

(4) *Organic Materials for Non-linear Optics*; Hann, R. A. and Bloor, D., Eds.; Royal Society of Chemistry: London, 1989.

(5) *Organic Materials for Non-linear Optics II*; Hann, R. A. and Bloor, D., Eds.; Royal Society of Chemistry: London, 1991.

(6) *Organic Materials for Non-linear Optics III*; Ashwell, G. J. and Bloor, D., Eds.; Royal Society of Chemistry: Cambridge, 1993.

(7) Tsunekawa, T.; Gotoh, T.; Iwamoto, M. *Chem. Phys. Lett.* **1990**, *166*, 353.

(8) Tsunekawa, T.; Gotoh, T.; Mataki, H.; Kondoh, T.; Iwamoto, M. *Proc. SPIE., Int. Soc. Opt. Eng.* **1990**, *1337*, 272.

(9) Tsunekawa, T.; Yamaguchi, K. *J. Phys. Chem.* **1992**, *96*, 10268.

(10) Nicoud, J. F.; Twieg, R. J. In *Nonlinear Optical Properties of Organic Molecules and Crystals*; Chemla, D. S. and Zyss, J., Eds.; Academic Press: Orlando, 1987; Vol. 1, p 227.

(11) Andre, J. M.; Morley, J. O.; Zyss, J. *Molecules in Physics, Chemistry, and Biology*; Maruani, J., Ed.; Kluwer: Dordrecht, 1988; Vol. 2.

(12) Morley, J. O. *J. Chem. Soc., Perkin Trans. 2* **1995**, 731.

(13) Whittall, I. R.; Humphrey, M. G.; Persoons, A.; Houbrechts, S. *Organometallics* **1996**, *15*, 1935.

(14) Singer, K. D.; Sohn, J. E.; King, L. A.; Gordon, H. M.; Katz, H. E.; Dirk, C. W. *J. Opt. Soc. Am. B* **1989**, *6*, 1339.

(15) Whittall, I. R.; Cifuentes, M. P.; Humphrey, M. G.; Luther-Davies, B.; Samoc, M.; Houbrechts, S.; Persoons, A.; Heath, G. A.; Hockless, D. C. R. *J. Organomet. Chem.* **1997**, *549*, 127.

(16) van Walree, C. A.; Franssen, O.; Marsman, A. W.; Flipse, M. C.; Jennekens, L. W. *J. Chem. Soc., Perkin Trans. 2* **1997**, 799.

(17) Whittall, I. R., *PhD Thesis*, Australian National University, **1997**.

(18) Marder, S. R.; Beratan, D. N.; Cheng, L. T. *Science* **1991**, *252*, 103.

(19) Marder, S. R.; Cheng, L. T.; Tiemann, B. G. *J. Chem. Soc., Chem. Commun.* **1992**, 672.

(20) Figueras, J.; Scullard, P. W.; Mack, A. R. *J. Org. Chem.* **1971**, *36*, 3497.

(21) Takahashi, S.; Kuroyama, Y.; Sonogashira, K.; Hagihara, N. *Synthesis* **1980**, 627.

(22) Vogel, A. *Textbook of Practical Organic Chemistry*, 4th ed.; Longman: London, 1978.

(23) Touchard, D.; Haquette, P.; Pirio, N.; Toupet, L.; Dixneuf, P. H. *Organometallics* **1993**, *12*, 3132.

(24) Bruce, M. I.; Wallis, R. C. *Aust. J. Chem.* **1979**, *32*, 1471.

(25) Whittall, I. R.; Humphrey, M. G.; Houbrechts, S.; Persoons, A.; Hockless, D. C. R. *Organometallics* **1996**, *15*, 5738.

(26) McDonagh, A. M., *Honours Thesis*, Australian National University, **1995**.

(27) Hodge, A. J.; Ingham, S. L.; Kakkar, A. K.; Khan, M. S.; Lewis, J.; Long, N. J.; Parker, D. G.; Raithby, P. R. *J. Organomet. Chem.* **1995**, *488*, 205.

(28) McDonagh, A. M.; Whittall, I. R.; Humphrey, M. G.; Skelton, B. W.; White, A. H. *J. Organomet. Chem.* **1996**, *519*, 229.

(29) Bruce, M. I.; Hameister, C.; Swincer, A. G.; Wallis, R. C. *Inorg. Synth.* **1982**, *21*, 78.

(30) Chaudret, B.; Commenges, G.; Poilblanc, R. *J. Chem. Soc., Dalton Trans.* **1984**, 1635.

(31) Bruce, M. I.; Nicholson, B. K.; bin Shawkataly, O. *Inorg. Synth.* **1989**, *26*, 324.

(32) teXsan: *Single Crystal Structure Analysis Software, Version 1.7-3*, Molecular Structure Corporation, The Woodlands, TX (1995).

(33) Stähelin, M.; Burland, D. M.; Rice, J. E. *Chem. Phys. Lett.* **1992**, *191*, 245.

(34) Clays, K.; Persoons, A. *Rev. Sci. Instrum.* **1992**, *63*, 3285.

(35) Houbrechts, S.; Clays, K.; Persoons, A.; Pikramenou, Z.; Lehn, J.-M. *Chem. Phys. Lett.* **1996**, *258*, 485.

Chapter 4

Branched Ruthenium Acetylide Complexes and Some of Their Nonlinear Optical Properties

Contents

Chapter 4

Branched Ruthenium Acetylide Complexes and Some of Their Nonlinear Optical Properties

4.1. Introduction

The traditional approach to the design of materials with enhanced molecular second-order optical nonlinearities has been to use molecules with extended π systems and significant molecular dipoles. This strategy was adopted in the design of the complexes presented in Chapters 2 and 3. Although there are many such molecules that exhibit large second-order optical nonlinearities, there are some disadvantages to this design approach. There is often a trade-off between the NLO efficiency and the optical transparency of these materials.[1] The proclivity of dipolar molecules to adopt centrosymmetric packing in the solid state (as in the examples in Section 3.4. and 1.4.1. where the dipoles align anti-parallel) is also a problem, as centrosymmetric packing in the bulk phase precludes macroscopic second-order optical nonlinearities. Furthermore, the symmetry of dipolar molecules often leads to small off-diagonal tensor components[2] of β (a brief description of the tensorial nature of hyperpolarizabilities is given in Section 1.2.1.).

Multipolar molecules may be effective in overcoming these problems. Molecules with no dipoles to "anti-align" are more likely to pack in a non-centrosymmetric fashion than dipolar molecules. Contributions to β from off-diagonal tensorial components may lead to significant second-order nonlinearities in octopolar molecules without loss of optical transparency.[3] Figure 4.1. shows some examples of multipolar arrangements of charges. Recent investigations have highlighted the potential of octopolar second-order NLO materials.[1,4-20] Although studies of organic multipolar systems have dominated the area, NLO measurements of the octopolar ruthenium complex shown in Figure 4.2. revealed a very large β_{HRS} value of 2200×10^{-30} esu when measured at 1320 nm. A recent report[21]

has, however, questioned whether the significant nonlinearity is attributable to octopolar or dipolar contributions.

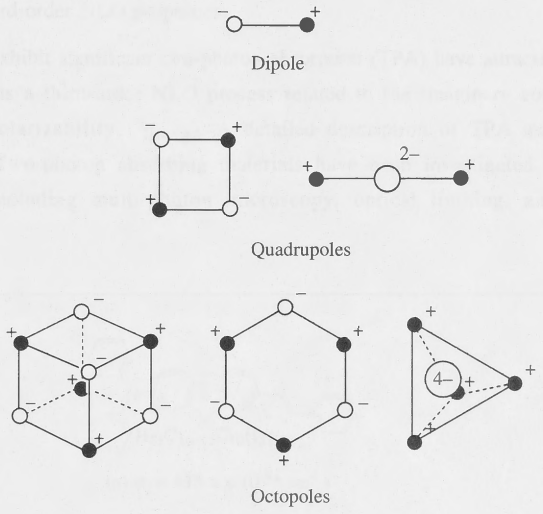

Figure 4.1. Some examples of multipolar arrangements of charges.

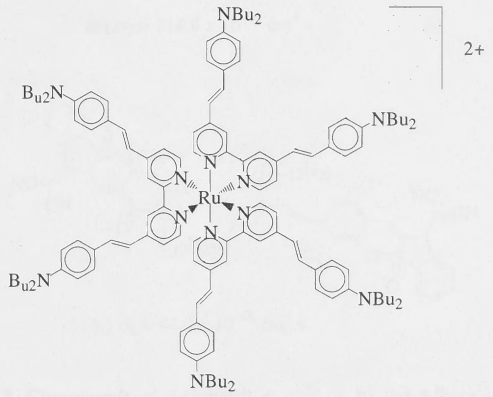

Figure 4.2. Ruthenium complex of Dhenaut *et al*[4] with $\beta_{HRS} = 2200 \times 10^{-30}$ esu.

There are few reports on the cubic optical nonlinearities of multipolar materials.[22,23] Greve *et al*[22] suggested that multidirectional charge-transfer transitions may induce large changes in electric moments higher than dipole moments. Such changes upon excitation may lead to enhanced third-order NLO properties.

Materials that exhibit significant two-photon absorption (TPA) have attracted some interest recently (TPA is a third-order NLO process related to the imaginary component of the second-hyperpolarizability, γ_{imag}). A detailed description of TPA may be found in reference 24. Two-photon absorbing materials have been investigated for a range of applications, including multi-photon microscopy, optical limiting, and optical data storage.[25]

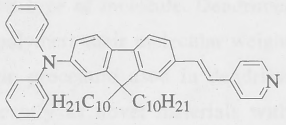

(a) $\sigma_2 = 115.6 \times 10^{-48}$ cm^4 s

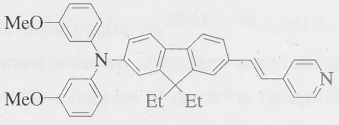

(b) $\sigma_2 = 114.8 \times 10^{-48}$ cm^4 s

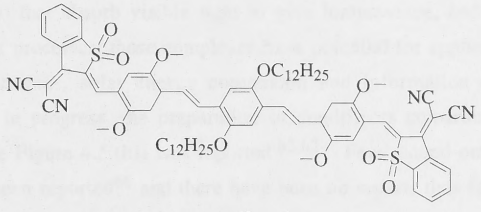

(c) $\sigma_2 = 44.0 \times 10^{-48}$ cm^4 s

Figure 4.3. Compounds of Reinhardt *et al*[26] (a, b) and Albota *et al*[27] (c) with large TPA cross-sections.

Recent studies have aimed at uncovering structure / property relationships for the two-photon absorbing characteristics of organic compounds.[26-29] Albota *et al*[27] suggested that π-conjugated molecules with large changes in quadrupole moment upon excitation are worthy of examination as TPA materials. In these studies, molecules with electron rich π-delocalized systems of varying geometries have been shown to have large TPA cross sections (see Figure 4.3.).

It is of interest, therefore, to investigate materials that incorporate all of the features mentioned above, i.e. compounds with multipolar symmetry and large electron-rich systems of π-delocalization, and exhibiting strong charge-transfer transitions. One relatively new type of compound that can accommodate these requirements is the dendritic molecule or dendrimer.

The name 'dendrimer' (from the Greek *dendros* = tree and *meros* = part) reflects the branching structure of this type of molecule. Dendrimers are hyperbranched polymers, but unlike more traditional polymers their molecular weights are well-defined. This is a result of the stepwise synthetic procedure used in dendrimer preparation. They have excited considerable interest recently as novel materials with uses in medical diagnostics and possible applications in areas such as molecular recognition, catalysis and photoactive device engineering.[30-32] Since the first report of 'cascade'-type compounds by Vögtle and co-workers[33] in 1978, a wide variety of dendritic structures has been reported. A number of reviews of the field have been published,[30-32,34-38] including reviews of metal-containing dendrimers.[39-42] The *meta*-connected phenylene-acetylene dendrimers prepared by Moore and co-workers[43-49] provide examples of dendritic molecules which contain large systems of π-delocalization (see Figure 4.4.). Transition metal-containing dendrimers have been reported,[50-65] some examples of which are shown in Figures 4.5. and 4.6. Balzani and co-workers[39,58-61] have prepared dendrimers containing ruthenium and osmium metal centres (see Figure 4.6.(b)) that absorb visible light to give luminesence, and undergo reversible multielectron redox processes; these complexes have potential for applications in areas such as molecular electronics, solar energy conversion and information storage. While the current work was in progress, the preparation of dendrimers constructed from platinum-acetylide units (see Figure 4.5.(b)) was reported.[52,62] Few second-order NLO studies on dendrimers have been reported[66] and there have been no reports thus far on the third-order NLO properties of dendrimers.

The aim of the work presented in this Chapter is to develop synthetic routes into dendrimers containing extensive π-delocalized systems using electron-rich alkynylruthenium units, to measure both the second- and third-order optical nonlinearities, and to determine structure / NLO property relationships for these novel complexes.

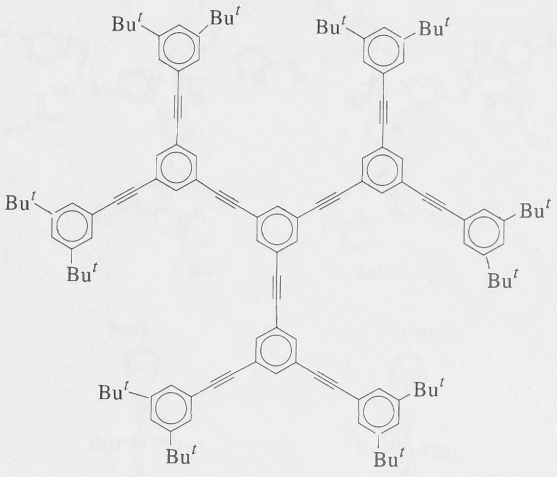

Figure 4.4. First generation phenylene-acetylene dendrimer prepared by Moore *et al.*[67]

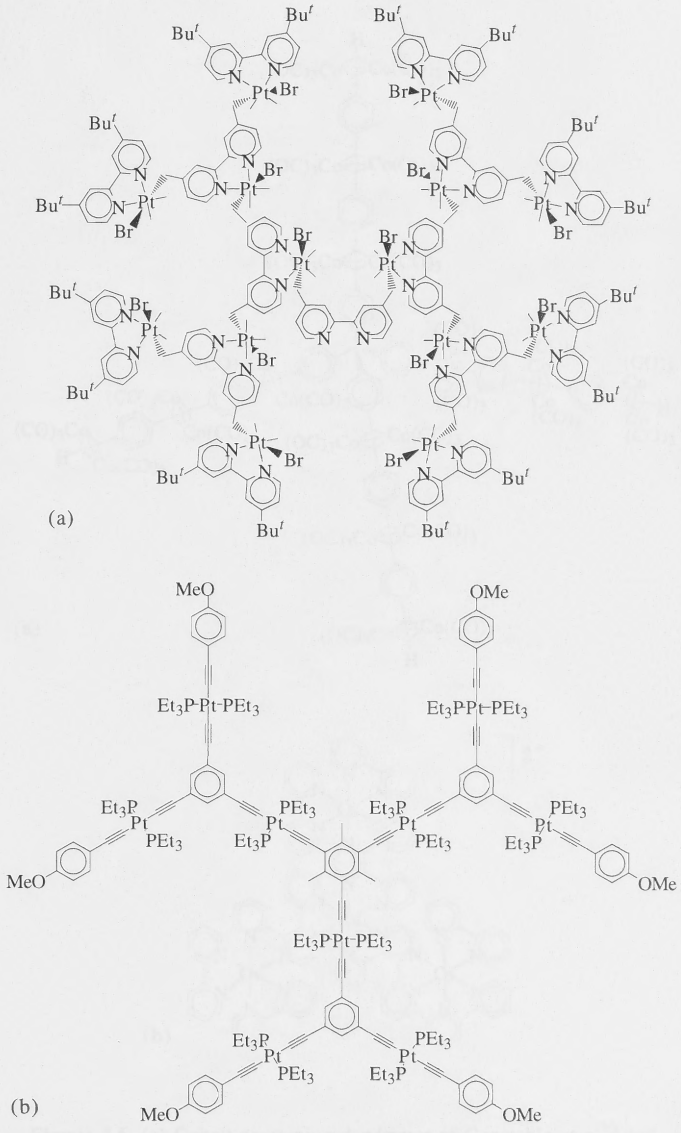

Figure 4.5. (a) Platinum-containing dendrimer of Puddephatt *et al*[53] and (b) platinum poly-yne dendrimer of Takahashi *et al*[52].

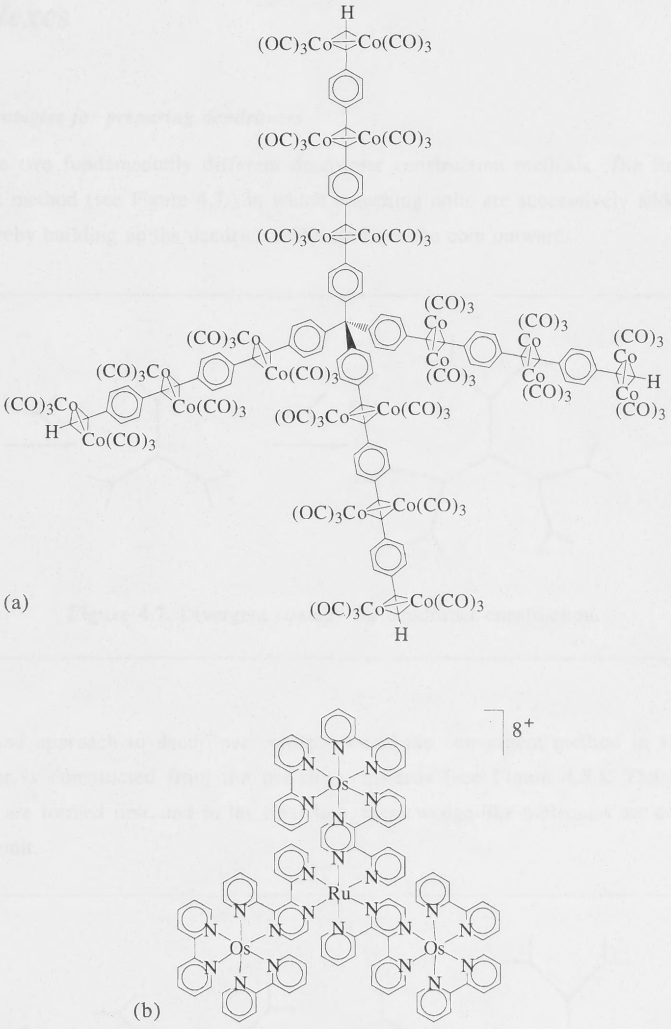

Figure 4.6. (a) Cobalt-containing dendrimer of Constable *et al*[50] and (b) osmium / ruthenium-containing dendrimer of Balzani *et al*[60].

4.2. Synthesis of branched ruthenium acetylide complexes

4.2.1. Strategies for preparing dendrimers

There are two fundamentally different dendrimer construction methods. The first is the divergent method (see Figure 4.7.) in which branching units are successively added to the core, thereby building up the dendritic molecule from the core outwards.

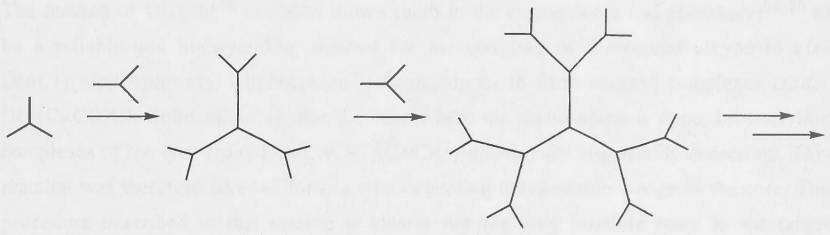

Figure 4.7. Divergent strategy for dendrimer construction.

The second approach to dendrimer construction is the convergent method in which the dendrimer is constructed from the periphery inwards (see Figure 4.8.). The dendritic branches are formed first, and in the final step, these wedge-like molecules are coupled to the core unit.

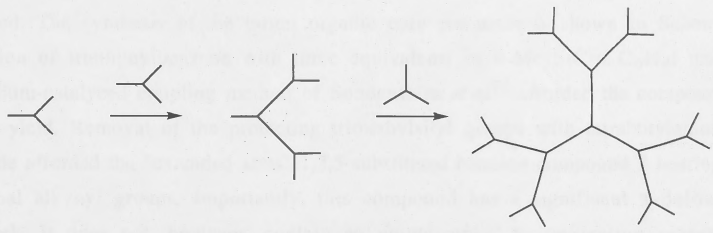

Figure 4.8. Convergent strategy for dendrimer construction.

A disadvantage of the divergent method is that defects that may form in the end-groups by incomplete reaction are propagated through to subsequent generations. Physical separation of these defective molecules is difficult because they differ only slightly from the non-defective molecules. In contrast, the convergent method is more favourable for the separation of defective units because such molecules differ significantly from the non-defective units. A disadvantage of the convergent method is the limited number of generations possible because of steric problems when coupling large wedges to a core. Because low generation, non-defective dendrimers were targeted in the current work, a convergent approach was adopted.

4.2.2. Synthesis of branched ruthenium acetylide complexes

The method of Dixneuf[68] has been shown (both in the current work and elsewhere)[68-76] to be a reliable and high-yielding method for the coupling of a terminal alkyne to *cis*-$[RuCl_2(diphosphine)_2]$ (diphosphine = dppm, dppe) to form alkynyl complexes *trans*-$[Ru(C{\equiv}CR)Cl(diphosphine)_2]$. For the case where the diphosphine is dppe, bis-acetylide complexes of the type *trans*-$[Ru(C{\equiv}CR^1)(C{\equiv}CR^2)(dppe)_2]$ are also readily accessible. This reaction was therefore adopted for use when coupling the dendritic wedge to the core. The procedure described in this section is clearly not the only possible route to the target molecules utilizing this alkynyl complex synthesis methodology, but it was found to be successful and therefore deveoped. An alternative synthesis, which was found to afford the desired reaction intermediates with by-products that were difficult to separate, was also explored, and subsequently rejected; it is discussed in more depth in section 4.2.4.

The first stage in the successful dendrimer synthesis was to prepare the organic skeleton of the dendrimer core. It has been reported by Whittall *et al*[77] that 1,3,5-triethynylbenzene is too small to accommodate three *trans*-$Ru(dppm)_2$ moietes around it; only two could be coupled. However, three $Au(PPh_3)$ units could be coordinated *via* ethynyl linkages to 1,3,5-triethynylbenzene, showing that the problem for the ruthenium complex was indeed steric. By extending the arms of the triethynylbenzene core, the steric congestion should be relieved. The synthesis of the target organic core precursor is shown in Scheme 4.1. Reaction of triethynylbenzene with three equivalents of $4\text{-}Me_3SiC{\equiv}CC_6H_4I$ using the palladium-catalyzed coupling method of Sonogashira *et al*[78] afforded the compound **8** in 71 % yield. Removal of the protecting trimethylsilyl groups with tetrabutylammonium fluoride afforded the "extended-arms" 1,3,5-substituted benzene compound **9** bearing three terminal alkynyl groups. Importantly, this compound has a significant π-delocalized network. It does not, however, contain an uninterrupted π-conjugation system, the conjugation being disrupted by the 1,3,5-substitution at the central benzene ring. Compounds **8** and **9** were characterized by mass spectrometry, IR and ^1H NMR

spectroscopy. The IR spectra of **8** and **9** show the characteristic ν(C≡C) at 2156 and 2106 cm^{-1}, respectively, and the H-C stretching band at 3296 cm^{-1} in the spectrum of **9**. The ^{1}H NMR spectra of **8** contains resonances at 0.24 ppm, assigned to the methyl protons, 7.44 ppm, assigned to the protons of the disubstituted rings, and 7.61 ppm, assigned to the protons of the central, trisubstituted ring. The ^{1}H NMR spectra of **9** is similar to that of **8** but with a signal at 3.17 ppm, assigned to the terminal alkyne, replacing that of the methyl groups observed in **8**.

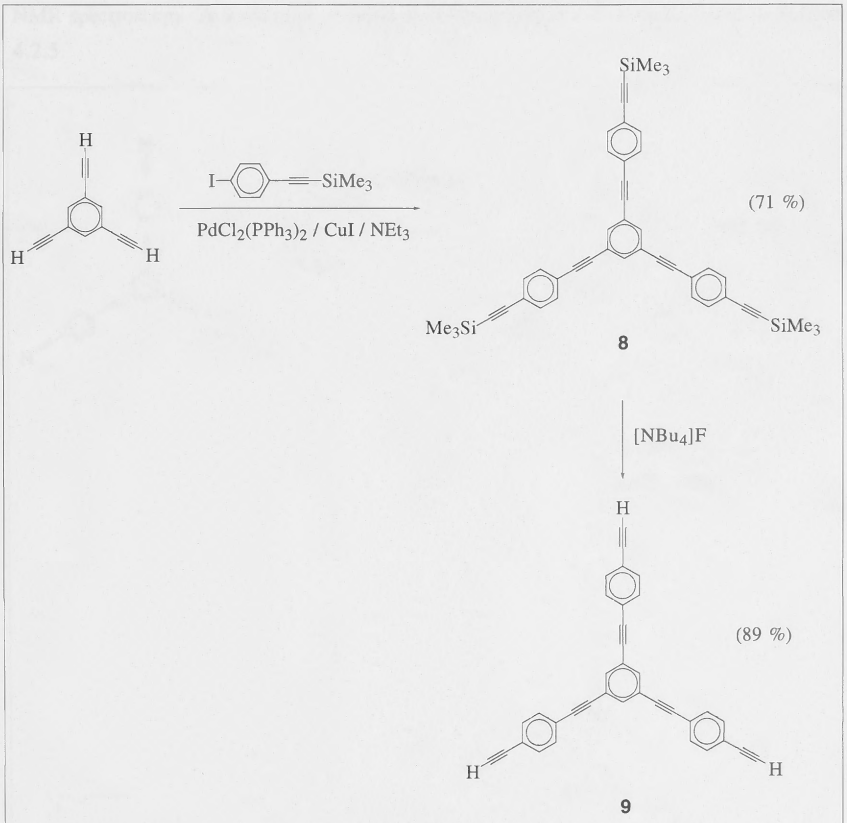

Scheme 4.1. Synthesis of the organic core compound.

The organometallic core complex was prepared by the reaction of *cis*-$[RuCl_2(dppe)_2]$, sodium hexafluorophosphate and **9** in dichloromethane at room temperature (see Scheme 4.2.). The ligand dppe was chosen in favour of dppm because trials showed that bis-acetylide complexes were more easily formed when the former ligand was coodinated to the metal centre (an important requirement for subsequent steps in dendrimer preparation). The intermediate vinylidene complex was not isolated, but deprotonated with base *in situ* to afford the complex **10** in 68 % yield. The new acetylide complex was characterized by FAB mass spectrometry, satisfactory microanalysis, UV-vis and IR spectroscopy, ^{1}H, ^{31}P and ^{13}C NMR spectroscopy. A discussion of selected characterization data may be found in Section 4.2.5.

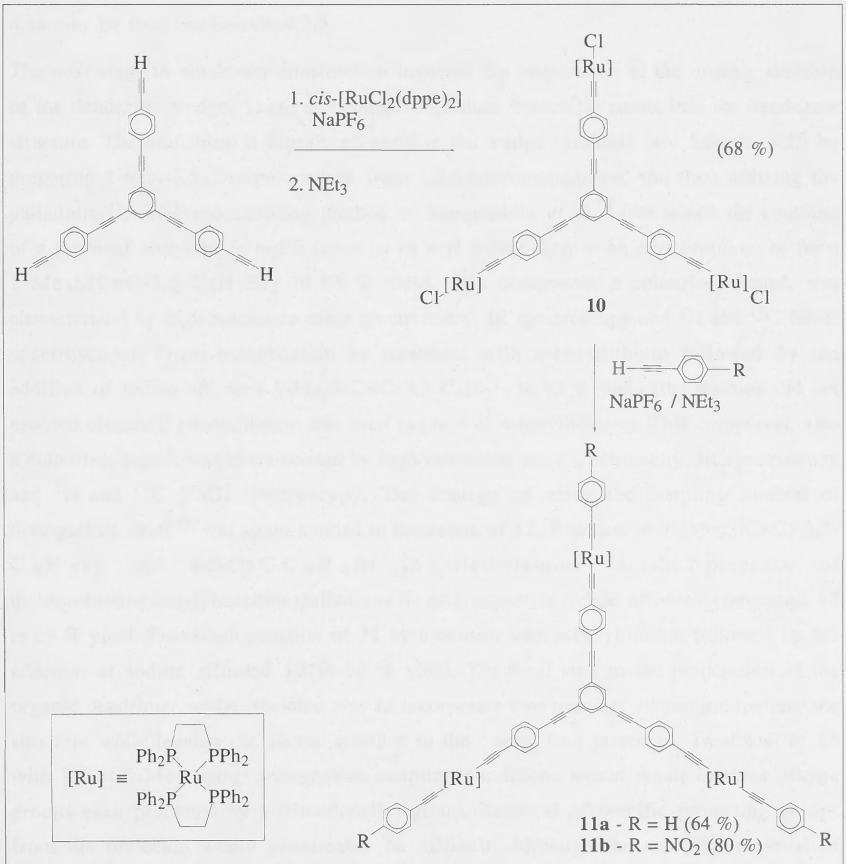

Scheme 4.2. Synthesis of **10** and **11a,b**.

The reaction of **10**, sodium hexafluorophosphate, triethylamine and 4-HC≡CC_6H_4R in dichloromethane (see Scheme 4.2.) afforded the complexes **11a** (R = H) and **11b** (R = NO_2) in 64 and 80 % yield, respectively. These new complexes with three bis(acetylide)ruthenium centres enable a comparison of physical data to be made with the targeted dendrimer complexes described below, which also have every ruthenium centre in a bis(acetylide) environment. Comparison of physical data of **11(a, b)** with **10** provides an opportunity to examine the effect of extending the π-delocalization through the metal centre. Comparison of **a** complexes with **b** complexes enables assessment of the effect of including an electron acceptor group on physical properties. Complexes **11(a, b)** were characterized by FAB mass spectrometry, satisfactory microanalyses, UV-vis and IR spectroscopy, ^1H, ^{31}P and ^{13}C NMR spectroscopy. A discussion of selected characterization data may be found in Section 4.2.5.

The next stage in dendrimer construction involved the preparation of the organic skeleton of the dendrimer wedge. These components introduce branching points into the dendrimer structure. The branching is introduced early in the wedge synthesis (see Scheme 4.3.) by preparing 1-iodo-3,5-dibromobenzene from 1,3,5-tribromobenzene, and then utilizing the palladium(II)-catalyzed coupling method of Sonogashira *et al.*[78] (for which the coupling of a terminal acetylene is much faster to an aryl iodide than to an aryl bromide) to form 1-Me_3SiC≡C-3,5-$C_6H_3Br_2$ in 93 % yield. This compound, a colourless liquid, was characterized by high resolution mass spectrometry, IR spectroscopy and ^1H and ^{13}C NMR spectroscopy. *Trans*-halogenation by treatment with *n*-butyllithium followed by the addition of iodine afforded 1-Me_3SiC≡C-3,5-$C_6H_3I_2$ in 93 % yield (the reaction did not proceed cleanly if *t*-butyllithium was used in place of *n*-butyllithium). This compound, also a colourless liquid, was characterized by high resolution mass spectrometry, IR spectroscopy and ^1H and ^{13}C NMR spectroscopy. The strategy of using the coupling method of Sonogashira *et al.*[78] was again applied in formation of **12**. Reaction of 1-(Me_3SiC≡C)-3,5-$C_6H_3I_2$ and 4-HC≡CC_6H_4Br in triethylamine in the presence of dichlorobis(triphenylphosphine)palladium(II) and copper(I) iodide afforded compound **12** in 69 % yield. *Trans*-halogenation of **12** by treatment with *n*-butyllithium followed by the addition of iodine afforded **13** in 82 % yield. The final step in the preparation of the organic dendrimer wedge skeleton was to incorporate two terminal alkyne groups into the structure while leaving the alkyne attached to the central ring protected. Treatment of **13** with HC≡C$SiMe_3$ using Sonogashira coupling conditions would result in three alkyne groups each protected by a trimethylsilyl group. Removal of specific protecting groups from the molecule would presumably be difficult. Although the selective removal of different silyl protecting groups (e.g. $SiMe_3$ and $SiPr^i_3$) from compounds containing multiple protected alkynes has been reported,[79,80] a more straightforward procedure for

incorporating a terminal alkyne directly onto an aryl iodide has been reported recently by Negishi *et al.*[81] Use of this method involves the preparation of Zn(C≡CH)Br *in situ* from Mg(C≡CH)Br and $ZnBr_2$. Addition of the aryl iodide **13** and dichlorobis(triphenylphosphine)palladium(II) afforded the compound **14** in 50 % yield. Compounds **12**, **13** and **14** were characterized by high resolution mass spectrometry, UV-vis and IR spectroscopy, and ^1H and ^{13}C NMR spectroscopy. Characterization data for these compounds are shown in Tables 4.1. and 4.2. and an NMR numbering is shown in Figure 4.9.

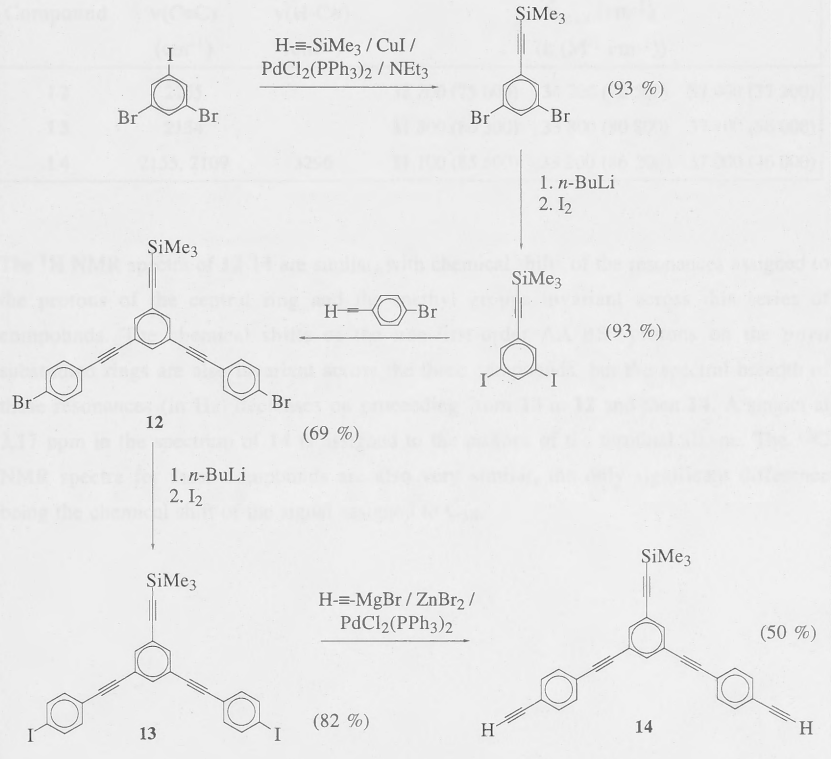

Scheme 4.3. Synthesis of the organic component of the dendrimer wedge.

The $\nu(C\equiv C)$ bands at 2154-5 cm^{-1} in **12-14** may be assigned to stretching modes associated with the $Me_3SiC\equiv C$ alkynyl groups by comparison with data obtained for compounds **8** and **9**. The $\nu(C\equiv C)$ band at 2109 cm^{-1} in the spectrum of **14** may similarly be assigned to the $HC\equiv C$ alkynyl groups with the C-H stretching band assigned to these groups observed at 3296 cm^{-1}. The UV-vis spectra for these compounds are similar, with strong absorption in the region associated with $\pi\rightarrow\pi^*$ transitions, and energies for these transitions decreasing upon progressing from **12** to **13** to **14**.

Table 4.1. IR and UV-vis data for **12-14**.

Compound	$\nu(C\equiv C)$ (cm^{-1})	$\nu(H\text{-}C\equiv)$ (cm^{-1})	$\bar{\nu}_{max}$ (cm^{-1}) (ε (M^{-1} cm^{-1}))		
12	2155		32 200 (75 600)	34 200 (72 500)	37 400 (37 200)
13	2154		31 800 (80 500)	33 800 (80 800)	37 100 (56 000)
14	2155, 2109	3296	31 100 (85 500)	33 200 (86 200)	37 000 (46 000)

The ^1H NMR spectra of **12-14** are similar, with chemical shifts of the resonances assigned to the protons of the central ring and the methyl groups invariant across this series of compounds. The chemical shifts of the non-first-order AA´BB´ protons on the *para* substituted rings are also invariant across the three compounds, but the spectral breadth of these resonances (in Hz) decreases on proceeding from **13** to **12** and then **14**. A singlet at 3.17 ppm in the spectrum of **14** is assigned to the protons of the terminal alkyne. The ^{13}C NMR spectra for these compounds are also very similar, the only significant difference being the chemical shift of the signal assigned to C_{38}.

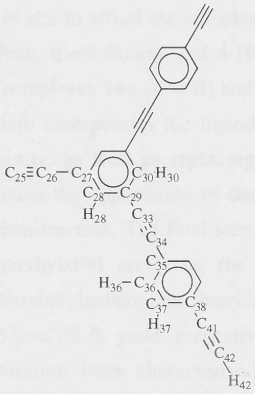

Figure 4.9. NMR numbering scheme for compounds **12**, **13** and **14**.

Table 4.2. NMR data for **12-14**.

Atom	^{1}H chemical shift (ppm)			^{13}C chemical shift (ppm)		
	12	**13**	**14**	**12**	**13**	**14**
Me	0.23	0.23	0.24	-0.2	-0.2	-0.2
25				103.0	103.0	103.0
26				96.0	96.0	96.0
27				124.0	124.0	124.0
28	7.57	7.56	7.57	134.5	134.5	134.6
29				123.6	123.6	123.6
30	7.58	7.58	7.60	134.1	134.1	134.2
33, 34				88.7, 89.4	89.0, 89.6	89.6, 89.9
35				121.6	122.2	122.2
36	m, 7.41	m, 7.44	m, 7.45	131.7	133.1	131.6
37	m, 7.41	m, 7.44	m, 7.45	133.0	137.6	132.1
38				122.9	94.6	123.1
41						83.1
42			3.17			79.1

The organometallic components of the wedge were introduced by reacting *cis*-$[RuCl_2(dppe)_2]$, sodium hexafluorophosphate and **14** in dichloromethane at room temperature (see Scheme 4.4.). The intermediate vinylidene complex was not isolated, but instead deprotonated with base *in situ* to afford the complex **15** in 66 % yield. The reaction of **15**, sodium hexafluorophosphate, triethylamine and 4-$HC{\equiv}CC_6H_4R$ in dichloromethane (see Scheme 4.4.) afforded the complexes **16a** (R = H) and **16b** (R = NO_2) in 71 and 85 % yield, respectively. This procedure incorporates the ligands that will eventually form the peripheral groups of the dendrimer, as well as replacing the chloro ligand on the two ruthenium centres thereby removing the opportunity of the wedge to couple with itself in the final step of the dendrimer construction. The final step in the wedge preparation is the removal of the protecting trimethylsilyl group by the treatment of dichloromethane solutions of **16a** and **16b** with tetrabutylammonium fluoride to give the complexes **17a** (R = H) and **17b** (R = NO_2) in 85 and 88 % yield, respectively. Each of the new acetylide complexes in the wedge preparation were characterized by FAB mass spectrometry, satisfactory microanalysis, UV-vis and IR spectroscopy, ^1H, ^{31}P and ^{13}C NMR spectroscopy. A discussion of selected characterization data may be found in Section 4.2.5.

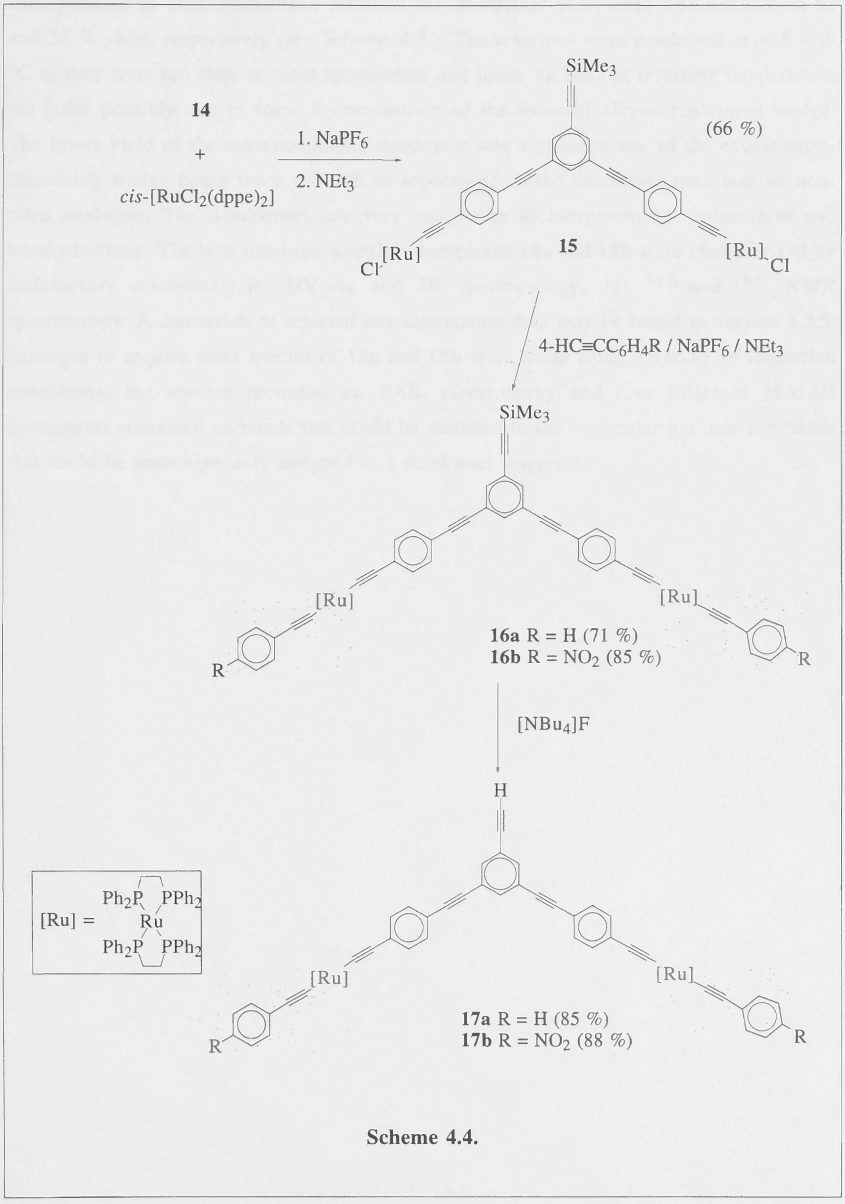
14
+
cis-[RuCl2(dppe)2]
1. NaPF6
2. NEt3
(66 %)
SiMe3
15
Cl
[Ru]
[Ru]
Cl
4-HC≡CC6H4R / NaPF6 / NEt3
SiMe3
[Ru]
[Ru]
R
R
16a R = H (71 %)
16b R = NO2 (85 %)
[NBu4]F
H
[Ru] =
Ph2P
PPh2
Ru
Ph2P
PPh2
[Ru]
[Ru]
R
R
17a R = H (85 %)
17b R = NO2 (88 %)

Scheme 4.4.

The reaction of **10** with three equivalents of **17a** or **17b**, sodium hexafluorophosphate and triethylamine in dichloromethane afforded the dendrimer complexes **18a** and **18b** in 52 and 32 % yield, respectively (see Scheme 4.5.). The reactions were conducted at ~35 - 38 °C as they were too slow at room temperature and lower yielding at refluxing temperature, the latter possibly due to some decomposition of the terminal alkyne-containing wedge. The lower yield of the nitro-containing dendrimer was a consequence of the excess nitro-containing wedge being more difficult to separate from the dendrimer than was its non-nitro analogue. The dendrimers are very soluble in dichloromethane, chloroform and tetrahydrofuran. The new dendritic acetylide complexes **18a** and **18b** were characterized by satisfactory microanalysis, UV-vis and IR spectroscopy, ^{1}H, ^{31}P and ^{13}C NMR spectroscopy. A discussion of selected characterization data may be found in Section 4.2.5. Attempts to acquire mass spectra of **18a** and **18b** were made using a variety of ionization conditions, but spectra recorded on FAB, electrospray and four different MALDI instruments contained no bands that could be assigned to the molecular ion, nor any bands that could be unambiguously assigned to a dendrimer fragment.

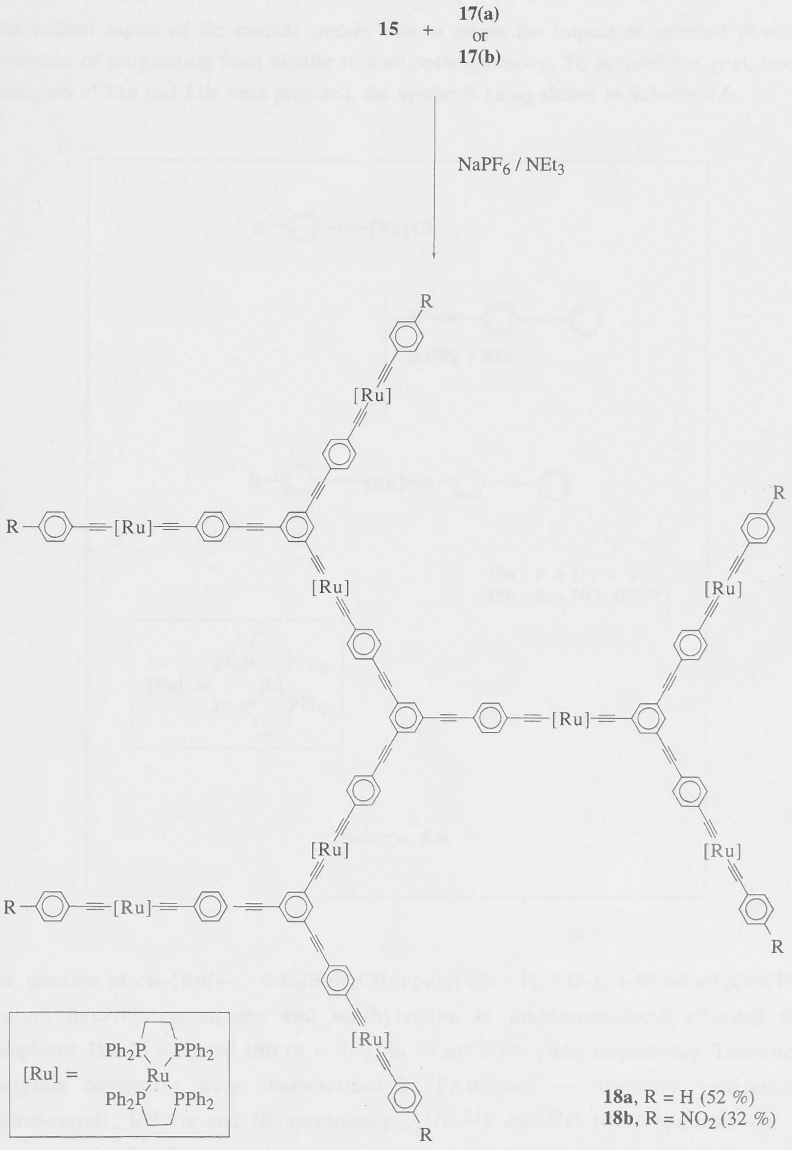
15 + 17(a) or 17(b)
NaPF6 / NEt3
[Ru] =
Ph2P PPh2
Ru
Ph2P PPh2
18a, R = H (52 %)
18b, R = NO2 (32 %)

Scheme 4.5.

4.2.3. Synthesis of linear ruthenium acetylide complexes

One critical aspect of the current studies was to assess the impact on selected physical properties of progressing from dipolar to multipolar geometry. To achieve this goal, linear analogues of **11a** and **11b** were prepared, the synthesis being shown in Scheme 4.6.

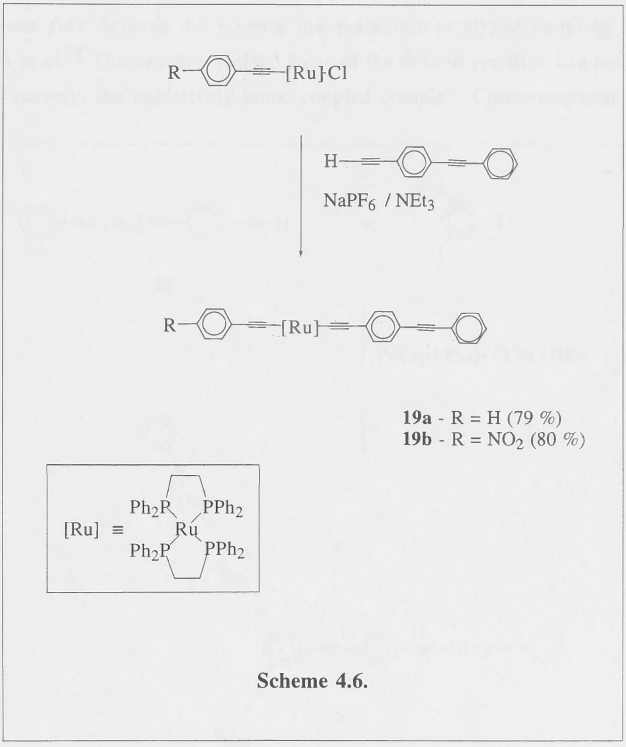

Scheme 4.6.

The reaction of *cis*-[Ru(4-C≡CC_6H_4R)Cl(dppe)$_2$] (R = H, NO_2), 4-HC≡C_6H_4C≡CPh, sodium hexafluorophosphate and triethylamine in dichloromethane afforded the complexes **19a** (R = H) and **19b** (R = NO_2) in 79 and 80 % yield, respectively. These new acetylide complexes were characterized by FAB mass spectrometry, satisfactory microanalysis, UV-vis and IR spectroscopy, ^{1}H, ^{31}P and ^{13}C NMR spectroscopy. A discussion of selected characterization data is included in Section 4.2.5.

4.2.4. An alternative synthetic procedure assayed for the preparation of branched acetylide complexes

As mentioned in Section 4.2., an alternative route to prepare branched ruthenium acetylide complexes was also investigated. This route uses 1,3,5-triiodobenzene as the core molecule. Problems with this proposed route became apparent when coupling complex **23** to 1,3,5-triiodobenzene (see Scheme 4.7.) using the palladium-catalyzed coupling reaction of Sonogashira *et al.*[78] This reaction yielded some of the desired complex **11a** but also gave a by-product, namely, the oxidatively homo-coupled complex. Chromatographic separation

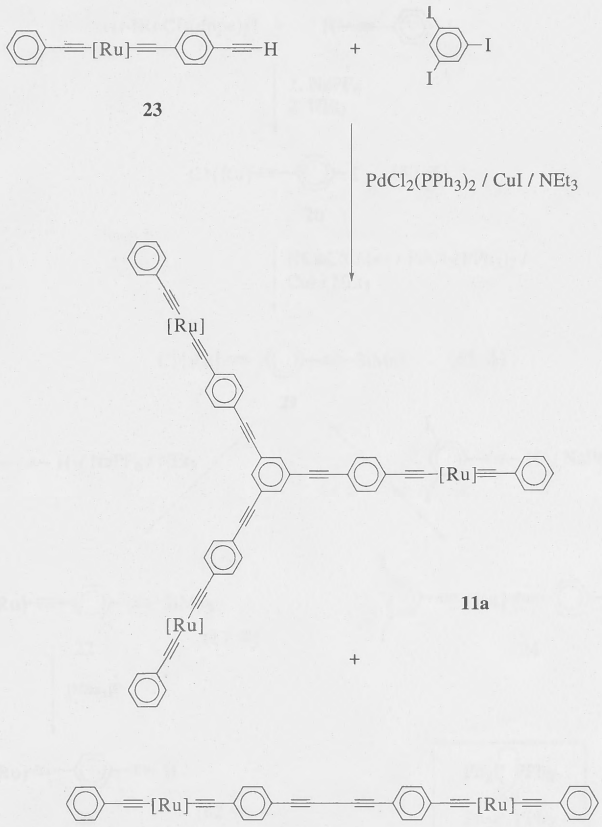

Scheme 4.7.

of these two complexes proved to be extremely difficult, only poor yields being obtained. The oxidative homo-coupling of terminal alkynes has been reported to proceed rapidly in the presence of palladium(II) and copper(I) catalysts and oxygen.[82] Procedures were therefore adopted to rigorously exclude oxygen from the reaction environment, but the oxidatively homo-coupled complex was still formed.

The proposed route to the dendrimer is outlined in Schemes 4.8. and 4.9. Thus, reaction of *cis*-[$RuCl_2(dppe)_2$], 4-HC≡CC_6H_4I and sodium hexafluorophosphate in dichloromethane afforded *trans*-[Ru(4-C≡CC_6H_4I)Cl(dppe)$_2$] (**20**) in 80 % yield (see Scheme 4.8).

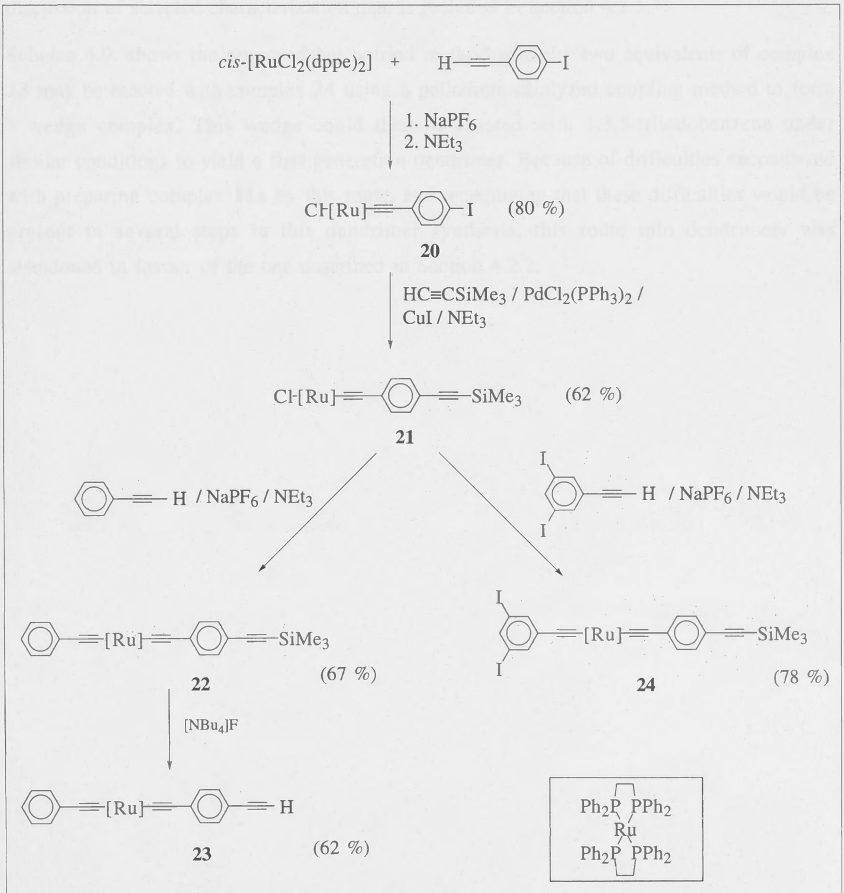

Scheme 4.8.

The reaction of **20** and trimethylsilylacetylene with catalytic amounts of dichlorobis(triphenylphosphine)palladium(II) and copper(I) iodide, and triethylamine, gave *trans*-[Ru(4-C≡CC_6H_4C≡C$SiMe_3$)Cl$(dppe)_2$] (**21**) in 62 % yield. Complex **21** could be reacted with either phenyacetylene or 1-HC≡C-3,5-$C_6H_3I_2$ in the presence of sodium hexafluorophosphate and triethylamine to afford the complexes **22** and **24** in 67 and 78 % yield, respectively. The trimethylsilyl protecting group was removed from complex **22** by treatment with tetrabutylammonium fluoride to afford complex **23** in 62 % yield. These new complexes were characterized by mass-spectrometry, satisfactory microanalyses (with the exception of **22**), UV-vis and IR spectroscopy, and ^1H and ^{31}P NMR spectroscopy. A discussion of selected characterization data is included in Section 4.2.5.

Scheme 4.9. shows the proposed but untried method whereby two equivalents of complex **23** may be reacted with complex **24** using a palladium-catalyzed coupling method to form a wedge complex. This wedge could then be reacted with 1,3,5-triiodobenzene under similar conditions to yield a first generation dendrimer. Because of difficulties encountered with preparing complex **11a** by this route, and recognizing that these difficulties would be present in several steps in this dendrimer synthesis, this route into dendrimers was abandoned in favour of the one described in Section 4.2.2.

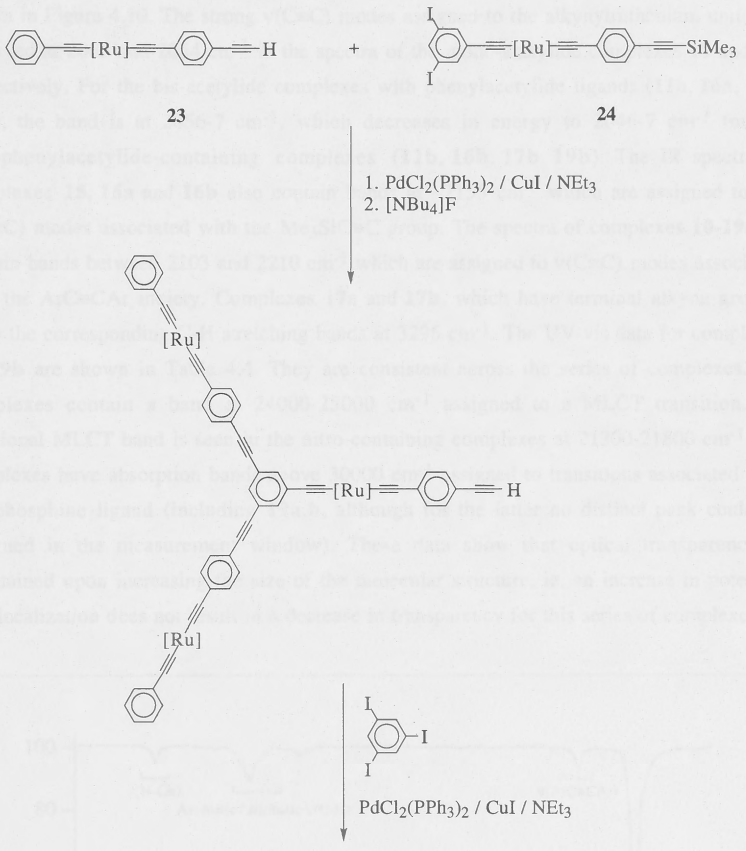
[Ru]
H
+
I
I
[Ru]
SiMe3
23
24
1. PdCl2(PPh3)2 / CuI / NEt3
2. [NBu4]F
[Ru]
[Ru]
[Ru]
H
I
I
I
PdCl2(PPh3)2 / CuI / NEt3
18a

Scheme 4.9.

4.2.5. Physical properties of acetylide complexes

The IR data for complexes **10-19b** are gathered in Table 4.3 and the spectrum of **17a** is shown in Figure 4.10. The strong ν(C≡C) modes assigned to the alkynylruthenium units are observed at 2065 and 2064 cm^{-1} in the spectra of the mono-acetylide complexes **10** and **15**, respectively. For the bis-acetylide complexes with phenylacetylide ligands (**11a**, **16a**, **17a**, **19a**), the band is at 2056-7 cm^{-1}, which decreases in energy to 2046-7 cm^{-1} for the nitrophenylacetylide-containing complexes (**11b**, **16b**, **17b**, **19b**). The IR spectra of complexes **15**, **16a** and **16b** also contain bands at ~2155 cm^{-1} which are assigned to the ν(C≡C) modes associated with the $Me_3SiC{\equiv}C$ group. The spectra of complexes **10-19a** all contain bands between 2203 and 2210 cm^{-1} which are assigned to ν(C≡C) modes associated with the ArC≡CAr moiety. Complexes **17a** and **17b**, which have terminal alkyne groups, show the corresponding C-H stretching bands at 3296 cm^{-1}. The UV-vis data for complexes **10-19b** are shown in Table 4.4. They are consistent across the series of complexes. All complexes contain a band at 24000-25000 cm^{-1} assigned to a MLCT transition. An additional MLCT band is seen in the nitro-containing complexes at 21300-21800 cm^{-1}. All complexes have absorption bands above 30000 cm^{-1} assigned to transitions associated with the phosphine ligand (including **19a**,**b**, although for the latter no distinct peak could be assigned in the measurement window). These data show that optical transparency is maintained upon increasing the size of the molecular structure, ie. an increase in potential π-delocalization does not result in a decrease in transparency for this series of complexes.

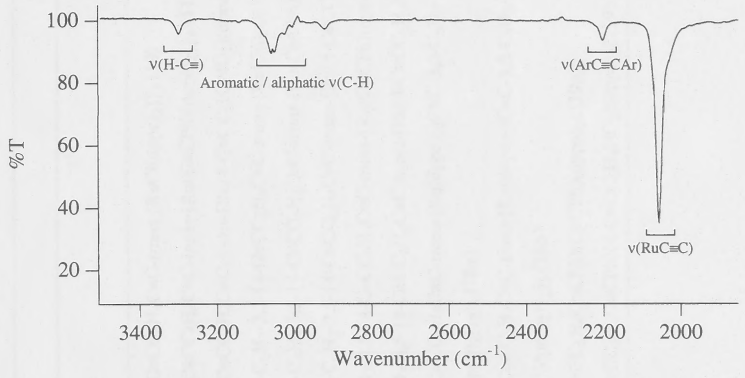

Figure 4.10. IR spectrum of complex **17a**.

Table 4.3. IR data for **10**-**19b**.

Compound	ν(RuC≡C) (cm^{-1})	ν(Me_3SiC≡C) (cm^{-1})	ν(ArC≡CAr) (cm^{-1})	ν(H-C≡) (cm^{-1})
1,3,5-C_6H_3{4-C≡CC_6H_4C≡C-*trans*-[RuCl(dppe)$_2$]}$_3$ (**10**)	2065		2204	
1,3,5-C_6H_3{4-C≡CC_6H_4C≡C-*trans*-[Ru(C≡CPh)(dppe)$_2$]}$_3$ (**11a**)	2057		2203	
1,3,5-C_6H_3{4-C≡CC_6H_4C≡C-*trans*-[Ru(4-C≡$CC_6H_4NO_2$)(dppe)$_2$]}$_3$ (**11b**)	2047		2204	
1-(Me_3SiC≡C)-C_6H_3-3,5-{4-C≡CC_6H_4C≡C-*trans*-[RuCl(dppe)$_2$]}$_2$ (**15**)	2064	2156	2205	
1-(Me_3SiC≡C)-C_6H_3-3,5-{4-C≡CC_6H_4C≡C-*trans*-[Ru(C≡CPh)(dppe)$_2$]}$_2$ (**16a**)	2057	2156	2204	
1-(Me_3SiC≡C)-C_6H_3-3,5-{4-C≡CC_6H_4C≡C-*trans*-[Ru(4-C≡$CC_6H_4NO_2$)(dppe)$_2$]}$_2$ (**16b**)	2047	2155	2206	
1-(HC≡C)-C_6H_3-3,5-{4-C≡CC_6H_4C≡C-*trans*-[Ru(C≡CPh)(dppe)$_2$]}$_2$ (**17a**)	2057		2202	3296
1-(HC≡C)-C_6H_3-3,5-{4-C≡CC_6H_4C≡C-*trans*-[Ru(4-C≡$CC_6H_4NO_2$)(dppe)$_2$]}$_2$ (**17b**)	2047		2204	3296
1,3,5-C_6H_3(4-C≡CC_6H_4C≡C-*trans*-[Ru(dppe)$_2$]C≡C-3,5-C_6H_3-{4-C≡CC_6H_4C≡C-*trans*-[Ru(C≡CPh)(dppe)$_2$]}$_2$)$_3$ (**18a**)	2056		2204	
1,3,5-C_6H_3(4-C≡CC_6H_4C≡C-*trans*-[Ru(dppe)$_2$]C≡C-3,5-C_6H_3-{4-C≡CC_6H_4C≡C-*trans*-[Ru(4-C≡$CC_6H_4NO_2$)(dppe)$_2$]}$_2$)$_3$ (**18b**)	2047		2206	
trans-[Ru(4-C≡CC_6H_4C≡CPh)(C≡CPh)(dppe)$_2$] (**19a**)	2056		2210	
trans-[Ru(4-C≡CC_6H_4C≡CPh)(4-C≡$CC_6H_4NO_2$)(dppe)$_2$] (**19b**)	2046			

Table 4.4. UV-vis data for **10-19b**.

Compound	$\tilde{\nu}_{max}$ (cm^{-1}) (ε (10^4 M^{-1} cm^{-1}))			
1,3,5-C_6H_3{4-C≡CC_6H_4C≡C-*trans*-[RuCl(dppe)$_2$]}$_3$ (**10**)		24 200 (9.9)	33 300 (6.6)	40 000 (13.7)
1,3,5-C_6H_3{4-C≡CC_6H_4C≡C-*trans*-[Ru(C≡CPh)(dppe)$_2$]}$_3$ (**11a**)		24 300 (11.6)	31 740 (9.8)	
1,3,5-C_6H_3{4-C≡CC_6H_4C≡C-*trans*-[Ru(4-C≡$CC_6H_4NO_2$)(dppe)$_2$]}$_3$ (**11b**)	21 800 (8.9)	24 800 (1.1)	32 700 (9.2)	41 000 (17.9)
1-(Me_3SiC≡C)-C_6H_3-3,5-{4-C≡CC_6H_4C≡C-*trans*-[RuCl(dppe)$_2$]}$_2$ (**15**)		24 300 (7.3)	33 400 (sh, 5.1)	39 900 (11.7)
1-(Me_3SiC≡C)-C_6H_3-3,5-{4-C≡CC_6H_4C≡C-*trans*-[Ru(C≡CPh)(dppe)$_2$]}$_2$ (**16a**)		24 500 (7.5)	32 100 (7.0)	
1-(Me_3SiC≡C)-C_6H_3-3,5-{4-C≡CC_6H_4C≡C-*trans*-[Ru(4-C≡$CC_6H_4NO_2$)(dppe)$_2$]}$_2$ (**16b**)	21 700 (5.9)	24 900 (7.1)	32 700 (sh, 5.9)	37 800 (9.4)
1-(HC≡C)-C_6H_3-3,5-{4-C≡CC_6H_4C≡C-*trans*-[Ru(C≡CPh)(dppe)$_2$]}$_2$ (**17a**)		24 600 (8.1)	32 000 (7.2)	
1-(HC≡C)-C_6H_3-3,5-{4-C≡CC_6H_4C≡C-*trans*-[Ru(4-C≡$CC_6H_4NO_2$)(dppe)$_2$]}$_2$ (**17b**)	21 600 (6.2)	25 000 (7.4)	32 500 (sh, 6.3)	
1,3,5-C_6H_3(4-C≡CC_6H_4C≡C-*trans*-[Ru(dppe)$_2$]C≡C-3,5-C_6H_3-{4-C≡CC_6H_4C≡C-*trans*-[Ru(C≡CPh)(dppe)$_2$]}$_2$)$_3$ (**18a**)		24 900 (42.1)	32 200 (29.1)	
1,3,5-C_6H_3(4-C≡CC_6H_4C≡C-*trans*-[Ru(dppe)$_2$]C≡C-3,5-C_6H_3-{4-C≡CC_6H_4C≡C-*trans*-[Ru(4-C≡$CC_6H_4NO_2$)(dppe)$_2$]}$_2$)$_3$ (**18b**)	21 400 (sh, 16.0)	25 300 (35.0)	32 700 (sh, 24.1)	
trans-[Ru(4-C≡CC_6H_4C≡CPh)(C≡CPh)(dppe)$_2$] (**19a**)		26 200 (3.8)		
trans-[Ru(4-C≡CC_6H_4C≡CPh)(4-C≡$CC_6H_4NO_2$)(dppe)$_2$] (**19b**)	21 300 (2.5)	26 800 (3.4)		

The ^{1}H NMR data for complexes **10-19b** are gathered in Table 4.5. and a numbering scheme is displayed in Figure 4.11. Not surprisingly, most of the signals observed are invariant across this series of complexes. One useful spectroscopic probe is the signal assigned to the protons adjacent to the nitro group, H_{47}, which are remote from the rest of the phenyl resonances in complexes **11b**, **16b**, **17b**, **18b**, **19b**.

The ^{1}H and ^{31}P NMR data for complexes **20-24** are shown in Table 4.6. All of the ^{1}H NMR spectra for these complexes contain resonances assigned to the protons of the ethylene bridge at ~2.6 ppm and resonances at ~6.9 to between 7.44 and 7.68 ppm which are assigned to the phenyl protons. The proton resonances of the trimethylsilyl groups are invariant for the complexes **21**, **22** and **24**. The chemical shift of the signal assigned to H_{11} moves downfield on progressing from complex **20** to **21**. Introduction of a second acetylide ligand moves this signal further downfield with the signals at 6.54, 6.58 and 6.69 ppm being tentatively assigned to H_{20} in complexes **22**, **23** and **24**, respectively, and the resonances at 6.79 ppm being assigned to H_{11}. The ^{31}P NMR spectra of the mono-acetylide complexes **20** and **21** contain the expected singlet resonances at ~50 ppm, while resonances at ~54 ppm are observed for the bis-acetylide complexes **22**, **23** and **24**.

In the UV-vis spectrum of **20**, a band assigned to the MLCT transition from the ruthenium atom to the acetylide ligand is observed at 29400 cm^{-1}. Replacing iodine with the trimethylsilyl-protected alkynyl group on progressing from **20** to **21** leads to a decrease in the energy of this transition, the MLCT band being observed at 27000 cm^{-1} for the complexes **21**, **22** and **24**. Replacement of the trimethylsilyl group with a proton on progressing from **22** to **23** leads to an increase in energy on the MLCT transition of ~700 cm^{-1}. The IR spectrum of **20** contains the expected $\nu(C{\equiv}C)$ mode associated with alkynylruthenium unit at 2068 cm^{-1}. This band is also observed in the spectra of complexes **21** and **22** at ~2060 cm^{-1}, together with a second band assigned to the $\nu(C{\equiv}C)$ mode associated with the $Me_3SiC{\equiv}C$ unit at 2148 cm^{-1}. Only one band is observed in the spectrum of complex **23** at 2057 cm^{-1}. Three bands are observed in the spectrum of complex **24**, those at 2046 and 2060 cm^{-1} being assigned to the alkynylruthenium modes and the one at 2149 cm^{-1} is assigned to the $Me_3SiC{\equiv}C$ unit.

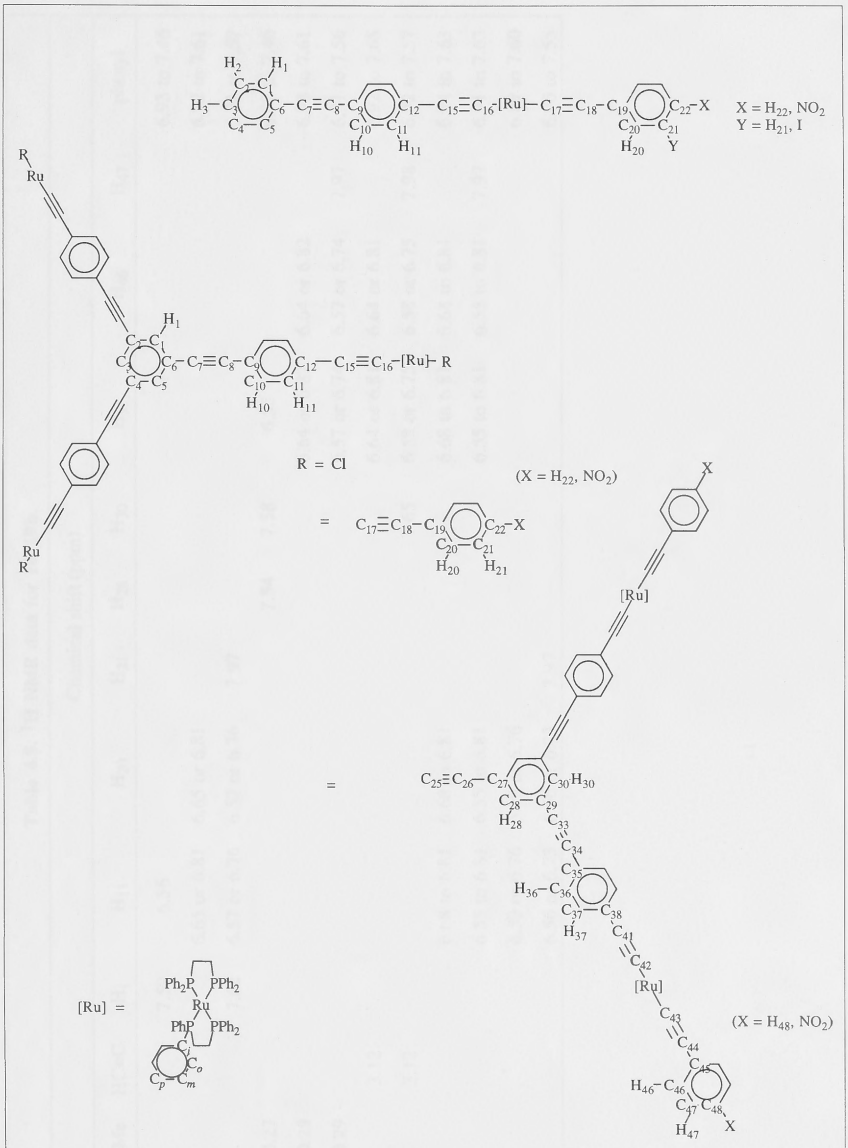

Figure 4.11. NMR numbering scheme for linear and branched compounds

Table 4.5. ^{1}H NMR data for **10-19b**.

Compound	Chemical shift (ppm)												
	CH_2	Me	HC≡C	H_1	H_{11}	H_{20}	H_{21}	H_{28}	H_{30}	H_{37}	H_{46}	H_{47}	phenyl
10	2.69			7.59	6.56								6.93 to 7.46
11a	2.63				6.65 or 6.81	6.65 or 6.81							6.92 to 7.61
11b	2.63			7.62	6.57 or 6.76	6.57 or 6.76	7.97						6.91 to 7.57
15	2.68	0.27						7.54	7.58	6.55			6.92 to 7.46
16a	2.63	0.29								6.64 or 6.82	6.64 or 6.82		6.93 to 7.61
16b	2.63	0.29								6.57 or 6.74	6.57 or 6.74	7.97	6.91 to 7.56
17a	2.63		3.12							6.64 or 6.81	6.64 or 6.81		6.92 to 7.65
17b	2.63		3.12						7.65	6.58 or 6.75	6.58 or 6.75	7.98	6.92 to 7.57
18a	2.64				6.68 to 6.81	6.68 to 6.81				6.68 to 6.81	6.68 to 6.81		6.94 to 7.63
18b	2.64				6.55 to 6.81	6.55 to 6.81				6.55 to 6.81	6.55 to 6.81	7.97	6.91 to 7.63
19a	2.61				6.59 or 6.76	6.59 or 6.76							6.89 to 7.60
19b	2.61				6.56 or 6.73	6.56 or 6.73	7.97						6.90 to 7.55

Table 4.6. ^{1}H and ^{31}P NMR data for **20**-**24**.

Complex	Chemical shift (ppm)						
	CH_2	Me	C≡CH	H_{11}	H_{20}	Ph	^{31}P
trans-[Ru(4-C≡CC_6H_4I)Cl(dppe)$_2$] (**20**)	2.63			6.30		6.90 to 7.44	50.1
trans-[Ru(4-C≡CC_6H_4C≡C$SiMe_3$)Cl(dppe)$_2$] (**21**)	2.66	0.24		6.46		6.87 to 7.40	49.8
trans-[Ru(4-C≡CC_6H_4C≡C$SiMe_3$)(C≡CPh)(dppe)$_2$] (**22**)	2.60	0.24		6.54 or 6.79	6.54 or 6.79	6.88 to 7.60	54.4
trans-[Ru(4-C≡CC_6H_4C≡CH)(C≡CPh)(dppe)$_2$] (**23**)	2.60		3.09	6.58 or 6.79	6.58 or 6.79	6.89 to 7.59	54.5
trans-[Ru(4-C≡CC_6H_4C≡C$SiMe_3$)(3,5-C≡C$C_6H_3I_2$)(dppe)$_2$] (**24**)	2.55	0.24		6.69 or 6.79	6.69 or 6.79	6.92 to 7.68	54.2

4.3. *Nonlinear optical investigations*

4.3.1. Results of second-order nonlinear optical measurements

Measurements of the first hyperpolarizability, β, of complexes **10**, **11**(**a**, **b**), **15-19**(**a**, **b**) and *trans*-[Ru(C≡CPh)Cl(dppe)$_2$], together with the organic compounds **8**, **12-14**, were performed at 1064 nm using the hyper-Rayleigh scattering technique (see Section 1.3.5.) by collaborators at the University of Leuven, Belgium and at RIKEN, Japan. The data are presented in Table 4.6.

The first hyperpolarizability data in Table 4.7. are reported as the square-roots of the rotational averages. In the HRS experiment, measurements of the rotational averages, $\langle\beta^2\rangle$, are made, where the angled brackets indicate averaging over all possible orientations in an isotropic solution. For one-dimensional dipolar molecules (such as those examined in Chapters 2 and 3), only the diagonal tensor component, β_{333}, is significant, so that $\beta = \beta_{333}$. In octopolar molecules, there are other non-vanishing tensor components, so that $\sqrt{\langle\beta^2\rangle} \neq \beta_{333}$. This property may also be used to obtain information about the symmetry of the molecule being measured. Depolarization measurements involve measuring the intensity of the scattered second-harmonic light parallel, $I_{zz}^{2\omega}$, and perpendicular, $I_{zx}^{2\omega}$, to the plane of the incident polarized laser beam. The ratio of these two quantities is dependant on the molecular symmetry. For dipolar molecules with C_{2v} symmetry,

$$\rho = \frac{I_{zz}^{2\omega}}{I_{zx}^{2\omega}} = 5$$

and for octopolar molecules with symmetry D_{3h} or C_{3h}

$$\rho = \frac{I_{zz}^{2\omega}}{I_{zx}^{2\omega}} = 1.5.$$

Depolarization measurements were undertaken by collaborators in RIKEN, Japan and were obtained for complexes **10** and **11a**. No β values were collected for the complex **19b** because a quadratic signal (with respect to the fundamental intensity) was not observed. Complex **10** was measured at both locations with consistent results, although a slightly lower value was obtained using the set-up at RIKEN, Japan.

Table 4.7. Results of hyper-Rayleigh scattering experiments.

Compound	$\tilde{\nu}_{max}$ (cm^{-1}) (ε (10^4 M^{-1} cm^{-1}))	$\sqrt{\langle\beta^2\rangle}$ [a] (10^{-30} esu)	$\rho = \frac{I_{zz}^{2\omega}}{I_{zx}^{2\omega}}$
1,3,5-C_6H_3(C≡C-4-C_6H_4C≡CSiMe_3) (**8**)	29 200 (0.5)	8[b]	
1,3,5-C_6H_3\{4-C≡CC_6H_4C≡C-*trans*-[RuCl(dppe)$_2$]\}$_3$ (**10**)	24 200 (9.9)	94[b] / 115	1.4 ± 0.2[b]
1,3,5-C_6H_3\{4-C≡CC_6H_4C≡C-*trans*-[Ru(C≡CPh)(dppe)$_2$]\}$_3$ (**11a**)	24 300 (11.6)	93[b]	2.1 ± 0.2[b]
1,3,5-C_6H_3\{4-C≡CC_6H_4C≡C-*trans*-[Ru(4-C≡C$C_6H_4NO_2$)(dppe)$_2$]\}$_3$ (**11b**)	21 800 (8.9)	1220	
1-(Me_3SiC≡C)-C_6H_3-3,5-(4-C≡CC_6H_4Br)$_2$ (**12**)	32 200 (7.6)	5.8	
1-(Me_3SiC≡C)-C_6H_3-3,5-(4-C≡CC_6H_4I)$_2$ (**13**)	31 800 (8.1)	8.9	
1-(Me_3SiC≡C)-C_6H_3-3,5-(4-C≡CC_6H_4C≡CH)$_2$ (**14**)	31 100 (8.6)	8.4	
1-(Me_3SiC≡C)-C_6H_3-3,5-\{4-C≡CC_6H_4C≡C-*trans*-[RuCl(dppe)$_2$]\}$_2$ (**15**)	24 300 (7.3)	101	
1-(Me_3SiC≡C)-C_6H_3-3,5-\{4-C≡CC_6H_4C≡C-*trans*-[Ru(C≡CPh)(dppe)$_2$]\}$_2$ (**16a**)	24 500 (7.5)	105	
1-(Me_3SiC≡C)-C_6H_3-3,5-\{4-C≡CC_6H_4C≡C-*trans*-[Ru(4-C≡C$C_6H_4NO_2$)(dppe)$_2$]\}$_2$ (**16b**)	21 700 (5.9)	900	
1-(HC≡C)-C_6H_3-3,5-\{4-C≡CC_6H_4C≡C-*trans*-[Ru(C≡CPh)(dppe)$_2$]\}$_2$ (**17a**)	24 600 (8.1)	104	
1-(HC≡C)-C_6H_3-3,5-\{4-C≡CC_6H_4C≡C-*trans*-[Ru(4-C≡C$C_6H_4NO_2$)(dppe)$_2$]\}$_2$ (**17b**)	21 600 (6.2)	1120	
1,3,5-C_6H_3(4-C≡CC_6H_4C≡C-*trans*-[Ru(dppe)$_2$]C≡C-3,5-C_6H_3-\{4-C≡CC_6H_4C≡C-*trans*-[Ru(C≡CPh)(dppe)$_2$]\}$_2$)$_3$ (**18a**)	24 900 (42.1)	160	
1,3,5-C_6H_3(4-C≡CC_6H_4C≡C-*trans*-[Ru(dppe)$_2$]C≡C-3,5-C_6H_3-\{4-C≡CC_6H_4C≡C-*trans*-[Ru(4-C≡C$C_6H_4NO_2$)(dppe)$_2$]\}$_2$)$_3$ (**18b**)	21 400 (sh, 16.0)	1880	
trans-[Ru(4-C≡CC_6H_4C≡CPh)(C≡CPh)(dppe)$_2$] (**19a**)	26 200 (3.8)	34[b]	
trans-[Ru(4-C≡CC_6H_4C≡CPh)(4-C≡C$C_6H_4NO_2$)(dppe)$_2$] (**19b**)	21 300 (2.5)	[c]	
trans-[Ru(C≡CPh)Cl(dppe)$_2$]	31 300 (1.8)	6[b]	

[a] All measurements performed at 1064 nm in tetrahydrofuran solvent, values ± 10 %.

[b] Measurement performed at RIKEN, Japan. [c] Quadratic signal (with respect to the fundamental itensity) not observed.

4.3.2. Discussion of second-order nonlinear optical results

The complexes bearing no nitro-substituents have absorption bands far from the second harmonic wavelength of 532 nm (see Figure 4.12. for UV-vis spectra of **11a** and **18a**), permitting assessment of the impact of structural variation on quadratic NLO merit. Incorporation of the ligated metal fragment in proceeding from the organic acetylenes **8** and **14** to the organometallic complexes **10** and **15** leads to a significant increase in β_{HRS}. Extending the delocalized π-system through the metal in progressing from **10** to **11a** and **15** to **16a**, though, is ineffective in increasing β, indicating that the *trans*-phenylalkynyl ligand is acting largely as a π-donor ligand (it has been reported that phenylalkynyl ligands are pseudo-halides in complexes of this type);[83] a similar lack of β enhancement on extending the π-system through a metal has been reported recently in a dipolar system.[84] Complex **19a** is a linear fragment of the octopolar complex **11a**, and also of the wedge complexes **16a** and **17a**. Not surprisingly, then, progressing from **19a** to **11a** results in a three-fold increase in oscillator strength of the UV-vis band assigned to the MLCT transition while progressing from **19a** to **16a** or **17a** results in a two-fold increase in the same parameter. Importantly, the quadratic NLO merit of two-dimensional complex **11a** is significantly improved compared to the one-dimensional complexes **19a** and *trans*-[Ru(C≡CPh)Cl(dppe)$_2$], with little loss of optical transparency (in progressing from **19a** to

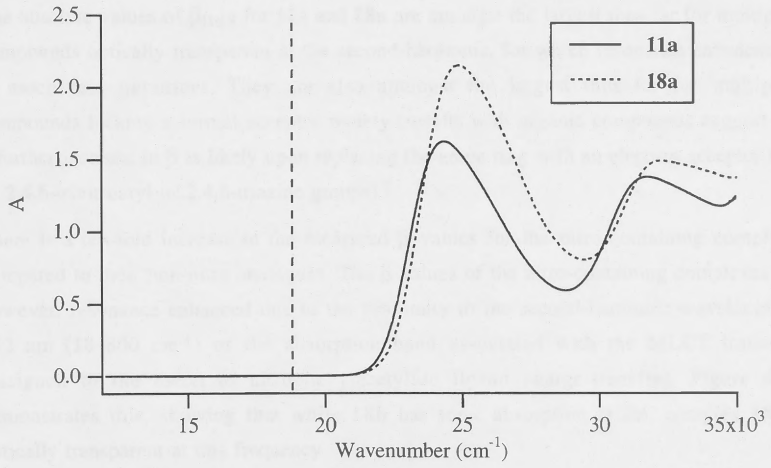

Figure 4.12. UV-vis spectra of **11a** and **18a**. The vertical dotted line indicates the second-harmonic frequency.

11a) accompanying the large increase in β. A similar increase in β is also seen in complexes **16a** and **17a**, although these complexes contain only two metal centres compared with three for **11a**.

The depolarization ratio of 1.4 for complex **10** is within experimental error of the ideal value of 1.5 expected for purely octopolar symmetry. Complex **11a** has a depolarization ratio of 2.1, a value larger than that expected for a molecule with octopolar symmetry. This increased value may result from a deviation from octopolar symmetry, most likely a lack of coplanarity of the arylethynyl groups. A decrease in molecular symmetry would result in an increase in ρ, as dipolar contributions to the first hyperpolarizability are introduced.

The dendrimer **18a** results from the coupling of **10** and **17a**. While its β value is larger than that of either of the component complexes, it is not substantially so, given that it contains nine metal centres, compared to three or two for the components. Improvements in nonlinearity in dipolar systems are usually accompanied by a loss in optical transparency. The present "multipolar" system is significant, then, in that there is no loss in transparency on progressing from **11a** to **18a**. In fact, a small gain in transparency is seen, which may indicate that the dendritic complex **18a** has a non-planar geometry. This onset of non co-planarity is consistent with the general observation that, upon increasing the size of dendritic systems, the initially planar disposition will eventually become a globular array. Unfortunately, depolarization measurements have not been obtained for the dendrimers.

The absolute values of β_{HRS} for **11a** and **18a** are amongst the largest thus far for multipolar compounds optically transparent at the second-harmonic, for which resonance enhancement is much less important. They are also amongst the largest thus far for multipolar compounds lacking a formal acceptor moiety (results with organic compounds suggest that a further increase in β is likely upon replacing the arene ring with an electron acceptor such as 2,4,6-trinitroaryl or 2,4,6-triazine groups).[9]

There is a ten-fold increase in the measured β values for the nitro-containing complexes compared to their non-nitro analogues. The β values of the nitro-containing complexes are, however, resonance enhanced due to the proximity to the second-harmonic wavelength of 532 nm (18 800 cm^{-1}) of the absorption band associated with the MLCT transition (assigned to the metal to nitrophenylacetylide ligand charge-transfer). Figure 4.13. demonstrates this, showing that while **18b** has some absorption at 2ω, complex **18a** is optically transparent at this frequency.

Complexes **16b** and **17b**, which both contain two metal-centres, possess similar β values. Only a small increase in β is observed on progressing to the three metal-centre complex

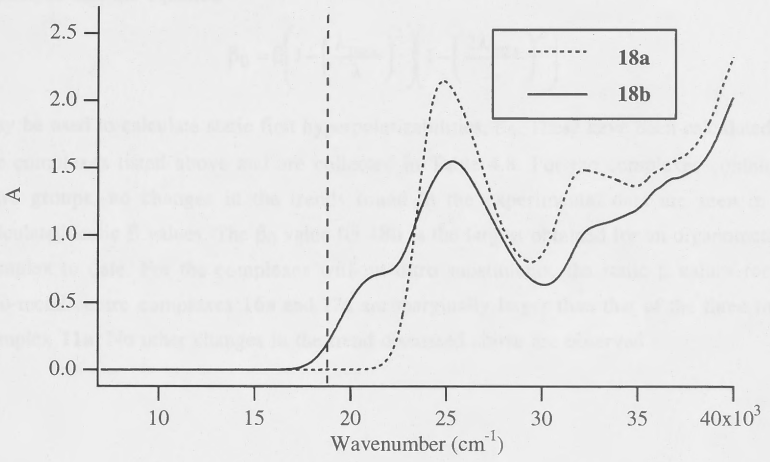

Figure 4.13. UV-vis spectra of **18a** and **18b**. The vertical dotted line indicates the second-harmonic frequency.

11b, a similar trend to that observed for the non-nitro analogues. A 50 % gain in β is found on progessing from **11b** to the nine metal-centre dendrimer **18b**. The β value of 1880 × 10^{-30} esu for the latter is quite large, comparable to that of the inorganic complex of Dhenaut *et al*[4] displayed in Figure 4.2., but, as mentioned above, this is due in part to resonance enhancement. The method used to calculate static β values discussed in Section 2.7.1. was based on the two-level description of β. However, the term Δμ, which is the difference between the ground and excited state dipole moment, must be zero for octopolar molecules. A three-level model has been proposed[85] that incorporates a doubly degenerate excited state with a dipole allowed transition between the ground and the excited states. Due to the degeneracy of the excited states, an expression for β_0 is obtained which resembles the two-level expression, so that (excluding constants),

$$\beta \propto \frac{\omega_{eg} f \mu_{1\bar{1}}}{\left(\omega_{eg}^2 - \omega^2\right)\left(\omega_{eg}^2 - (2\omega)^2\right)}$$

where ω_{eg} is the frequency of the optical transition, f is the oscillator strength, ω is the frequency of the exciting radiation, and $\mu_{1\bar{1}}$ is the transition dipole moment between the

two degenerate excited states. The resonant term is the simple expression from the two-level model, so that the equation

$$\beta_0 = \beta\left(1-\left(\frac{\lambda_{max}}{\lambda}\right)^2\right)\left(1-\left(\frac{2\lambda_{max}}{\lambda}\right)^2\right)$$

may be used to calculate static first hyperpolarizabilities, β_0. These have been calculated for the complexes listed above and are collected in Table 4.8. For the complexes containing nitro groups, no changes in the trends found in the experimental data are seen in the calculated static β values. The β_0 value for **18b** is the largest obtained for an organometallic complex to date. For the complexes without nitro substituents, the static β values for the two-metal-centre complexes **16a** and **17a** are marginally larger than that of the three-metal complex **11a**. No other changes in the trend discussed above are observed.

Table 4.8. Experimental and static first hyperpolarizabilities.

Compound	$\tilde{\nu}_{max}$ (cm^{-1})	$\sqrt{\langle\beta^2\rangle}$ [a] (10^{-30} esu)	$\sqrt{\langle\beta_0^2\rangle}$ (10^{-30} esu)
1,3,5-C_6H_3{4-C≡CC_6H_4C≡C-*trans*-[RuCl(dppe)$_2$]}$_3$ (**10**)	24 200	94[b] / 115	32 / 39
1,3,5-C_6H_3{4-C≡CC_6H_4C≡C-*trans*-[Ru(C≡CPh)(dppe)$_2$]}$_3$ (**11a**)	24 300	93[b]	31
1,3,5-C_6H_3{4-C≡CC_6H_4C≡C-*trans*-[Ru(4-C≡$CC_6H_4NO_2$)(dppe)$_2$]}$_3$ (**11b**)	21 800	1220	254
1-(Me_3SiC≡C)-C_6H_3-3,5-{4-C≡CC_6H_4C≡C-*trans*-[RuCl(dppe)$_2$]}$_2$ (**15**)	24 300	101	34
1-(Me_3SiC≡C)-C_6H_3-3,5-{4-C≡CC_6H_4C≡C-*trans*-[Ru(C≡CPh)(dppe)$_2$]}$_2$ (**16a**)	24 500	105	37
1-(Me_3SiC≡C)-C_6H_3-3,5-{4-C≡CC_6H_4C≡C-*trans*-[Ru(4-C≡$CC_6H_4NO_2$)(dppe)$_2$]}$_2$ (**16b**)	21 700	900	182
1-(HC≡C)-C_6H_3-3,5-{4-C≡CC_6H_4C≡C-*trans*-[Ru(C≡CPh)(dppe)$_2$]}$_2$ (**17a**)	24 600	104	37
1-(HC≡C)-C_6H_3-3,5-{4-C≡CC_6H_4C≡C-*trans*-[Ru(4-C≡$CC_6H_4NO_2$)(dppe)$_2$]}$_2$ (**17b**)	21 600	1120	220
1,3,5-C_6H_3(4-C≡CC_6H_4C≡C-*trans*-[Ru(dppe)$_2$]C≡C-3,5-C_6H_3-{4-C≡CC_6H_4C≡C-*trans*-[Ru(C≡CPh)(dppe)$_2$]}$_2$)$_3$ (**18a**)	24 900	160	59
1,3,5-C_6H_3(4-C≡CC_6H_4C≡C-*trans*-[Ru(dppe)$_2$]C≡C-3,5-C_6H_3-{4-C≡CC_6H_4C≡C-*trans*-[Ru(4-C≡$CC_6H_4NO_2$)(dppe)$_2$]}$_2$)$_3$ (**18b**)	21 400 (sh)	1880	350
trans-[Ru(4-C≡CC_6H_4C≡CPh)(C≡CPh)(dppe)$_2$] (**19a**)	26 200	34[b]	14
trans-[Ru(C≡CPh)Cl(dppe)$_2$]	31 300	6[b]	3

[a] All measurements performed at 1064 nm, values ± 10 %.

[b] Measurement performed at RIKEN, Japan.

4.3.3. Results of third-order nonlinear optical measurements

Measurements of third-order optical nonlinearities were performed at the Australian National University using the Z-scan technique (see Section 1.3.8.) operating at 800 nm. The results are presented in Table 4.9. The linear complex **19b** was not measured because it was insufficiently soluble in a range of suitable solvents.

Figure 4.14. shows experimental data plots from the Z-scan experiment on solutions of **11b**. A tightly focussed laser beam provides a gradient of intensity, with the greatest intensity at the focus, z = 0 (the Gaussian beam spot size radius at the focus is about 49 μm). The upper set of curves in Figure 4.14. shows the open aperture experiment for various concentrations. They reveal a significant increase in absorption with increasing beam intensity (i. e. there is a reduction in transmittance as the sample approaches z = 0). This is indicative of two-photon absorption (TPA). From these curves, the nonlinear absorption coefficient β_2, and the related imaginary part of γ, may be calculated. The TPA cross-section, σ_2, may also be calculated from β_2; σ_2 values are included in Table 4.9. to

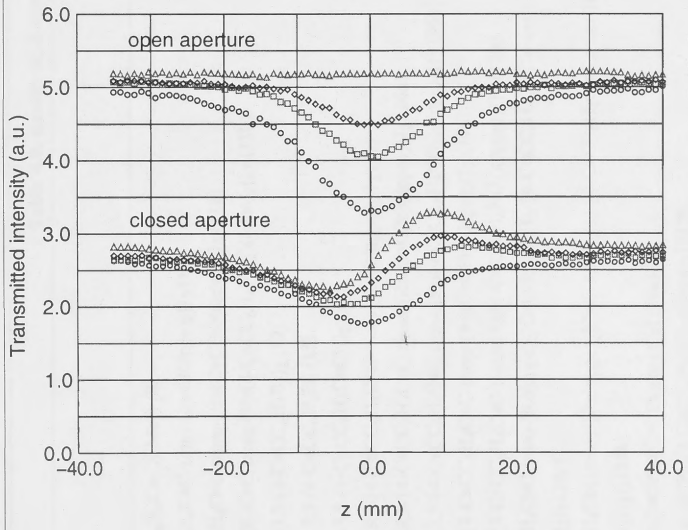

Figure 4.14. Z-scan measurements on solutions of **11b**. The $1/e^2$ Gaussian beam spot size radius at the focus, w_0, is about 49 μm.

Table 4.9. Results of Z-scan experiments.

Compound	$\tilde{\nu}_{max}$ (cm^{-1}) (ε (10^4 M^{-1} cm^{-1}))	γ_{real} (10^{-36} esu)	γ_{imag} (10^{-36} esu)	σ_2[a] (10^{-50} cm^4 s)
1,3,5-C_6H_3($C\equiv C$-4-$C_6H_4C\equiv CSiMe_3$) (**8**)	29200 (0.5)	95 ± 20	0	0
1,3,5-C_6H_3\{4-$C\equiv CC_6H_4C\equiv C$-*trans*-[RuCl(dppe)$_2$]\}$_3$ (**10**)	24200 (9.9)	-330 ± 100	2200 ± 500	530 ± 100
1,3,5-C_6H_3\{4-$C\equiv CC_6H_4C\equiv C$-*trans*-[Ru($C\equiv$CPh)(dppe)$_2$]\}$_3$ (**11a**)	24300 (11.6)	-600 ± 200	2900 ± 500	700 ± 120
1,3,5-C_6H_3\{4-$C\equiv CC_6H_4C\equiv C$-*trans*-[Ru(4-$C\equiv CC_6H_4NO_2$)(dppe)$_2$]\}$_3$ (**11b**)	21800 (8.9)	-5000 ± 1000	5600 ± 1000	1300 ± 200
1-($Me_3SiC\equiv C$)-C_6H_3-3,5-(4-$C\equiv CC_6H_4Br$)$_2$ (**12**)	32 200 (7.6)	53 ± 20	5 ± 3	1 ± 1
1-($Me_3SiC\equiv C$)-C_6H_3-3,5-(4-$C\equiv CC_6H_4I$)$_2$ (**13**)	31 800 (8.1)	77 ± 30	4 ± 3	1 ± 1
1-($Me_3SiC\equiv C$)-C_6H_3-3,5-(4-$C\equiv CC_6H_4C\equiv CH$)$_2$ (**14**)	31 100 (8.6)	67 ± 30	7 ± 5	2 ± 1
1-($Me_3SiC\equiv C$)-C_6H_3-3,5-\{4-$C\equiv CC_6H_4C\equiv C$-*trans*-[RuCl(dppe)$_2$]\}$_2$ (**15**)	24300 (7.3)	-510 ± 500	4700 ± 1500	1100 ± 360
1-($Me_3SiC\equiv C$)-C_6H_3-3,5-\{4-$C\equiv CC_6H_4C\equiv C$-*trans*-[Ru($C\equiv$CPh)(dppe)$_2$]\}$_2$ (**16a**)	24500 (7.5)	-700 ± 100	2270 ± 300	550 ± 70
1-($Me_3SiC\equiv C$)-C_6H_3-3,5-\{4-$C\equiv CC_6H_4C\equiv C$-*trans*-[Ru(4-$C\equiv CC_6H_4NO_2$)(dppe)$_2$]\}$_2$ (**16b**)	21700 (5.9)	-5200 ± 1000	5200 ± 1000	1300 ± 250
1-($HC\equiv C$)-C_6H_3-3,5-\{4-$C\equiv CC_6H_4C\equiv C$-*trans*-[Ru($C\equiv$CPh)(dppe)$_2$]\}$_2$ (**17a**)	24600 (8.1)	-830 ± 100	2200 ± 300	530 ± 70
1-($HC\equiv C$)-C_6H_3-3,5-\{4-$C\equiv CC_6H_4C\equiv C$-*trans*-[Ru(4-$C\equiv CC_6H_4NO_2$)(dppe)$_2$]\}$_2$ (**17b**)	21600 (6.2)	-4900 ± 1000	4900 ± 1000	1200 ± 250
1,3,5-C_6H_3(4-$C\equiv CC_6H_4C\equiv C$-*trans*-[Ru(dppe)$_2$]$C\equiv C$-3,5-C_6H_3-\{4-$C\equiv CC_6H_4C\equiv C$-*trans*-[Ru($C\equiv$CPh)(dppe)$_2$]\}$_2$)$_3$ (**18a**)	24900 (42.1)	-5050 ± 500	20100 ± 2000	4800 ± 500
1,3,5-C_6H_3(4-$C\equiv CC_6H_4C\equiv C$-*trans*-[Ru(dppe)$_2$]$C\equiv C$-3,5-C_6H_3-\{4-$C\equiv CC_6H_4C\equiv C$-*trans*-[Ru(4-$C\equiv CC_6H_4NO_2$)(dppe)$_2$]\}$_2$)$_3$ (**18b**)	21400 (sh, 16.0)	-14900 ± 3000	18200 ± 3000	4400 ± 700
trans-[Ru(4-$C\equiv CC_6H_4C\equiv$CPh)($C\equiv$CPh)(dppe)$_2$] (**19a**)	26200 (3.8)	-670 ± 300[d]	1300 ± 300[d]	310 ± 70
trans-[Ru(4-$C\equiv CC_6H_4C\equiv$CPh)(4-$C\equiv CC_6H_4NO_2$)(dppe)$_2$] (**19b**)	21300 (2.5)	[b]		
trans-[Ru($C\equiv$CPh)Cl(dppe)$_2$]	31300 (1.8)	-170 ± 40[d]	71 ± 20[d]	20 ± 5

[a] Calculated using the equation $\sigma_2 = \frac{\hbar\omega\beta_2}{N}$ where $\hbar$ is Plancks constant on 2π, ω is the exciting frequency, β_2 is the two-photon absorption coefficient and N is the concentration. [b] Not measured due to lack of solubility.

permit comparison with literature values. Importantly, the Z-scan measurements were performed using low repetition rate (30 Hz) 100 fs pulses; excited state absorption should therefore be negligible. The bottom set of curves show the closed aperture experiment (performed concurrently with the open aperture experiment). Analysis of the concentration dependance of these curves reveals the defocussing nature of the complex at this wavelength. From these data, the real component of γ may be obtained.

4.3.4. Discussion of third-order nonlinear optical results

The significant γ_{imag} values are indicative of TPA, which becomes important as the linear absorption maximum approaches 2ω (i.e. twice the exciting laser frequency, in this case 25 000 cm^{-1} or 400 nm).[24] Figure 4.15. shows the close proximity to 2ω of the absorption band assigned to a MLCT transition. It is not possible at present to determine whether the negative γ_{real} values are indicative of zero-frequency negative cubic hyperpolarizabilities, or result from two-photon dispersion effects (as mentioned in Section 1.2.1., resonant behaviour of the cubic hyperpolarizability involves a rapidly changing real part and enhanced imaginary part). However, the organic compound **8**, which exhibits no TPA, has a positive γ_{real} value.

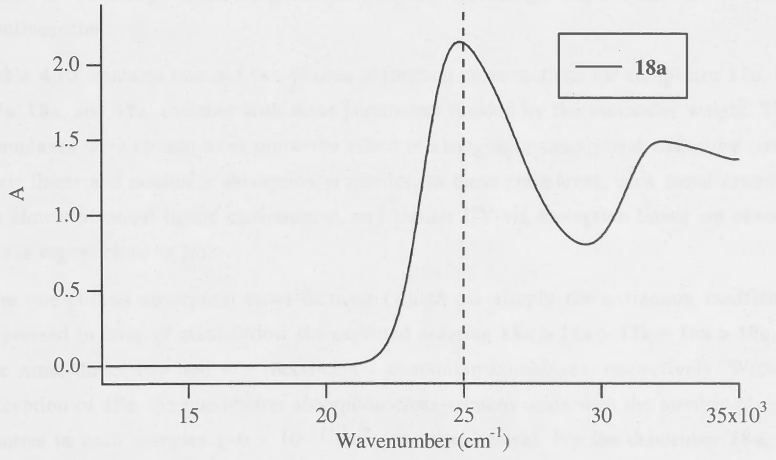

Figure 4.15. UV-vis of **18a**. The vertical dotted line indicates the position of 2ω.

Furthermore, Table 1.19. contains examples of ruthenium acetylide complexes with positive γ_{real} and substantial γ_{imag} values, together with similar complexes exhibiting negative γ_{real} with substantial γ_{imag} values. It is likely, therefore, that the negative γ_{real} values result from two-photon dispersion effects, with the sign of γ_{real} sensitive to small differences in the energies of absorption bands of the complexes. Not unexpectedly, introduction of the ligated metal on proceeding from **8** to **10** or **14** to **15** results in significant increases in both γ_{real} and γ_{imag}. Inspection of γ values for **19a** and **11a** reveals a significant increase in the imaginary component on progressing from the linear to the multipolar complex, but no increase in γ_{real}. Both real and imaginary components of the third-order hyperpolarizability for the dendrimer **18a** are much larger than those of its components **17a** and **10** or the related complex **11a**. In particular, progressing from **11a** to **18a** results in increases in both γ_{real} and γ_{imag} proportionately greater than either the increase in the number of phenylethynyl groups or the extinction coefficient. Comparison of the nitro-containing complexes **11b**, **16b** and **17b** to their non-nitro analogues reveals large increases in both real and imaginary γ values. Comparison of the dendrimer complexes shows a large increase in γ_{real}, but no change in γ_{imag}, on progressing from **18a** to **18b**. These results suggest that the introduction of a nitro-group has a significant effect on the cubic nonlinearity, but the degree to which this is affected by two-photon dispersion is not readily ascertained from these data. Future experiments may allow for measurements of γ over a range of wavelengths, enabling insight into the wavelength dependence of the optical nonlinearities.

Table 4.10. contains one and two-photon absorption cross-sections for complexes **11a**, **16a**, **17a**, **18a**, and **19a**, together with these parameters divided by the molecular weight. These complexes were chosen to examine the effect of changing geometry and molecular size on their linear and nonlinear absorption properties. In these complexes, each metal centre has an almost identical ligand environment, and similar UV-vis absorption bands are observed in the region close to 2ω.

The one-photon absorption cross-sections (which are simply the extinction coefficients expressed in units of area) follow the expected ordering **18a** > **11a** > **17a** ≈ **16a** > **19a**, i.e. the nine, three, two and one metal-centre containing complexes, respectively. With the exception of **18a**, the one-photon absorption cross-sections scale with the number of metal centres in each complex (~6×10^{-17} cm^2 per metal centre). For the dendrimer **18a**, this scaling factor does not hold, a much higher figure per metal-centre being observed. This trend is reflected in the σ / MW values, with the complexes with one, two or three metal centres ranging from 5.0 to 6.0×10^{-20} cm^2 mol g^{-1}, but with **18a** having a value of 6.9×10^{-20} cm^2 mol g^{-1}. Examination of the TPA cross-sections reveals the same ordering as for

Table 4.10. One and two-photon absorption cross-sections for selected complexes.

Compound	$\tilde{\nu}_{max}$ (cm^{-1})	σ (10^{-17} cm^2)	σ / MW (10^{-20} cm^2 mole g^{-1})	σ_2[a] (10^{-50} cm^4 s)	σ_2 / MW[a] (10^{-51} cm^4 s mole g^{-1})
1,3,5-C_6H_3{4-C≡CC_6H_4C≡C-*trans*-[Ru(C≡CPh)(dppe)$_2$]}$_3$ (**11a**)	24300	19	5.5	700	2.0
1-(Me_3SiC≡C)-C_6H_3-3,5-{4-C≡CC_6H_4C≡C-*trans*-[Ru(C≡CPh)(dppe)$_2$]}$_2$ (**16a**)	24500	13	5.4	550	2.3
1-(HC≡C)-C_6H_3-3,5-{4-C≡CC_6H_4C≡C-*trans*-[Ru(C≡CPh)(dppe)$_2$]}$_2$ (**17a**)	24600	14	6.0	530	2.3
1,3,5-C_6H_3(4-C≡CC_6H_4C≡C-*trans*-[Ru(dppe)$_2$]C≡C-3,5-C_6H_3-{4-C≡CC_6H_4C≡C-*trans*-[Ru(C≡CPh)(dppe)$_2$]}$_2$)$_3$ (**18a**)	24900	70	6.9	4800	4.7
trans-[Ru(4-C≡CC_6H_4C≡CPh)(C≡CPh)(dppe)$_2$] (**19a**)	26200	6	5.0	310	2.6

[a] Error is ~ 15 %.

the linear absorption parameter, with complexes **11a**, **16a**, **17a**, and **19a** having σ_2 values between 200-300 $\times 10^{-50}$ cm^4 s per metal-centre, but complex **18a** having a value of ~500 $\times 10^{-50}$ cm^4 s per metal-centre. Similarly, the σ_2 / MW values reveal a larger TPA coefficient per unit of molecular mass for the dendrimer complex **18a** than for the smaller related complexes. Clearly, both linear and nonlinear absorption characteristics are altered upon proceeding from the smaller ruthenium-acetylide complexes to the dendrimer. Both of the dendritic complexes **18a** and **18b** show σ_2 values comparable in magnitude to those of the bis(styryl)benzene derivatives reported by Albota *et al.*[27] (up to 44 $\times 10^{-48}$ cm^4 s) and the heterocyclic compounds reported by Reinhardt *et al.*[26] (up to 115.6 $\times 10^{-48}$ cm^4 s). In the present case, it is likely that the size and two-dimensional nature of the π-delocalized system combined with the strong MLCT transition all contribute to the large observed σ_2 value.

4.4. Conclusions

Routes into branched and dendritic complexes containing extensive π-delocalized systems were assayed, and examples were prepared from electron-rich ruthenium-acetylide units using a convergent synthesis. The alkynylruthenium dendrimers are soluble in a range of solvents and oxidatively stable.

Measurements of second-order NLO properties showed that varying the molecular size and geometry impacts significantly on the optical nonlinearity. Very large quadratic hyperpolarizabilities were measured for several of the branched complexes, comparable to the largest values for organometallics reported in the literature. The multipolar complexes lacking a formal acceptor group have some of the largest nonlinearities thus far for compounds of this type. Modication of the electronic properties of the molecule by the introduction of strong acceptor groups induced large increases in second-order nonlinearities.

Third-order NLO measurements revealed significant TPA behaviour, again, comparable to some of the largest reported in the literature. Both linear and nonlinear absorption characteristics are altered upon proceeding from the smaller complexes to the dendrimers. While one and two-photon absorption cross-sections were found to scale with the number of metal centres in each molecule for complexes containing one, two or three metal centres, a much higher figure per metal-centre was observed for the dendritic complexes. This nonlinear increase in third-order NLO properties provides an incentive to further investigate the NLO behaviour of dendritic macromolecules.

4.5 Experimental

4.5.1. General Conditions, Reagents and Instruments

General Conditions

All reactions were performed under a nitrogen atmosphere with the use of Schlenk techniques unless otherwise stated. Dichloromethane was dried by distilling over calcium hydride, methanol was dried by distilling over magnesium / iodine, and diethylether and tetrahydrofuran were dried by distilling over sodium / benzophenone; other solvents were used as received. "Pet. spirit" refers to a fraction of petroleum ether of boiling range 60-80 °C. Chromatography was on silica gel (230-400 mesh ASTM) or ungraded basic alumina.

Reagents

The following were prepared by literature procedures: 1,3,5-triethynylbenzene,[86] 4-$Me_3SiC{\equiv}CC_6H_4I$,[87] 4-$HC{\equiv}CC_6H_4Br$,[78] 4-$HC{\equiv}CC_6H_4NO_2$,[78] 4-$HC{\equiv}CC_6H_4C{\equiv}CPh$,[88] *trans*-$[Ru(4\text{-}C{\equiv}CC_6H_4NO_2)Cl(dppe)_2]$,[68] *trans*-$[Ru(C{\equiv}CPh)Cl(dppe)_2]$.[68] Dichlorobis(triphenylphosphine)palldium (II) was prepared by stirring two equivalents of triphenylphosphine with palladium(II) chloride in dimethylformamide at reflux for 2 h. The resulting precipitate was collected and recrystallized from chloroform. *n*-Butyllithium (solution in hexane) (Merck) and *t*-butyllithium (solution in pentane) (Aldrich) were titrated with diphenylacetic acid in diethylether before use to determine their exact concentration.[89] *cis*-$[RuCl_2(dppe)_2]$ was prepared by modifying the literature procedure[90] in the following way: (i) dppe was substituted for dppm, (ii) reflux time in toluene was 2 h, and (iii) the product was recrystallized by the addition of methanol to a dichloromethane solution. Sodium hexafluorophosphate (Aldrich) was recrystallized from acetonitrile before use. Copper(I) iodide (Unilab), tetra-*n*-butylammonium fluoride (1 M solution in tetrahydrofuran) (Aldrich), 1,3,5-tribromobenzene (Aldrich), iodine (M&B), sodium thiosulphate (Univar), trimethylsilylacetylene (Aldrich), zinc(II) bromide (Aldrich), ethynylmagnesium bromide (0.5 M solution in tetrahydrofuran) (Aldrich), phenylacetylene (Aldrich), and anhydrous magnesium sulfate (Aldrich) were used as received.

Instruments

EI (electron impact) mass spectra (both unit resolution and high resolution (HR)) were recorded using a VG Autospec instrument (70 eV electron energy, 8 kV accelerating potential) and secondary ion mass spectra were recorded using a VG ZAB 2SEQ instrument (30 kV Cs^+ ions, current 1 mA, accelerating potential 8 kV, 3-nitrobenzyl alcohol matrix) at the Research School of Chemistry, Australian National University; peaks are reported as *m/z*

(assignment, relative intensity). Microanalyses were carried out at the Research School of Chemistry, Australian National University. Infrared spectra were recorded as dichloromethane solutions using a Perkin-Elmer System 2000 FT-IR. ^{1}H, ^{13}C and ^{31}P NMR spectra were recorded using a Varian Gemini-300 FT NMR spectrometer and are referenced to residual chloroform (7.24 ppm), *d*-chloroform (77.0 ppm) or external 85% H_3PO_4 (0.0 ppm), respectively. The assignments follow the numbering schemes shown in Figure 4.11. UV-Vis spectra of solutions in tetrahydrofuran in 1 cm cells were recorded using either a Cary 4 or Cary 5 spectrophotometer. Melting points were measured using an Electrothermal melting point apparatus.

4.5.2. Syntheses of Organic Precursors

*1,3,5-C_6H_3(C≡C-4-C_6H_4C≡CSiMe_3)$_3$ (**8**)*

To a solution of 1,3,5-triethynylbenzene (190 mg, 1.26 mmol) and 4-$Me_3SiC{\equiv}CC_6H_4I$ (1.139 g, 3.79 mmol) in triethylamine (70 ml) was added dichlorobis(triphenylphosphine)-palladium(II) (44 mg, 0.063 mmol) and copper(I) iodide (60 mg, 0.32 mmol). The mixture was stirred for 2 h and then filtered through a glass sinter. The filtrate was reduced to dryness *in vacuo*. The residue was purified by silica column chromatography eluting with pet. spirit. The solvent was then removed from the eluate using a rotary evaporator. Recrystallization by slow evaporation of a dichloromethane / methanol mixture afforded 600 mg of pale yellow microcrystals (71%). MS: 666 ($[M]^+$, 100). IR (cm^{-1}): 2157 ν(C≡C). ^{1}H NMR (δ, 300 MHz, $CDCl_3$); 0.24 (s, 27H, $SiMe_3$), 7.44 (s, 12H, H_{10} and H_{11}), 7.61 (s, 3H, H_1). M.p. 140 °C (decomp.).

*1,3,5-C_6H_3(C≡C-4-C_6H_4C≡CH)$_3$ (**9**)*

To a solution of **8** (300 mg, 0.45 mmol) in dichloromethane was added 2 mL of tetra-*n*-butylammonium fluoride solution (1 M in tetrahydrofuran) and the mixture stirred for 15 min. The solvent was then removed *in vacuo*. The residue was dissolved in a minimum amount of pet. spirit and purified by silica column chromatography eluting with pet. spirit. The solvent was then removed from the eluate using a rotary evaporator. Slow evaporation of a dichloromethane / methanol solution afforded 180 mg of a white powder (89%). MS: 450 ($[M]^+$, 100). IR (cm^{-1}): 3296 ν(HC≡), 2108 ν(C≡C). ^{1}H NMR (δ, 300 MHz, $CDCl_3$); 3.17 (s, 3H, C≡CH), 7.46 (s, 12H, H_{10} and H_{11}), 7.63 (s, 3H, H_1). M.p. 126 °C.

1,3-dibromo-5-iodobenzene

1,3,5-tribromobenzene (5.0 g, 15.9 mmol) was dissolved in diethylether (150 mL) and cooled to -78 °C in a dry-ice / acetone bath. *n*-Butyllithium (10.4 mL of a 1.54 M solution in hexane, 16.0 mmol) was slowly added and the mixture stirred for 30 min. A solution of iodine (5.0 g, 19.7 mmol) in diethylether (80 mL) was then added dropwise *via* a cannula.

The mixture was stirred at -78 °C for 10 min and then at room temperature for 30 min. After washing the mixture with saturated aqueous sodium thiosulphate solution, the organic layer was separated and dried using magnesium sulphate. The mixture was filtered and the solvent removed using a rotary evaporator. The product was purified by silica column chromatography eluting with pet. spirit. Yield was 4.5 g (78 %). MS: 362 ($[M]^+$, 100), 235 ($[C_6H_3Br_2]^+$, 40). Anal. Calcd: C 19.92, H 0.84 %. Found: C 20.13, H 0.79 %. ^{1}H NMR: (δ, 300 MHz, $CDCl_3$); 7.62 (t, J_{HH} = 2 Hz, 1H, H_{30}), 7.78 (d, J_{HH} = 2 Hz, 2H, H_{28}). ^{13}C NMR: (δ, 75 MHz, $CDCl_3$); 94.5 (C_{27}), 123.3 (C_{29}), 133.6 (C_{30}), 138.5 (C_{28}).

1,3-dibromo-5-(trimethylsilylethynyl)benzene

1,3-Dibromo-5-iodobenzene (1.0 g, 2.8 mmol) was dissolved in tetrahydrofuran (30 mL). Trimethylsilylacetylene (0.40 mL, 2.8 mmol) and triethylamine (20 mL) were then added and the mixture cooled in an ice bath. Dichlorobis(triphenylphosphine)palladium(II) (15 mg, 0.02 mmol) and copper(I) iodide (10 mg, 0.05 mmol) were added and the mixture stirred at 0 °C for 30 min. The ice bath was then removed and stirring was continued for 90 min while the mixture warmed to room temperature. The mixture was filtered and the solvent removed *in vacuo*. The product was purified by column chromatography on silica, eluting with pet. spirit. Removal of the solvent on a rotary evaporator yielded 0.85 g of a colorless liquid (93 %). HR MS (EI) $C_{11}H_{12}Si^{81}Br_2$: calc. 333.9034, found 333.9043; $C_{11}H_{12}Si^{79}Br^{81}Br$: calc. 331.9055, found 331.9058; $C_{11}H_{12}Si^{79}Br_2$: calc. 329.9075, found 329.9069. IR (cm^{-1}): 2167 ν(C≡C). ^{1}H NMR: (δ, 300 MHz, $CDCl_3$); 0.22 (s, 9H, Me), 7.51 (d, J_{HH} = 2 Hz, 2H, H_{28}), 7.59 (t, J_{HH} = 2 Hz, 1H, H_{30}). ^{13}C NMR: (δ, 75 MHz, $CDCl_3$); -0.3 (Me), 97.5 (C_{26}), 101.6 (C_{25}), 122.5 (C_{29}), 126.5 (C_{27}), 133.3 (C_{28}), 134.1 (C_{30}). Density: 1.4 g mL^{-1}.

1,3-diiodo-5-(trimethylsilylethynyl)benzene

1,3-Dibromo-5-(trimethylsilylethynyl)benzene (1.77 g, 5.33 mmol) was dissolved in diethylether (100 mL) and the resultant solution cooled to -78 °C in a dry-ice / acetone bath. *t*-Butyllithium (13.5 mL, 1.6 M solution in hexane, 21.6 mmol) was slowly added and the mixture stirred for 30 min. A solution of iodine (3.8 g, 15.0 mmol) in diethylether (50 mL) was then added slowly via a cannula. The mixture was stirred at -78 °C for 10 min and then allowed to warm to room temperature with stirring for a period of 30 min. After washing the mixture with saturated aqueous sodium thiosulfate solution, the organic layer was separated and dried using magnesium sulfate. The mixture was filtered and the solvent removed from the filtrate using a rotary evaporator. The product, a clear viscous liquid, was purified by column chromatography on silica, eluting with pet. spirit. Yield was 2.12 g (93 %). HR MS (EI) $C_{11}H_{12}SiI_2$: calc. 425.8798, found 425.8796. IR (cm^{-1}): 2162 ν(C≡C). ^{1}H

NMR: (δ, 300 MHz, $CDCl_3$); 0.21 (s, 9H, Me), 7.74 (d, J_{HH} = 2 Hz, 2H, H_{28}), 7.97 (t, J_{HH} = 2 Hz, 1H, H_{30}). ^{13}C NMR: (δ, 75 MHz, $CDCl_3$); –0.2 (Me), 94.0 (C_{29}), 97.5 (C_{26}), 101.3 (C_{25}), 126.6 (C_{27}), 139.6 (C_{28}), 145.0 (C_{30}). Density: 1.3 g mL^{-1}.

1-ethynyl-3,5-diiodobenzene

1,3-diiodo-5-(trimethylsilylethynyl)benzene was dissolved in a 1:1 mixture of dichloromethane / methanol. Potassium carbonate (2 molar equivalents) was added and the mixture stirred at room temperature for 1 h. The mixture was filtered, and the solvent removed using a rotary evaporator and the residue purified by column chromatography on silica, to yield an off-white powder in 85% yield. MS: 354 ($[M]^+$, 100), 227 ($[M - I]^+$, 30), 100 ($[M - I_2]^+$, 35). ^1H NMR: (δ, 300 MHz, $CDCl_3$); 3.14 (s, 1H, C≡CH), 7.76 (d, J_{HH} = 2 Hz, 2H, H_{28}), 8.01 (t, J_{HH} = 2 Hz, 1H, H_{30}). ^{13}C NMR: (δ, 75 MHz, $CDCl_3$); 79.8 (C_{25}), 80.2 (C_{26}), 94.0 (C_{29}), 125.6 (C_{27}), 139.8 (C_{28}), 145.5 (C_{30}).

*1-Me_3SiC≡C-3,5-(4-BrC_6H_4C≡C)$_2$-C_6H_3 (**12**)*

1,3-Diiodo-5-(trimethylsilylethynyl)benzene (2.25 g, 5.29 mmol) and 4-bromoethynylbenzene (2.00 g, 11.05 mmol) were dissolved in triethylamine (50 mL) and the resultant solution cooled in an ice bath for 10 min. Dichlorobis(triphenylphosphine)palladium(II) (100 mg, 0.14 mmol) and copper(I) iodide (50 mg, 0.26 mmol) were added with stirring and the mixture allowed to warm to room temperature. After stirring for 2 h, the mixture was filtered and the filtrate taken to dryness *in vacuo*. The residue was purified by column chromatography on silica, eluting with pet. spirit. Removal of solvent on a rotary evaporator yielded 1.95 g (69 %) of a colorless powder. HR MS (EI) $C_{27}H_{20}Si^{79}Br^{81}Br$: calc. 531.9681, found 531.9699; $C_{27}H_{20}Si^{79}Br_2$ calc. 529.9701, found 529.9712. UV-vis ($\tilde{\nu}_{max}$, cm^{-1} (ε, M^{-1} cm^{-1})): 32 200 (75 600), 34 200 (72 500), 37 400 (37 200). IR (cm^{-1}): 2155 ν(C≡C). ^1H NMR: (δ, 300 MHz, $CDCl_3$); 0.23 (s, 9H, Me), 7.41 (AA´BB´, 8H, H_{36}, H_{37}), 7.57 (d, J_{HH} = 2 Hz, 2H, H_{28}), 7.58 (t, J_{HH} = 2 Hz, 1H, H_{30}). ^{13}C NMR: (δ, 75 MHz, $CDCl_3$); -0.2 (Me), 88.7, 89.4 (C_{33}, C_{34}), 96.0 (C_{26}), 103.0 (C_{25}), 121.6 (C_{35}), 122.9 (C_{38}), 123.6 (C_{29}), 124.0 (C_{27}), 131.7 (C_{36}), 133.0 (C_{37}), 134.1 (C_{30}), 134.5 (C_{28}).

*1-Me_3SiC≡C-3,5-(4-IC_6H_4C≡C)$_2$-C_6H_3 (**13**)*

Compound **12** (1.70 g, 3.19 mmol) was dissolved in diethylether (~100 mL) and the resultant solution cooled to -78 °C in a dry-ice / acetone bath. *t*-Butyllithium (8.7 mL, 1.5 M solution in hexane, 13.1 mmol) was slowly added and the mixture stirred for 30 min. A solution of iodine (2.10 g, 8.27 mmol) in diethylether (50 mL) was then added slowly via a cannula. The mixture was stirred at -78 °C for 10 min and then allowed to warm to room temperature with stirring for a period of 30 min. After washing the mixture with saturated aqueous sodium thiosulfate solution, the organic layer was separated and dried using

magnesium sulfate. The mixture was filtered and the solvent removed using a rotary evaporator. The product was precipitated from a dichloromethane / pet. spirit solution by slow evaporation to yield 1.65 g (82 %) of a colourless solid. HR MS (EI) $C_{27}H_{20}SiI_2$: calc. 625.9424, found 625.9427. UV-vis ($\bar{\nu}_{max}$, cm^{-1} (ε, M^{-1} cm^{-1})): 31 800 (80 500), 33 800 (80 800), 37 100 (56 000). IR (cm^{-1}): 2154 ν(C≡C). ^1H NMR: (δ, 300 MHz, $CDCl_3$); 0.23 (s, 9H, Me), 7.44 (AA´BB´, 8H, H_{36}, H_{37}), 7.56 (d, J_{HH} = 1.5 Hz, 2H, H_{28}), 7.58 (t, J_{HH} = 1.5 Hz, 1H, H_{30}). ^{13}C NMR: (δ, 75 MHz, $CDCl_3$); -0.2 (Me), 89.0, 89.6 (C_{33}, C_{34}), 94.6 (C_{38}), 96.0 (C_{26}), 103.0 (C_{25}), 122.2 (C_{35}), 123.6 (C_{29}), 124.0 (C_{27}), 133.1 (C_{36}), 134.1 (C_{30}), 134.5 (C_{28}), 137.6 (C_{37}).

*1-Me_3SiC≡C-3,5-(4-HC≡CC_6H_4C≡C)$_2$-C_6H_3 (**14**)*

Zinc(II) bromide (1.08 g, 4.8 mmol) was flame dried under vacuum in a Schlenk tube and tetrahydrofuran (10 mL) was added. A solution of ethynylmagnesium bromide (10 mL, 0.5 M in tetrahydrofuran, 5.0 mmol) was added and the mixture stirred for 5 min. Compound **13** (1.0 g, 1.6 mmol) was added, followed by dichlorobis(triphenylphosphine)palladium(II) (200 mg, 0.3 mmol), and the mixture was stirred for 2 h. After washing the mixture with aqueous ammonium chloride, the organic layer was separated and dried with magnesium sulfate. The mixture was filtered and the solvent removed on a rotary evaporator. The product was purified by column chromatography on silica eluting with 1:19 dichloromethane / pet. spirit. Removal of the solvent afforded 340 mg (50 %) of a white powder . HR MS (EI) $C_{31}H_{22}Si$: calc. 422.1491, found 422.1488. UV-vis ($\bar{\nu}_{max}$, cm^{-1} (ε, M^{-1} cm^{-1})): 31 100 (85 500), 33 200 (86 200), 37 000 (46 000). IR (cm^{-1}): 2155, 2109 ν(C≡C), 3296 ν(HC≡). ^1H NMR: (δ, 300 MHz, $CDCl_3$); 0.24 (s, 9H, Me), 3.17 (s, 2H, H_{42}), 7.45 (m, 8H, H_{36}, H_{37}), 7.57 (d, J_{HH} = 1.5 Hz, 2H, H_{28}), 7.60 (t, J_{HH} = 1.5 Hz, 1H, H_{30}). ^{13}C NMR: (δ, 75 MHz, $CDCl_3$); -0.2 (Me), 79.1 (C_{42}), 83.1 (C_{41}), 89.6, 89.9 (C_{33}, C_{34}), 96.0 (C_{26}), 103.0 (C_{25}), 122.2 (C_{35}), 123.1 (C_{38}), 123.6 (C_{29}), 124.0 (C_{27}), 131.6 (C_{36}), 132.1 (C_{37}), 134.2 (C_{30}), 134.6 (C_{28}).

4.5.3. Syntheses of Ruthenium-containing Complexes

*1,3,5-C_6H_3{4-C≡CC_6H_4C≡C-trans-[$RuCl(dppe)_2$]}$_3$ (**10**)*

To a solution of **9** (0.090 g, 0.20 mmol) and *cis*-[$RuCl_2$(dppe)$_2$] (1.00 g, 1.02 mmol) in dichloromethane (25 mL) was added sodium hexafluorophosphate (0.20 g, 1.2 mmol). The mixture was stirred at room temperature for 12 h. Triethylamine (1 mL) was added and the mixture stirred for a further 5 min. The solvent was removed *in vacuo* and the residue absorbed onto alumina (basic, grade 3) and placed onto an alumina column. This was eluted firstly with 1:19 acetone:diethylether (400 mL) to remove *trans*-[$RuCl_2$(dppe)$_2$] and then with dichloromethane (200 mL) to remove the product. Evaporation of the solvent afforded a yellow powder, yield 440 mg (68 % based on **9**). MS: 3249 ([M]$^+$, 20), 898

([Ru(dppe)$_2$]$^+$, 100). Anal. Calcd for $C_{192}H_{159}Cl_3P_{12}Ru_3$: C 71.01, H 4.94 %. Found: C 70.90, H 5.20 %. UV-vis ($\tilde{\nu}_{max}$, cm^{-1} (ε, M^{-1} cm^{-1})): 24 200 (99 000), 33 300 (66 000), 40 000 (137 000). IR (cm^{-1}): 2204, 2065 ν(C≡C). ^{1}H NMR: (δ, 300 MHz, $CDCl_3$); 2.69 (m, 24H, CH_2), 6.56 (d, J_{HH} = 8 Hz, 6H, H_{11}), 6.93 to 7.46 (m, 126H, phenyl), 7.59 (s, 3H, H_1). ^{13}C NMR: (δ, 75 MHz, $CDCl_3$); 30.6 (m, CH_2), 88.3, 91.5 (C_7, C_8), 116.2 (C_{15}), 127.0 (C_m), 127.2 (C_m), 128.9 (C_p), 130.0, 130.9 (C_{10}, C_{11}), 134.2 (C_o), 134.4 (C_o), 135.5 (C_i), 136.3 (C_i). ^{31}P NMR: (δ, 121 MHz, $CDCl_3$); 49.9 (s).

1,3,5-C_6H_3{4-C≡CC_6H_4C≡C-trans-[Ru(C≡CPh)(dppe)$_2$]}$_3$ (***11a***)

To a solution of **10** (155 mg, 0.048 mmol) and phenylacetylene (0.05 mL, 0.46 mmol) in dichloromethane (15 mL) was added sodium hexafluorophosphate (50 mg, 0.30 mmol) and triethylamine (0.5 mL). The mixture was stirred for 5 h at room temperature. The solvent was removed *in vacuo* and the residue dissolved in dichloromethane and absorbed onto alumina, which was then placed on to an alumina column. It was eluted firstly with 1:19 dichloromethane / pet. spirit to remove excess phenylacetylene and then with 3:2 dichloromethane / pet. spirit to remove the product. Evaporation of the solvent afforded a yellow powder, yield 0.105 g (64 %). MS: 3445 ([M]$^+$, 0.4), 3343 ([M - C≡CPh]$^+$, 0.8), 898 ([Ru(dppe)$_2$]$^+$, 100). Anal. Calcd for $C_{216}H_{174}P_{12}Ru_3$: C 75.32, H 5.09 %. Found: C 74.98, H 5.60 %. UV-vis ($\tilde{\nu}_{max}$, cm^{-1} (ε, M^{-1} cm^{-1})): 24 300 (116 000), 31 740 (98 100). IR (cm^{-1}): 2203, 2057 ν(C≡C). ^{1}H NMR: (δ, 300 MHz, $CDCl_3$); 2.63 (m, 24H, CH_2), 6.65 (d, J_{HH} = 8 Hz, 6H, H_{11} or H_{20}), 6.81 (d, J_{HH} = 8 Hz, 6H, H_{11} or H_{20}), 6.92 to 7.61 (m, 138H, phenyl and H_1 (obscured)). ^{13}C NMR: (δ, 75 MHz, $CDCl_3$); 31.4 (m, CH_2), 88.3, 91.6 (C_7, C_8), 116.2 (C_{15}), 117.2 (C_{18}), 127.0 (C_m), 127.4 (C_{20} or C_{21}), 128.6 (C_p), 128.7 (C_p), 129.9 (C_{10} or C_{11}), 130.5 (C_{12}), 130.9 (C_{10} or C_{11}), 134.1 (C_o), 134.3 (C_o), 136.9 (m, C_i)). ^{31}P NMR: (δ, 121 MHz, $CDCl_3$); 54.5 (s).

1,3,5-C_6H_3{4-C≡CC_6H_4C≡C-trans-[Ru(4-C≡C$C_6H_4NO_2$)(dppe)$_2$]}$_3$ (***11b***)

To a solution of **10** (100 mg, 0.031 mmol) and 4-HC≡C$C_6H_4NO_2$ (30 mg, 0.20 mmol) in dichloromethane (5 mL) was added sodium hexafluorophosphate (35 mg, 0.21 mmol) and triethylamine (0.5 mL). The mixture was stirred for 2 h at refluxing temperature. The solvent was removed *in vacuo* and the residue dissolved in dichloromethane and absorbed onto alumina, which was then placed onto an alumina column. It was eluted firstly with 1:2 dichloromethane / pet. spirit to remove excess acetylene, and then with dichloromethane to remove the product. Evaporation of the solvent afforded a red powder, yield 88 mg (80 %). MS: 3580 ([M]$^+$, 1), 1044 ([Ru(4-C≡C$C_6H_4NO_2$)(dppe)$_2$]$^+$, 10), 898 ([Ru(dppe)$_2$]$^+$, 100). Anal. Calcd for $C_{216}H_{171}N_3O_6P_{12}Ru_3$: C 72.48, H 4.81, N 1.17 %. Found: C 72.10, H 4.80, N 1.21 %. UV-vis ($\tilde{\nu}_{max}$, cm^{-1} (ε, M^{-1} cm^{-1})): 21 800 (89 300), 24 800 (11 200), 32 700 (91 500), 41 000 (179 000). IR (cm^{-1}): 2204, 2047 ν(C≡C). ^{1}H NMR: (δ, 300 MHz,

$CDCl_3$); 2.63 (m, 24H, CH_2), 6.57 (d, J_{HH} = 8 Hz, 6H, H_{11} or H_{20}), 6.76 (d, J_{HH} = 8 Hz, 6H, H_{11} or H_{20}), 6.91 to 7.57 (m, 126H, phenyl), 7.62 (s, 1H, H_1), 7.97 (d, J_{HH} = 8 Hz, 6H, H_{21}). ^{13}C NMR: (δ, 75 MHz, $CDCl_3$); 31.4 (m, CH_2), 88.4, 91.6 (C_7, C_8), 116.9 (C_{15}), 118.8 (C_{18}), 123.5 (C_{21} or C_{20}), 127.3 (C_m), 128.9 (C_p), 129.0 (C_p), 129.9 (C_{10} or C_{11}), 130.7 (C_{12}), 131.2 (C_{10} or C_{11}), 134.0 (C_o), 134.2 (C_o), 136.4 (m, C_i), 137.3 (C_{19}), 142.7 (C_{22}). ^{31}P NMR: (δ, 121 MHz, $CDCl_3$); 54.5 (s).

*1-($Me_3SiC{\equiv}C$)-C_6H_3-3,5-{4-$C{\equiv}CC_6H_4C{\equiv}C$-trans-[$RuCl(dppe)_2$]}$_2$ (**15**)*

To a solution of **14** (100 mg, 0.24 mmol) and *cis*-[$RuCl_2(dppe)_2$] (550 mg, 0.57 mmol) in dichloromethane (20 mL) was added sodium hexafluorophosphate (160 mg, 0.95 mmol). The mixture was stirred at room temperature for 20 h. Triethylamine (1 mL) was added and the mixture stirred for a further 5 min. The solvent was removed *in vacuo* and the residue absorbed onto alumina (basic, ungraded) and placed onto an alumina column. This was eluted firstly with 4:1 diethylether / pet. spirit and then with 1:1 diethylether / dichloromethane to remove the product. Evaporation of the solvent afforded a yellow powder. Yield 0.360 g (66 % based on **14**). MS: 2288 ($[M]^+$, 7), 2252 ($[M - Cl]^+$, 3), 898 ($[Ru(dppe)_2]^+$, 100). Anal. Calcd for $C_{135}H_{116}Cl_2P_8Ru_2Si$: C 70.89, H 5.11 %. Found: C 70.52, H 5.11 %. UV-vis ($\bar{\nu}_{max}$, cm^{-1} (ε, M^{-1} cm^{-1})): 24 300 (72 700), 33 400 (sh, 51 000), 39 900 (117 000). IR (cm^{-1}): ν(C≡C) 2064, 2156, 2205. ^1H NMR: (δ, 300 MHz, $CDCl_3$); 0.27 (s, 9H, Me), 2.68 (m, 16H, CH_2), 6.55 (d, J_{HH} = 8 Hz, 4H, H_{37}), 6.92 to 7.46 (m, 84H, phenyl), 7.54 (d, J_{HH} = 2 Hz, 2H, H_{28}), 7.58 (t, J_{HH} = 2 Hz, 1H, H_{30}). ^{13}C NMR: (δ, 75 MHz, $CDCl_3$); –0.1 (Me), 30.6 (CH_2), 126.9 (C_m), 127.2 (C_m), 128.8 (C_p), 134.1 (C_o), 134.3 (C_o), 135.5 (m, C_i), 136.2 (m, C_i). ^{31}P NMR: (δ, 121 MHz, $CDCl_3$); 50.0 (PPh_2).

*1-($Me_3SiC{\equiv}C$)-C_6H_3-3,5-{4-$C{\equiv}CC_6H_4C{\equiv}C$-trans-[$Ru(C{\equiv}CPh)(dppe)_2$]}$_2$ (**16a**)*

To a solution of **15** (720 mg, 0.31 mmol) and phenylacetylene (0.20 mL) in dichloromethane (20 mL) was added sodium hexafluorophosphate (320 mg, 1.9 mmol) and triethylamine (1 mL) with stirring. The mixture was stirred for 2 h at reflux. The solvent was removed *in vacuo* and the residue dissolved in dichloromethane and absorbed onto alumina, which was then placed on to an alumina column (basic, ungraded). It was eluted firstly with 1:19 dichloromethane / pet. spirit to remove excess phenylacetylene and then with 3:2 dichloromethane / pet. spirit to remove the product. Evaporation of the solvent afforded a yellow powder which was recrystallized from dichloromethane / methanol, yield 540 mg (71 %). MS: 2420 ($[M]^+$, 3), 999 ($[Ru(C{\equiv}CPh)(dppe)_2]^+$, 3), 898 ($[Ru(dppe)_2]^+$, 20). Anal. Calcd for $C_{151}H_{126}P_8Ru_2Si$: C 74.99, H 5.25 %. Found: C 75.00, H 5.43 %. UV-vis ($\bar{\nu}_{max}$, cm^{-1} (ε, M^{-1} cm^{-1})): 24 500 (74 500), 32 100 (70 000). IR (cm^{-1}): 2057, 2156, 2204 ν(C≡C). ^1H NMR: (δ, 300 MHz, $CDCl_3$); 0.29 (s, 9H, Me), 2.63 (m, 16H, CH_2), 6.64 (d, J_{HH} = 8 Hz, 4H, H_{37} or H_{46}), 6.82 (d, J_{HH} = 8 Hz, 4H, H_{37} or H_{46}), 6.93 to 7.61

(m, 93H, phenyl). ^{13}C NMR: (δ, 75 MHz, $CDCl_3$); –0.1 (Me), 31.4 (CH_2), 127.0 (C_m), 128.6 (C_p), 134.1 (C_o), 134.3 (C_o), 136.9 (m, C_i). ^{31}P NMR: (δ, 121 MHz, $CDCl_3$); 50.0 (PPh_2).. ^{31}P NMR: (δ, 121 MHz, $CDCl_3$); 54.5 (PPh_2).

*1-($Me_3SiC{\equiv}C$)-C_6H_3-3,5-{4-$C{\equiv}CC_6H_4C{\equiv}C$-trans-[Ru(4-$C{\equiv}CC_6H_4NO_2$)(dppe)$_2$]}$_2$ (**16b**)*

To a solution of **15** (140 mg, 0.061 mmol) and 4-$HC{\equiv}CC_6H_4NO_2$ (35 mg, 0.24 mmol) in dichloromethane (5 mL) was added sodium hexafluorophosphate (40 mg, 0.24 mmol) and triethylamine (0.5 mL). The mixture was stirred for 2 h at reflux. The solvent was removed *in vacuo* and the residue dissolved in dichloromethane and then passed through an alumina plug eluting with dichloromethane. The solvent was removed and the residue dissolved in the minimum amount of dichloromethane. Pet. spirit (~ 30 mL) was added with stirring whereupon the product precipitated from solution. It was then collected by filtration, yield 130 mg (85 %). MS: 2509 ([M]$^+$, 5), 1044 ([Ru(4-$C{\equiv}CC_6H_4NO_2$)(dppe)$_2$]$^+$, 10), 898 ([Ru(dppe)$_2$]$^+$, 100). Anal. Calcd for $C_{151}H_{124}N_2O_4P_8Ru_2Si$: C 72.30, H 4.98, N 1.12 %. Found: C 71.70, H 4.86, N 1.08 %. UV-vis ($\bar{\nu}_{max}$, cm^{-1} (ε, M^{-1} cm^{-1})): 21 700 (58 900), 24 900 (71 200), 32 700 (sh, 59 300), 37 800 (94 200). IR (cm^{-1}): 2047, 2155, 2206 ν(C≡C). ^{1}H NMR: (δ, 300 MHz, $CDCl_3$); 0.29 (s, 9H, Me), 2.63 (m, 16H, CH_2), 6.57 (d, J_{HH} = 8 Hz, 4H, H_{37} or H_{46}), 6.74 (d, J_{HH} = 8 Hz, 4H, H_{37} or H_{46}), 6.91 to 7.56 (m, 87H, phenyl), 7.97 (d, J_{HH} = 8 Hz, 4H, H_{47}). ^{13}C NMR: (δ, 75 MHz, $CDCl_3$); –0.1 (Me), 31.3 (CH_2), 127.2 (C_m), 128.9 (C_p), 133.9 (C_o), 134.1 (C_o), 136.3 (m, C_i), 142.6 (C_{48}). ^{31}P NMR: (δ, 121 MHz, $CDCl_3$); 54.5 (PPh_2).

*1-($HC{\equiv}C$)-C_6H_3-3,5-{4-$C{\equiv}CC_6H_4C{\equiv}C$-trans-[Ru($C{\equiv}CPh$)(dppe)$_2$]}$_2$ (**17a**)*

To a solution of **16a** (400 mg, 0.17 mmol) in dichloromethane (15 mL) was added 0.2 mL of tetra-*n*-butylammonium fluoride solution (1 M in THF) and the resultant mixture stirred for 1 h. The mixture was then placed atop a short alumina (basic, ungraded) column and eluted with dichloromethane. Methanol (~40 mL) was then added to the eluted solution and the total volume of solvent was reduced to ~30 mL using a rotary evaporator. The precipitated product was collected by filtration and dried *in vacuo*, yield 330 mg (85 %). MS: 2347 ([M]$^+$, 5), 898 ([Ru(dppe)$_2$]$^+$, 45). Anal. Calcd for $C_{148}H_{118}P_8Ru_2$: C 75.76, H 5.07 %. Found: C 75.37, H 5.07 %. UV-vis ($\bar{\nu}_{max}$, cm^{-1} (ε, M^{-1} cm^{-1})): 24 600 (80 700), 32 000 (72 100). IR (cm^{-1}): 2057, 2202 ν(C≡C), 3296 ν(H-C≡). ^{1}H NMR: (δ, 300 MHz, $CDCl_3$); 2.63 (m, 16H, CH_2), 3.12 (s, 1H, C≡CH), 6.64 (d, J_{HH} = 8 Hz, 4H, H_{37} or H_{46}), 6.81 (d, J_{HH} = 8 Hz, 4H, H_{37} or H_{46}), 6.92 to 7.65 (m, 93H, phenyl). ^{13}C NMR: (δ, 75 MHz, $CDCl_3$); 31.4 (CH_2), 78.0 (C_{25}), 82.3 (C_{26}), 127.0 (C_m), 128.6 (C_p), 134.0 (C_o), 134.3 (C_o), 137.0 (m, C_i). ^{31}P NMR: (δ, 121 MHz, $CDCl_3$); 54.5 (PPh_2).

*1-(HC≡C)-C_6H_3-3,5-{4-C≡CC_6H_4C≡C-trans-[Ru(4-C≡C$C_6H_4NO_2$)(dppe)$_2$]}$_2$ (**17b**)*

To a solution of **16b** (100 mg, 0.041 mmol) in dichloromethane (15 mL) was added 0.2 mL of tetra-*n*-butylammonium fluoride solution (1 M in THF) and the resultant mixture stirred for 1 h. The mixture was then placed atop a short alumina (basic, ungraded) column and eluted with dichloromethane. Methanol (~20 mL) was then added to the eluted solution and the total volume of solvent was reduced to ~10 mL using a rotary evaporator. The precipitated product was collected by filtration, washed with pet. spirit, and dried *in vacuo*. Yield was 85 mg (88 %). MS: 2436 ([M]$^+$, 2), 1044 ([Ru(4-C≡C$C_6H_4NO_2$)(dppe)$_2$]$^+$, 10), 898 ([Ru(dppe)$_2$]$^+$, 100). Anal. Calcd for $C_{148}H_{116}N_2O_4P_8Ru_2$: C 72.96, H 4.80, N 1.15 %. Found: C 73.21, H 4.74, N 1.19 %. UV-vis ($\bar{\nu}_{max}$, cm^{-1} (ε, M^{-1} cm^{-1})): 21 600 (61 700), 25 000 (74 000), 32 500 (sh, 62 700). IR (cm^{-1}): 2047, 2204 ν(C≡C), 3296 ν(HC≡). ^{1}H NMR: (δ, 300 MHz, $CDCl_3$); 2.63 (m, 16H, CH_2), 3.12 (s, 1H, C≡CH), 6.58 (d, J_{HH} = 8 Hz, 4H, H_{37} or H_{46}), 6.75 (d, J_{HH} = 8 Hz, 4H, H_{37} or H_{46}), 6.92 to 7.57 (m, 88H, phenyl), 7.65 (s, 1H, H_{30}), 7.98 (d, J_{HH} = 8 Hz, 4H, H_{47}). ^{13}C NMR: (δ, 75 MHz, $CDCl_3$); 31.3 (CH_2), 78.1 (C_{25}), 82.3 (C_{26}), 127.2 (C_m), 128.9 (C_p), 133.9 (C_o), 134.1 (C_o), 136.4 (m, C_i), 142.6 (C_{48}). ^{31}P NMR: (δ, 121 MHz, $CDCl_3$); 54.5 (PPh_2).

*1,3,5-C_6H_3(4-C≡CC_6H_4C≡C-trans-[Ru(dppe)$_2$]C≡C-3,5-C_6H_3-{4-C≡CC_6H_4C≡C-trans-[Ru(C≡CPh)(dppe)$_2$]}$_2$)$_3$ (**18a**)*

To a solution of **10** (80 mg, 0.025 mmol) and **17a** (190 mg, 0.081 mmol) in dichloromethane (20 mL) was added sodium hexafluorophosphate (30 mg, 0.18 mmol) and triethylamine (0.5 mL) with stirring. The mixture was stirred for 24 h in an oil bath held at 38 °C. The solvent was removed *in vacuo* and the residue dissolved in dichloromethane and absorbed onto alumina, which was then placed on to an alumina column (basic, ungraded). It was eluted firstly with diethylether to remove excess **17a** and then with dichloromethane to remove the product. Methanol (~40 mL) was then added to the eluted solution and the total volume of solvent was reduced to ~10 mL using a rotary evaporator. The precipitated product was collected by filtration and dried *in vacuo*. Yield was 130 mg (52 %). Anal. Calcd for $C_{636}H_{510}P_{36}Ru_9$: C 75.06, H 5.05 %. Found: C 74.83, H 5.23 %. UV-vis ($\bar{\nu}_{max}$, cm^{-1} (ε, M^{-1} cm^{-1})): 24 900 (421 000), 32 200 (291 000). IR (cm^{-1}): 2056, 2204 ν(C≡C). ^{1}H NMR: (δ, 300 MHz, $CDCl_3$); 2.64 (m, 72H, CH_2), 6.68 to 6.81 (m, 36H, H_{11}, H_{28}, H_{37}, H_{46}), 6.94 to 7.63 (m, 402H, phenyl). ^{13}C NMR: (δ, 75 MHz, $CDCl_3$); 31.4 (CH_2), 127.0 (C_m), 128.6 (C_p), 128.7 (C_p), 134.1 (C_o), 134.3 (C_o), 136.9 (m, C_i). ^{31}P NMR: (δ, 121 MHz, $CDCl_3$); 54.4 (s, 24P, "outer" PPh_2), 54.3 (s, 12P, "inner" PPh_2).

1,3,5-C_6H_3(4-C≡CC_6H_4C≡C-trans-[Ru(dppe)$_2$]C≡C-3,5-C_6H_3-{4-C≡CC_6H_4C≡C-trans-[Ru(4-C≡$CC_6H_4NO_2$)(dppe)$_2$]}$_2$)$_3$ ***(18b)***

To a solution of **10** (77 mg, 0.024 mmol) and **17b** (190 mg, 0.078 mmol) in dichloromethane (15 mL) was added sodium hexafluorophosphate (25 mg, 0.15 mmol) and triethylamine (0.5 mL) with stirring. The mixture was stirred for 18 h in an oil bath held at 35 °C. The solvent was removed *in vacuo* and the residue dissolved in dichloromethane and absorbed onto alumina, which was then placed on to an alumina column (basic, ungraded). It was eluted firstly with diethylether to remove excess **17b** and then with dichloromethane to remove the product. The solvent was then removed using a rotary evaporator and 80 mg (32 %) of red powder was collected. Anal. Calcd for $C_{636}H_{504}N_6O_{12}P_{36}Ru_9$: C 73.12, H 4.86, N 0.80 %. Found: C 73.35, H 4.92, N 1.03 %. UV-vis ($\bar{\nu}_{max}$, cm^{-1} (ε, M^{-1} cm^{-1})): 21 400 (sh, 160 000), 25 300 (350 000), 32 700 (sh, 241 000). IR (cm^{-1}): 2047, 2206 ν(C≡C). ^{1}H NMR: (δ, 300 MHz, $CDCl_3$); 2.64 (m, 72H, CH_2), 6.55 to 6.81 (m, 36H, H_{11}, H_{28}, H_{37}, H_{46}), 6.91 to 7.63 (m, 384H, phenyl), 7.97 (d, J_{HH} = 8 Hz, 12H, H_{47}). ^{13}C NMR: (δ, 75 MHz, $CDCl_3$); 31.3 (CH_2), 127.0 (C_m), 128.9 (C_p), 133.9 (C_o), 134.1 (C_o), 136.5 (m, C_i), 142.6 (C_{48}). ^{31}P NMR: (δ, 121 MHz, $CDCl_3$); 53.8 (s, 24P, "outer" PPh_2), 54.1 (s, 12P, "inner" PPh_2).

trans-[Ru(4-C≡CC_6H_4C≡CPh)(C≡CPh)(dppe)$_2$] ***(19a)***

To a solution of *trans*-[Ru(C≡CPh)Cl(dppe)$_2$] (200 mg, 0.19 mmol) and 4-HC≡CC_6H_4C≡CPh (50 mg, 0.25 mmol) in dichloromethane (10 mL) was added sodium hexafluorophosphate (65 mg, 0.39 mmol) and triethylamine (1 mL) with stirring. The mixture was stirred for 6 h at room temperature. The solvent was removed *in vacuo* and the residue dissolved in dichloromethane and absorbed onto alumina, which was then placed on to an alumina column. It was eluted firstly with 1:9 dichloromethane / pet. spirit to remove excess acetylene and then with dichloromethane to remove the product. Addition of pet. spirit and then evaporation of the solvent afforded yellow microcrystals. Yield was 0.180 g (78 %). MS: 1200 ($[M]^+$, 5), 1099 ($[M(C≡C{C_6}H_4C≡CPh)(dppe)_2]^+$, 75), 999 ($[M(C≡CPh)(dppe)_2]^+$, 65), 897 ($[M(dppe)_2 - H]^+$, 100). Anal. Calcd for $C_{77}H_{64}Cl_2P_4Ru$: C 71.96, H 5.02 %. Found: C 71.96, H 5.03 %. UV-vis ($\bar{\nu}_{max}$, cm^{-1} (ε, M^{-1} cm^{-1})): 26 200 (38 000). IR (cm^{-1}): 2210, 2056 ν(C≡C). ^{1}H NMR: (δ, 300 MHz, $CDCl_3$); 2.61 (m, 8H, CH_2), 6.59 (d, J_{HH} = 8 Hz, 2H, H_{11} or H_{20}), 6.76 (d, J_{HH} = 8 Hz, 2H, H_{11} or H_{20}), 6.89 to 7.60 (m, 50H, phenyl). ^{13}C NMR: (δ, 75 MHz, $CDCl_3$); 31.4 (CH_2), 127.0 (C_m), 128.6 (C_p), 134.1 (C_o), 134.3 (C_o), 136.9 (C_i). ^{31}P NMR: (δ, 121 MHz, $CDCl_3$); 54.2 (PPh_2).

*trans-[Ru(4-C≡CC$_6$H$_4$C≡CPh)(4-C≡CC$_6$H$_4$NO$_2$)(dppe)$_2$] (**19b**)*

To a solution of *trans*-[Ru(4-C≡CC$_6$H$_4$NO$_2$)Cl(dppe)$_2$] (120 mg, 0.11 mmol) and 4-HC≡CC$_6$H$_4$C≡CPh (45 mg, 0.22 mmol) in dichloromethane (10 mL) was added sodium hexafluorophosphate (40 mg, 0.24 mmol) and triethylamine (0.5 mL) with stirring. The mixture was stirred for 2 h at reflux and then allowed to cool to room temperature. The mixture was then placed atop a short alumina (basic, ungraded) column and eluted with dichloromethane. Pet. spirit (~50 mL) was then added to the eluted solution and the total volume of solvent was reduced to ~30 mL using a rotary evaporator. The precipitated product was collected by filtration, washed with pet. spirit, and dried *in vacuo*, yield 110 mg (79 %). MS: 1245 ([M]$^+$, 5), 898 ([M(dppe)$_2$]$^+$, 35). Anal. Calcd for C$_{76}$H$_{61}$NO$_2$P$_4$Ru: C 73.30, H 4.94, N 1.12 %. Found: C 72.89, H 5.19, N 1.48 %. UV-vis ($\tilde{\nu}_{max}$, cm^{-1} (ε, M^{-1} cm^{-1})): 21 300 (24 700), 26 800 (33 900). IR (cm^{-1}): 2046 ν(C≡C). ^{1}H NMR: (δ, 300 MHz, CDCl$_3$); 2.61 (m, 8H, CH$_2$), 6.56 (d, J_{HH} = 8 Hz, 2H, H$_{11}$ or H$_{20}$), 6.73 (d, J_{HH} = 8 Hz, 2H, H$_{11}$ or H$_{20}$), 6.90 to 7.55 (m, 47H, phenyl), 7.97 (d, J_{HH} = 8 Hz, 2H, H$_{21}$). ^{13}C NMR: (δ, 75 MHz, CDCl$_3$); 31.3 (CH$_2$), 127.2 (C$_m$), 128.9 (C$_p$), 133.9 (C$_o$), 134.1 (C$_o$), 136.3 (m, C$_i$), 142.6 (C$_{48}$). ^{31}P NMR: (δ, 121 MHz, CDCl$_3$); 53.7 (PPh$_2$).

*trans-[Ru(4-C≡CC$_6$H$_4$I)Cl(dppe)$_2$] (**20**)*

A mixture of *cis*-[RuCl$_2$(dppe)$_2$] (500 mg, 0.52 mmol), 4-HC≡CC$_6$H$_4$I (240 mg, 1.05 mmol) and sodium hexafluorophosphate (200 mg, 1.19 mmol) was stirred in dichloromethane (20 mL) for 6 h at room temperature. Pet. spirit (30 mL, deoxygenated) was added via cannula and the total solvent volume reduced to ~25 mL *in vacuo*. The mixture was filtered using Schlenk techniques and the residue dissolved in dichloromethane (20 mL). Sodium methoxide (65 mg, 1.19 mmol in 2 mL of MeOH) was added to deprotonate the vinylidene complex formed. The solvent was removed *in vacuo* and the residue purified by column chromatography eluting with 4:1 dichloromethane / pet. spirit. The product was precipitated by removing the dichloromethane on a rotary evaporator. Upon filtering, 480 mg of yellow powder was isolated (80 %). MS: 1160 ([M]$^+$, 17), 1125 ([M - Cl]$^+$, 32), 897 ([Ru(dppe)$_2$]$^+$, 23), 499 ([Ru(dppe)]$^+$, 16). Anal. Calcd for C$_{60}$H$_{52}$ClIP$_4$Ru: C 62.10, H 4.52 %. Found: C 62.34, H 4.30 %. UV-vis ($\tilde{\nu}_{max}$, cm^{-1} (ε, M^{-1} cm^{-1})): 29 400 (24 500). IR (cm^{-1}); 2068 ν(C≡C). ^{1}H NMR: (δ, 300 MHz, CDCl$_3$); 2.63 (m, 8H, CH$_2$), 6.30 (d, J_{HH} = 8 Hz, 2H, H$_{11}$), 6.90 to 7.44 (42H, Ph). ^{31}P NMR: (δ, 121 MHz, CDCl$_3$); 50.1 (PPh$_2$).

*trans-[Ru(4-C≡CC$_6$H$_4$C≡CSiMe$_3$)Cl(dppe)$_2$] (**21**)*

trans-[Ru(4-C≡CC$_6$H$_4$I)Cl(dppe)$_2$] (500 mg, 0.43 mmol) and trimethylsilylacetylene (180 μL, 1.27 mmol) were dissolved in tetrahydrofuran (15 mL). Dichlorobis(triphenyl-

phosphine)palladium(II) (10 mg, 0.014 mmol), copper(I) iodide (10 mg, 0.052 mmol) and triethylamine (2 mL) were added with stirring. The mixture was stirred for 20 min at room temperature. The solvent was then removed *in vacuo* and the residue dissolved in dichloromethane and passed through an alumina plug, eluting with dichloromethane. Pet. spirit was added (~50 mL) and the solvent removed using a rotary evaporator, affording 300 mg (62 %) of the product as a yellow powder. MS: 1130 ($[M]^+$, 100), 1095 ($[M - Cl]^+$, 20), 897 ($[Ru(dppe)_2 - H]^+$, 25), 499 ($[Ru(dppe)]^+$, 25). Anal. Calcd for $C_{65}H_{61}ClP_4RuSi$: C 69.05, H 5.44 %. Found: C 68.51, H 5.50 %. UV-vis ($\tilde{\nu}_{max}$, cm^{-1} (ε, M^{-1} cm^{-1})): 27 000 (33 100). IR (cm^{-1}); 2148, 2065 ν(C≡C). ^1H NMR: (δ, 300 MHz, $CDCl_3$); 0.24 (s, 9H, Me), 2.66 (m, 8H, CH_2), 6.46 (d, J_{HH} = 8 Hz, 2H, H_{11}), 6.87 to 7.40 (42H, Ph). ^{31}P NMR: (δ, 121 MHz, $CDCl_3$); 49.8 (PPh_2).

*trans-[Ru(4-C≡CC_6H_4C≡C$SiMe_3$)(C≡CPh)(dppe)$_2$] (**22**)*

trans-[Ru(4-C≡CC_6H_4C≡C$SiMe_3$)Cl(dppe)$_2$] (720 mg, 0.64 mmol), phenylacetylene (140 μL, 1.28 mmol), sodium hexafluorophosphate (220 mg, 1.31 mmol) and triethylamine were stirred in dichloromethane for 4 h at room temperature. The solvent was then removed *in vacuo* and the residue purified by column chromatography, eluting first with pet. spirit to remove excess acetylene, and then with 4:1 dichloromethane / pet. spirit to remove the product. The solvent was removed using a rotary evaporator and 500 mg (67 %) of the product as a yellow powder was collected. MS: 1196 ($[M]^+$, 25), 898 ($[Ru(dppe)_2]^+$, 50). UV-vis ($\tilde{\nu}_{max}$, cm^{-1} (ε, M^{-1} cm^{-1})): 27 000 (40 200). IR (cm^{-1}); 2148, 2058 ν(C≡C). ^1H NMR: (δ, 300 MHz, $CDCl_3$); 0.24 (s, 9H, Me), 2.60 (m, 8H, CH_2), 6.54 (d, J_{HH} = 8 Hz, 2H, H_{11} or H_{20}), 6.79 (d, J_{HH} = 8 Hz, 2H, H_{11} or H_{20}), 6.88 to 7.60 (45H, Ph). ^{31}P NMR: (δ, 121 MHz, $CDCl_3$); 54.4 (PPh_2).

*trans-[Ru(4-C≡CC_6H_4C≡CH)(C≡CPh)(dppe)$_2$] (**23**)*

trans-[Ru(4-C≡CC_6H_4C≡C$SiMe_3$)(C≡CPh)(dppe)$_2$] (440 mg, 0.36 mmol) was dissolved in dichloromethane (20 mL) and tetra-*n*-butylammonium fluoride (0.40 mL, 1 M solution in tetrahydrofuran) was added with stirring. The mixture was stirred 30 min at room temperature. The solvent was then removed *in vacuo* and the residue purified by column chromatography on alumina, eluting with 2:3 dichloromethane / pet. spirit. The solvent was removed using a rotary evaporator and 335 mg (81 %) of yellow powder was collected. MS: 1160 ($[M]^+$, 17). Anal. Calcd for $C_{70}H_{58}P_4Ru$: C 74.79, H 5.20 %. Found: C 74.48, H 5.20 %. UV-vis ($\tilde{\nu}_{max}$, cm^{-1} (ε, M^{-1} cm^{-1})): 27 700 (35 400). IR (cm^{-1}); 2057 ν(C≡C), 3294 ν(H-C≡). ^1H NMR: (δ, 300 MHz, $CDCl_3$); 2.60 (m, 8H, CH_2), 3.09 (s, 1H, C≡CH), 6.58 (d, J_{HH} = 8 Hz, 2H, H_{11} or H_{20}), 6.79 (d, J_{HH} = 8 Hz, 2H, H_{11} or H_{20}), 6.89 to 7.59 (45H, Ph). ^{31}P NMR: (δ, 121 MHz, $CDCl_3$); 54.5 (PPh_2).

*trans-[Ru(4-C≡CC$_6$H$_4$C≡CSiMe$_3$)(3,5-C≡CC$_6$H$_3$I$_2$)(dppe)$_2$] (**24**)*

trans-[Ru(4-C≡CC$_6$H$_4$C≡CSiMe$_3$)Cl(dppe)$_2$] (150 mg, 0.13 mmol), 1-HC≡C-3,5-C$_6$H$_3$I$_2$ (70 mg, 0.20 mmol), sodium hexafluorophosphate (45 mg, 0.26 mmol) and triethylamine (1 mL) were stirred in dichloromethane for 5 h at room temperature. The solvent was then removed *in vacuo* and the residue purified by column chromatography, eluting first with 1:9 dichloromethane / pet. spirit to remove excess acetylene, and then with 1:1 dichloromethane / pet. spirit to remove the product. The solvent was removed using a rotary evaporator and 150 mg (78 %) of the product as a yellow powder was collected. MS: 1448 ([M]$^+$, 30), 898 ([Ru(dppe)$_2$]$^+$, 100). Anal. Calcd for C$_{73}$H$_{64}$I$_2$P$_4$RuSi: C 60.55, H 4.45 %. Found: C 60.69, H 4.48 %. UV-vis ($\bar{\nu}_{max}$, cm^{-1} (ε, M^{-1} cm^{-1})): 27 000 (56 200). IR (cm^{-1}); 2149, 2060, 2046 ν(C≡C). ^{1}H NMR: (δ, 300 MHz, CDCl$_3$); 0.24 (s, 9H, Me), 2.55 (m, 8H, CH$_2$), 6.69 (d, J_{HH} = 8 Hz, 2H, H$_{11}$ or H$_{20}$), 6.79 (d, J_{HH} = 2 Hz, 2H, H$_{11}$ or H$_{20}$), 6.92 to 7.68 (43H, Ph). ^{31}P NMR: (δ, 121 MHz, CDCl$_3$); 54.2 (PPh$_2$).

4.7.4. Hyper-Rayleigh scattering measurements

A Nd:YAG laser (Q-switched Nd:YAG Quanta Ray GCR130-10, 1064 nm, 8 ns pulses, 10 Hz) was focussed into a cylindrical cell (14 mL) containing the sample. The intensity of the incident beam was varied by rotation of a half-wave plate placed between crossed polarizers. Part of the laser pulse was sampled by a photodiode to measure the vertically polarized incident light intensity. The frequency doubled light was collected by an efficient condenser system and detected by a photomultiplier. The harmonic scattering and linear scattering were distinguished by appropriate filters; gated integrators were used to obtain intensities of the incident and harmonic scattered light. All measurements were performed in tetrahydrofuran using *p*-nitroaniline ($\beta = 21.4 \times 10^{-30}$ esu) as a reference.

4.7.5. Z-scan measurements

Z-scan measurements were performed at 800 nm using a system consisting of a Coherent Mira Ar-pumped Ti-sapphire laser generating a mode-locked train of approximately 100 fs pulses and a home-built Ti-sapphire regenerative amplifier pumped with a frequency-doubled Q-switched pulsed YAG laser (Spectra Physics GCR) at 30 Hz and employing chirped pulse amplification. THF solutions were examined in a 0.1 cm path length cell. The closed-aperture and open-aperture Z-scans were recorded at a few concentrations of each compound and the real and imaginary part of the nonlinear phase shift determined by numerical fitting using equations given in reference 91. The real and imaginary part of the hyperpolarizability of the solute was then calculated by linear regression from the concentration dependencies. The nonlinearities and light intensities were calibrated using measurements of a 1 mm thick silica plate for which the nonlinear refractive index $n_2 = 3 \times 10^{-16}$ cm^2 W^{-1} was assumed.

4.6. References

(1) Zyss, J. *Nonlinear Opt.* **1991**, *1*, 3.

(2) Zyss, J.; Ledoux, I. *Chem. Rev.* **1994**, *94*, 77.

(3) Brasselet, S.; Zyss, J. *Opt. Mater.* **1998**, *9*, 307.

(4) Dhenaut, C.; Ledoux, I.; Samuel, I. D. W.; Zyss, J.; Bourgault, M.; Bozec, H. L. *Nature* **1995**, *374*, 339.

(5) Stadler, S.; Feiner, F.; Bräuchle, C.; Brandl, S.; Gompper, R. *Chem. Phys. Lett.* **1995**, *245*, 292.

(6) Stadler, S.; Dietrich, R.; Bourhill, G.; Bräuchle, C. *Opt. Lett.* **1996**, *21*, 251.

(7) Stadler, S.; Bräuchle, C.; Brandl, S.; Gompper, R. *Chem. Mater.* **1996**, *8*, 676.

(8) Verbiest, T.; Clays, K.; Samyn, C.; Wolff, J.; Reinhoudt, D.; Persoons, A. *J. Am. Chem. Soc.* **1994**, *116*, 9320.

(9) Wortmann, R.; Glania, C.; Kramer, P.; Matschimer, R.; Wolff, J. J.; Kraft, S.; Treptow, B.; Barbu, E.; Längle, D.; Görlitz, G. *Chem. Eur. J.* **1997**, *3*, 1765.

(10) Lequan, M.; Branger, C.; Simon, J.; Thami, T.; Chauchard, E.; Persoons, A. *Adv. Mater.* **1994**, *6*, 851.

(11) Zyss, J.; Dhenaut, C.; Chauvan, T.; Ledoux, I. *Chem. Phys. Lett.* **1993**, *206*, 409.

(12) Blanchard-Desce, M.; Baudin, J.-B.; Ruel, O.; Jullien, L.; Brasselet, S.; Zyss, J. *Opt. Mater.* **1998**, *9*, 276.

(13) Verbiest, T.; Clays, K.; Persoons, A.; Meyers, F.; Brédas, J. L. *Opt. Lett.* **1993**, *18*, 525.

(14) Verbiest, T.; Houbrechts, S.; Kauranen, M.; Clays, K.; Persoons, A. *J. Mater. Chem.* **1997**, *7*, 2175.

(15) Chui, T. W.; Wong, K. Y. *J. Chem. Phys.* **1998**, *109*, 1391.

(16) Lambert, C.; Nöll, G.; Schmälzlin, E.; Meerholz, K.; Bräuchle, C. *Chem. Eur. J.* **1998**, *4*, 2129.

(17) Sastre, A.; Torres, T.; Díaz-García, M. A.; Agulló-López, F.; Dhenaut, C.; Brasselet, S.; Ledoux, I.; Zyss, J. *J. Am. Chem. Soc.* **1996**, *118*, 2746.

(18) Ray, P. C.; Das, P. K. *Chem. Phys. Lett.* **1995**, *244*, 153.

(19) Brédas, J. L.; Meyers, F. In *Organic Materials for Non-linear Optics III*; Ashwell, G. J. and Bloor, D., Eds.; Royal Society of Chemistry: Cambridge, 1993, p 129.

(20) Zyss, J.; Van, T. C.; Dhenaut, C.; Ledoux, I. *Chem. Phys.* **1993**, *177*, 281.

(21) Vance, F. W.; Hupp, J. T. *J. Am. Chem. Soc.* **1999**, *121*, 4047.

(22) Greve, D. R.; Schougaard, S. B.; Geisler, T.; Petersen, J. C.; Bjørnholm, T. *Adv. Mater.* **1997**, *9*, 1113.

(23) Gubler, U.; Spreiter, R.; Bosshard, C.; Günter, P.; Tykwinski, R. R.; Diederich, F. *Appl. Phys. Lett.* **1998**, *73*, 2396.

(24) Sutherland, R. L. *Handbook of Nonlinear Optics*; Thompson, B. J., Ed.; Marcel Dekker: New York, 1996; Vol. 52.

(25) Bhawalkar, J. D.; He, G. S.; Prasad, P. N. *Rep. Prog. Phys.* **1996**, *59*, 1041.

(26) Reinhardt, B. A.; Lawrence, L. B.; Clarson, S. J.; Dillard, A. G.; Bhatt, J. C.; Kannan, R.; Yuan, L.; He, G. S.; Prasad, P. N. *Chem. Mater.* **1998**, *10*, 1863.

(27) Albota, M.; Beljonne, D.; Bredas, J. L.; Ehrlich, J. E.; Fu, J. Y.; Heikal, A. A.; Hess, S. E.; Kogej, T.; Levin, M. D.; Marder, S. R.; McCordmaughon, D.; Perry, J. W.; Rockel, H.; Rumi, M.; Subramaniam, C.; Webb, W. W.; Wu, I. L.; Xu, C. *Science* **1998**, *281*, 1653.

(28) Perry, J. W.; Mansour, K.; Lee, I. Y. S.; Wu, X. L.; Bedworth, P. V.; Chen, C. T.; Ng, D.; Marder, S. R.; Miles, P.; Wada, T.; Tian, M.; Sasabe, H. *Science* **1996**, *273*, 1533.

(29) Perry, J. W.; Khundkar, L. R.; Coulter, D. R.; Alvarez Jr, D.; Marder, S. R.; Wei, T. H.; Spence, M. J.; van Stryland, E. W.; Hagen, D. J. In *Organic Molecules for Nonlinear Optics and Photonics*; Messier, J., Kajzar, F. and Prasad, P., Eds.; Kluwer: Dordrecht, 1991; Vol. 194, p 369.

(30) Fischer, M.; Vogtle, F. *Angew. Chem., Int. Ed.* **1999**, *38*, 885.

(31) Archut, A.; Vogtle, F. *Chem. Soc. Rev.* **1998**, *27*, 233.

(32) Zeng, F. W.; Zimmerman, S. C. *Chem. Rev.* **1997**, *97*, 1681.

(33) Buhleier, E.; Wehner, W.; Vögtle, F. *Synthesis* **1978**, 155.

(34) Tomalia, D. A.; Naylor, A. M.; Goddard, W. A. *Angew. Chem., Int. Ed. Engl.* **1990**, *29*, 138.

(35) Mekelburger, H. B.; Jaworek, W.; Vögtle, F. *Angew. Chem., Int. Ed. Engl.* **1992**, *31*, 1571.

(36) Issberner, J.; Moors, R.; Vögtle, F. *Angew. Chem., Int. Ed. Engl.* **1994**, *33*, 2413.

(37) Ardoin, N.; Astruc, D. *Bull. Soc. Chim. Fr.* **1995**, *132*, 875.

(38) Newkome, G. R.; Moorefield, C. N.; Vögtle, F. *Dendritic Molecules: Concepts, Syntheses, Perspectives*; VCH: Weinheim, 1996.

(39) Balzani, V.; Campagna, S.; Denti, G.; Juris, A.; Serroni, S.; Venturi, M. *Coord. Chem. Rev.* **1994**, *132*, 1.

(40) Moss, J. R. *Platinum Metals Rev.* **1995**, *39*, 33.

(41) Gorman, C. *Adv. Mater.* **1998**, *10*, 295.

(42) Hearshaw, M. A.; Moss, J. R. *J. Chem. Soc., Chem. Commun.* **1999**, 1.

(43) Xu, Z.; Moore, J. S. *Macromolecules* **1991**, *24*, 5893.

(44) Xu, Z.; Moore, J. S. *Angew. Chem., Int. Ed. Engl.* **1993**, *32*, 246.

(45) Xu, Z.; Moore, J. S. *Angew. Chem., Int. Ed. Engl.* **1993**, *32*, 1354.

(46) Xu, Z.; Kahr, M.; Walker, K. L.; Wilkins, C. L.; Moore, J. S. *J. Am. Chem. Soc.* **1994**, *116*, 4537.

(47) Devadoss, C.; Bharathi, P.; Moore, J. S. *J. Am. Chem. Soc.* **1996**, *118*, 9635.

(48) Shortreed, M. R.; Swallen, S. F.; Shi, Z. Y.; Tan, W.; Xu, Z.; Devadoss, C.; Moore, J. S.; Kopelman, R. *J. Phys. Chem. B* **1997**, *101*, 6318.

(49) Pesak, D. J.; Moore, J. S. *Tetrahedron* **1997**, *53*, 15331.

(50) Constable, E. C.; Eich, O.; Housecroft, C. E.; Johnston, L. A. *J. Chem. Soc., Chem. Commun.* **1998**, 2661.

(51) Constable, E. C.; Eich, O.; Housecroft, C. E. *J. Chem. Soc., Dalton Trans.* **1999**, 1363.

(52) Onitsuka, K.; Fujimoto, M.; Ohshiro, N.; Takahashi, S. *Angew. Chem., Int. Ed.* **1999**, *38*, 689.

(53) Achar, S.; Puddephatt, R. J. *Angew. Chem., Int. Ed. Engl.* **1994**, *33*, 847.

(54) Moulines, F.; Djakovitch, L.; Boese, R.; Gloaguen, B.; Thiel, W.; Fillaut, J. L.; Delville, M. H.; Astruc, D. *Angew. Chem. Int. Ed. Engl.* **1993**, *32*, 1075.

(55) Köllner, C.; Pugin, B.; Togni, A. *J. Am. Chem. Soc.* **1998**, *120*, 10274.

(56) Larré, C.; Donnadieu, B.; Caminade, A. M.; Majoral, J. P. *Chem. Eur. J.* **1998**, *4*, 2031.

(57) Liao, Y. H.; Moss, J. R. *J. Chem. Soc., Chem. Commun.* **1993**, 1774.

(58) Balzani, V.; Campagna, S.; Denti, G.; Juris, A.; Serroni, S.; Venturi, M. *Acc. Chem. Res.* **1998**, *31*, 26.

(59) Denti, G.; Campagna, S.; Serroni, S.; Ciano, M.; Balzani, V. *J. Am. Chem. Soc.* **1992**, *114*, 2944.

(60) Serroni, S.; Juris, A.; Venturi, M.; Campagna, S.; Resino, I. R.; Denti, G.; Credi, A.; Balzani, V. *J. Mater. Chem.* **1997**, *7*, 1277.

(61) Serroni, S.; Denti, G.; Campagna, S.; Juris, A.; Ciano, M.; Balzani, V. *Angew. Chem., Int. Ed. Engl.* **1992**, *31*, 1493.

(62) Leininger, S.; Stang, P. J.; Huang, S. *Organometallics* **1998**, *17*, 3981.

(63) Newkome, G. R.; Güther, R.; Moorefield, C. N.; Cardullo, F.; Echegoyen, L.; Perez-Cordero, E.; Luftmann, H. *Angew. Chem., Int. Ed. Engl.* **1995**, *34*, 2023.

(64) Miedaner, A.; Curtis, C. J.; Barkley, R. M.; DuBois, D. L. *Inorg. Chem.* **1994**, *24*, 5482.

(65) Alonso, B.; Cuadrado, I.; Moran, M.; Losada, J. *J. Chem. Soc., Chem. Commun.* **1994**, 2575.

(66) Put, E. J. H.; Clays, K.; Persoons, A.; Biemans, H. A. M.; Liujkx, C. P. M.; Meijer, E. W. *Chem. Phys. Lett.* **1996**, *260*, 136.

(67) Moore, J. S. *Acc. Chem. Res.* **1997**, *30*, 402.

(68) Touchard, D.; Haquette, P.; Guesmi, S.; LePichon, L.; Daridor, A.; Toupet, L.; Dixneuf, P. H. *Organometallics* **1997**, *16*, 3640.

(69) Uno, M.; Dixneuf, P. H. *Angew. Chem., Int. Ed.* **1998**, *37*, 1714.

(70) Touchard, D.; Guesmi, S.; LePichon, L.; Daridor, A.; Dixneuf, P. H. *Inorg. Chim. Acta* **1998**, *280*, 118.

(71) Touchard, D.; Haquette, P.; Pirio, N.; Toupet, L.; Dixneuf, P. H. *Organometallics* **1993**, *12*, 3132.

(72) McCleverty, J. A. *Polyhedron* **1989**, *8*, 1669.

(73) McDonagh, A. M.; Whittall, I. R.; Humphrey, M. G.; Skelton, B. W.; White, A. H. *J. Organomet. Chem.* **1996**, *519*, 229.

(74) McDonagh, A. M.; Whittall, I. R.; Humphrey, M. G.; Hockless, D. C. R.; Skelton, B. W.; White, A. H. *J. Organomet. Chem.* **1996**, *523*, 33.

(75) Naulty, R. H.; McDonagh, A. M.; Whittall, I. R.; Cifuentes, M. P.; Humphrey, M. G.; Houbrechts, S.; Maes, J.; Persoons, A.; Heath, G. A.; Hockless, D. C. R. *J. Organomet. Chem.* **1998**, *563*, 137.

(76) McDonagh, A. M.; Humphrey, M. G.; Samoc, M.; Luther-Davies, B.; Houbrechts, S.; Wada, T.; Sasabe, H.; Persoons, A. *J. Am. Chem. Soc.* **1999**, *121*, 1405.

(77) Whittall, I. R.; Humphrey, M. G.; Houbrechts, S.; Maes, J.; Persoons, A.; Schmid, S.; Hockless, D. C. R. *J. Organomet. Chem.* **1997**, *544*, 277.

(78) Takahashi, S.; Kuroyama, Y.; Sonogashira, K.; Hagihara, N. *Synthesis* **1980**, 627.

(79) Faust, R.; Diederich, F.; Volker, G.; Seiler, P. *Chem. Eur. J.* **1995**, *1*, 111.

(80) Lavastre, O.; Olivier, L.; Dixneuf, P. H.; Sibandhit, S. *Tetrahedron* **1996**, *52*, 5495.

(81) Negishi, E.; Kotora, M.; Xu, C. *J. Org. Chem.* **1997**, *62*, 8957.

(82) Nguyen, P.; Yuan, Z.; Agocs, L.; Lesley, G.; Marder, T. B. *Inorg. Chim. Acta.* **1994**, *220*, 289.

(83) McGrady, J. E.; Lovell, T.; Stranger, R.; Humphrey, M. G. *Organometallics* **1997**, *16*, 4004.

(84) Coe, B. J.; Harris, J. A.; Harrington, L. J.; Jeffery, J. C.; Rees, L. H.; Houbrechts, S.; Persoons, A. *Inorg. Chem.* **1998**, *37*, 3391.

(85) Joffre, M.; Yarron, D.; Silbey, R. J.; Zyss, J. *J. Chem. Phys.* **1992**, *97*, 5607.

(86) Trumbo, D. L.; Marvel, C. S. *J. Polym. Sci.* **1986**, *A24*, 2311.

(87) Hsung, R. P.; Chidsey, C. E. D.; Sita, L. R. *Organometallics* **1995**, *14*, 4808.

(88) Lavastre, O.; Cabioch, S.; Dixneuf, P. H.; Vohlidal, J. *Tetrahedron* **1997**, *53*, 7595.

(89) Kofron, W. G.; Baclowski, L. M. *J. Org. Chem.* **1976**, *41*, 1879.

(90) Chaudret, B.; Commenges, G.; Poilblanc, R. *J. Chem. Soc., Dalton Trans.* **1984**, 1635.

(91) Sheik-Bahae, M.; Said, A. A.; Wei, T.; Hagan, D. J.; van Stryland, E. W. *IEEE J. Quantum Electr.* **1990**, *26*, 760.